EFFECT OF DIVALENT CATIONS AND SOLUBILIZERS IN APOFERRITIN AND GAMMA D-CRYSTALLIN SOLUTIONS: NUCLEATION, CRYSTALLIZATION AND LIGHT SCATTERING STUDIES

A Dissertation
Presented to
The Academic Faculty

By

Quinta Mgbeke Nwanosike

In Partial Fulfillment
Of the Requirements for the Degree
Doctor of Philosophy in Chemical Engineering
School of Chemical and Biomolecular Engineering

Georgia Institute of Technology

December, 2009

EFFECT OF DIVALENT CATIONS AND SOLUBILIZERS IN APOFERRITIN AND GAMMA D-CRYSTALLIN SOLUTIONS: NUCLEATION, CRYSTALLIZATION AND LIGHT SCATTERING STUDIES

Approved by:

Dr. Ronald W. Rousseau, Advisor
School of Chemical and Biomolecular
Engineering
Georgia Institute of Technology

Dr. Athanassios Sambanis, Co-Advisor
School of Chemical and Biomolecular
Engineering
Georgia Institute of Technology

Dr. Amyn Teja
School of Chemical and Biomolecular
Engineering
Georgia Institute of Technology

Dr. Athanasios Nenes
School of Chemical and Biomolecular
Engineering
Georgia Institute of Technology

Dr. Ingeborg Schmidt-Krey
School of Biology
Georgia Institute of Technology

Date Approved: November 2nd, 2009

Of all tyrannies, a tyranny exercised for the good of its victims may be the most oppressive. It may be better to live under robber barons than under omnipotent moral busybodies. The robber baron's cruelty may sometimes sleep, his cupidity may at some point be satiated; but those who torment us for our own good will torment us without end, for they do so with the approval of their own conscience.

C. S. Lewis
The Humanitarian Theory of Punishment[1]

To my loving husband Diondré
and
for Loretta, Helen, Carol and Eugene

ACKNOWLEDGEMENTS

I would like to thank my thesis advisors, Dr. Ronald Rousseau and Dr. Athanassios Sambanis, for their guidance through the maze that is graduate school. Many thanks go to my thesis committee, Dr. Amyn Teja, Dr. Athanasios Nenes and Dr. Ingeborg Schmidt-Krey, who were instrumental in shaping my research. I offer my gratitude to the members of the crystallization group who offered ideas and opinions and a (willing?) ear, especially Karsten Bartling, Apichit Svang-Ariyaskul, Stephanie Barthe, Krystle Chavez, and George Dumont. Special thanks also go to Dr. Athanassios Sambanis, Dr. Andreas Bommarius and Dr. Sven Behrens and their group members who provided advice, training, materials and equipment for my experiments. David Detwiler, my able undergraduate assistant, provided invaluable help in the lab especially with protein production. In addition, Pei-Yoong Koh provided valuable insight into my research, patiently sitting through slide after slide of my presentations.

I would like to acknowledge the Cecil J. "Pete" Silas Endowment and the Georgia Research Alliance which provided funding for this research.

Above all, I would like to thank my husband Diondré who always believed in me, even when I didn't, and has the utmost faith in my abilities.

TABLE OF CONTENTS

LIST OF TABLES

LIST OF FIGURES

NOMENCLATURE

a_e Activity of solute in equilibrium with crystals

A Dimensionless second virial coefficient

B_{22} Second virial coefficient (mol mL/g^2)

B_{23} Cross second virial coefficient (mol mL/g^2)

c Solute concentration (mg/mL)

D Diffusion coefficient (μm^2/s)

d_f Fractal dimension

ΔG Free energy (J/mol)

ΔG^o Standard free energy (J/mol)

ΔH^o Standard enthalpy (J/mol)

k_B Boltzmann's constant (1.38 x 10^{-23} J/K)

K Equilibrium constant

k_D Diffusivity slope (mL/mg)

M_w Molecular weight (kDa or g/mol)

N_A Avogadro constant (6.02 x 10^{23} mol^{-1})

R Universal gas constant (8.314 J/mol-K)

R_h Hydrodynamic radius (nm)

ΔS^o Standard entropy (J/mol-K)

t Time (s)

T   Temperature (°C or K)

Greek Letters

γ	Activity coefficient
η_o	Solvent viscosity
λ	Wavelength
σ	Supersaturation
υ	Protein partial molar volume (mL/mg)
φ	Solute volume fraction

Subscripts

2, 3	Species in binary mixture
cryst	Crystallization
nuc	Nucleation

Abbreviations

BSA   Bovine serum albumin

CV   Column volume

DLCA   Diffusion-limited cluster-cluster aggregation

DLS   Dynamic light scattering

DTT   Dithiothreitol

EDTA   Ethylenediaminetetraacetic acid

HGD   Human gamma D-crystallin

HPLC   High performance liquid chromatography

NDSB   Non-detergent sulfobetaine

PAGE   Polyacrylamide gel electrophoresis

REACT   Roche European American Cataract Trial

RLCA   Reaction-limited cluster-cluster aggregation

SDS   Sodium dodecyl sulfate

SEC   Size exclusion chromatography

sHSP   Small heat shock protein

SLS   Static light scattering

SUMMARY

Crystallization of proteins in the human body can lead to the development of diseases such as sickle cell anemia and cataract. Understanding the processes involved in protein crystallization can help us gain a better understanding of such diseases. Furthermore, protein crystallization is necessary for protein structure resolution which is the first step towards determination of protein function. This is important since resolution of protein structure is the first step towards establishing structure/function relations, and possibly at performing specific structural modifications that may change the function in desirable directions. Another important application of protein crystallization is in downstream processing in the pharmaceutical industry where it is used for separation and as a final purification step. The present study increases knowledge of interactions between protein molecules during crystallization and hence the crystallization process.

Crystallization of a lens protein, human gamma D-crystallin (HGD), was studied in relation to cataract formation. The crystallization habits of this protein were determined in the presence of divalent cations which are found at elevated concentrations in cataractous lenses. Results indicate that the divalent cations studied enhance crystallization of HGD.

A thermodynamic property, the osmotic second virial coefficient, was measured in protein solutions and its value was correlated with the occurrence of crystallization. It was found that the second virial coefficient successfully predicted crystallization of HGD. A new method was developed for indirect measurement of the second virial

coefficient using dynamic light scattering. This new method is more robust and efficient than the traditional static light scattering method.

Finally the ability of solubilizers to prevent crystallization of proteins was studied. A commercial solubilizer, NDSB-201, was found to increase the energy barrier to nucleation. Although this did not prevent crystallization, it resulted in fewer and smaller crystals being obtained. The naturally occurring alpha A-crystallin was a superior solubilizer to NDSB-201, as it suppressed aggregation and prevented crystallization of HGD under conditions for which NDSB-201 did not.

The findings in the present study provide insight into the processes by which protein crystallization occurs. Using the second virial coefficient to assess whether a protein will crystallize out of solution, approaches for retardation and prevention of protein crystallization, and implications for future research, are discussed.

CHAPTER 1: INTRODUCTION

Crystallization of proteins in the human body can lead to the development of diseases such as sickle cell anemia and cataracts. Understanding the phenomena involved in protein crystallization can help us gain a better understanding of such diseases Furthermore, protein crystallization is used in determining the three dimensional structure of proteins through x-ray diffraction.[2] This is important since resolution of protein structure is the first step towards establishing structure/function relations, and possibly at performing specific structural modifications that may change the function in desirable directions. Another important application of protein crystallization is in downstream processing in the pharmaceutical industry where it is used for separation and as a final purification step. The present study increases knowledge of interactions between protein molecules during crystallization.

Human gamma D-crystallin (HGD) is one of the major proteins found in the human lens and crystallization of this protein has been linked to several types of cataract. Abnormally elevated concentrations of divalent cations such as Ca^{2+} and Ba^{2+} have been found in cataractous lenses and may play a part in cataract formation.[3] The effects of divalent cations on the crystallization habits of HGD were thus investigated in the present study. Temperature is another important factor in cataract formation. Studies show that the temperature in the lens decreases from 34°C to 32.5°C from the age of 15 weeks to 80 years. While this temperature change may seem inconsequential, temperature is known to affect the solubility of some proteins. For example, Bénas *et al.*[4] found that the solubility of lysozyme in solutions containing rubidium chloride increased by 30% with an increase

in temperature of only 2°C (26°C to 28°C). Therefore the effect of temperature on the solubility of HGD was also investigated. HGD was obtained by production with recombinant *Escherichia coli* clones.

Ordinarily, trial-and-error is used to determine conditions favorable for protein crystal growth. However there are over 20 factors that affect protein crystallization. These factors include pressure, precipitant type and concentration, type and ionic strength of solvent, metal ions, temperature and pH. Therefore, random screening is time-consuming and expensive, requiring numerous experiments and a large amount of material. George and Wilson discovered a correlation between the value of the second virial coefficient, B_{22}, and crystallization of a number of proteins including lysozyme and bovine serum albumin (BSA).[5; 6] The present study investigates the correlation between B_{22} and the occurrence of crystallization for HGD and makes use of this correlation to reduce the number of crystallization screening experiments for HGD. Usually B_{22}, which is a measure of protein-protein interactions in a particular solvent, is evaluated using static light scattering (SLS). However, this method requires relatively large amounts of protein and is notoriously unreliable especially in solutions containing aggregates.[7] This was of particular concern in the present work because the protein solutions that were studied often contained aggregates, which are precursors to crystals. In this work, a more reliable and robust method was developed whereby dynamic light scattering (DLS) can be used to measure B_{22} indirectly. This new method is also more efficient as it requires much less material and time than SLS. Whereas SLS averages out fluctuations caused by Brownian motion of protein molecules, DLS makes use of deviations from the average scattering intensity to evaluate the diffusion coefficient of the protein molecules. In

addition, the use of DLS enables real-time monitoring of the aggregation process in a protein solution. Therefore information about the Gibbs free energy associated with the nucleation process can be obtained with DLS. Probes are currently in development for *in vivo* ophthalmic studies via DLS.[8; 9] Therefore there is potential for use of our newly developed method as a diagnostic tool for biomedical applications.

Once conditions conducive for crystallization were established, attempts were made to prevent crystallization through the use of solubilizers which are known to increase the solubility of proteins in solution. A naturally occurring solubilizer, alpha A-crystallin, which is also found in the lens was used for this part of the study along with a commercial solubilizer, non-detergent sulfobetaine 201 (NDSB-201). The purpose of this part of the study was to inhibit or delay crystallization. Preventing protein crystallization or precipitation would be of potential benefit in biomedical applications and in particular in developing treatments for crystallization-related diseases, such as cataracts.

The overall objective of the present study is to increase knowledge of interactions between protein molecules during crystallization. The specific aims of the present study are summarized as follows:

1. To determine the conditions that favor crystallization of human gamma D-crystallin.

This was accomplished by carrying out crystallization experiments with varying protein concentration while simultaneously varying the temperature or the concentration of divalent cations.

2. To establish a direct correlation between the sign and magnitude of the second virial coefficient and the incidence of crystallization of human HGD.

After determination of conditions conducive for crystallization, B_{22} of protein solutions was measured using DLS. The results were then correlated with the results from Specific Aim 1.

3. To determine the role of human alpha A-crystallin chaperone as a solubilizer in solutions of HGD.

The effects of alpha A-crystallin were determined by measuring B_{22} and evaluating nucleation terms. Comparisons of these terms were then made with those from identical protein solutions containing no alpha A-crystallin. The solubilizing effects of alpha A-crystallin were then compared with those of NDSB-201.

The specific aims and the related research to address each of these are presented in CHAPTERS 4 through 8 of this thesis. CHAPTER 4 addresses the determination of conditions of protein concentration, temperature and divalent cation concentration conducive for crystallization, which is Specific Aim 1. The measurement of B_{22} by SLS was found to be unreliable for the aggregating systems under study. As such a new method was developed in CHAPTER 5 using DLS to indirectly measure B_{22}. Another lens protein, apoferritin, was used in the development of this method as it had been used for SLS studies by a previous member of our lab which provided results for comparison with the new method.[10] The use of DLS permitted determination of nucleation terms such as interfacial energy and critical free energy. These results are presented in CHAPTER 6 for both apoferritin and HGD along with B_{22} measurements. The correlation between B_{22} and the occurrence of crystallization is addressed in this chapter and this satisfies Specific Aim 2. The effects of solubilizers on nucleation terms, B_{22} and crystallization of HGD were examined in CHAPTER 7. Thus Specific Aim 3 was addressed in this chapter.

Conclusions and recommendations for future work are discussed in CHAPTER 8. The Appendices provide step-by-step procedures on the methods used in the present study. APPENDIX A deals with expression and purification of HGD, APPENDIX B focuses on high performance liquid chromatography - size exclusion chromatography which was used for protein purification, and APPENDIX C contains the procedure used for dynamic light scattering studies. Results from SLS experiments with apoferritin are given in APPENDIX D.

Overall the present study enhances understanding of intermolecular interactions of HGD and apoferritin during crystallization. In addition, it provides a more rational means for screening crystallization conditions. The newly developed method which uses DLS makes determination of intermolecular interactions easier, more robust and more efficient as it is faster and requires less material. These findings can be applied to prevent or impede cataracts and other protein condensation diseases. They may also lead to development of diagnostic tools for protein condensation diseases.

CHAPTER 2: BACKGROUND

2.1 PROTEIN CRYSTALLIZATION

Aggregation of molecules in an ordered and repetitive manner from a supersaturated solution results in crystal formation. A crystal is a highly organized solid whose constituent particles, i.e. atoms, ions or molecules, are arranged in an orderly manner in all three spatial dimensions.[11] Crystal structure is highly dependent upon solution conditions including temperature. The angles between the different faces of a crystal are characteristic of the material being crystallized. A solid may exhibit more than one crystal structure and this is referred to as polymorphism. Polymorphs exhibit different stabilities and different physical properties. This is of particular relevance to pharmaceuticals as therapeutic efficacy may vary from one polymorph to another. Although simple organic molecules can be crystallized in a few minutes, it may take weeks for proteins to crystallize as they are much bigger and therefore diffuse much slower.[12]

There are many different applications of protein crystallization. It is used in determining the three dimensional structure of proteins through x-ray diffraction.[2] This is important since resolution of protein structure is the first step towards establishing structure/function relations, and possibly at performing specific structural modifications that may change the function in desirable directions. Another important application of

protein crystallization is in downstream processing in the pharmaceutical industry where it is used for separation and as a final purification step.

Protein crystallization has been linked to diseases such as sickle cell anemia and cataracts.[13] With sickle-cell anemia, a mutant form of hemoglobin which has a lower solubility in its deoxygenated form is expressed. As such, it forms crystals or fibers within the red blood cells.[13; 14] The formation of aggregates, crystals or precipitates of the proteins found in the lens of the eye has been linked to cataracts.[15]

2.1.1 Factors Affecting Crystallization

Crystallization is affected by many different variables. These include temperature; protein concentration; type and concentration of precipitating agent; and type, concentration and pH of buffer.[2] Screening is necessary to determine the conditions that favor crystallization.

Crystallization of proteins can be induced by creating supersaturated solutions. Addition of precipitating agents such as inorganic salts, polymers and organic solvents can induce supersaturation. Precipitants are thought to induce supersaturation by competing with the protein for water molecules thereby reducing the amount of water available to dissolve the protein. Other factors that affect crystallization are protein concentration, presence of metal ions, pH and temperature.[12] A list of factors which influence crystallization is shown in Table 2-1.

Determining conditions that favor crystallization is empirical and requires comprehensive screening experiments. An understanding of protein interactions with

solvents and other solutes may lead to prediction of crystal formation.[16] George and Wilson induced crystallization in several proteins including bovine serum albumin, ovalbumin and lysozyme by addition of precipitants such as polyethylene glycol 8000 and NaCl.[6] They observed that the value of the second virial coefficient of protein solutions correlates to solution conditions favorable for the crystallization of proteins.[6] In the present study, the effect of temperature and different types and concentrations of divalent cations on crystallization of proteins was studied.

Table 2-1: Factors that influence crystallization of proteins (Adapted from McPherson[17])

1	Temperature
2	Gravity
3	pH
4	Precipitant type and concentration
5	Purity of the protein
6	Ionic strength
7	Mechanical perturbations
8	Metal ions
9	Detergents / solubilizers
10	Isoelectric point

2.1.2 Supersaturation

Crystallization comprises three phenomena: supersaturation, nucleation and growth. A saturated solution is one which contains the maximum possible solute

concentration at a given condition and which is thermodynamically stable.[11] Thus crystals cannot grow from a saturated solution. A supersaturated solution results from changing the solution conditions of a saturated solution, such that the new solution contains more solute than its maximum solubility and is thermodynamically unstable. However, a supersaturated solution may be metastable, i.e. it may remain unchanged for a long period of time if there are no external influences such as introduction of seed crystals. Supersaturation is the driving force necessary for crystallization to occur.[18] The greater the supersaturation, the further from equilibrium the solutions is and therefore the greater the crystallization driving force. Supersaturation may be achieved in several ways including cooling, evaporation and addition of precipitants.

Supersaturation may be divided into three regions namely the labile, intermediate and metastable regions which are illustrated in a protein phase diagram in Figure 2-1. The solubility line is well-defined whereas the limits of the metastable and intermediate regions are variable. Below the solubility line, crystallization is impossible. Crystal growth occurs in the metastable region although nuclei do not form spontaneously. In the intermediate region, both crystal growth and nucleation occur while in the labile region nuclei form spontaneously from a clear solution.[17]
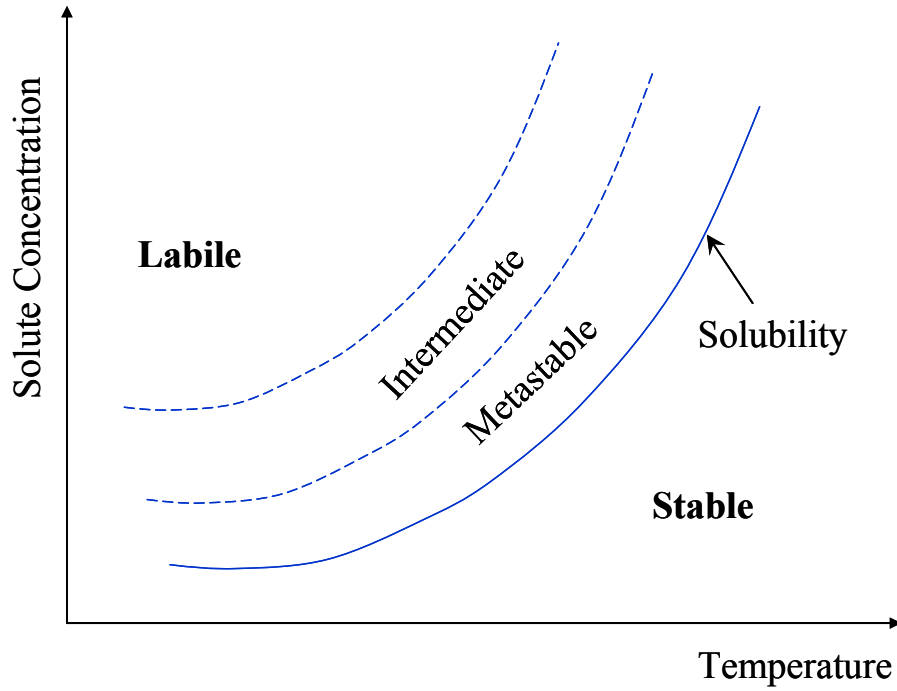
Figure 2-1: Protein phase diagram showing the regions that comprise supersaturation. Crystallization is impossible below the solubility line.[11; 18]

There are many representations for supersaturation. One of the most often used expressions is the concentration driving force

$$\Delta c = c - s \qquad\qquad\qquad 2\text{-}1$$

where c is the solute concentration and s is the solubility of the protein at those conditions. In the present study, supersaturation is represented by σ and is defined by

$$\sigma = \ln\frac{c}{s} \qquad\qquad\qquad 2\text{-}2$$

This representation is most often used when studying the energy changes associated with nucleation. As nucleation was investigated in the present study, Equation 2-2 was used to represent supersaturation.

2.1.3 Nucleation Kinetics

Nucleation is the formation of an ordered solid phase, a nucleus, from a liquid or amorphous phase. This results in crystal formation via transfer of solute from the liquid phase to the solid phase. It differs from growth in that solute is not deposited on an already existing crystal. The nucleation process is illustrated in Figure 2-2. Protein monomers aggregate reversibly resulting in random clusters and aggregates which break apart and re-form. The existence of an energy barrier prevents nucleation from occurring spontaneously except in cases where supersaturation is large enough to overcome the barrier. If the aggregates can overcome the energy barrier they reach a critical size where they become stable nuclei and rearrangement from random aggregates to crystals results.[17] The rate of crystal growth is influenced by diffusion of solute molecules from the bulk solution to the growing crystal surface, as well as by incorporation of solute molecules into the crystal lattice.

Aggregates have hydrophobic interiors which is energetically favorable. However, the molecules at the surface have greater contact and thus competition with water, which is less energetically favorable. Thus the surface molecules need to gain entry to the interior and the number of interior molecules must increase in relation to the number of exterior molecules. The aggregates thus increase in size and become more

stable.[18] As supersaturated solutions are unstable, a solid state, the nucleus, must be created in order for equilibrium to be achieved. This is the rate limiting step for the crystallization process. The energy barrier can be overcome by increasing the supersaturation of the system.
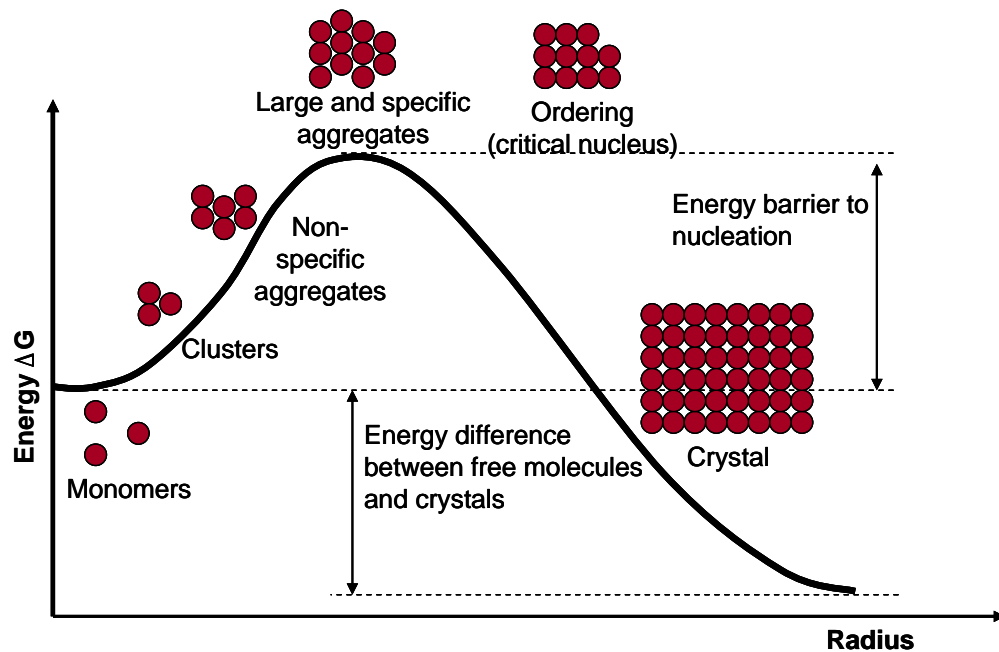
Figure 2-2: Free energy of nucleation as a function of particle radius. The schematic illustrates the nucleation process.(Adapted from McPherson, 1998[17])

There are two types of nucleation: primary and secondary nucleation.[18] Existing crystals do not play a role in primary nucleation. The mechanisms involved in primary nucleation are homogeneous and heterogeneous nucleation. Both mechanisms involve formation of crystals by successive addition of protein molecules. They both require high levels of supersaturation and display a high order dependence on supersaturation.

Therefore, small changes in supersaturation can drastically change the nucleation rate. Homogeneous nucleation is the formation of nuclei from a clear solution. On the other hand, heterogeneous nucleation requires the presence of insoluble material such as dust which provide nucleation sites. Secondary nucleation requires that solute crystals be present in the system. It can occur at low supersaturation. There are three main mechanisms by which secondary nucleation occurs. With initial breeding, seed crystals are added to the solution. Smaller crystals dislodged from the surface of the larger crystals provide nucleation sites. The second mechanism is contact nucleation whereby crystals collide with the vessel and with each other, breaking off smaller crystal pieces which can act as secondary nucleation sites. The third mechanism is shear breeding where crystal precursors are removed from the surface of growing crystals by a supersaturated solution. The different mechanisms involved in nucleation are illustrated in Figure 2-3.
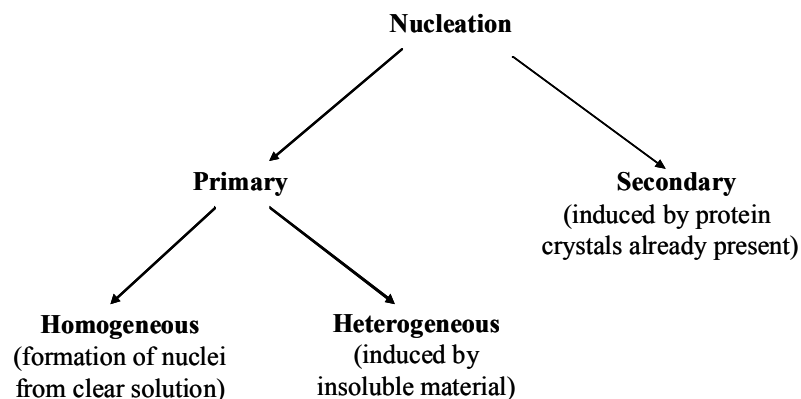
Figure 2-3: Schematic illustration mechanisms by which nucleation occurs (Adapted from Mullin, 2004[18])

The free energy change ΔG for the formation of a spherical crystalline aggregate has two contributions: a volume energy term and a surface energy term. This may be illustrated as shown in Figure 2-4.
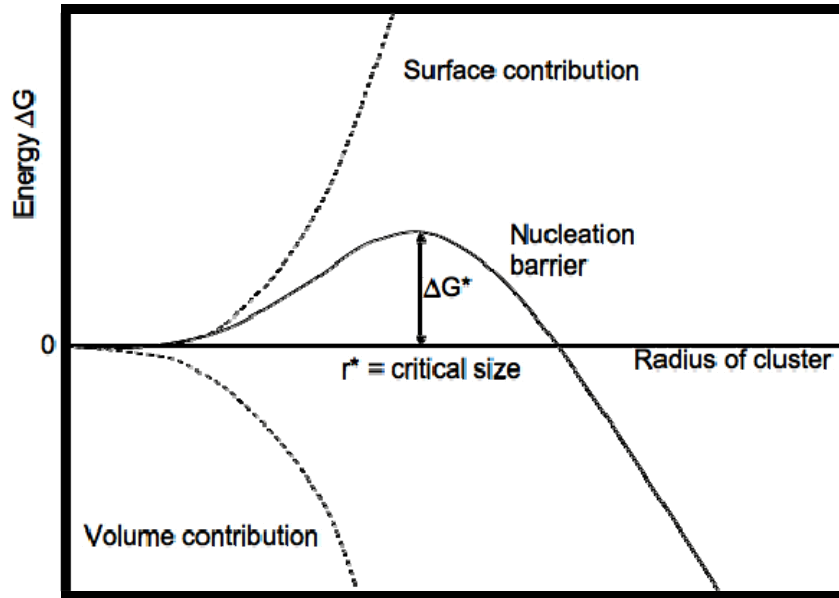
Figure 2-4: Free energy of nucleation as a function of radius. The surface and volume energy contributions add up to the overall free energy.(Adapted from Mullin, 2004[18])

ΔG is calculated using [19]

$$\Delta G = \frac{-4\pi.r^3 k_B T\sigma}{3.\Omega} + 4\pi.r^2\gamma \qquad \text{2-3}$$

where r is the radius of the aggregate, k_B is Boltzmann's constant, T is the absolute temperature, σ is the supersaturation, Ω is the protein monomer volume in solution, and γ

is the interfacial energy. The interfacial energy γ is the amount of energy necessary to create a unit of surface area of the growing crystal.[19] The solution supersaturation is determined from $\sigma = \ln(c/s)$ where c is the protein concentration and s is the solubility of the protein.

The critical radius, R_c, may be calculated using Equation 2-4 below. This equation is obtained by setting to zero the first derivative of ΔG with respect to the radius.

$$R_c = \frac{2\pi\gamma}{k_B T \sigma}$$

2-4

Equation 2-4 is taken from an article by Malkin and McPherson.[19] However, the article contains a typographical error with a factor of 4 instead of a factor of 2. In the present work, Equation 2-4, which uses the correct factor of 2, is used to evaluate R_c. The critical radius is the size beyond which aggregation is no longer reversible. At this point, the aggregates have overcome the energy barrier and irreversible aggregation results in growth. Below R_c the aggregates are unstable and stochastically grow and dissociate.

Upon determination of R_c and γ, the critical free energy change, ΔG_c, may be calculated using Equation 2-9. This equation is obtained by combining Equations 2-3 and 2-4 and setting $\Delta G = \Delta G_c$. This gives

$$\Delta G_c = \frac{-4\pi(k_B T \sigma)}{3\Omega} \frac{8\Omega^3 \gamma^3}{(k_B T \sigma)^3} + 4\pi\gamma \frac{4\Omega^2 \gamma^2}{(k_B T \sigma)^2}$$

2-5

$$\Delta G_c = \frac{-32\pi}{3}\frac{\Omega^2\gamma^3}{(k_BT\sigma)^2} + \frac{16\pi\gamma^3\Omega^2}{(k_BT\sigma)^2} \qquad\qquad 2\text{-}6$$

$$\Delta G_c = \frac{-\dfrac{32\pi}{3}\Omega^2\gamma^3 + 16\pi\gamma^3\Omega^2}{(k_BT\sigma)^2} \qquad\qquad 2\text{-}7$$

$$\Delta G_c = \frac{16.\pi.\Omega^2\gamma^3}{(k_BT\sigma)^2}\left(\frac{-2}{3}+1\right) \qquad\qquad 2\text{-}8$$

$$\Delta G_c = \frac{16\pi.\Omega^2\gamma^3}{3(k_BT\sigma)^2} \qquad\qquad 2\text{-}9$$

The critical free energy is calculated using Equation 2-9. The higher the value of ΔG_c, the less likely it is that irreversible aggregation will occur and the slower the rate of aggregation. If ΔG_c is very low, a very strong attraction results between protein molecules. This strong attraction does not allow them adequate time to orient themselves as they come together and. precipitates may form rather than crystals.[20]

The nucleation rate J can be calculated using $J = A \exp\left[-\Delta G_c / (k_BT)\right]$ where A is a pre-exponential constant[18] The main variables determining the nucleation rate J are interfacial energy, temperature and supersaturation. The nucleation rate J decreases as the value of ΔG_c increases. Therefore, values of ΔG_c may be used to gain insight into nucleation rates at different conditions even when A cannot be determined.

2.1.4 Phase Diagrams

Phase diagrams are plots of protein solubility or concentration against experimental variables, such as precipitant concentration, keeping other variables constant. Batch crystallization is used to develop phase diagrams.[17]
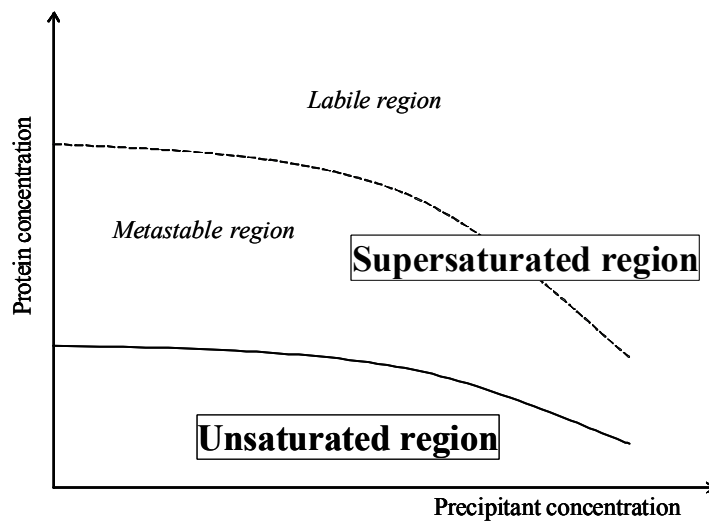
Figure 2-5: Protein phase diagram showing the different regions of supersaturation.(Adapted from McPherson, 2004[17])

Figure 2-5 shows the three main regions of a phase diagram: unsaturated, metastable and labile. Crystals dissolve in the unsaturated region. In the metastable region, stable nuclei grow but do not form spontaneously. In the labile region, stable nuclei form and grow spontaneously.

Crystals are formed by nucleation. Homogeneous nucleation results from a supersaturated solution while heterogeneous nucleation is crystal formation from

insoluble material such as seed crystals or dust. It is necessary to enter the labile region to grow nuclei spontaneously or homogeneously. However, amorphous precipitate forms in the upper part of the labile region. Even when no precipitate forms, an infinite number of microcrystals may form. The metastable region must be entered to obtain fewer, larger crystals. It is best to start in the lower part of the labile region where nuclei form spontaneously. As the nuclei grow, protein concentration decreases until the metastable region is entered and growth of fewer and larger crystals can occur.[11] In the present study, nucleation was induced from a clear solution, i.e. homogeneously.

2.1.5 Protein Crystallization Methods

The key to crystallizing proteins is lowering the energy barrier to nucleation or infusing energy into the system. The energy barrier may be lowered by addition of catalysts such as enzymes.[17] Energy may be added to a system by adding heat or by inducing supersaturation through seeding. There are a number of methods for inducing supersaturation including batch crystallization, vapor diffusion and dialysis. A list of common methods is shown in Table 2-2.

Batch crystallization is the oldest crystallization method presented in Table 2-2 and it has been in use for over 150 years. It is one of the most widely used techniques because of its simplicity and reliability upon optimization of crystallization conditions. It involves mixing of an unsaturated protein solution with a precipitating agent which creates supersaturation. Alternatively, supersaturation may be induced by changing the temperature. After a period of time ranging from hours to weeks, spontaneous nucleation

occurs. A major disadvantage of this method is that only one solution can be tested at a time. This difficulty can be overcome by setting up arrays of vessels each testing a different condition. A modification of this method involves microbatch crystallization under paraffin oil which is illustrated in Figure 2-6. The paraffin oil prevents evaporation while the microbatch set-up allows for high throughput screening of crystallization conditions requiring only microliter volumes of protein solutions.[21]

Table 2-2: Common crystallization methods [17]

1	Bulk crystallization
2	Batch crystallization
3	Evaporation
4	Bulk dialysis
5	Concentration dialysis
6	Microdialysis
7	Liquid bridge
8	Free interface diffusion
9	Vapor diffusion on plates (sitting drop)
10	Vapor diffusion in hanging drops
11	Sequential extraction
12	pH-induced crystallization
13	Temperature-induced crystallization
14	Crystallization by addition of precipitants

Paraffin oil **Protein solution**
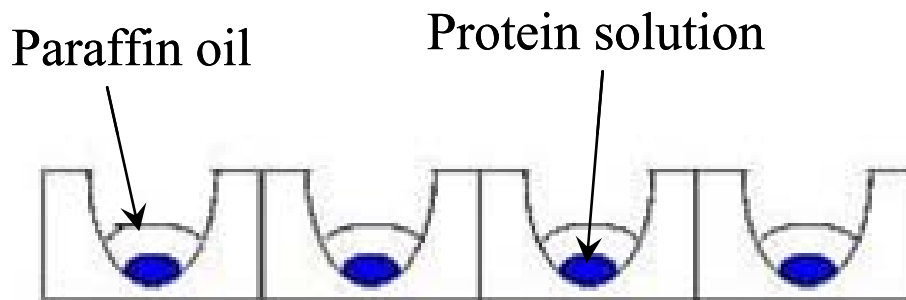
Figure 2-6: Illustration of microbatch crystallization under paraffin oil.
As little as 1 μL of protein solution may be required.
(Source: http://www-structmed.cimr.cam.ac.uk/Course/Crystals/Theory/methods.html)

Another commonly used method is vapor diffusion. It can be used to screen a large number of conditions and is both economic and convenient. There are two main ways in which vapor diffusion is carried out: hanging drop where a drop of the protein solution with precipitant is suspended from a surface, and sitting drop where the drop is supported by a surface. Hanging drop and sitting drop vapor diffusion are illustrated in Figure 2-7. Generally, the protein solution is first mixed with the additive such as precipitant. A drop of the mixture is placed in the headspace of a tightly closed chamber containing a large amount of the additive. The additive thus saturates the headspace and water diffuses from the drop into the headspace. This causes the concentration of protein and additive to increase continuously, allowing different concentrations to be examined in one experiment.[2] However, it is difficult to measure intermediate concentrations with this method. In addition, many variables are associated with this method including the contact angle of the drop, the volume of the drop and the distance between the drop and the reservoir.

Hanging drop   Sitting drop
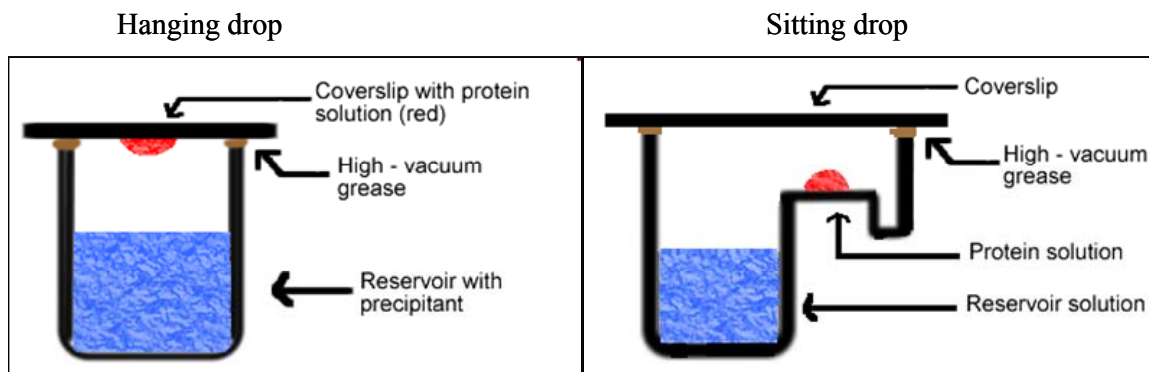
Figure 2-7: Schematic showing the two set-ups for vapor diffusion. The protein drop is suspended in hanging drop, but is placed on a pedestal for sitting drop.
(Source: http://www.bio.davidson.edu/courses/MolBio/MolStudents/spring2003/Kogoy/protein.html)

Multiwell microbatch crystallization was utilized in the present study. The microbatch apparatus used was developed by Bartling *et al.*[21] It consists of an automated stage which allowed timed image acquisition and online monitoring of the multiwell tray. A linear temperature gradient could be applied for temperature experiments. The microbatch apparatus will be further described in CHAPTER 3.

2.2 PROTEIN CRYSTALLIZATION AND THE SECOND VIRIAL COEFFICIENT

The second virial coefficient, B_{22}, is a thermodynamic property which is a measure of solute-solute and solute-solvent interactions in dilute solutions solutions.[6; 16] Studies have shown that a negative second virial coefficient corresponds to overall attractive interactions between solute molecules which could result in crystallization, precipitation or aggregation.[7] A positive second virial coefficient corresponds to repulsive interactions between solute molecules, resulting in the solute remaining in solution.[6; 7] When

21

repulsive and attractive interactions are equal, the solution is called a theta solvent and has a B_{22} value of zero.[6] This state is analogous to the Boyle temperature where real gases behave ideally and B_{22} is zero.[22]

George and Wilson studied crystallization of a number of proteins including lysozyme, bovine serum albumin and ovalbumin, and induced crystallization by addition of precipitants such as NaCl and polyethylene glycol 8000.[6] They found that values of B_{22} which correspond to crystallization lie within a narrow range of slightly negative values. They call this range of values from -1 x 10^{-4} to -8 x 10^{-4} mol mL g^{-2} the crystallization slot.[6]

Figure 2-8 is a schematic depicting the crystallization slot. Values greater than -1 x 10^{-4} mol mL g^{-2} were measured in solutions where no crystallization occurred while values less than -8 x 10^{-4} mol mL g^{-2} were measured in solutions where precipitation was observed. The crystallization slot was achieved for many different proteins under many different crystallization conditions including solvents containing alcohols, additives such as inorganic salts, various molecular weight polyethylene glycols, and mixtures of inorganic salts and alcohols.[5] Therefore it can be concluded that B_{22} can predict the occurrence of crystallization regardless of the driving force for crystallization.
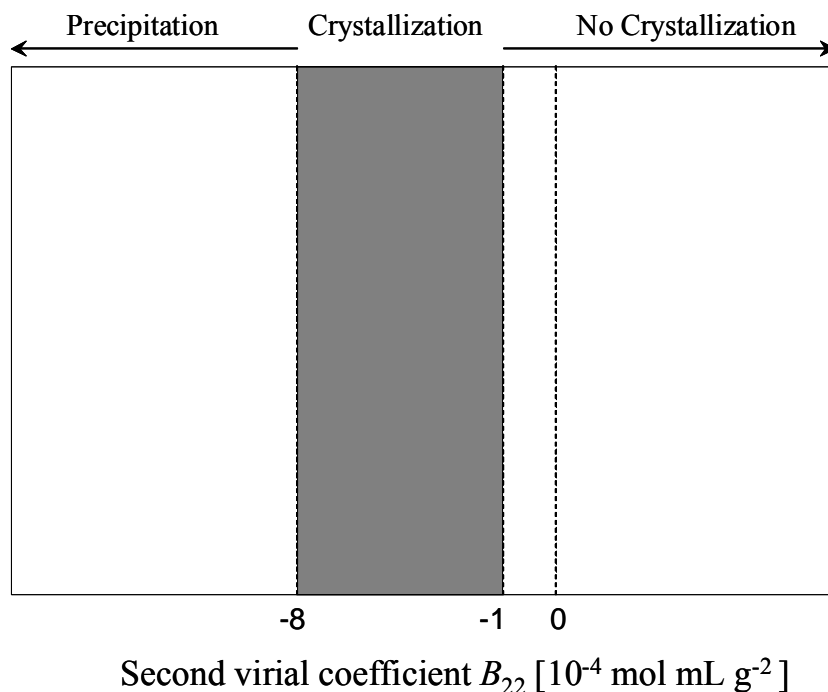
Figure 2-8: Protein crystallization slot
Schematic showing behavior of proteins in solution relative to the value of the second virial coefficient B_{22}. Crystallization occurs between -1 and -8 x 10^{-4} mol mL g^{-2}, a range of values referred to as the crystallization slot. More negative values of B_{22} are obtained under precipitating conditions while no crystallization or precipitation is observed at greater values of B_{22}.

Trial-and-error is often used to determine conditions suitable for crystal growth. [6] As shown in Table 2-1, there are over 20 different variables which can affect crystallization, including temperature, pH and protein purity and concentration. Therefore numerous screening experiments have to be carried out to determine conditions suitable for growing protein crystals.[16] Correlating the value of B_{22} to conditions conducive for crystallization eliminates the need for extensive screening experiments.[16] Bartling[10] successfully correlated the occurrence of crystallization of apoferritin in solutions containing $CdCl_2$ with the second virial coefficient of the solutions. In the present study,

attempts were made to replicate Bartling's results and correlate crystallization of human gamma D-crystallin to the value of the second virial coefficient.

2.2.1 Measurement of B_{22}

Static light scattering (SLS) is the method most commonly used to measure B_{22}. However, B_{22} has also been measured using small angle x-ray and neutron scattering, self-interaction chromatography, [23; 24; 25] size exclusion chromatography, [23; 26] sedimentation equilibrium, [27] and membrane osmometry.[7; 20; 23; 27] These methods all have difficulties associated with them. For example, membrane osmometry is unreliable as proteins adsorb onto membranes or block membrane pores.[7] Sedimentation is time-consuming and requires large amounts of protein which limits the number of solution conditions which can be studied. SLS is convenient because it is non-destructive and the protein sample can be recovered after the experiment. However, it also requires relatively large amounts of protein and in addition is very sensitive to aggregates in the solution, which may be impossible to avoid at very negative B_{22}.[7]

Protein cross interactions B_{23} have only been directly determined through the use of membrane osmometry.[7] However, for SLS and other methods, mixing rules can be applied to determine B_{23} of a mixture of two proteins in solution after measuring B_{22} of the individual pure protein solutions. Mixing rules can also be applied to mixtures of more than two proteins. The equation used in the present study for a binary mixture is shown below:[28]

$$B = \sum_i \sum_j y_i y_j B_{ij} \qquad\qquad 2\text{-}10$$

where y is the mole fraction of components i and j, B_{ij} are the virial coefficients and B is the second virial coefficient of the mixture which may be measured by any of the methods mentioned above. The mixing rule for a binary mixture was used in the present study to determine the cross second virial coefficient of a mixture of alpha A-crystallin and human gamma D-crystallin.

2.2.2 Static Light Scattering

The basic premise of static light scattering (SLS) is that it measures the scattering intensity of a protein in solution relative to background scattering.[29] If the size of the molecule is less than $\lambda/20$, where λ is the wavelength of the laser, then there is no angular dependence and all data can be collected at 90°.[6]

Data from static light scattering are interpreted using the Rayleigh equation shown below:

$$\frac{Kc}{R_{90}} = \frac{1}{M} + 2B_{22}c \qquad\qquad 2\text{-}11$$

where

$$K = \frac{4\pi^2 n_o^2 (dn/dc)^2}{N_A \lambda^4}$$

and c is the protein concentration, R_{90} is the excess Rayleigh ratio at 90°, M is the molecular weight of the protein, n_o is the solvent refractive index, (dn/dc) is the differential refractive index increment of the solvent containing the solute, N_A is Avogadro's number and λ is the wavelength of the laser.

A plot of Kc/R_{90} against c is called a Debye plot and its slope and intercept yield B_{22} and M respectively. Measurement of B_{22} of a theta solvent would result in a horizontal line. A non-crystallizing solvent would yield a sloped line above that of the theta solvent while a crystallizing or precipitating solution would yield a sloped line below the horizontal line as illustrated in Figure 2-9.
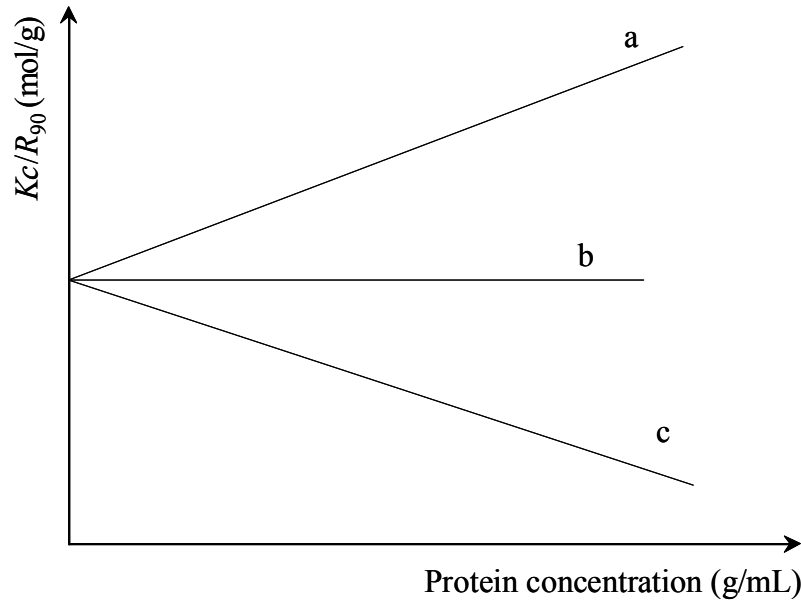
Figure 2-9: Schematic illustrating the different types of slope obtained from static light scattering corresponding to the value of the second virial coefficient B_{22} in three different solutions; (a) non-crystallizing (positive B_{22}). (b) Theta solvent i.e. $B_{22} = 0$. (c) Crystallizing or precipitating (negative B_{22})

2.3 THE CRYSTALLINS

The crystallins are structural water-soluble proteins found in the lens of the mammalian eye. Three classes of crystallins are found in mammalian lenses, namely alpha-, beta- and gamma-crystallins. They are the major proteins maintaining lens transparency and they represent up to 90% of the soluble lens protein.[30] The high refractive index of the lens is due to the high concentration of these proteins, up to 430 mg/mL,[31] and the absence of organelles from the lens fiber cells. Organelles may interfere with the lens' function by scattering light.[32] There is almost no protein turnover in the lens. Therefore, the proteins in the center of the lens are approximately the same age as the individual.[15] This also implies that the crystallins sustain substantial damage over time through post-biosynthetic modifications such as oxidation and deamidation.[15]

Alpha-crystallin makes up 40% of the soluble lens protein.[15] There are two alpha-crystallin genes, alpha A and alpha B. is Approximately 40 subunits of alpha A- and alpha B-crystallin make up the structure of alpha-crystallin, in a ratio of approximately 3:2.[15] Expression of alpha A-crystallin is limited to the lens. Alpha B-crystallin is systemically expressed but is found primarily in the eye lens. Both alpha A- and alpha B-crystallin belong to the small heat shock protein (sHSP) family.[33] In addition to being structural, both alpha-crystallin and its subunits exhibit chaperone-like activity by inhibiting aggregation and insolubilization of the crystallin proteins, including themselves, due to conditions of stress. Such stress may be generated by oxidation, elevated temperature and chemical reduction, for example.[34] Alpha-crystallin chaperones

proteins by incorporating them into large complexes thus preventing their nonspecific aggregation.[33]

Figure 2-10: 3-D structure of human beta B1-crystallin
(Source: http://www.ebi.ac.uk/pdbsum/1oki)

Figure 2-11: 3-D structure of human gamma S-crystallin
(Source: http://www.ebi.ac.uk/pdbsum/1ha4)

Like alpha-crystallin, beta-crystallin is a heterogeneous oligomeric protein whereas gamma-crystallin is a monomer.[35] Beta-crystallin has an average molecular weight of 200 kDa with subunits around 20 to 30 kDa, and gamma-crystallin has an average molecular weight of 20 kDa.[36] The beta and gamma subunits are structurally related.[37] The beta-crystallin subunits present in the human lens are βB1, βB2, βB3, βA1/A3, βA2,, and βA4.[38] The 3-D structure of human βB1-crystallin is shown in Figure 2-10.

There are seven gamma-crystallin genes (γA, γB, γC, γD, γE, γF, γS), the most abundant of which are γC and γD.[15; 39; 40] The first six, γA-F, are similar in sequence but the gamma S-crystallin gene is less similar in sequence and is situated on another chromosome.[15] The 3-D structure of human gamma S-crystallin is shown in Figure 2-11. Point mutations in the γC and γD genes have been linked to many genetic cataracts demonstrating the importance of these two proteins to lens transparency.[40] The relationship between the crystallins is illustrated in Figure 2-12.

Alpha A-Crystallin

Alpha-Crystallin

Alpha B-Crystallin

Beta B1-Crystallin

Beta B2-Crystallin

Beta B3-Crystallin

Crystallin

Beta-Crystallin

Beta A1/A3-Crystallin

Beta A2-Crystallin

Beta A4-Crystallin

Gamma A-Crystallin

Gamma B-Crystallin

Gamma C-Crystallin

Gamma-Crystallin

Gamma D-Crystallin

Gamma E-Crystallin

Gamma F-Crystallin

Gamma S-Crystallin
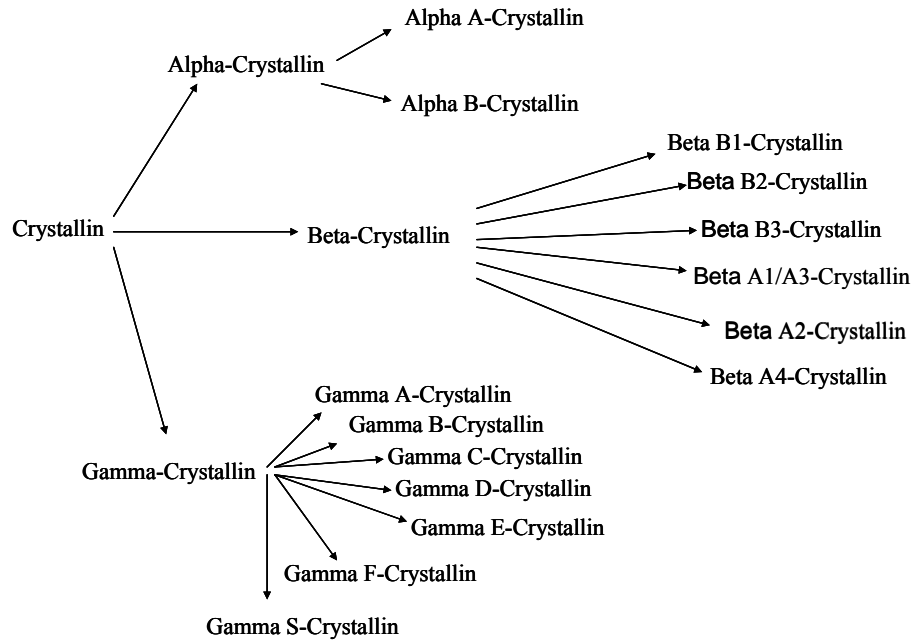
Figure 2-12: Schematic illustrating relationship between the crystallins.

2.4 APOFERRITIN

Ferritin is an iron-storage protein found in every tissue in the body as well as in most living organisms.[41] The structure of ferritin is shown in Figure 2-13. It comprises 24 polypeptide chains[42] which are arranged to form a hollow shell 7 to 8 nm wide within which up to 4500 iron ions can be stored as a complex with the protein.[42; 43] Ferritin has a molecular weight of approximately 456 kDa[44] and an outer diameter of 12 to 13 nm.[42] By taking up iron, ferritin plays a detoxification role as iron catalyzes the formation of reactive oxygen species which cause oxidative damage.[42] Iron-free ferritin is called apoferritin.[45]
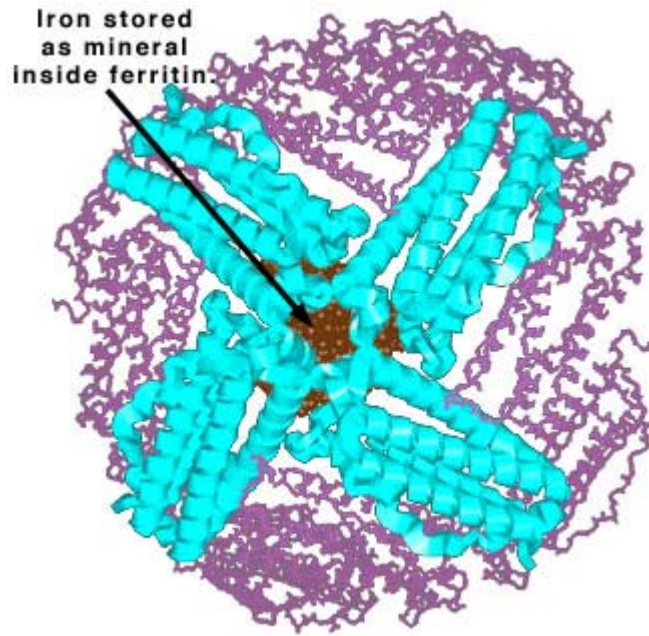
Figure 2-13: Structure of the ferritin complex
(Source: http://www.coe.drexel.edu/ret/personalsites/2005/Geisler/startframe.html)

In vertebrates, apoferritin is a hetero-oligomer of the heavy H-chain, which has 182 amino acids, and the light L-chain, which has 174 amino acids.[41] Apoferritin molecules found in different organs in the body contain different ratios of H-chain to L-chain.[42] Apoferritin rich in L-chains is most often found in organs that store iron, i.e. the liver and the spleen. The H-chain is thought to play a part in iron sequestration as overexpression of the H-chain leads to anemia.[41]

2.5 CATARACTS

Cataract disease affects the lens of the eye. Figure 2-14 illustrates the position of the lens relative to the other parts of the eye. Cataract disease is characterized by progressive loss

31

of lens transparency, accumulation of molecules that absorb in the UV-Vis range, and formation of fluid-filled vacuoles, especially in diabetics when sugar levels are high in the lens. [46] Elevated levels of divalent cations such as Ca^{2+}, Fe^{2+} and Cu^{2+} ions are also associated with cataract.[47]
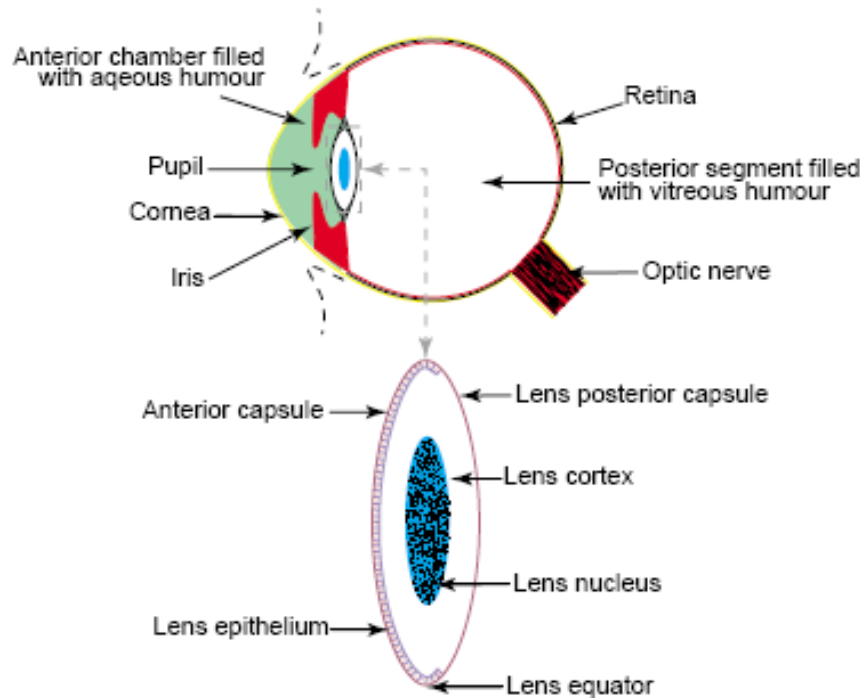
Figure 2-14: Structure of the eye showing location and structure of the lens. The lens comprises non-vascularized tissue that focuses images on the retina.[48]

Cataracts are the leading cause of blindness, affecting an estimated 16–20 million people worldwide.[15] Ageing is the major risk factor for cataract. Cataracts can also be caused by metabolic disturbances, trauma, drugs, smoking, heavy alcohol consumption and congenital disorders.[47] Systemic diseases such as diabetes can also be factor and Figure 2-15 shows the lens of a diabetic with advanced cataract.[15] Currently, the only cure for cataracts is surgical removal of the lens and replacement with a plastic

intraocular lens.[15] A slit is made in the side of the cornea and a probe is inserted to break up the cataractous lens and suction it out. An intraocular lens is implanted in its place. This process is illustrated in Figure 2-16. A better understanding of this disease may lead to development of non-invasive cures. The results from the present study increase understanding of the protein crystallization process, which can be applied to cataract formation and may lead to prevention or stagnation of cataract disease.
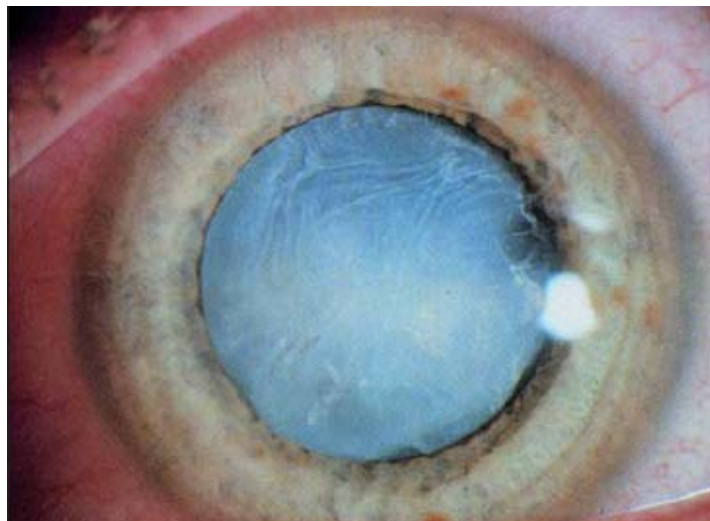
Figure 2-15: Advanced cataract in the lens of a diabetic patient.[32]

a   b
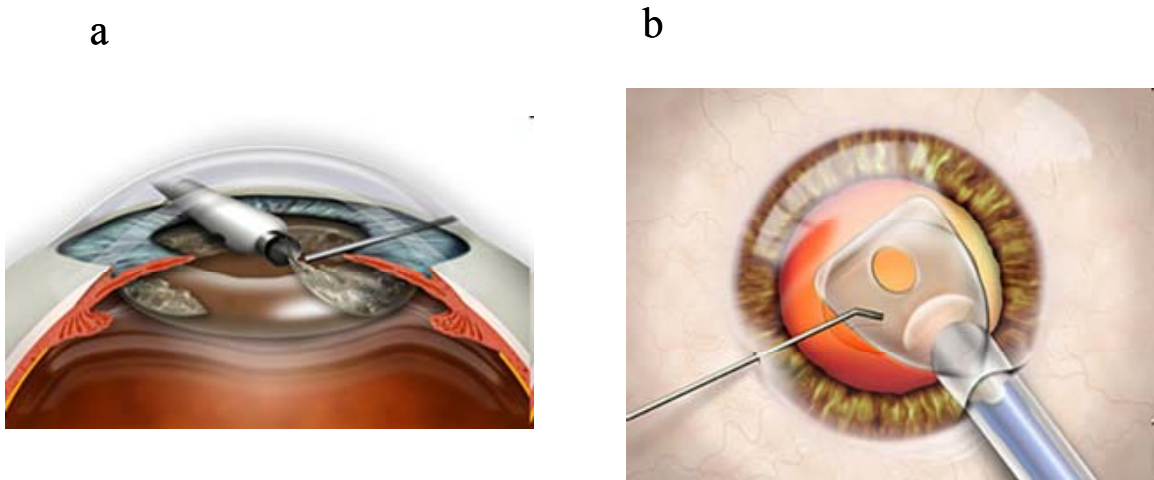
Figure 2-16: Surgical correction for cataract (a) A probe is inserted into the cornea to break up the cataractous lens and suction it out. (b) An artificial lens is implanted to replace the cataractous lens.
(Source: http://www.allaboutvision.com/conditions/cataract-surgery.htm)

2.6 THE ROLE OF CRYSTALLINS AND APOFERRITIN IN CATARACT FORMATION

Modification of the crystallins, either through mutations, post-biosynthetic modifications such as oxidative stress and thermal stress, occurs with time.[14; 47] Since there is no turnover of lens proteins, the damage from modifications tends to accumulate leading to altered interaction between the crystallins or leading to them unfolding.[15] The modifications often result in reduced crystallin solubility in the form of aggregation, precipitation or crystallization of crystallins, which in turn leads to occurrence of cataract.[15; 48; 49; 50] Protein crystals or precipitates with molecular masses above 50 MDa diffract light and hence interfere with vision[15; 51] as illustrated in Figure 2-17.
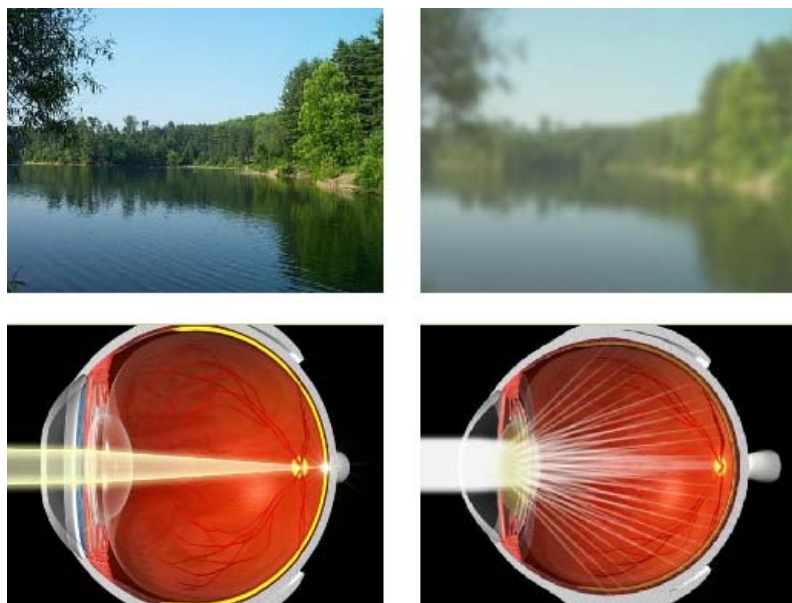
Figure 2-17: Transmission of light by the lens.
Transmission through a normal lens (left) and diffusion of light by a lens with cataract (right) resulting in unfocused vision. (Source: http://www.harvardeye.com/cataract/cataracts.html)

Human beta-crystallin remains soluble even with extensive modification.[15] However, gamma-crystallin has been linked to cataracts which are caused by mutations but the differences between the wildtype and the mutant proteins are usually small. Point mutations in gamma C- and gamma D-crystallin are the genetic basis for many dominant cataracts.[40] For instance, the R58H mutation in human gamma D-crystallin (HGD) causes the aculeiform cataract. The mutation results in crystallization of the mutant protein which is an order of magnitude less soluble than the wildtype protein.[49] Crystal deposits of HGD have been identified in the lenses of individuals with coralliform cataracts.[52] The 3-D structure of human gamma D-crystallin is shown in Figure 2-18.

Figure 2-18: 3-D structure of human gamma D-crystallin
(Source: http://www.ebi.ac.uk/pdbsum/1hk0)

The lenses of young mammals exhibit cold cataract in which the center of the lens becomes opaque when cooled but rapidly clarifies when warmed. Large amounts of gamma-crystallin have been linked to cold cataract as gamma-crystallin has long been known to undergo reversible cryoprecipitation.[14; 53]

Post-biosynthetic modifications of alpha-crystallin have been shown to compromise its chaperone function, resulting in the formation of light-scattering aggregates of lens proteins which proceed to form cataracts. The lens UV-filter 3-hydroxykynurenine readily catalyzes the oxidation of methionine residues in both alpha A- and alpha B-crystallin, making the overall alpha-crystallin molecule a poorer chaperone and contributing to cataract.[54]

Mutations in the beta B3-crystallin gene have been associated with recessive genetic cataracts. A mutation in the beta A3/beta A1-crystallin coding gene causes a dominant cataract in mice.[37]

UV-A causes oxidative damage to the crystallins which leads to cataractogenesis. Antioxidants present in the lens include catalase, peroxidase, glutathione and ascorbic acid. Levels and activity of these antioxidants decrease with age while oxidative stress increases, making the lens more vulnerable to cataracts.[46] The eyes are more susceptible to UV damage with age as the number of UV filters in the lenses decreases linearly with age.[55]

Studies show that treatment of patients with hyperbaric oxygen (HBO) leads to subsequent cataract formation. It has been suggested that high concentrations of oxygen in the tissues leads to corresponding levels of tissue H_2O_2. Very low levels of oxygen are present in the lens with a steep gradient from the exterior of the lens to its center. It may be that the increased liquefaction of the vitreous humor with age enables more retinal oxygen to diffuse into the lens thus contributing to cataract.[47]
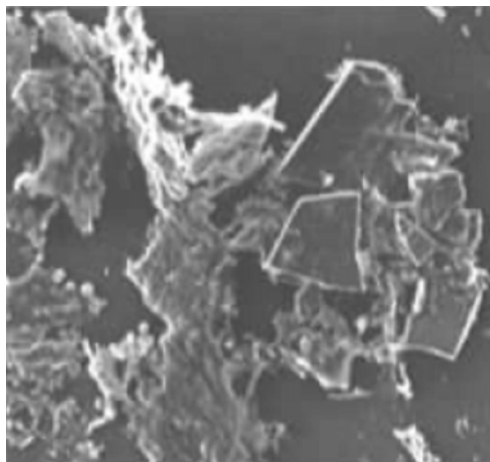
Figure 2-19: Gamma-crystallin crystals deposits found in lens fiber removed from patient suffering from congenital cataract[52]

Unlike the other crystallins, gamma-crystallins have attractive interactions between them both in the lens and *in vitro*.[13; 53] These attractive interactions increase the likelihood of gamma-crystallin undergoing phase separation and aggregation, thus leading to cataract formation.[13] Figure 2-19 shows crystals of gamma-crystallin extracted from the lens of a patient suffering from coralliform cataract caused by mutations in the gamma D-crystallin gene.[52] Non-genetic forms of cataract involving crystal formation in the lens have also been reported.[13] Since gamma D-crystallin has been linked to many cataracts, it was used for crystallization experiments in the present study.

Apoferritin has been implicated in the development of Hereditary Hyperferritinemia Cataract Syndrome (HHCS), which is inherited, and characterized by early onset of cataract.[41] HHCS is thought to occur as a result of a mutation in the L-chain which leads to overexpression of the L-chain. This overexpression may affect the antioxidant properties of the lens as well as the solubility of the other proteins in the lens.[41] Crystals of L-rich ferritin have been found in lenses of HHCS patients.[56] L-rich ferritin complexes with few, if any, iron ions, making it similar to apoferritin. For this reason, apoferritin was used by Bartling *et al.*[10] in investigations into the effect of $CdCl_2$ on crystallization of ferritin in HHCS.

2.7 THE ROLE OF DIVALENT CATIONS IN CATARACT

Divalent cations play important roles in metabolic processes in the body. For instance, Ca^{2+} is required for activation of Calpain 2, an enzyme found in the lens and involved

with signal transduction.[48] The concentrations of divalent cations, including Ca^{2+}, Ba^{2+}, Cd^{2+}, Cu^{2+}, Pb^{2+} and Zn^{2+}, have been shown to increase in cataractous lenses.[3; 48] Table 2-3 shows concentrations of various divalent cations in normal and cataractous lenses.[3] It can be seen that the concentration of Cd^{2+} is approximately 20 times higher in cataractous lenses. One study evaluated the impact of a 5-week oral Pb^{2+} (~30μg/dL) exposure on the alpha A-crystallin profile in the lens of Fisher 344 rats. It was found that exposure to Pb^{2+} led to the crystallins undergoing post-biosynthetic modifications leading to lens opacities.[30] Injection of frogs with $BaCl_2$ and $CaCl_2$ resulted in formation of cataracts in the lenses of the frogs.[57] Studies have shown that divalent cations cause increased attractive interactions between proteins in solution unlike monovalent cations which increase repulsion between protein molecules.[58] Divalent cations were used in the present study to induce crystallization.

Apoferritin is normally crystallized by addition of cadmium ions.[59] Previous crystallization studies were conducted by Bartling[9] and Bartling *et al.*[10; 44] with apoferritin in solutions containing $CdCl_2$. Bartling discovered that crystallization was successfully induced at concentrations of $CdCl_2$ above 13 mM. At higher $CdCl_2$ concentration, the final size of crystals obtained was smaller.

Table 2-3: Divalent cation concentrations in lenses (From Cekic, 1998[3]). Concentrations (ppm) of Cadmium, Copper, Lead and Calcium in cataractous and normal lenses grouped according to different smoking habits. [3; 60]

Lenses	Concentration (µg/g dry tissue weight = ppm)			
Cataractous	Cd^{2+}	Cu^{2+}	Pb^{2+}	Ca^{2+}
Overall	0.99	2.11	5.17	82.31
Males	1.05	2.13	5.00	80.36
Females	0.88	2.04	5.53	86.83
1−10 cigarettes/day	1.01			
> 20 cigarettes/day	1.19			
Non−smokers	0.79			
Normal				
Overall	0.045	0.69	0	15.11
Males	0.055	0.66	0	15.18
Females	0.032	0.72	0	15.01

2.8 POTENTIAL FOR DEVELOPMENT OF THERAPUETIC DRUGS

At present, the only way to cure cataract is to surgically remove the lens and replace it with a plastic intraocular lens.[36; 48] Administration of antioxidant cocktails helps in slowing down age-related cataract according to the Roche European American Cataract Trial (REACT).[46] A recent study found that supplementation of the antioxidant lutein in patients with age-related cataract led to improvement in visual function. Natural sources of antioxidants include green and black tea, *gingko biloba* (which contains EGb761), tumeric (contains curcumin) and *Withania somnifera*.[46]

Alpha A- and alpha B-crystallin have been shown to increase the solubility of the mutant T5P gamma C-crystallin both in vitro and in transfected cells, as well as to significantly reduce the size of its aggregates. It has previously been shown that the alpha-crystallins interact with both the beta- and gamma-crystallins, assisting in their

refolding and preventing their aggregation.[40] Understanding how cataracts are formed on the molecular level may provide a means to prevent them or treat them without surgery.

The alpha A-crystallin null mouse suffers from cataract caused by inclusion bodies containing alpha B-crystallin as well as gamma-crystallin. This implies that alpha A-crystallin plays a part in maintaining solubility of gamma-crystallin.[15] Alpha A-crystallin has been shown to prevent non-specific aggregation of proteins by incorporating them into large complexes.[40] It may therefore prevent the occurrence of crystallization of HGD. Solubilizers are known to increase hydration of proteins resulting in increased protein solubility and possibly preventing crystal formation. Non-detergent sulfobetaine 201 (NDSB-201) has been shown to act as a solubilizer in protein solutions.[61] As such, the solubilizing effects of alpha A-crystallin are compared with the effect of NDSB-201.

Solubilizers are molecules which increase the solubility of proteins by causing them to become preferentially hydrated. Alpha-crystallin behaves like a solubilizer when it carries out its chaperoning activities. Solubilizers are useful in separating proteins from inclusion bodies or biological membranes during protein purification. Examples of solubilizers include urea, non-detergent sulfobetaines (NDSBs), detergents and salts.[61] A study on NDSBs showed that they prevent protein aggregation and precipitation at low ionic strengths without denaturing proteins.[61; 62] The structure of NDSB-201 is illustrated in Figure 2-20. Detergents attach their hydrophilic tails to the hydrophobic regions of the protein and thus allow the hydrophilic part of the protein to interact with water, increasing the solubility of the protein. Sucrose has also been reported to maintain protein

41

solubility under harsh conditions.[62] The use of solubilizers may suppress crystallization and thus may lead to prevention of cataract disease.
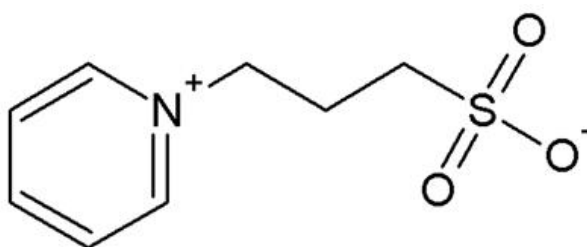
Figure 2-20: Structure of NDSB-201 showing oppositely charged ends of a carbon bridge
(Source: http://www.gbiosciences.com/NDSB_201-desc.aspx)
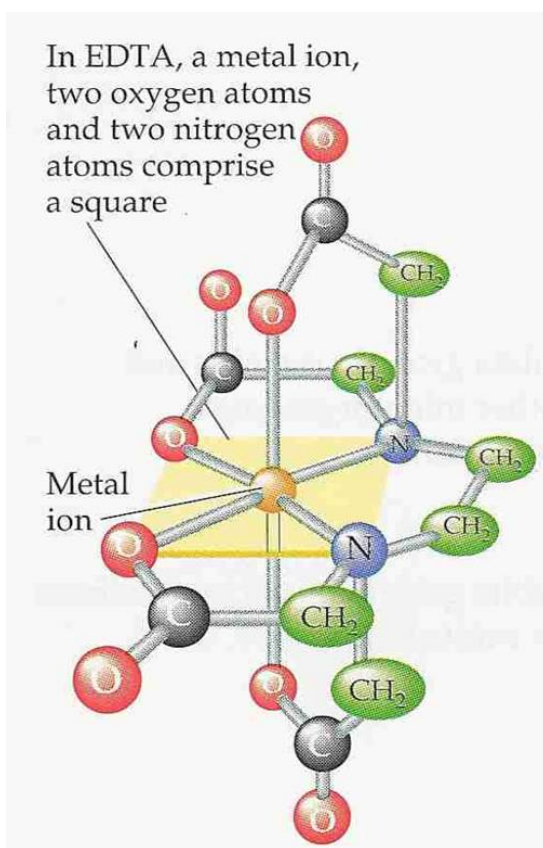
Figure 2-21: Schematic of EDTA chelating a metal ion.
(Source: http://www.benbest.com/nutrceut/EDTA.html)

Chelating agents such as ethylenediaminetetraacetic acid (EDTA) form multiple bonds with metal ions thus inactivating them. Figure 2-21 shows EDTA chelating a metal ion. Injection of chelating agents into dogs and rabbits resulted in retinal detachment and blindness.[63] This may be because divalent cations are essential for functioning of the body. Lower concentrations of chelating agents may suppress crystallization brought about by high concentrations of divalent cations. In the present study, the solubilizing effects of NDSB-201 and alpha A-crystallin were investigated.

CHAPTER 3: METHODOLOGY

3.1 EXPRESSION AND ISOLATION OF PROTEINS

3.1.1 Gamma D-Crystallin

Commercially available human gamma D-crystallin (HGD) and alpha A-crystallin are costly. For instance, the cost of alpha A-crystallin from Sigma Aldrich (St. Louis, MO) is $400 for 1 mg. Approximately 50 mg of each protein is needed per experiment making commercial purchase impractical. As a result, these proteins were obtained by expression using *Escherichia coli* clones obtained from the Petrash Lab at Washington University in St. Louis, MO. The protocol described below for expression of HGD using *Escherichia coli* was developed by the Petrash Lab at Washington University in St. Louis.[64; 65; 66]

Over-expression of HGD was achieved in *Escherichia coli* strain BL21-DE3. Approximately 10 batches of HGD were produced over the course of the present study. For each batch, four cultures of 400 mL each were grown in 2 liter baffled shaker flasks. Isopropyl-1-thio-beta-D-galactopyranoside (IPTG) at a final concentration of 0.1 mM was added to each flask to induce expression of HGD at an OD_{600} of approximately 0.8 and cultures were grown for another 2.5 to 4 hours. Cells were collected by centrifugation (10,000 x g, 15 minutes, 4°C) and the cell pellets frozen at −80°C for at least 12 hours and up to a week. The freeze-thaw process aided in breaking open the bacterial cell walls.

Extraction of proteins from the cell pellet was done using 10 μg/mL DNase (Fisher Scientific, Pittsburgh, PA), an N-lysis buffer (50 mM Tris Cl pH = 7.5, 0.3 M NaCl, 0.5 EDTA) and 0.05 mg/mL lysozyme (Sigma-Aldrich Co., St. Louis, MO). DNase degrades the DNA of the bacteria, making the solution containing the pellets less viscous. The purpose of the lysozyme was to break down bacterial cell walls.[67] The solution produced from the extraction process is called the whole cell lysate (WCL).

Dialysis was carried out next to exchange the N-lysis buffer for chromatography buffer (20 mM tris-acetate buffer, pH 6.0, 0.5 mM dithiothreitol and 0.5 mM ethylenediaminetetraacetic acid) in preparation for ion exchange chromatography. Buffer exchange of the WCL was achieved using dialysis bags with a molecular weight cutoff (MWCO) of 12 − 14 kDa (Fisher Scientific, Pittsburgh, PA). Dialysis of the WCL was done against 2 L of cold chromatography buffer in a cold room. The solution in the beaker was stirred to reduce the time required for the WCL and the chromatography buffer in the beaker to reach equilibrium. After equilibrium was achieved, approximately 3 hours later, the dialysis bag was transferred to a beaker with a fresh solution of chromatography buffer. After 2 more hours, the dialysis bags were moved to another beaker of fresh solution and left for 12 hours. This process resulted in the formation of a white precipitate, mostly composed of lysozyme,[64] which was removed by centrifugation (10,000 x g, 15 minutes, 4°C). The supernatant contained HGD and other proteins expressed by the bacteria.
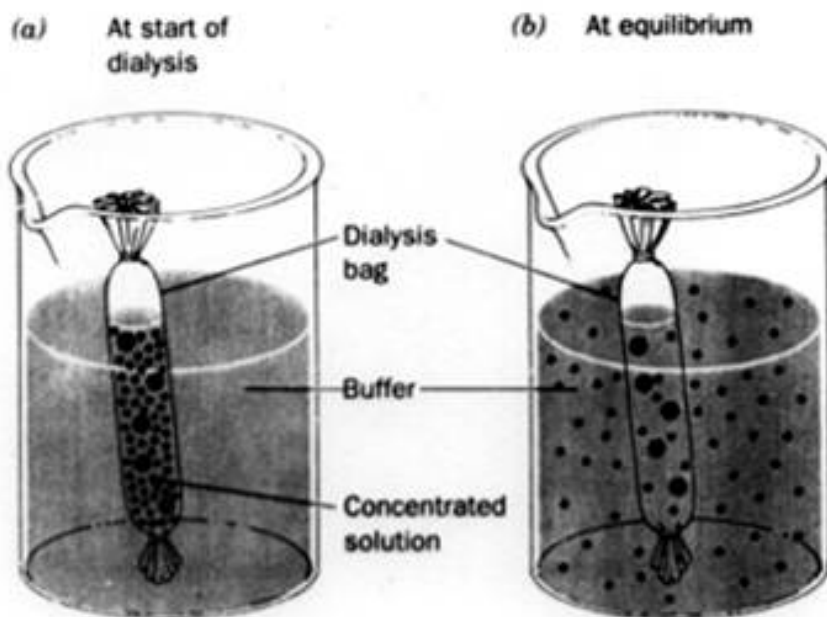
Figure 3-1: Illustration of buffer exchange via dialysis.
At equilibrium, the concentration of salts from the buffers is the same in the dialysis bag and in the beaker. The bag must be transferred to a beaker with fresh buffer for further buffer exchange to take place. (Source: http://www.bio.mtu.edu/campbell/bl482/lectures/lec5/482w52.htm)

Cation exchange chromatography was carried out next to separate HGD from the other proteins expressed by the bacteria. The chromatography buffer consisted of 20 mM tris-acetate buffer (pH 6.0) to which 0.5 mM dithiothreitol (DTT) and 0.5 mM ethylenediaminetetraacetic acid (EDTA) were added. DTT prevents thiol-mediated aggregation while EDTA protects the protein from metalloproteases. The amount of protein in the supernatant was determined by total protein assay using Bradford reagent (Pierce Biotechnology, Rockford, IL). The supernatant was manually applied with a syringe to a Macro-Prep S cation exchange column (BioRad Laboratories, Hercules, CA) shielded from ambient light and already equilibrated with chromatography buffer at 1 ml/min. Enough protein was loaded to put 80% of the maximum column loading. A wash was applied to remove unadsorbed material and the bound protein was eluted using 5

46

column volumes (CV) of 6% v/v Na acetate in the chromatography buffer. A flowchart of the manual chromatography process is outlined in Figure 3-2. After the protein was eluted from the column, residual protein was removed with 5 CV of 1 M Na acetate in chromatography buffer followed by 5 CV of pure chromatography buffer. The process was repeated until all the protein was purified. Five CV of 30% v/v ethanol were run over the column and the column was stored at 4°C.

Measure whole cell lysate protein concentration with Bradford reagent

Rinse column with 5 column volumes (CV) of 100% salt buffer

Equilibrate with 5CV no-salt buffer

Load enough sample to put 80% of max loading

Re-equilibrate with 5CV no-salt buffer

Run salt gradient with 6% salt (~5CV)

Rinse column with 5CV 100% salt buffer

Equilibrate with 5CV no-salt buffer

Wash column with 5CV of 30% ethanol. Store in 30% ethanol in refrigerator

Figure 3-2: Flowchart of the manual cation exchange chromatography process

Sodium dodecyl sulfate – polyacrylamide gel electrophoresis (SDS-PAGE) was used to detect the presence of HGD in the elution fractions by comparing migration rates

47

with a molecular weight standard. This involves denaturing proteins with sodium dodecyl sulfate (SDS), which also binds strongly to the proteins, giving them a negative charge, and running the proteins through a gel.[12] Separation is only based on size and is done by applying an electric current across the gel as shown in Figure 3-3. Larger molecules move more slowly through the gel. A mixture of known polypeptides is used as the molecular weight standard. The purity of a protein can also be assessed. When a protein sample is purified by SDS-PAGE, all the proteins in the sample separate according to size only. The different proteins appear as separate "bands" in the gel. More than one protein band implies that impurities, or unwanted proteins, are present.
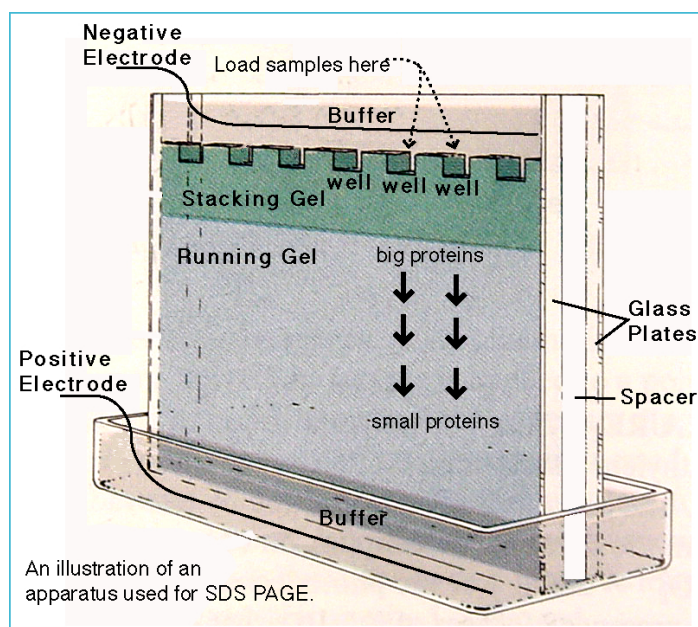
Figure 3-3: Schematic of SDS-PAGE apparatus showing how an electric current is applied across a gel to cause migration of proteins. SDS binds to the proteins giving them a negative charge so movement results in separation based on size alone. Larger molecules move more slowly through the gel.
(Source: http://web.chemistry.gatech.edu/~williams/bCourse_Information/4581/techniques/gel_elect/page_protein.html)

In the present study, Nupage Novex 10% Bis-Tris gels (Invitrogen, Carlsbad, CA) were utilized for SDS-PAGE. Figure 3-4 shows a gel obtained after purification of HGD. Lane 2 shows the whole cell lysate which has many proteins expressed by the *E. coli* clones including HGD at 20 kDa. The other proteins represent impurities for HGD.
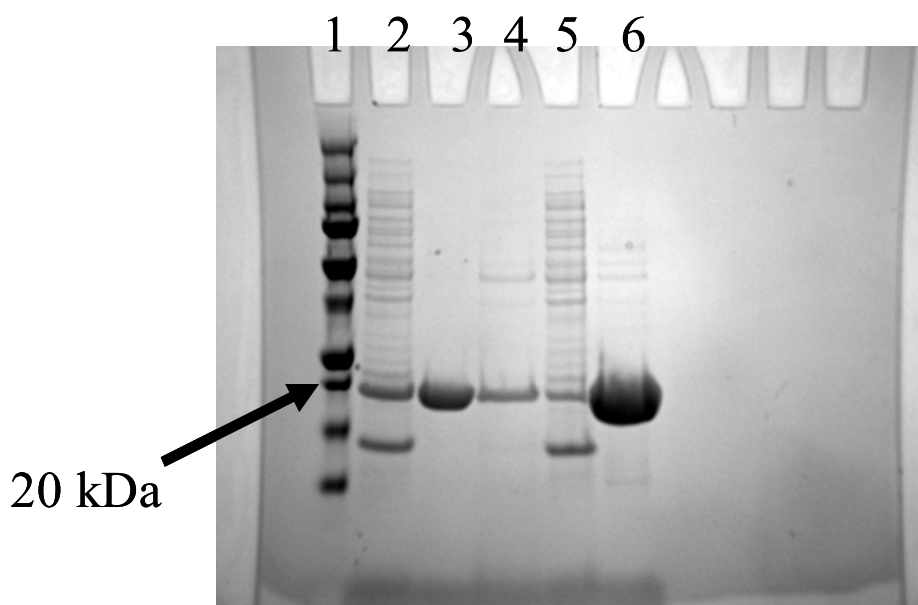
Figure 3-4: SDS-PAGE gel of HGD obtained after ion exchange chromatography.
Lane 1: Molecular weight standard containing proteins of different molecular weights; Lane 2: whole cell lysate or unpurified protein; Lane 3: HGD eluted by 6% v/v Na acetate in chromatography buffer; Lane 4: residual protein eluted with 1 M Na acetate in chromatography buffer; Lane 5: protein which did not bind to the column when the whole cell lysate was run over it ; Lane 6: concentrated HGD (from 6% v/v Na acetate in chromatography buffer)

HGD was concentrated using Microcon and Centricon centrifugal filter units with a 10 kDa membrane cutoff (Millipore, Billerica, MA). In preparation for crystallization experiments, HGD was dialyzed into 100 mM phosphate buffer (pH 7.4, 10 mM DTT) or 50 mM tris-HCl (pH 7.4, 150 mM NaCl, 10 mM NaN_3 and 10 mM DTT) using 10 kDa MWCO dialysis cassettes (Pierce Biotechnology, Rockford, IL). Figure 3-5 shows how

the dialysis cassettes are loaded with a syringe. The cassette is then immersed in buffer and kept afloat by a buoy. After dialysis, the protein was stored at −80°C until needed for crystallization or light scattering experiments.
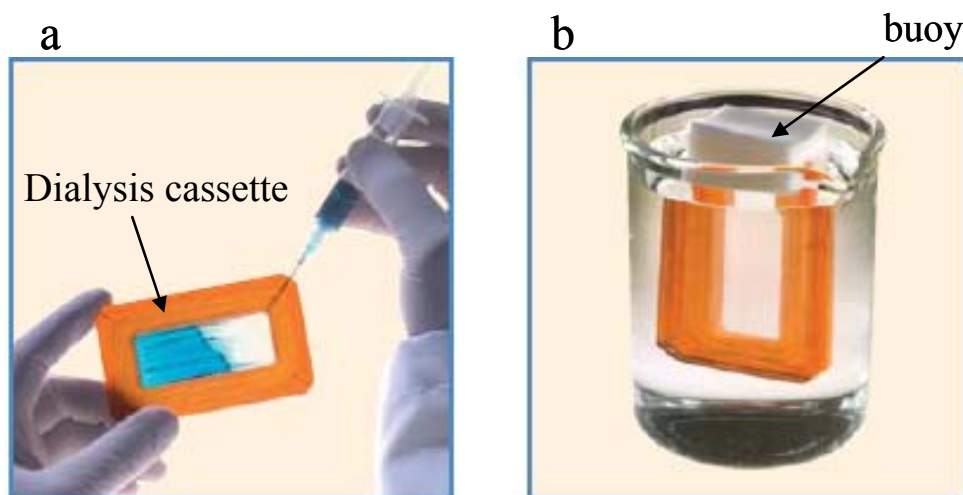
Figure 3-5: Buffer exchange using dialysis cassettes (a) Dialysis cassette is loaded with a syringe (b) The cassette is kept afloat in the beaker of buffer by a buoy .
(Source: http://www.piercenet.com/Objects/View.cfm?Type=Page&ID=B76E5F7B-B7C3-4BED-92B4-7BB8F6EF9D5E)

3.1.2 Apoferritin

The protocol described here for apoferritin was developed by Bartling *et al*.[10; 44] Size exclusion chromatography - high performance liquid chromatography (SEC-HPLC) was used to prepare apoferritin for crystallization and light scattering experiments. Horse spleen apoferritin (Sigma-Aldrich Co., St. Louis, MO) was dialyzed at 4°C overnight into 50 mM Tris-HCl buffer (pH 7.4 with 150 mM NaCl and 10 mM NaN_3) using dialysis cassettes with a 10 kDa molecular weight cutoff (Pierce Biotechnology, Rockford, IL). Preparative SEC-HPLC was then carried out to separate apoferritin monomers from

oligomers and subunits. A HiPrep 16/60 Sephacryl S-300 High Resolution column (Amersham Biosciences, Piscataway, NJ) was utilized for this separation with 50 mM Tris-HCl buffer (pH 7.4 with 150 mM NaCl and 10 mM NaN_3) as the mobile phase at a flow-rate of 0.5 mL/min.

SEC-HPLC was carried out using a CM4000 LDC analytical pump, an SCL-10A VP Shimadzu system controller, and an SPD-10AV Shimadzu detector at a wavelength of 280 nm (Shimadzu Scientific Instruments, Columbia, MD). The chromatogram was recorded using CLASS-VP 7.2.1 software (Shimadzu Scientific Instruments, Columbia, MD).

3.1.3 Material Preparation

Stock solutions of NDSB-201 (EMD, Gibbstown, NJ), $BaCl_2$ (Sigma-Aldrich Co., St. Louis, MO) and $CaCl_2$ (Sigma-Aldrich Co., St. Louis, MO) were prepared by dissolving the appropriate amount in 50 mM tris-HCl buffer (pH 7.4, 10 mM NaN_3). Appropriate amounts of cadmium chloride (MP Biomedicals, Solon, OH) were dissolved in ultrapure HPLC-grade water (Alfa Aesar, Ward Hill, MA) to prepare stock solutions. Human alpha A-crystallin was purchased from ProSpec (Rehovot, Israel) and used as received in 20 mM Tris-HCl buffer (pH 7.5).

Protein solutions were prepared by first mixing buffer and stock protein solution and then adding the appropriate metal chloride to obtain the final desired concentration of both protein and metal chloride. Fresh solutions were prepared for each experiment and

used immediately. All protein and buffer solutions were filtered through a 0.2 μm Whatman filter (VWR International, West Chester, PA) prior to mixing.

3.2 CRYSTALLIZATION

3.2.1 Crystallization Apparatus

Crystallization experiments were carried out using a multi-well plate and the set-up shown in Figure 3-6. The apparatus was developed by Bartling *et al.*[21] The set-up comprises a multi-well plate mounted on a thermal gradient plate which in turn sits on an insulation plate. All three rest on the automated stage of a microscope which is used to view the individual wells. There are water channels on either side of the thermal gradient plate attached to a heating and cooling water bath to create a temperature gradient along the x-axis of the multi-well plate. The temperature gradient was found to be linear in the present study and in a study by Bartling *et al.*[21] In other experiments, solution conditions were varied on an isothermal plate. The other factor varied along the x-axis was concentration of divalent cation. In both isothermal and non-isothermal experiments, protein concentration was varied along the y-axis.

x

y

A

B

C

A: Multi-well plate
B: Thermal Gradient Plate
C: Insulation Plate

Automated Stage

TOP WORK
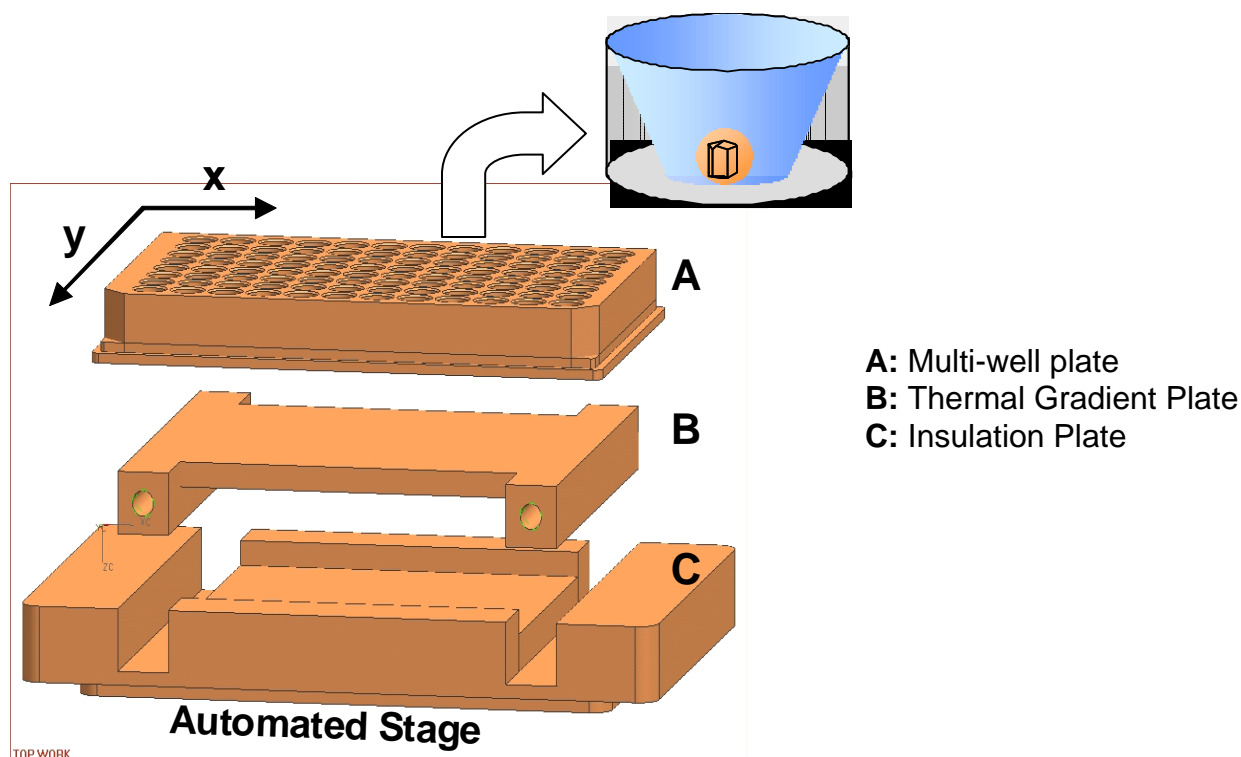
Figure 3-6: Crystallization setup showing an isolated well from the multi-well plate.[21]

To carry out crystallization, paraffin oil was pipetted into each well in the multi-well plate and then the protein solution was pipetted under the oil to prevent evaporation of the aqueous phase and hence false results. This process is called microbatch crystallization under oil.[21] This method was useful because small amounts of protein, 4 μL of protein solution per well, were needed. The microbatch multiwell setup was also a high-throughput method and as such allowed for many different conditions to be tested on one multiwell plate.[21] Batch crystallization was chosen because this is the method by which crystallization occurs in the lens during cataract formation.

The complete crystallization apparatus is shown in Figure-3-7. The multi-well plate sits on the stage of the microscope. The microscope is attached to a digital camera

which is in turn connected to a computer. Through a macro program on the computer, images are taken of each well at regular time intervals. The microscope is housed in a Plexiglas box for uniform temperature control.
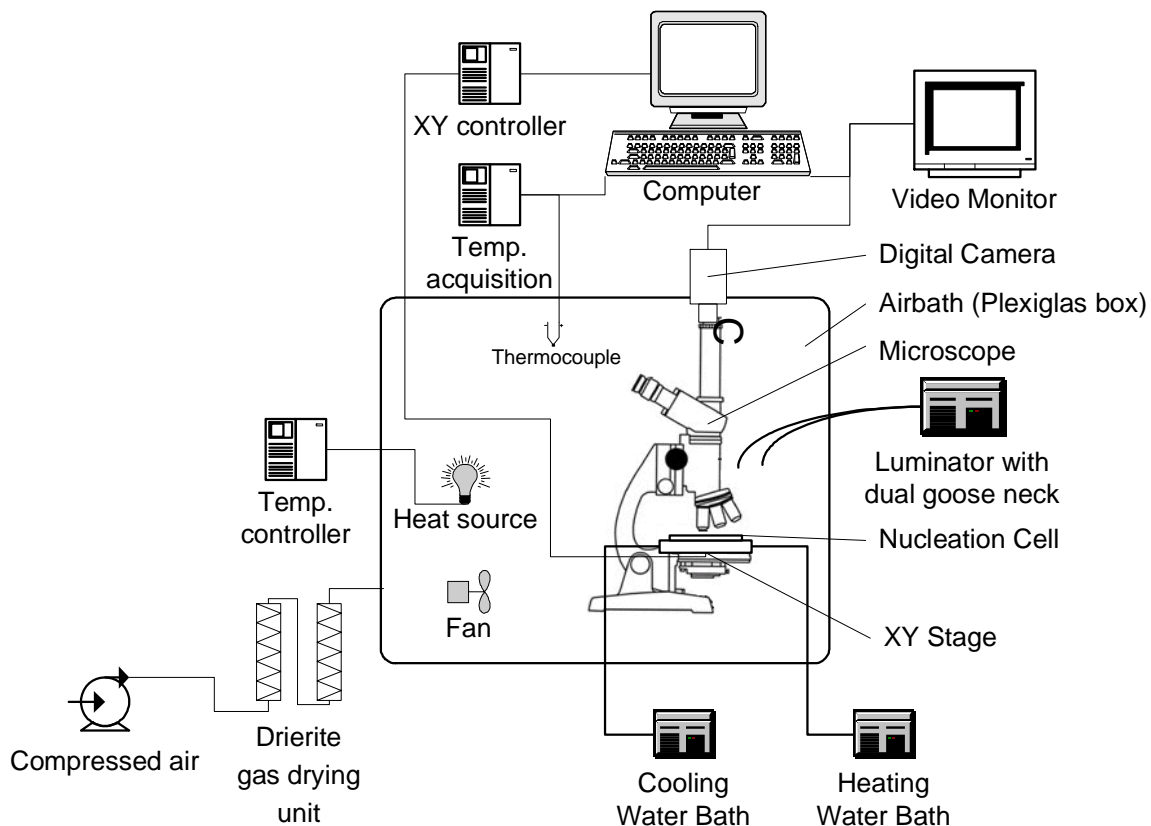
Figure-3-7: Crystallization apparatus[21]

3.2.2 Determination of Phase Diagrams

The solubility of proteins was determined in some cases by measuring the concentration of the supernatant in equilibrium with crystals grown for at least 3 weeks. In other cases,

the microbatch multi-well system described by Bartling[21] was used. A crystallization grid was set up as shown in Figure 3-8 with protein concentration varied along the vertical axis and precipitant concentration varied along the horizontal axis. Each well had a unique concentration of protein and divalent cation. After approximately 4 weeks, crystals were obtained in the shaded region though crystals did not grow in every well. Crystals not growing in every well in the shaded region may be attributed to different rates of crystal growth in each well since nucleation is stochastic.

Each of the conditions where crystals were obtained was noted on a graph of protein concentration against temperature or precipitant temperature. The solubility line was formed by joining the wells on the outer boundary of the region with crystals as illustrated in Figure 3-8.
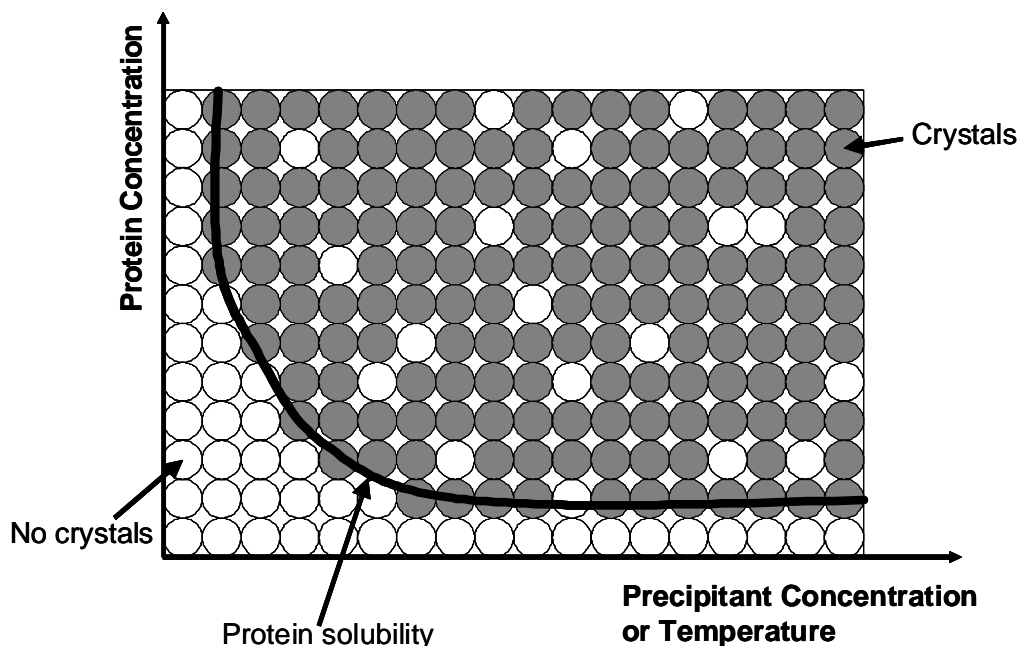
Figure 3-8: Multiwell microbatch set-up used to determine protein phase diagrams. Crystals were obtained in ~ 50% of the wells in the shaded region. The solubility curve is drawn to the boundary between the region where crystals were observed and the region where no crystals were observed.

3.3 LIGHT SCATTERING

3.3.1 Static Light Scattering

Data from static light scattering were interpreted using the Rayleigh equation shown below:

$$\frac{Kc}{R_{90}} = \frac{1}{M} + 2B_{22}c \qquad \text{3-1}$$

where

$$K = \frac{4\pi^2 n_o^2 (dn/dc)^2}{N_A \lambda^4} \qquad \text{3-2}$$

and c is the protein concentration, R_{90} is the excess Rayleigh ratio at 90°, M is the molecular weight of the protein, n_o is the solvent refractive index, (dn/dc) is the refractive index increment, which is how the refractive index of a solution varies with concentration, N_A is Avogadro's number and λ is the wavelength of the laser.[6] The second virial coefficient can be obtained from the slope of the plot of (Kc/R_{90}) against c.
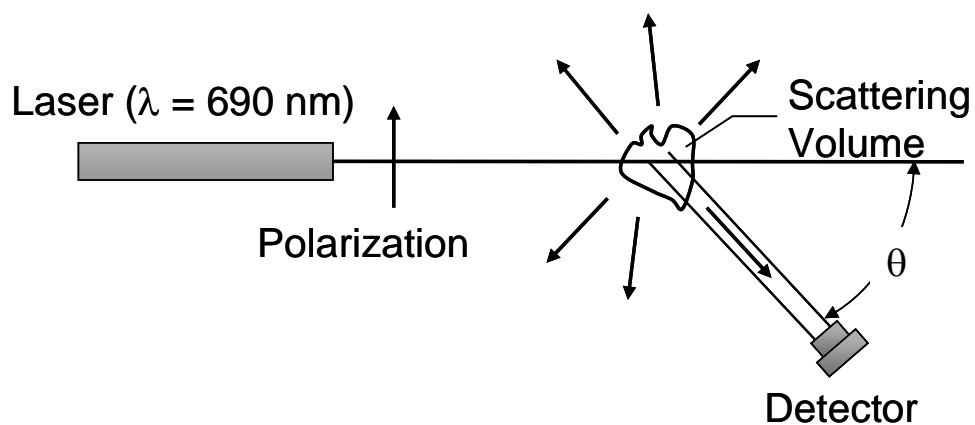
Figure 3-9: Static light scattering apparatus[10]

Data from static light scattering are represented as a Debye plot. Light scattering intensity is obtained at one scattering angle, 90°, as a function of different concentrations of the protein as shown in Figure 3-10. The slope of the plot gives the second virial coefficient while the average molecular weight is obtained from the intercept using Equation 3-1.
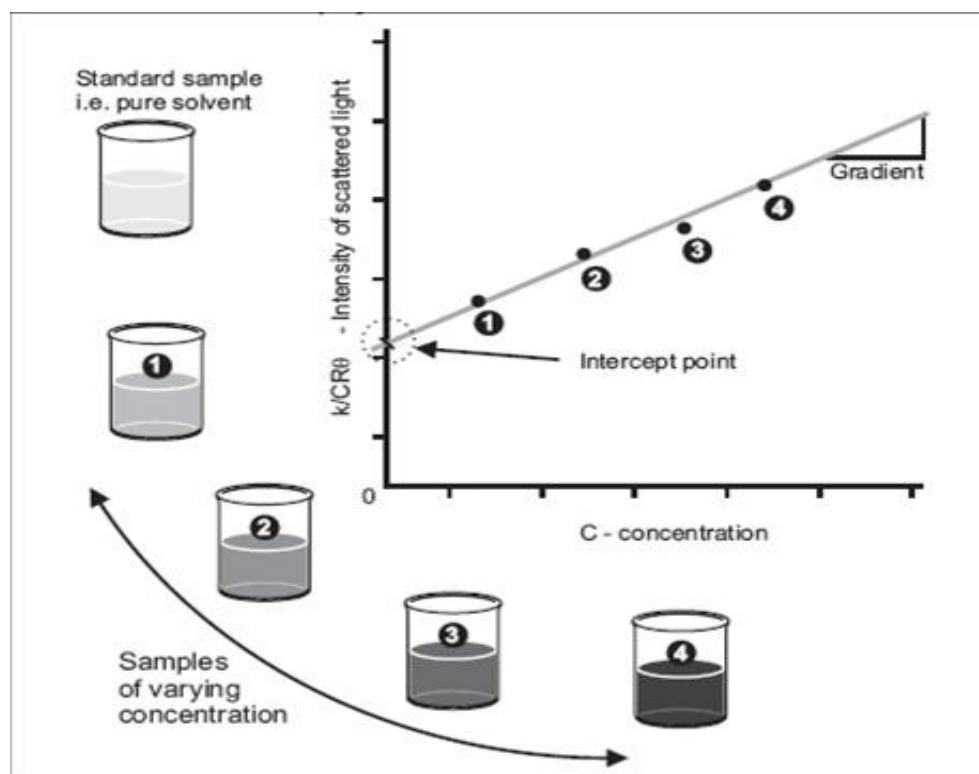
Figure-3-10: Debye plot showing how the MW is obtained from the intercept and the second virial coefficient from the slope. Four or more different protein concentrations are used and background scattering is determined using the pure buffer.
(Source: http://www.nbtc.cornell.edu/facilities/downloads/Zetasizer%20chapter%2015.pdf)

The light scattering system consisted of an ALV 5000/E/EPP instrument, an ALV/LSE-5004 digital correlator and ALV-60X0 4.0 software (ALV, Langen, Germany). A 22 mW laser (632.80 nm) served as the light source. Samples were placed in 2.5 mL cylindrical glass cuvettes (ALV, Langen, Germany) and capped. Three 10-second measurements were taken at each angle with no more than 5% deviation between the measurements. For rapidly aggregating solutions, the deviation was increased to 10%.

Five different protein concentrations were utilized for static light scattering: 0.1, 0.2, 0.3, 0.4 and 0.5 mg/mL. The stock protein solution was first diluted with buffer and finally the stock divalent cation solution was added to the protein and the mixture was

gently vortexed. Measurements were taken immediately thereafter. All protein, buffer and cation solutions were filtered through a 0.2 μm Whatman filter (VWR International, West Chester, PA) prior to mixing.

3.3.2 Dynamic Light Scattering

Dynamic light scattering (DLS) makes use of the same laser set-up as SLS. Protein molecules scatter the laser light in all directions. Since the laser is coherent and monochromatic, and the molecules are undergoing Brownian motion, the scattering intensity exhibits a time-dependent fluctuation.[68] Whereas SLS averages out fluctuations, DLS makes use of deviations from the average scattering intensity to evaluate the diffusion coefficient.

An autocorrelation function can be derived from this fluctuation. From Adel at al, we can see that the autocorrelation function *G(t)* is related to the delay time, i.e. the time scale of movement of the scattering molecules, as follows:[69]

$$G(t) = A\exp\left(-2\frac{t}{\tau}\right) + B \qquad\qquad 3\text{-}3$$

where *A* is a system-specific constant, τ is delay time and *B* is the baseline. The apparent diffusion coefficient *D* is related to the delay time by

$$D = \frac{1}{q^2 \tau}$$

3-4

with the scattering wave vector q defined by

$$q = \frac{4\pi n}{\lambda} \sin \frac{\theta}{2}$$

3-5

where n is the refractive index of the solvent, θ is the scattering angle, and λ is the wavelength of the laser. Once the diffusion coefficient is obtained, the hydrodynamic radius of the aggregates can be determined from the Stokes-Einstein equation.

$$R_h = \frac{k_B T}{6\pi \eta_o D}$$

3-6

where k_B is the Boltzmann constant, T is absolute temperature, η_o is the solvent viscosity and R_h is the hydrodynamic radius. The diffusion coefficient is related to the diffusivity slope k_D as follows:[70]

$$D = D_{p,o}(1 + k_D c)$$

3-7

where D is the collective diffusion coefficient, $D_{p,o}$ is the diffusion coefficient at infinite dilution, and c is protein concentration. A plot of D against c yields $D_{p,o}$ as the intercept and k_D can be obtained from the slope.

Buffer and protein were first mixed and the divalent cation was added last to obtain the final desired concentration of both protein and divalent cation. The mixture was gently vortexed and then placed inside the ALV 5000/E/EPP instrument (ALV, Langen, Germany). The samples were kept in the machine for the full duration of the experiment. The hydrodynamic radius of the particles in solution was obtained from the third cumulant of a computer-generated Cumulant analysis.

CHAPTER 4: EVALUATING CRYSTALLIZATION THERMODYNAMICS OF GAMMA D-CRYSTALLIN

4.1 ABSTRACT

Crystallization of human gamma D-crystallin (HGD), a lens protein, has been linked to the occurrence of cataracts. Crystallization of HGD was carried out using a microbatch grid over a temperature range from 300 K to 305 K to determine HGD concentrations suitable for tracking crystal growth over time. The results from this study were then used to determine the solubility of HGD, and hence the thermodynamic crystallization properties of HGD, over this temperature range. It was observed that the solubility of HGD increased with increasing temperature, and the dependence on temperature was used to estimate the enthalpy of crystallization as −455 kJ/mol, while the Gibbs free energy of crystallization ranged from −34.9 kJ/mol to −31.1 kJ/mol. Over a temperature range from 301 K to 304 K, the entropy of crystallization was determined to decrease from −1398 J/mol-K to −1394 J/mol-K which disfavors crystallization. Therefore the large negative enthalpy compensates for the loss of entropy determined over the temperature range studied allowing crystallization to occur. The entropy loss was attributed to trapping of ~55 water molecules per HGD molecule in the crystal structure.

The solubility of HGD in the presence of $CaCl_2$ and $BaCl_2$ was also determined and found to decrease with increasing salt concentration. This can be explained by increased attraction of Ca^{2+} and Ba^{2+} for water molecules at higher concentrations of

BaCl$_2$ and CaCl$_2$, resulting in decreased HGD solubility. The results from the present study advance knowledge of the factors needed to control crystallization of HGD in solutions with divalent cations and at different temperatures.

4.2 INTRODUCTION

Cataract disease is characterized by a progressive loss of lens transparency. Left untreated, it may result in complete blindness. In fact, it is the leading cause of blindness worldwide[9] with approximately 10 million new cases diagnosed every year.[3] At present, the only cure for cataracts is removal of the lens and replacement with a plastic lens. The majority of cataract patients are unable to afford this surgery, making it even more imperative that the link between crystallization of lens proteins and cataract formation be better understood.[48]

The crystallins are a family of lens proteins that make up 90% of all proteins in the lens.[35] They are water-soluble and are responsible for the structure and transparency of the lens.[49; 71] Three types of crystallins can be found in the human lens: namely, alpha-crystallin, beta-crystallin and gamma-crystallin. There are seven different proteins within the gamma-crystallin family: γA-, γB-, γC-, γD-, γE-, γF- and γS-crystallin.[72] Though γC- and γD-crystallin are the most abundantly expressed of the gamma-crystallins in the human lens,[40] human gamma D-crystallin (HGD) has been linked to numerous cataracts including punctate and aculeiform cataract.[73] Also, x-ray scattering and osmotic pressure studies show that the gamma-crystallins have attractive interactions in solution and tend

63

to exist as aggregates *in vitro* while the other crystallins have repulsive interactions in solution.[13; 53]

Many factors have been linked to cataracts including age, smoking and diseases like diabetes.[32] The temperature in the eye decreases with age, which may result in decreased solubility of the lens proteins. In diabetes, sorbitol, a metabolized form of glucose, is present in very high concentrations throughout the body and therefore reduces the solubility of lens protein by drawing water from the lens by osmosis.[74]

Elevated concentrations of divalent cations such as Ba^{2+}, Ca^{2+} and Cd^{2+} have also been found in cataractous lenses.[75; 76] For example, one study found that the concentration of Cd^{2+} is increased 20-fold in cataractous lenses.[3] These cations are found naturally in the lens and play various roles in the metabolism of the eye.[32; 63] The mechanisms that result in elevated concentrations of divalent cations are not well-understood, although it is thought that cigarettes and alcohol are a possible source.[3] All these factors may culminate in cataracts forming and are aggravated by the fact that there is no protein turnover in the lens.[71]

In the present study, the effects of temperature and the precipitants $BaCl_2$ and $CaCl_2$ on crystallization of HGD were examined. The thermodynamics of crystallization of HGD were determined as a function of temperature. Determining the conditions conducive for crystallization of HGD may provide a means to control or prevent crystallization of this protein. The results from the present study provide information that may be used to prevent conditions conducive for cataracts and other protein condensation diseases.

4.3 MATERIALS AND METHODS

4.3.1 Solution Preparation

HGD was expressed using recombinant *E. coli* BL21-DE3 clones obtained from the Petrash Lab at Washington University in St. Louis, MO using the method described by Andley *et al.*[64] After purification, buffer exchange into either 100 mM phosphate buffer (pH 7.4, 10 mM dithiothreitol (DTT), 10 mM NaN$_3$) for the linear growth rate experiment and determination of the temperature phase diagram, or 50 mM tris-HCl buffer (pH 7.4 with 150 mM NaCl, 10 mM NaN$_3$ and 10 mM DTT) for determination of the precipitant phase diagrams was accomplished either by dialysis using a 10 kDa MWCO dialysis cassette (Pierce Biotechnology, Rockford, IL) or via centrifugation with a 10 kDa MWCO Centricon centrifugal filter unit (Millipore, Billerica, MA). HGD was then concentrated via centrifugation with the Centricon centrifugal filter unit (Millipore, Billerica, MA) and stored at -80°C until use.

Protein concentration was determined by total protein assay using Bradford reagent (Pierce Biotechnology, Rockford, IL). Ultrapure HPLC-grade water (Alfa Aesar, Ward Hill, MA) was used for all buffers. All solutions were filtered through a 0.2μm Whatman filter (VWR International, West Chester, PA) prior to use.

Stock solutions of $CaCl_2$ (Sigma-Aldrich Co., St. Louis, MO) and $BaCl_2$ (Sigma-Aldrich Co., St. Louis, MO) were prepared by dissolving the appropriate amounts in 50 mM Tris-HCl buffer (pH 7.4).

4.3.2 Crystallization Experiments

Linear growth rates of crystals of HGD at different concentrations were determined by preparing 1-mL solutions of pure HGD in 100 mM phosphate buffer (pH 7.4, 10 mM DTT, 10 mM NaN_3) in Eppendorf tubes (Fisher Scientific, Pittsburgh, PA) and allowing crystals to grow for a week at 298 ± 0.43 K. Three concentrations were used, 10, 20 and 30 mg/mL, and four solutions were prepared for each concentration. The solutions were left undisturbed for one week to facilitate growth of crystals to a measurable size. Measurements were then taken approximately every 24 hours for 4 days. To measure crystal size, approximately 20 μL of each solution was pipetted onto a micro slide (Corning Glass Works, Corning, NY), covered with a micro cover (VWR International, West Chester, PA) and the remainder of the solution was discarded. The 20 μL samples were taken from the near the bottom of the Eppendorf solution in every case. A Meiji Techno (Santa Clara, CA) video-microscope was utilized for polarized light microscopy (PLM) and images of crystals were taken with a DKC-5000 digital camera (Sony Electronics, San Diego, CA). Crystal length measurements were taken with Image-Pro Plus 4.0 (Media Cybernetics, Silver Spring, MD). Photomicrographs were taken of each crystal in the 20 μL drop as follows: successive frames containing crystals were photographed until each crystal in the drop had been photographed. The length of the

longest side of each crystal in the drop was measured using optical microscopy and averaged for each solution. A single set of experiments was performed to determine the linear growth rates.

For determination of phase diagrams of HGD, 50 mM tris-HCl buffer (pH 7.4 with 150 mM NaCl and 10 mM NaN$_3$) and the multi-well micro batch crystallization set-up described by Bartling et al.[21] were used. Crystallization was carried out under paraffin oil (Hampton, Aliso Viejo, CA) to prevent evaporation and condensation of solvent, and oxidation of the protein in solution. A crystallization grid was set up as shown in Figure 4-1 with protein concentration varied along the vertical axis and precipitant concentration or temperature varied along the horizontal axis. For determination of precipitant phase diagrams, each well had a unique concentration of protein and divalent cation whereas for the temperature phase diagram, identical protein solutions were used for each well in a row. After approximately 4 weeks, crystals were observed in the shaded region in about 50% of the wells. Each of these points was noted on a graph of protein concentration against temperature or precipitant concentration, and the wells on the outer boundary between the region with crystals and the region with no crystals formed the solubility relationship as shown in the qualitative schematic in Figure 4-1. The outermost wells in the region containing crystals form the solubility curve. The closer a well is to the solubility line, the closer the initial protein concentration approaches the protein concentration in equilibrium with the crystals. In the wells in the region where crystals did not form, the final protein concentration is reasonably assumed to be equal to the initial protein concentration. While it is obvious that solutions where crystals formed were supersaturated, it cannot be said for certain that solutions with no crystals were not

supersaturated. It was assumed that there is a high probability that the area above the curve represents supersaturated conditions. Similarly, it was assumed that below the curve, it was still possible that supersaturated conditions may have existed although the probability was much lower than for the area above the curve.

It should be noted that the microbatch method was not used for linear growth experiments because of occasional equipment failure upon heating of the plate, and the small size of the crystals obtained when the equipment did work. In addition, the low concentrations and low volumes used resulted in small crystals being obtained. This made it difficult to use the microbatch method to track crystal lengths in the linear growth experiment. Therefore, Eppendorf tubes were used to determine linear growth rates as described in the beginning of this section.
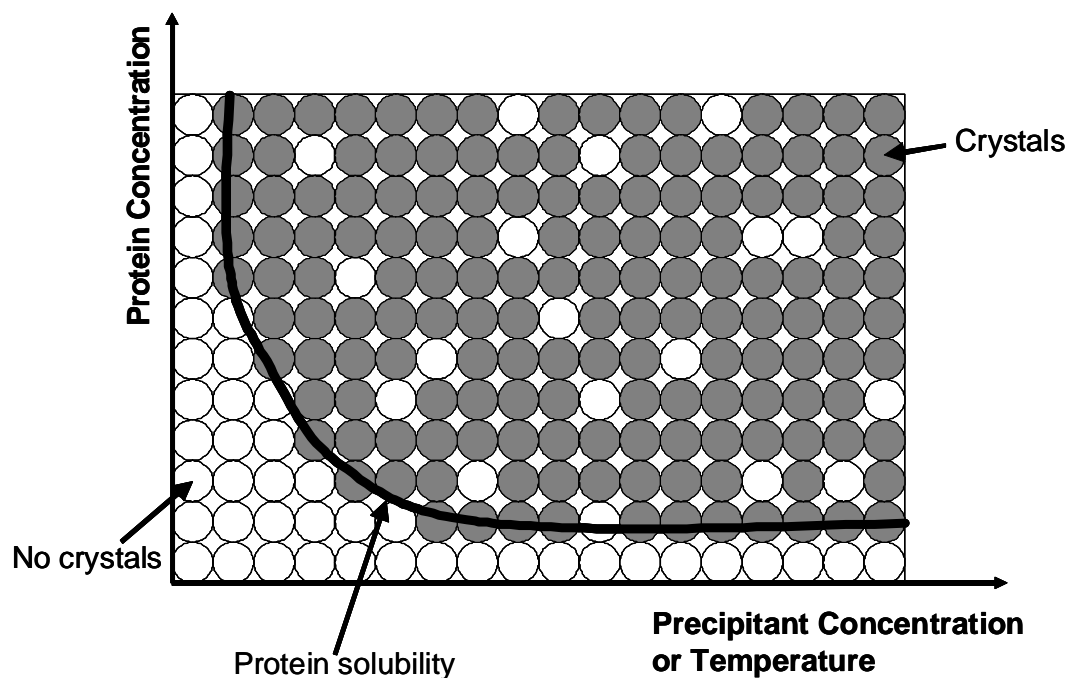
Figure 4-1: Multiwell microbatch set-up used to determine protein phase diagrams. Crystals were obtained in ~ 50% of the wells in the shaded region. The solubility curve is drawn to the boundary between the region where crystals were observed and the region where no crystals were observed.

4.4 RESULTS AND DISCUSSION

4.4.1 Linear Growth Rates

For three different initial concentrations of HGD, 10, 20 and 30 mg/mL, the length of the longest side of all crystals observed was tracked over time at 298 K. Initially, these experiments were designed to see if crystal growth would occur, and to compare crystal sizes under the conditions studied. They were not designed to characterize the crystal growth kinetics of HGD. However, since information on crystal sizes was obtained, approximate crystal growth rates were determined. A single experiment was used to determine linear growth rates of HGD at the three concentrations. Crystals were obtained at all concentrations of HGD and appeared to be tetragonal, which is consistent with findings from previous studies.[77] A schematic of the tetragonal crystal structure is shown in Figure 4-2 (left). Two of the three sides are of the same length, and all axes are perpendicular to each other. A photomicrograph of an actual crystal of HGD grown in phosphate buffer containing 20 mg/mL of HGD at 25°C is also shown in Figure 4-2 (right).
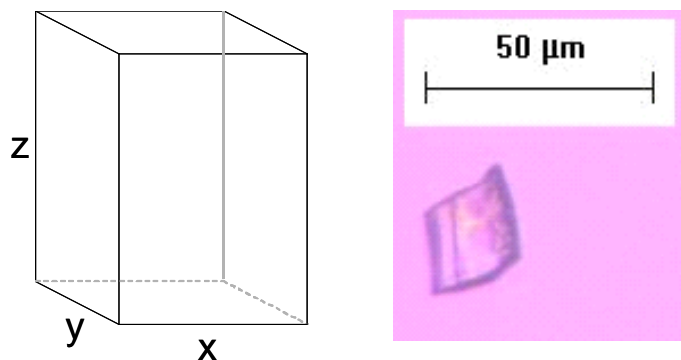
Figure 4-2: Sketch of a tetragonal crystal (adapted from Mullin[18]) along with a photomicrograph of an actual crystal of HGD grown at 25°C in phosphate buffer containing 20 mg/mL of HGD. The schematic shows that two sides of the crystal are the same length i.e. $x = y \neq z$, and all axes are mutually perpendicular. The crystal in the photomicrograph is not perfectly tetragonal and this may be a result of impurities in the solution.

As explained in the Section 4.3.2, four solutions were prepared in Eppendorf tubes for each concentration and one sample from each tube was examined at one time point only. A 20-µL sample was extracted from the solution in the Eppendorf tube and examined for crystals under an optical microscope. Each solution was used only once and discarded after use. The number of crystals observed in each 20-µL sample ranged from 5 to 24 and the longest side of each crystal was measured. As nucleation is stochastic, nucleation rates can vary for solutions with identical conditions, resulting in variation in the number of crystals obtained in each solution, and thereby affecting sizes of resulting crystals. No crystals were obtained in control experiments carried out with phosphate buffer containing no HGD.

Photomicrographs of crystals obtained at 10, 20 and 30 mg/mL HGD at different times are shown in Figure 4-3, Figure 4-4 and Figure 4-5 respectively. The crystals shown represent a sample of all the crystals obtained under the specific solution conditions. Irregularities in the crystal shapes may be attributed to the crystal growing

70

environment (Eppendorf tubes) and incorporation of impurities into the crystal. Some of the crystals shown in Figure 4-4 c appear to be more rod-shaped than tetragonal although the reason for this is not clear.

The purpose of the photomicrographs was to examine the average size of crystals obtained. As explained in SECTION 4.3.2, a 20 µL drop was extracted from each sample and examined under a microscope. Either a 10X or a 20X magnification was used in order to get photomicrographs that were as sharp as possible. Photomicrographs were taken of all crystals in the drop in successive frames until the entire drop had been examined. It can be seen in Figure 4-3, Figure 4-4 and Figure 4-5 that the size of crystals in the 10 mg/mL, 20 mg/mL and 30 mg/mL HGD solutions was approximately the same in all three solutions for the duration of the experiment. Figure 4-6 shows a plot of the length of crystals obtained as a function of time with four data points for each initial concentration. The error bars, which represent standard deviations from the average crystal length, show that there is no statistical difference between the crystal lengths at all three concentrations and at all time points. The number of crystals obtained for each sample at each time point are shown in Table 4-1 along with the mean size and the standard deviation of the crystals. Using the TTEST function in Excel, the p values was determined to be 0.22 for the 10 mg/mL and 20 mg/mL data sets, 0.17 between the 10 mg/mL and 30 mg/mL data sets, and 0.31 between the 20 mg/mL and 30 mg/mL data sets. Since the p values are all ≥ 0.17, there is indeed no statistical difference between the data.

Table 4-1: The number of crystals in 20-µL drops obtained at each time point for each concentration of HGD

Concentration (mg/mL)	Time (h)	Number of Crystals	Mean Crystal Size (µm)	Standard Deviation
10	161	5	19.35	3.13
	185	12	18.97	4.81
	210	24	19.86	8.06
	236	24	22.34	8.85
20	161	13	19.02	1.54
	185	19	21.40	7.72
	210	21	23.16	8.06
	236	16	24.82	12.00
30	161	8	15.19	4.74
	185	24	24.01	13.73
	210	19	23.43	9.10
	236	9	22.26	7.48
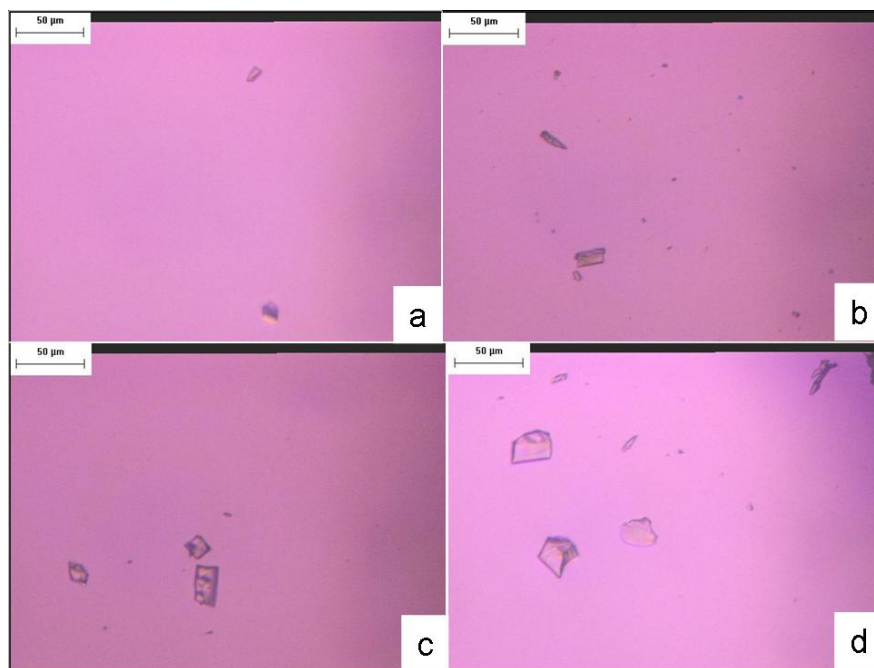
Figure 4-3: Photomicrographs of crystals in samples from the 10 mg/mL HGD solution taken at different times. The size of crystals increased with time. The crystals in the photomicrographs represent the typical size of crystals obtained in each of the solutions. Crystals are shown after (a) 161 hours (b) 185 hours (c) 210 hours (d) 236 hours.
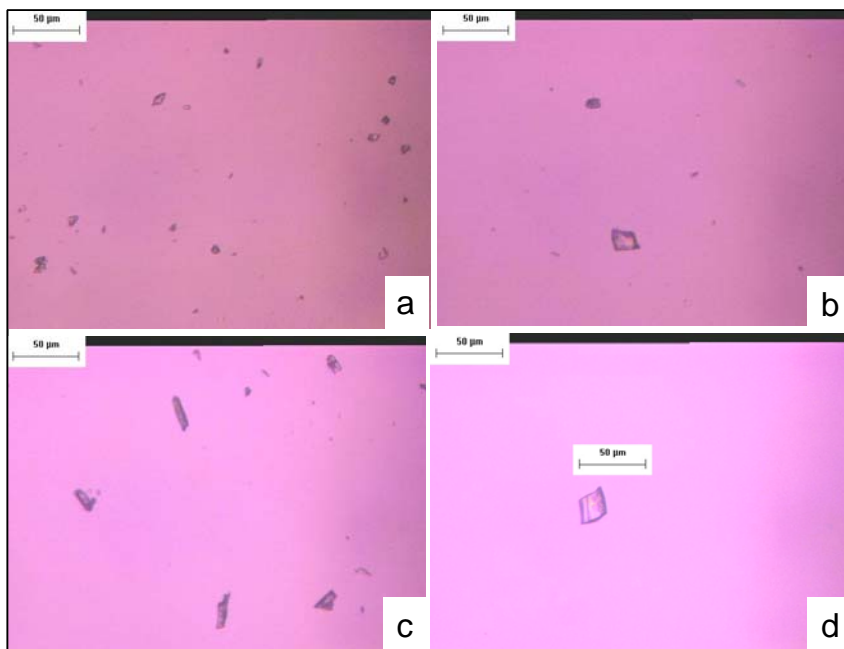
Figure 4-4: Photomicrographs of crystals in samples from the 20 mg/mL HGD solution taken at different times. The crystals in the photomicrographs represent the typical size of crystals obtained in each of the solutions. Crystals are shown after (a) 161 hours (b) 185 hours (c) 210 hours (d) 236 hours.
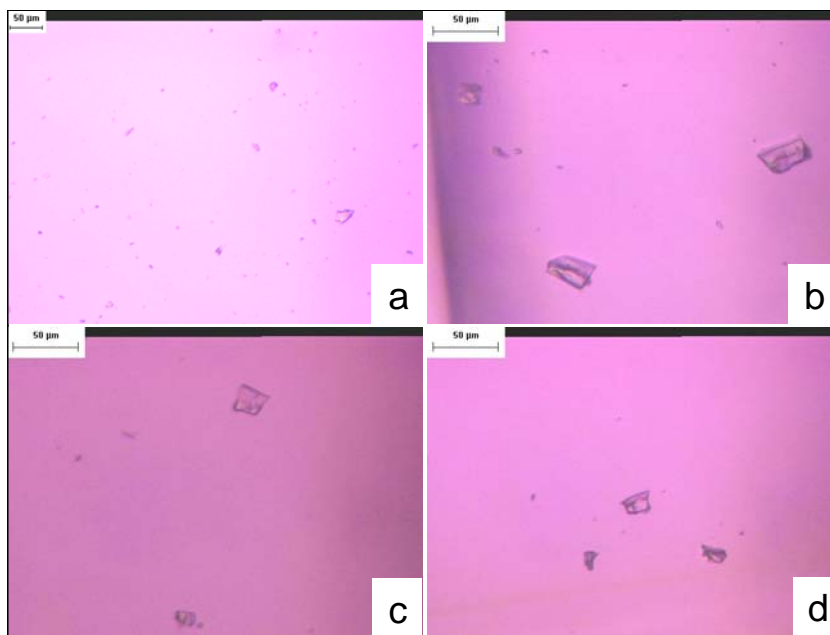
Figure 4-5: Photomicrographs of crystals in samples from the 30 mg/mL HGD solution taken at different times. The crystals in the photomicrographs represent the typical size of crystals obtained in each of the solutions. Crystals are shown after (a) 161 hours (b) 185 hours (c) 210 hours (d) 236 hours.
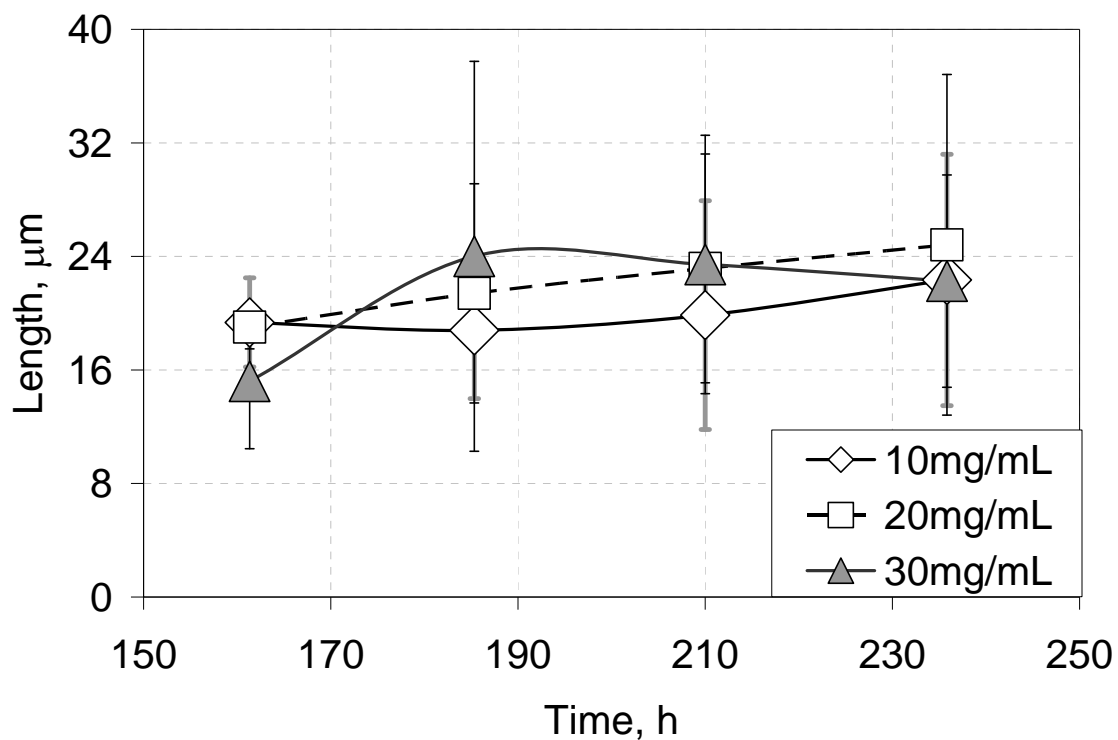
Figure 4-6: Length of crystals of HGD at 10, 20 and 30 mg/mL of HGD tracked over time. A different sample was used at each time point for each concentration. The error bars represent population standard deviations.

As explained earlier in this section, the experiments from which the data in this section were obtained were not designed to measure the kinetics of crystal growth. In addition, only one experiment was carried out. The results do, however, give a rough idea of the growth trends of crystals of HGD under the conditions studied.

4.4.2 Liquid-Liquid Phase Separation

Liquid-liquid phase separation (LLPS) is a phenomenon whereby protein-rich liquid drops form within a protein solution.[78] HGD was observed to exhibit LLPS in the present

study in determination of both the temperature and precipitant (Ba^{2+} and Ca^{2+}) phase diagrams. LLPS has been observed in fewer than 20 proteins including the gamma-crystallins, arachin, and lysozyme.[78] Crystals often grow out of the protein-rich phase, thus LLPS is thought to promote crystallization.[78] Figure 4-7 shows three microwells each containing 5 mg/mL HGD: one with no crystals, one with LLPS, and one with a "skin" formation. All three wells contained HGD in the presence of 100 mM phosphate buffer at 32°C after one week. In many cases, crystals grew in wells where LLPS was first noted which is compatible with the theory that LLPS is a metastable transition with respect to crystallization.[78] Indeed, Figure 4-7 shows that crystals of HGD are coexisting with LLPS. Temperature-induced LLPS has previously been reported in HGD[79] but the present study is the first time, to the knowledge of the author, that LLPS has been reported to be induced in HGD by addition of Ba^{2+} and Ca^{2+}.

"Skin" formations like the one shown in Figure 4-7 were observed in approximately 2% of the wells in the temperature phase diagram experiment. In such cases, the skin did not re-dissolve. Skin formations are considered a negative crystallization result like amorphous precipitate. In the present study, crystals rarely grew out of solutions containing skins and were not considered in the phase diagram determination if they did. It is not known what causes skins to grow but it is sometimes attributed to denatured protein.[80] Skin formations are easily distinguishable from LLPS by their wrinkled surfaces.
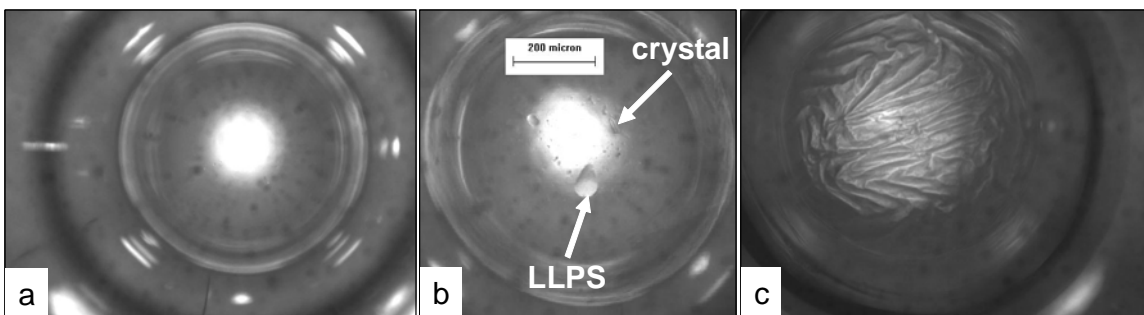
Figure 4-7: Observations made in microwells during determination of the temperature phase diagram. (a) Microwell with no crystals. (b) Liquid-liquid phase separation of 5 mg/mL pure HGD in 100 mM phosphate buffer at 32°C observed after 1 week and coexisting with crystals of HGD. (c) Skin formation observed in some wells. Its wrinkled surface distinguishes the skin from LLPS.

4.4.3 Temperature Phase Diagram

The temperature phase diagram for pure HGD was determined using microbatch crystallization and a range of concentrations of HGD from 1 mg/mL to 5 mg/mL. Initially, the experiment was set up to determine concentrations of HGD which would yield crystals large enough for their growths to be tracked by microscopy. However, the crystals obtained were too small for this purpose. The results were used instead to determine solubility of HGD.

The microbatch set up used in the present study was developed by Bartling *et al.*[21] who determined that the temperature gradient along the microbatch plate was linear provided that the surrounding temperature was midway between the temperature ranges of the plate. The temperature of the surroundings was controlled by placing the plate in a Plexiglas box with a heat lamp and a temperature controller. The temperature gradient across the plate was generated by two water baths on either end of the plate. Experiments were carried out to measure the temperature in each well and they confirmed that the

temperature gradient across the plate was linear. In the present study, temperature was varied from 26.8°C to 31.4°C across the plate. Well temperatures were determined by setting up a similar experiment in which the temperature across the plate was also varied from 26.8°C to 31.4°C. The well temperatures were allowed to equilibrate and then the temperature in each well was measured in random order with a thermocouple. The measurements were repeated two more times over a two hour period. Figure 4-8 shows a plot of average well temperature vs. well number. It can be seen from the plot that edge temperatures did not follow the linear trend obtained for the interior wells. As a result, the first two wells and the last two wells were not used. The error bars in the plot represent standard deviations with n = 3.
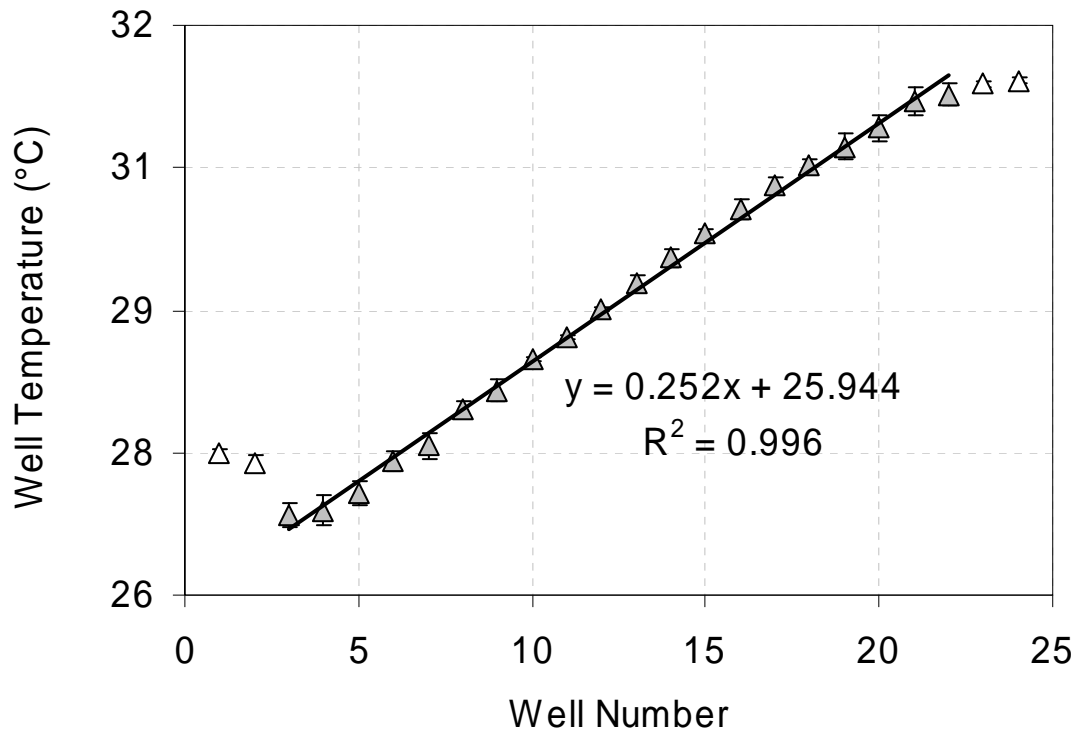
Figure 4-8: Plot showing linear temperature gradient across a multiwell plate. The clear triangles represent the edge wells while the grey triangles represent the interior wells. Only the gray triangles were used to evaluate the linear plot. The error bars represent standard deviations with n = 3.

Temperature was varied linearly across the plate from 26.8°C to 31.4°C. A grid of concentrations of HGD and temperatures used in determination of the phase diagram is shown in Table 4-2. Crystals were allowed to grow for 2 weeks. Conditions where crystals were obtained are marked by an "X" and conditions that did not yield crystals are marked with an "O." The results from Table 4-2 were plotted on a graph of HGD concentration against temperature with no processing of data as shown in Figure 4-9. The solubility line is obtained by joining the outer points of the region where crystals were obtained i.e. the outermost wells containing crystals for each HGD concentration form the solubility boundary. Stochastic aggregation of protein molecules is thought to be the first step in crystallization. At a critical radius R_c, the aggregates overcome the energy barrier and irreversible aggregation results in growth. Below R_c the aggregates are unstable and stochastically grow and dissociate. The stochastic nature of nucleation may result in solutions of the same supersaturation forming crystals at different rates. Therefore, varying amounts of time are needed for nucleation and equilibration of solid and liquid phases. This may explain the apparent randomness of crystals obtained in the present study.

It was observed that the solubility of HGD has a normal dependence on temperature, i.e. solubility increased with increasing temperature as shown in Figure 4-9 which is consistent with results from previous studies[13; 79] although the equilibrium temperatures determined in the present study are lower. As temperature increases, the energy barrier to nucleation also increases (Mullin 2001, pages 186 - 187).[18] Therefore, even though the HGD molecules have more energy at higher temperatures, they also have

a higher energy barrier to overcome and this leads to increasing solubility of HGD at higher temperatures.

Table 4-2: Grid showing concentrations of HGD and temperatures used in determining the temperature phase diagram for HGD. The concentration of HGD was varied from 1 to 5 mg/mL, and temperature from 25.87 to 34.13°C. "X" designates where crystals were observed and "O" designates where no crystals were observed. The outermost wells with crystals for each HGD concentration were taken as the solubility boundary. The "X"es which form the solubility curve are marked in red.

		Temperature (°C)																		
		26.8	26.9	27.1	27.4	27.6	28.0	28.2	28.5	28.7	29.0	29.3	29.6	29.8	30.1	30.3	30.5	30.7	30.9	31.2	31.3
	1	O	O	O	O	O	O	O	O	O	O	O	O	O	O	O	O	O	O	O	O
	1	O	O	O	O	O	O	O	O	O	O	O	O	O	O	O	O	O	O	O	O
	1	O	O	O	O	O	O	O	**X**	O	O	O	O	O	O	O	O	O	O	O	O
	1	O	O	O	O	**X**	O	O	O	O	O	O	O	O	O	O	O	O	O	O	O
	3	X	X	X	X	X	X	O	O	O	O	O	O	O	O	O	O	O	O	O	O
HGD concentration (mg/mL)	3	X	X	X	O	O	O	O	X	X	O	O	O	O	**X**	O	O	O	O	O	O
	3	O	O	X	O	O	O	O	O	O	O	O	O	O	O	O	O	O	O	O	O
	3	X	X	O	X	X	O	O	X	X	O	O	O	O	O	O	O	O	O	O	O
	5	X	O	X	X	O	O	X	O	X	O	O	X	O	O	O	**X**	O	O	O	O
	5	O	X	O	O	O	O	O	O	O	O	O	O	O	O	O	O	O	O	O	O
	5	X	O	X	O	O	X	O	O	O	X	O	O	O	O	O	O	O	O	O	O
	5	O	X	O	X	O	O	X	O	O	O	O	O	O	O	O	O	O	O	O	O

Crystals obtained were on the order of 20 μm and appeared to match the tetragonal structure previously described.[81] No visual change in crystal form was observed over the temperature range studied. Higher concentrations of HGD yielded more crystals suggesting that crystallization was taking place close to the labile region of the phase diagram where precipitation or formation of microcrystals occurs. More

crystals were also obtained at lower temperatures, possibly as a result of lower energy

barriers to nucleation at lower temperatures.[18] This is consistent with findings in previous

crystallization studies e.g. Bartling et al.[44] also observed more crystals of apoferritin at

lower temperatures.
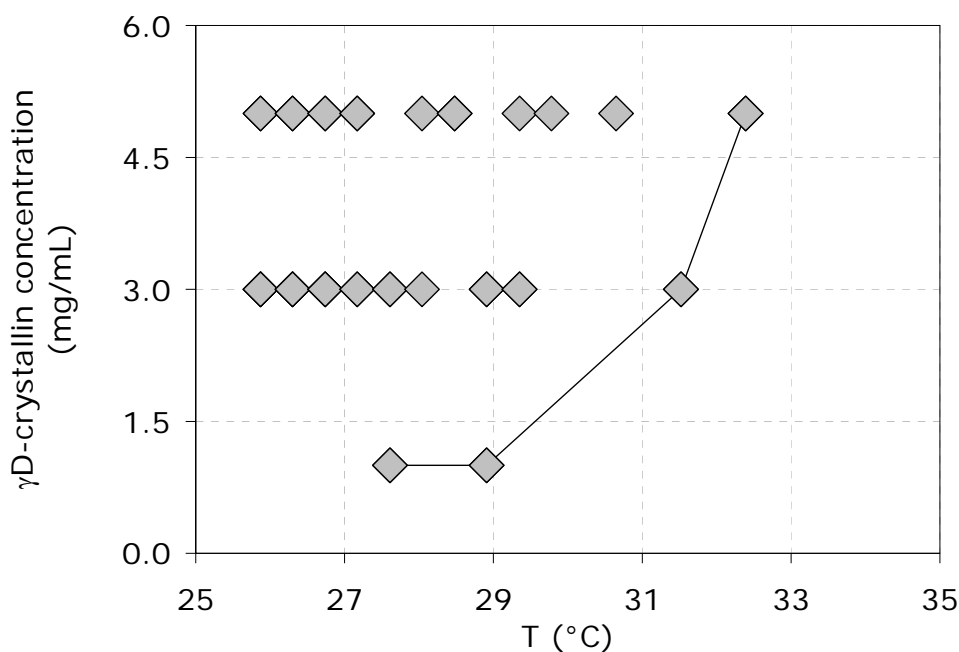
Figure 4-9: Temperature phase diagram of pure HGD obtained by microbatch crystallization.
The diamonds represent concentration and temperatures where crystals were observed. The line through the
points is a guide for the eye and represents the solubility line. Two or more crystals were obtained at each
point on the solubility line except for the 3 mg/mL concentration where only one crystal was observed.

4.4.4 Precipitant Phase Diagram

A phase diagram was determined for HGD in the presence of two precipitants, $CaCl_2$ and

$BaCl_2$, at 298 K. Two independent experiments were carried out for each divalent cation

and crystals were allowed to grow for 4 weeks in each case. Conditions used in

determination of the HGD phase diagram with BaCl$_2$ are shown in Table 4-3 while

conditions used in determination of the HGD phase diagram with CaCl$_2$ are shown in

Table 4-4. Conditions where crystals were obtained are marked with a "Y" or an "X" for

the first and second microbatch experiment respectively. It can be seen in both Table 4-3

and Table 4-4 that more crystals were obtained in the second set of experiments, i.e. there

are more "X"es than "Y"s. This may be attributed to the stochastic nature of the

nucleation process. The divalent cation concentrations were varied from 0.0 to 12.0

mg/mL while HGD concentration was varied from 0.00 mg/mL to 0.30 mg/mL. These

low concentrations were used in order to preserve HGD which was available in limited

quantities. The range of concentrations of HGD used span the concentration (0.2 mg/mL)

used for experiments in the chapters that follow. Crystallization experiments with

solutions containing 0.2 mg/mL of HGD and 10 mM BaCl$_2$ or 10 mM CaCl$_2$ yielded

crystals and this gave confidence that crystals would be obtained at the low concentration

used.

Table 4-3: Grid showing data obtained using 2 microbatch experiments to determine the phase diagram of HGD in the presence of BaCl$_2$ at 298 K. Both HGD concentration and BaCl$_2$ concentration were varied. Wells where crystals were obtained are marked with a "Y" representing the first experiment and/or an "X" for the second experiment. Wells where no crystals were observed are marked with an "O." The X'es and Y's which form the solubility curve are marked in red.

		BaCl$_2$ concentration, mM							
		0.0	1.0	2.0	4.0	6.0	8.0	10.0	12.0
	0.00	O	O	O	O	O	O	O	O
	0.01	O	O	O	O	O	O	O	O
HGD concentration, mg/mL	0.05	O	O	O	X	Y, X	X	O	Y, X
	0.10	O	Y, X	X	O	Y, X	O	O	X
	0.15	O	Y, X	Y, X	X	O	Y, X	X	Y, X
	0.20	O	X	X	O	Y, X	Y, X	O	Y, X
	0.30	O	X	X	O	O	Y, X	Y, X	Y, X

81

Table 4-4: Grid showing data obtained using 2 microbatch experiments to determine the phase diagram of HGD in the presence of $CaCl_2$ at 298 K. Both HGD concentration and $BaCl_2$ concentration were varied. Wells where crystals were obtained are marked with a "Y" representing the first experiment and/or an "X" for the second experiment. Wells where no crystals were observed are marked with an "O." The X'es and Y's which form the solubility curve are marked in red.

		CaCl₂ concentration, mM							
		0.0	1.0	2.0	4.0	6.0	8.0	10.0	12.0
	0.00	O	O	O	O	O	O	O	O
	0.01	O	O	O	O	O	O	O	Y, X
HGD concentration, mg/mL	0.05	O	O	O	Y, X	X	Y, X	Y, X	X
	0.10	O	Y, X	Y, X	Y, X	X	X	O	Y, X
	0.15	O	O	O	O	Y, X	X	X	Y, X
	0.20	O	Y, X	Y, X	X	X	X	X	X
	0.30	O	Y, X	X	Y, X	X	Y, X	Y, X	Y, X
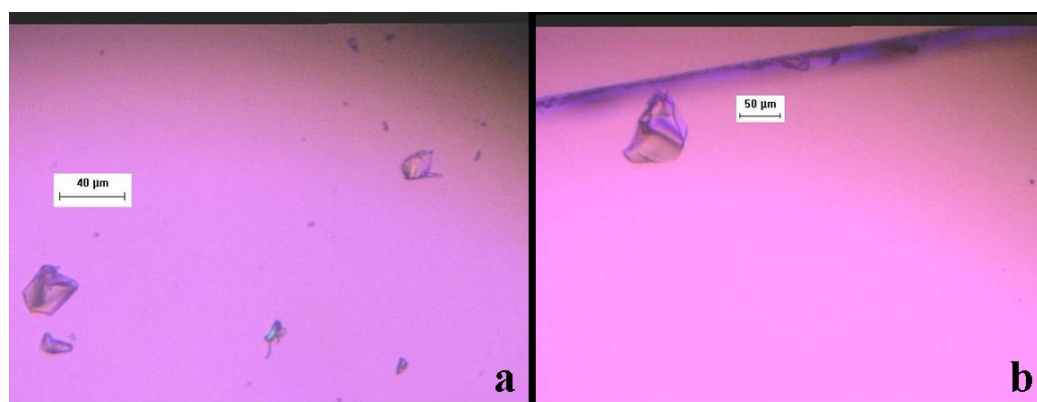
Figure 4-10: Photomicrographs of tetragonal HGD crystals obtained during determination of the phase diagram in the presence of $CaCl_2$. (a) 0.2 mg/mL HGD in solution containing 10 mM $CaCl_2$ (b) 0.3 mg/mL HGD in solution containing 12 mM $CaCl_2$

Figure 4-10 shows photomicrographs of crystals obtained with 0.2 mg/mL HGD-10 mM $CaCl_2$ and 0.3 mg/mL HGD-12 mM $CaCl_2$. The crystals obtained appear to be tetragonal which is consistent with findings from previous studies.[77] The phase diagrams are shown in Figure 4-11 as a plot of HGD concentration against divalent cation

concentration. The solubility curve was taken to pass through the wells on the outer boundary between the region with crystals and the region with no crystals. A salting-out effect was observed with both $CaCl_2$ and $BaCl_2$ as solubility of HGD decreased with increasing precipitant concentration. Divalent cations are thought to induce crystallization of proteins by binding to water, effectively increasing the concentration of the protein in the "free" water.[82] HGD has attractive interactions in solution[53] so addition of the divalent cations increased the attraction between HGD molecules as the concentration of the protein increased, hence the salting-out effect. HGD behaves similarly in solutions containing either $CaCl_2$ or $BaCl_2$ at the conditions examined in the present study. These results imply that in the lens, increasing concentrations of the divalent cations under study may lead to crystallization of HGD. Concentrations of Ca^{2+} as high as 64 mM have been reported in cataractous lenses.[83] As much lower concentrations of Ca^{2+} were used in the present study ($\leq$ 12 mM), this suggests that divalent cations have a strong effect on the solubility of HGD.
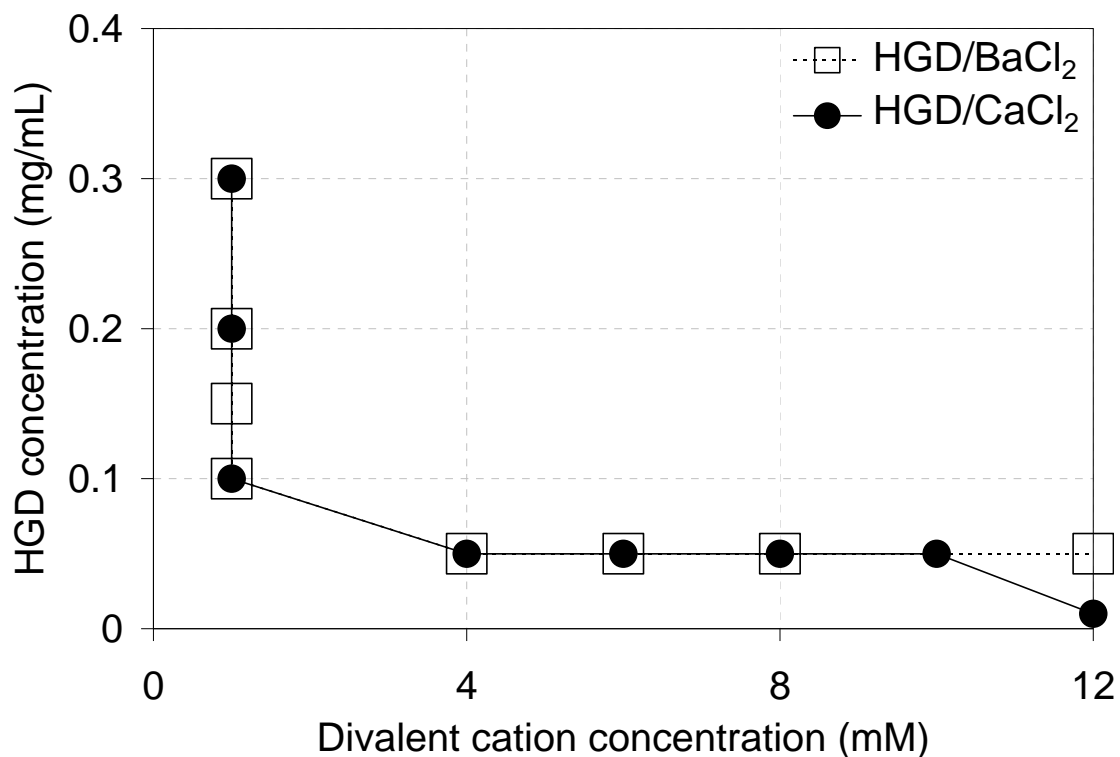
Figure 4-11: Precipitant concentration phase diagram for HGD in the presence of $CaCl_2$ or $BaCl_2$ at a temperature of 298 K.

4.4.5 Enthalpy and Free Energy of Crystallization

Thermodynamic properties were determined for the temperature phase diagram of pure HGD using results from SECTION 4.4.3. As explained in the aforementioned section, the experiment was initially set up to track crystal growth over time. However, the crystals obtained were too small for this purpose and as such the results were used instead to determine solubility of HGD. The thermodynamic properties determined were then compared with results from the literature.

The standard enthalpy of crystallization ΔH^o_{cryst} was evaluated from a modified form of the van't Hoff equation which was derived from the Gibbs-Helmholtz equation as follows.[84; 85] For a closed system,

$$dG = -SdT + VdP \qquad\qquad 4\text{-}1$$

where S is entropy, T is the absolute temperature, V is volume, and P is pressure. At constant pressure,

$$\left(\frac{\partial G}{\partial T}\right)_P = -S \qquad\qquad 4\text{-}2$$

The dependence of the ratio G/T on T can be found using the quotient rule:

$$\left[\frac{\partial(G/T)}{\partial T}\right]_P = \frac{1}{T}\left(\frac{\partial G}{\partial T}\right)_P - \frac{G}{T^2} \qquad\qquad 4\text{-}3$$

Combining Equations 4-2 and 4-3, we obtain

$$\left[\frac{\partial(G/T)}{\partial T}\right]_P = \frac{-ST - G}{T^2} = \frac{-H}{T^2} \qquad\qquad 4\text{-}4$$

where H is enthalpy. The Gibbs free energy change may be written as

$$\Delta G^o = -RT \ln K_{cryst}$$

<div align="right">4-5</div>

where R is the universal gas constant and K_{cryst} is defined by Smith *et al.*[28] as

$$K_{cryst} = \frac{a_{s,cryst}}{a_{s,sol'n}} = \frac{x_{s,cryst} f_s^S}{\gamma_s x_{s,sol'n} f_s^L}$$

<div align="right">4-6</div>

where $a_{s,cryst}$ is the activity of the solute in the crystal, $a_{s,sol'n}$ is the activity of the solute in the solution, $x_{s,cryst}$ is the mole fraction of the solute in the crystal, f_s^S is the fugacity of pure solid solute at the temperature and pressure of the system, γ_s is the activity coefficient of the solute in liquid solution, $x_{s,sol'n}$ is the mole fraction of the solute in solution, and f_s^L is the fugacity of pure liquid solute at the temperature and pressure of the system. Assuming that the value of $x_{s,cryst}$ is close to unity since the crystal is mostly made up of solute, and that f_s^S is equal to f_s^L at equilibrium, Equation 4-6 simplifies to

$$K_{cryst} = \frac{1}{\gamma_s x_{s,sol'n}}$$

<div align="right">4-7</div>

with $x_{s,sol'n}$ evaluated using

$$x_{s,sol'n} = \frac{n_p}{n_p + n_w}$$

<div align="right">4-8</div>

where n_p is the number of moles of HGD in the solution at the points on the solubility curve, and n_w is the number of moles of water in the solution. Using results from Equation 4-4 and Equation 4-5, we obtain

$$\left(\frac{\partial \ln K_{cryst}}{\partial T}\right)_P = -\left[\frac{\partial\left(\Delta G^o_{cryst} / RT\right)}{\partial T}\right]_P = \frac{\Delta H^o_{cryst}}{RT^2} \qquad \text{4-9}$$

where ΔG^o_{cryst} is the change of the standard Gibbs free energy upon crystallization. If the solution is assumed to be ideal i.e. $\gamma_e \approx 1$, we can combine Equations 4-7 and 4-9 to obtain

$$\left[\frac{\partial \ln x_{s,sol'n}}{\partial T}\right]_P = -\frac{\Delta H^o_{cryst}}{RT^2} \qquad \text{4-10}$$

or

$$\ln x_{s,sol'n} = \frac{\Delta H^o_{cryst}}{RT} + \text{constant} \qquad \text{4-11}$$

which is a modified form of the van't Hoff equation. Thus ΔH^o_{cryst} may be obtained from the slope of the plot of $\ln x_{s,sol'n}$ against $1/T$.

   A summary of the results from the present study and results from an HGD solubility study by Pande et al.[13] are shown in Table 4-5 and Table 4-6, respectively. The HGD concentrations and corresponding temperatures in Table 4-5 were obtained from

the solubility data in Figure 4-9. Figure 4-12, which shows a graph of Ln $x_{s.soln}$ against

$1/T$ was plotted using data from Table 4-5. Using Equation 4-11, the value of ΔH^o_{cryst} was

determined to be −455 kJ/mol from the graph in Figure 4-12. The value of ΔH^o_{cryst}

determined for HGD in the present study is much lower than the value (−61.5 kJ/mol)

reported by Pande et al.[13] After reviewing the procedures used in both studies, the only

logical explanation is the presence of aggregates in the HGD solution used in the present

study as aggregates in a protein solution may shift the position of the solubility curve.[78]

Pande et al.[13] used 20 mM dithiothreitol (DTT) to prevent thiol-mediated aggregation of

HGD molecules. The average size of HGD molecules in a solution containing 20 mM

DTT was determined by Pande et al.[38] to be 2.3 nm, which is also the size of a single

molecule of HGD.[86; 87] A 10 mM solution of DTT was used in the present study to

prevent aggregation of HGD molecules. Although the HGD solution used for the

temperature phase diagram was not examined for aggregates, dynamic light scattering

experiments have shown that the average radius in the HGD solutions used for other

experiments in the present study was 18 nm. Since the radius of a single molecule of

HGD is 2.5 nm,[86; 87] a radius of 18 nm suggests that aggregates were present in HGD

samples. The presence of aggregates in the HGD solution may explain why the solubility

curve determined in the present study is different from that determined by Pande et al.[13]

In spite of the discrepancy in values determined for ΔH^o_{cryst}, both the present study as

well as the study by Pande et al.[13] determined that the dependence of solubility of HGD

on temperature was normal, i.e. higher solubility at higher temperatures. However, it can

be argued that the partially oxidized HGD used in the present study is more like the HGD

involved in protein condensation diseases such as cataract. Hence the results from the present study are relevant to protein condensation diseases.

Table 4-5: Thermodynamic properties obtained from the present study. The equilibrium temperatures and concentrations were obtained from the solubility curve in Figure 4-9.

Temperature (°C)	Concentration (mg/mL)	Mole fraction $x_{s,soln}$	ΔS^{o}_{cryst} (J/mol-K)	ΔG^{o}_{cryst} (kJ/mol)
27.7	1	9.0×10^{-7}	−1397.5	−34.8
28.5	1	9.0×10^{-7}	−1393.5	−34.9
30.0	3	2.7×10^{-6}	−1395.1	−32.3
30.5	5	4.5×10^{-6}	−1396.9	−31.1

Table 4-6: Thermodynamic results extracted from the study by Pande *et al.*[13] Rather than mole fractions, volume fractions φ_p were used in this study and evaluated using $\varphi_p = cv$ where c is the concentration of HGD on the solubility line and v is the specific volume of HGD taken to be 7.1×10^{-4} mL/mg.[13]

Temperature (°C)	Concentration (mg/mL)	Volume fraction φ	ΔS^{o}_{cryst} (J/mol-K)	ΔG^{o}_{cryst} (kJ/mol)
2.3	2	0.001	−189.71	−15.04
13.7	4	0.003	−186.40	−13.83
16.2	6	0.004	−186.86	−13.23
19.0	12	0.008	−190.43	−11.66
27.3	16	0.011	−186.60	−11.24
29.4	26	0.018	−189.17	−10.06
35.7	43	0.030	−188.81	−8.99
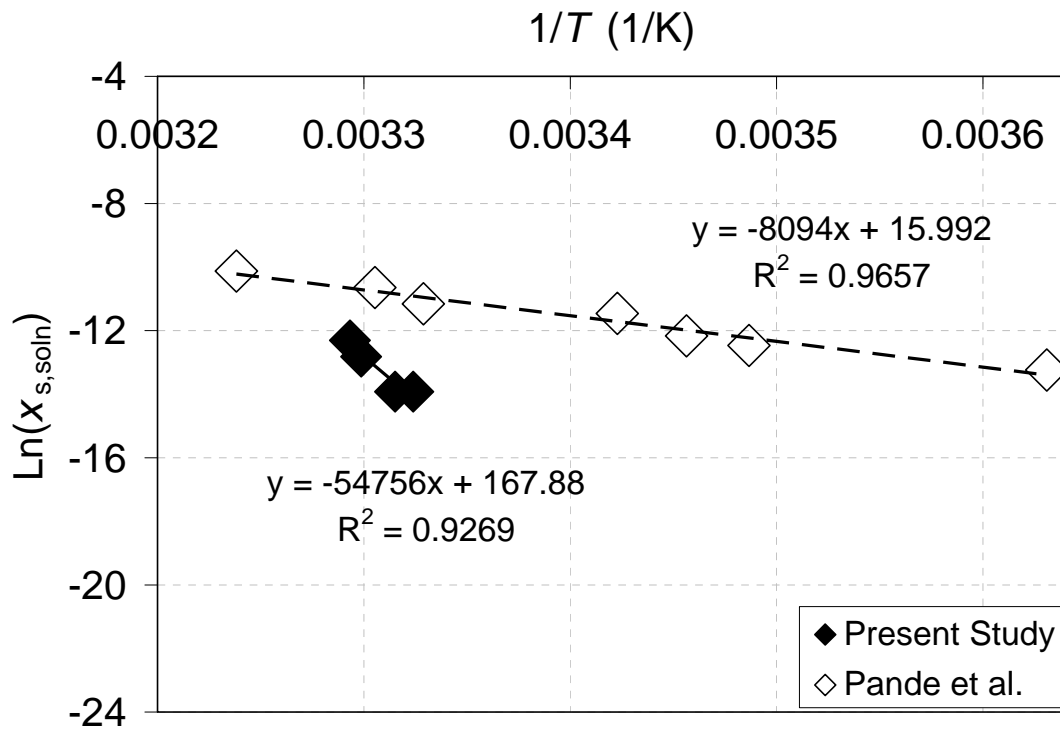
Figure 4-12: Determination of the enthalpy of crystallization. The solubility curve shown in Figure 4-9 was used to obtain the present plot. Results from the study by Pande *et al.*[13] are shown for comparison.

ΔG^o_{cryst} was calculated using the equation below:

$$\Delta G^o_{cryst} = RT \ln a_e \cong RT \ln x_{s,sol'n} \qquad\qquad 4\text{-}12$$

The resulting values of ΔG^o_{cryst} determined for HGD ranged from -34.9 kJ/mol at 302 K to -31.1 kJ/mol at 304 K. These values of ΔG^o_{cryst} are comparable to values reported in literature such as the ΔG^o_{cryst} of crystallization of hemoglobin C which was determined to be -21.3 kJ/mol at 289 K.[88] The negative values for ΔG^o_{cryst} along with the negative value for enthalpy indicate that the crystallization process is thermodynamically feasible for

HGD under the conditions studied. The change in the standard entropy ΔS^{o}_{cryst} was evaluated from

$$\Delta G^{o}_{cryst} = \Delta H^{o}_{cryst} - T\Delta S^{o}_{cryst} \qquad\qquad 4\text{-}13$$

Values for ΔS^{o}_{cryst} ranged from -1393.5 J/mol-K at 302 K to -1397.5 J/mol-K at 301 K, showing a slight decrease in entropy, which disfavors crystallization. The discrepancy in entropy values between the present study and the study by Pande et al.[13] may be attributed to the narrow temperature range used for determination of solubility of HGD in the present study.

Proteins in solution are thought to be associated with specific arrangements of water molecules.[85] During crystallization, as the protein molecules rearrange to form the new phase, the water molecules also undergo rearrangement, with the trapping of more water molecules around the protein molecules, or the release of some water molecules. Entropy change during crystallization is thought to be due to trapping or release and rearrangement of water molecules ($\Delta S^{o}_{solvent}$), as well as incorporation of protein molecules to the surface of the crystal ($\Delta S^{o}_{protein}$), i.e.[88; 89]

$$\Delta S^{o}_{cryst} = \Delta S^{o}_{protein} + \Delta S^{o}_{solvent} \qquad\qquad 4\text{-}14$$

While $\Delta S^{o}_{protein}$ is expected to be negative, $\Delta S^{o}_{solvent}$ may be positive or negative depending on whether water molecules are released or trapped, respectively. Therefore, ΔS^{o}_{cryst} may be positive or negative. The term $\Delta S^{o}_{protein}$ is assumed to be insignificant as

has been discovered for hemoglobin C and apoferritin.[85] Thus in cases where water molecules are trapped, crystallization is thermodynamically feasible if $\Delta H^{o}_{cryst} < 0$ and of greater magnitude than $T\Delta S^{o}_{cryst}$. Conversely, when water molecules are released, crystallization is thermodynamically feasible if $\Delta H^{o}_{cryst} < 0$, or if $\Delta H^{o}_{cryst} > 0$ but of smaller magnitude than $T\Delta S^{o}_{cryst}$.

Using the assumption that $\Delta S^{o}_{protein}$ is insignificant, the entropy of crystallization of HGD under the conditions in the present study can be solely attributed to the reordering of water molecules. This entropy effect can be compared with the entropy change associated with the melting of ice at 273 K, $\Delta S^{o}_{ice} = 22$ J, following an analogy first proposed by Tanford.[90] The analogy is based on the transfer of water molecules to a more ordered state during freezing. Previous studies with lysozyme showed that 7 or 8 water molecules are trapped in the crystal for each lysozyme molecule incorporated into the crystal.[85] Similar studies with apoferritin showed that 20 to 30 water molecules are released for each molecule of apoferritin incorporated into the crystal.[85] A comparison of the entropy values from the present study with the entropy of the melting of ice suggests that approximately 55 molecules of water are trapped rather than released in HGD crystals for each molecule of HGD incorporated into the crystal, in addition to the water molecules already associated with HGD molecules in solution. It is not well-understood why water molecules are trapped in some protein crystals but released in others.

The insight into the thermodynamics of protein crystallization developed in the present study increases understanding of the processes associated with protein condensation diseases such as cataract. Since crystallization of HGD is more favorable at lower temperatures, decreasing temperatures in the eye may promote development of

cataracts. The abundance of water in the lens may also be a contributing factor since water is trapped during crystallization of HGD.

4.5 CONCLUSIONS

The equilibrium phase boundary for HGD was experimentally determined over a temperature range from 300 K to 305 K. The phase diagrams of HGD in the presence of $BaCl_2$ and $CaCl_2$ were determined at 298 K. A salting-out effect was observed in both cases as higher concentrations of the cations resulted in lower solubility of HGD. The salting-out effect was attributed to the increased hydration of the divalent cations at higher concentrations of the salt, resulting in lowered protein solubility.

Thermodynamic analyses of crystallization of HGD as a function of temperature yielded a negative Gibbs free energy, which favors crystallization at the conditions studied. The entropy of crystallization was determined to range from −1397 J/mol-K at 301 K to −1393 J/mol-K at 302 K. It was determined that there was a small decrease in entropy, which disfavors crystallization. The loss of entropy was attributed to the trapping of ~ 55 water molecules for each molecule of HGD incorporated into the crystal. Crystallization was therefore possible because of the high negative enthalpy of −455 kJ/mol.

The results from this chapter serve to further the understanding of the thermodynamics of crystallization of proteins involved in protein condensation diseases. The findings indicate that HGD, a protein involved in cataract disease, is more likely to crystallize at the lower temperatures examined in the present study. They also indicate

that in the presence of Ba^{2+} or Ca^{2+}, the solubility of HGD is lowered, which may increase the likelihood of cataract formation in the lens. Thus, cataract formation may be impeded if the concentration of divalent cations is prevented from increasing above physiological levels.

CHAPTER 5: EVALUATING INTERMOLECULAR INTERACTIONS BY LIGHT SCATTERING TECHNIQUES

5.1 ABSTRACT

The second virial coefficient, B_{22}, has long been used as a measure of protein-protein interactions in solution. The value of B_{22} measured in protein solutions may be used to predict crystallization in these solutions. Although static light scattering (SLS) is the most common method for measuring B_{22}, it requires a significant amount of material, effort and time. In this work, we demonstrate that dynamic light scattering (DLS) measurements can be used in evaluating intermolecular interactions in protein solutions and assessing B_{22}. Results obtained with apoferritin show that DLS alone may be used to derive the second virial coefficient with less material and time than SLS. Additional advantages of DLS measurements, especially in cases of active protein aggregation and for biological fluid specimens, are discussed.

5.2 INTRODUCTION

Several human degenerative diseases such as cataract, Alzheimer's and Parkinson's disease can be linked to aggregation and crystallization of proteins.[91; 92; 93] Crystallization of proteins is also a key step in the purification and separation of pharmaceutical

products.[25; 94] According to the classical model of nucleation,[95] the initial stage of protein crystallization is the stochastic aggregation of protein molecules. When the aggregate reaches a critical size, it forms a nucleus. The nucleus rearranges to a crystalline form and additional molecules are added to the nucleus leading to crystal growth. Many factors can lead to proteins crystallizing or precipitating out of solution, including temperature, pH, and elevated divalent cation concentration[3; 32] in the case of cataract.[20; 94; 96] As a result, predicting crystallization is difficult and still largely depends on random screening experiments.[16; 97]

Light scattering methods may be used to study the pre-crystallization state of proteins in solution[98] and therefore track aggregation and predict crystallization. Static light scattering (SLS) yields the second virial coefficient B_{22}, while dynamic light scattering (DLS) yields the diffusivity slope, k_D, which is a measure of solute-solute interactions. The sign of B_{22} signifies the type of interaction of the protein molecules with each other. A negative B_{22} indicates greater attraction between solute molecules than between solute and solvent, while a positive second virial coefficient indicates a greater attraction between the solute and the solvent than between solute molecules.[23; 68] The diffusivity slope, however, is only indicative of solute-solute interactions.[105] When k_D is negative, the particles have attractive interactions while a positive k_D implies repulsive interactions.[68] Both terms are negative under crystallizing or precipitating conditions, and positive in solutions where the protein remains in solution. Thus, the value of k_D or B_{22} can be correlated to the occurrence of crystallization.

While SLS may be used to measure B_{22} directly, it requires significant amounts of material and time.[7] DLS requires much less material than SLS and is quicker and easier

to carry out. SLS is also very sensitive to the formation of aggregates, which may skew the measurements, especially in cases where there are significant attractive interactions in the solution. In contrast, DLS measures the size of the aggregates in solution and this information is then used to calculate k_D. DLS is also relatively more tolerant of aggregates as it measures fluctuations about an average intensity whereas static light scattering (SLS) averages out intensity measurements.[29] While values of k_D may also be used to predict crystallization, it is advantageous to determine B_{22} values as there is a universal range of B_{22} values within which crystallization of most proteins is likely to occur. A similar range of k_D values can be determined but such a range is unique to each protein since the molecular weight of the protein and friction effects must be taken into account. Therefore, the crystallization window for k_D must be determined for each protein whereas the B_{22} window is universal for all proteins.

Here, we report on the development of a methodology to assess intermolecular solute interactions and the second virial coefficient from DLS measurements alone. SLS and DLS measurements were carried out with apoferritin and yielded essentially the same results. These results correlate with the crystallization outcome, indicating that the signs of both B_{22} and k_D may be used to predict crystallization.

5.3 THEORY

5.3.1 Dynamic Light Scattering

Dynamic light scattering (DLS) makes use of a laser. Macromolecules in solution, in this case, protein molecules, scatter the laser light in all directions. Since the laser is coherent and monochromatic, and the molecules are undergoing Brownian motion, the scattering intensity exhibits a time-dependent fluctuation.[68] An autocorrelation function can be derived from this fluctuation. From Adel at al, we can see that the autocorrelation function $G(t)$ is related to the delay time, i.e. the time scale of movement of the scattering molecules, as follows:[69]

$$G(t) = A \exp\left(-2\frac{t}{\tau}\right) + B \qquad \text{5-1}$$

where A is a system-specific constant, τ is delay time and B is the baseline. The apparent diffusion coefficient D is related to the delay time by[69]

$$D = \frac{1}{q^2 \tau} \qquad \text{5-2}$$

with the scattering wave vector q defined by[69]

$$q = \frac{4\pi n}{\lambda} \sin\frac{\theta}{2} \qquad \text{5-3}$$

where n is the refractive index of the solvent, θ is the scattering angle, and λ is the wavelength of the laser. Once the diffusion coefficient is obtained, the hydrodynamic radius of the aggregates can be determined from the Stokes-Einstein equation.[69]

$$R_h = \frac{k_B T}{6 \pi \eta_o D}$$ 5-4

where k_B is the Boltzmann constant, T is absolute temperature, η_o is the solvent viscosity and R_h is the hydrodynamic radius. The diffusion coefficient is related to k_D as follows:[69]

$$D = D_{p,o}(1 + k_D\, c)$$ 5-5

where D is the diffusion coefficient, $D_{p,o}$ is the diffusion coefficient at infinite dilution, and c is protein concentration. Traditionally, k_D is determined by varying c and measuring D at the corresponding concentrations. By plotting D against c, k_D can be obtained from the slope.

In the present study, protein amounts were limited and as such only one concentration was used. Aggregation of apoferritin was induced by addition of $CdCl_2$ and measurements were taken immediately upon addition of $CdCl_2$. Since aggregation is a dynamic process, both D and k_D are changing with time. By making the assumption that c is constant, Equation 5-5 may be re-written as follows:

$$\frac{D(t)}{D_o} = 1 + k_D(t)c \qquad\qquad\qquad\qquad\qquad 5\text{-}6$$

with D_o taken as the diffusion coefficient at time zero. Therefore, at time zero, $k_D = 0$. This is the first time, to the knowledge of the author, that Equation 5-5 has been used as a dynamic equation and with concentration constant. The efficacy of this method with be demonstrated in this chapter. Once the diffusivity slope is determined at each time point, B_{22} may be evaluated using:[69]

$$k_D = 2B_{22}M_w - k_s - v \qquad\qquad\qquad\qquad 5\text{-}7$$

where M_w is the molecular weight, k_s is a friction term, and v is the partial specific volume. The first term in the expression usually dominates in polymer solutions and is therefore used as an approximation in the present study.[69] The solutions used in the present study are very dilute thus friction effects, i.e. k_s, may be safely ignored. The value of v for HGD, 7.1 x 10^{-4} mL/mg,[13] is also negligible compared to the $2B_{22}M_w$ term.

Dynamic light scattering has been used by Brown and Zhou[99] to measure B_{22} values for polymers. Muschol and Rosenberger[70] showed that values of k_D can be related to the occurrence of crystallization of proteins. However, no evidence of the use of dynamic light scattering for measurement of B_{22} for proteins has been found by the author. In addition, this method has never before been demonstrated as useful for apoferritin in solutions of $CdCl_2$ as it is in the present study.

5.3.2 Derivation for Equation Relating B_{22} and k_D[100]

Diffusion arises because of movement of molecules due to concentration gradients. Assuming a concentration gradient along the x-axis, the diffusion flux or rate of flow of solute molecules across a unit area perpendicular to the x-axis, J, is give by Fick's law,

$$J = -D\frac{\partial c}{\partial x} \qquad\qquad 5\text{-}8$$

where D is the translational diffusion coefficient and c is the solute concentration. Combining Equation 5-8 with the equation of continuity below,

$$\frac{\partial c}{\partial t} = -\frac{\partial J}{\partial x} \qquad\qquad 5\text{-}9$$

we get the one-dimensional diffusion equation

$$\frac{\partial c}{\partial t} = D\frac{\partial^2 c}{\partial x^2} \qquad\qquad 5\text{-}10$$

D may be expanded as shown below: [100]

$$D = D_{p,o}\left(1 + k_D c + ...\right) \qquad\qquad 5\text{-}11$$

where $D_{p,o}$ is the diffusion coefficient at infinite dilution and k_D is the diffusivity slope.

According to the thermodynamics of irreversible processes, J is proportional to the force per molecule X which causes the flow. In this case, X is the negative gradient of the solute chemical potential per molecule μ_1, i.e.

$$J = LX = -L\frac{\partial \mu_1}{\partial x} \qquad \text{5-12}$$

The velocity of flow is $J/c = X/f$ where f is the translational frictional coefficient of each molecule. Therefore, $L = c/f$ and

$$\frac{\partial \mu_1}{\partial x} = \frac{\partial \mu_1}{\partial c}\frac{\partial c}{\partial x} = \frac{M_w}{N_A c}(1-cv)\frac{\partial \pi}{\partial c}\frac{\partial c}{\partial x} \qquad \text{5-13}$$

where π is the osmotic pressure, M_w is the molecular weight of the solute, N_A is Avogadro's number, v is the partial specific volume of the solute. The Gibbs-Duhem equation was used to obtain the second equality. Combining Equations 5-11, 5-12 and 5-13, and using the following relationships,

$$\frac{\partial \pi}{\partial c} = \frac{RT}{M_w}\left(1 + 2M_w B_{22}c + ...\right) \qquad \text{5-14}$$

$$R = k_B N_A \qquad \text{5-15}$$

$$f = f_o\left(1 + k_s c\right)$$

<div align="right">5-16</div>

where R is the universal gas constant, T is the absolute temperature, k_B is Boltzmann's constant and f_o is the friction coefficient at infinite dilution, we obtain

$$D\frac{\partial c}{\partial x} = \frac{c}{f}\frac{M_w}{cN_A}(1 - c\upsilon)\frac{\partial \pi}{\partial c}\frac{\partial c}{\partial x}$$

<div align="right">5-17</div>

$$D = \frac{M_w}{N_A f}(1 - c\upsilon)\frac{\partial \pi}{\partial c} = \frac{k_B T}{f}(1 - c\upsilon)(1 + 2B_{22}M_w + ...)$$

<div align="right">5-18</div>

which leads to

$$D_{p,o} = \frac{k_B T}{f_o}$$

<div align="right">5-19</div>

which is Einstein's relation between the diffusion and friction coefficients, and

$$k_s + k_D = 2B_{22}M_w - \upsilon$$

<div align="right">5-20</div>

5.3.3 Static Light Scattering

Static light scattering (SLS) compares the intensity of laser light scattered by a protein solution with the laser's incident intensity. This ratio is called the Rayleigh ratio. By varying the concentration of the protein solution, the molecular weight of the sample and the second virial coefficient may be obtained from the Rayleigh equation below:

$$\frac{Kc}{R_\theta} = \frac{1}{M_w} + 2B_{22}c \qquad\qquad 5\text{-}21$$

K is a system-specific constant which may be calculated as follows:

$$K = \frac{4\pi^2 n_o^2 (dn/dc)^2}{N_A \lambda^4} \qquad\qquad 5\text{-}22$$

where n_o is the refractive index of the solvent, (dn/dc) is the refractive index increment of the solvent-solute system, N_A is Avogadro's constant and λ is the wavelength of the laser.

Upon determination of the molecular weight of the protein, a dimensionless second virial coefficient A may be calculated from[101]

$$\frac{KcM_w}{R_\theta} = 1 + 2A\varphi \qquad\qquad 5\text{-}23$$

An approximate value of the protein volume fraction φ may be determined using the hydrodynamic diameter d_h as.

$$\varphi = \frac{N_A \pi c \, d_h^3}{6 M_w}$$

5-24

Therefore, the dimensionless form of the second virial coefficient may be calculated from the dimensional second virial coefficient as follows:[44]

$$A = \frac{6 B_{22} M_w^2}{N_A \pi d_h^3}$$

5-25

The dimensionless second virial coefficient was calculated in order to ease comparison of second virial coefficient values from the present study with previous studies.

5.4 MATERIALS AND METHODS

5.4.1 Protein Preparation

Horse spleen apoferritin (Sigma-Aldrich Co., St. Louis, MO) was dialyzed at 4°C overnight into 50 mM Tris-HCl buffer (pH 7.4 with 150 mM NaCl and 10 mM NaN$_3$) using dialysis cassettes with a 10 kDa molecular weight cutoff (Pierce Biotechnology,

Rockford, IL). Preparative size exclusion high performance liquid chromatography (SEC-HPLC) was then carried out to separate apoferritin monomers from oligomers and subunits. A HiPrep 16/60 Sephacryl S-300 High Resolution column (Amersham Biosciences, Piscataway, NJ) was utilized for this separation with 50 mM Tris-HCl buffer (pH 7.4 with 150 mM NaCl and 10 mM NaN_3) as the mobile phase at a flow-rate of 0.5 mL/min. SEC-HPLC was carried out using a CM4000 LDC analytical pump, an SCL-10A VP Shimadzu system controller, and an SPD-10AV Shimadzu detector at a wavelength of 280 nm (Shimadzu Scientific Instruments, Columbia, MD). The chromatogram was recorded using CLASS-VP 7.2.1 software (Shimadzu Scientific Instruments, Columbia, MD).

The purified protein was then concentrated via centrifugation with an Amicon centrifugal filter unit (Millipore Corporation, Billerica, MA) and stored at 4°C until use. Appropriate amounts of cadmium chloride (MP Biomedicals, Solon, OH) were dissolved in ultrapure HPLC-grade water (Alfa Aesar, Ward Hill, MA).

Protein concentration was determined by total protein assay using Bradford reagent (Pierce Biotechnology, Rockford, IL). Fresh solutions were prepared for each experiment and used within 2 minutes.

5.4.2 Methods

5.4.2.1 Static and Dynamic Light Scattering

Multi-angle static and dynamic light scattering were carried out simultaneously. The light scattering system consisted of an ALV 5000/E/EPP instrument, an ALV/LSE-5004 digital correlator and ALV-60X0 4.0 software (ALV, Langen, Germany). Scattering intensity was measured from 90° to 110° at 10° increments. A 22 mW laser (632.80 nm) served as the light source. Samples were placed in 2.5 mL cylindrical glass cuvettes (ALV, Langen, Germany) and capped. Three 10-second measurements were taken at each angle with no more than 5 % deviation between the measurements. For rapidly aggregating solutions, the deviation was increased to 10 %. A (dn/dc) value of 0.195 was used.[102]

Five different protein concentrations were utilized for static light scattering: 0.1, 0.2, 0.3, 0.4 and 0.5 mg/mL. A stock apoferritin solution was first diluted with buffer and finally cadmium chloride solution was added to the solution which was then gently vortexed. Measurements were taken immediately thereafter. Five concentrations of cadmium chloride were used: 0 mM (i.e. no cadmium chloride), 5 mM, 10 mM, 13 mM, and 20 mM.

Dynamic light scattering was carried out independently of static light scattering at 90° for 30 seconds per run, 10 seconds between each run and a total of 1000 runs. Only one concentration of apoferritin was used in this case, 0.2 mg/mL. Five different concentrations of cadmium chloride were used: 0 mM, 10 mM, 13 mM, and 20 mM. Buffer and apoferritin were first mixed and cadmium chloride was added last to obtain the final desired concentration of both apoferritin and cadmium chloride. The mixture was gently vortexed and then placed inside the ALV 5000/E/EPP instrument (ALV, Langen, Germany). The samples were kept in the machine for the full duration of the

experiment. The hydrodynamic radius of the particles in solution was obtained from the third cumulant of a computer-generated Cumulant analysis. The results from the DLS experiments were compared with the results from the DLS portion of the simultaneous SLS/DLS experiments.

All measurements were taken at 298 ± 0.43 K.

5.4.2.2 Crystallization experiments

Crystallization of apoferritin was carried out at 298 K under the same solution conditions as the light scattering experiments using the multiwell batch crystallization set-up described by Bartling *et al.*[21]

5.5 RESULTS AND DISCUSSION

5.5.1 Simultaneous Static and Dynamic Light Scattering

5.5.1.1 Static Light Scattering

Simultaneous SLS and DLS were carried out with apoferritin at concentrations between 0.1 mg/mL and 0.5 mg/mL, and various $CdCl_2$ concentrations ranging from 0 mM to 20 mM. Average Kc/R_θ values are shown in Table 5-1 along with apoferritin molecular

weight at each concentration, calculated volume fraction and KcM/R_θ values. Values of

Kc/R_θ used to determine average Kc/R_θ values are given in APPENDIX D. Each

experiment was carried out at least twice. Figure 5-1 shows the plot of Kc/R_θ against

apoferritin concentration at all concentrations of $CdCl_2$. The molecular weight of

apoferritin was obtained from the intercept of the plot. In each case, the molecular weight

of apoferritin was determined to be between 320,000 g/mol and 400,000 g/mol, which is

close to the expected 456,000 g/mol.[10] For each concentration of $CdCl_2$, KcM/R_θ was

plotted against the protein volume fraction, and A was obtained from the slope as shown

in Figure 5-2. Results from the DLS portion of simultaneous SLS/DLS are summarized in

Table 5-3.

Table 5-1: Table of average Kc/R_θ values obtained from static light scattering and the corresponding calculated values of φ and KcM/R_θ.

$CdCl_2$ Concentration (mM)	Protein Concentration (mg/mL)	Kc/R_θ (mol/g)	Molecular Weight (g/mol)	Volume fraction φ	KcM/R_θ
0	0.1	3.0×10^{-6}	366,311	3.5×10^{-4}	1.10
	0.2	3.2×10^{-6}		7.1×10^{-4}	1.16
	0.4	3.7×10^{-6}		1.4×10^{-3}	1.35
	0.5	3.9×10^{-6}		1.7×10^{-3}	1.44
5	0.1	3.2×10^{-6}	350,405	3.6×10^{-4}	1.12
	0.2	3.6×10^{-6}		7.4×10^{-4}	1.25
	0.3	3.7×10^{-6}		1.1×10^{-3}	1.28
	0.4	4.3×10^{-6}		1.5×10^{-3}	1.49
10	0.1	3.4×10^{-6}	321,520	4.0×10^{-4}	1.10
	0.2	3.6×10^{-6}		8.0×10^{-4}	1.15
	0.3	4.0×10^{-6}		1.2×10^{-3}	1.28
13	0.3	2.4×10^{-6}	402,037	9.6×10^{-4}	0.95
	0.4	2.3×10^{-6}		1.3×10^{-3}	0.93
	0.5	2.3×10^{-6}		1.6×10^{-3}	0.92
20	0.1	2.9×10^{-6}	321,621	4.0×10^{-4}	0.92
	0.3	2.5×10^{-6}		8.0×10^{-4}	0.82
	0.4	2.3×10^{-6}		1.2×10^{-3}	0.73
	0.5	2.0×10^{-6}		1.6×10^{-3}	0.63
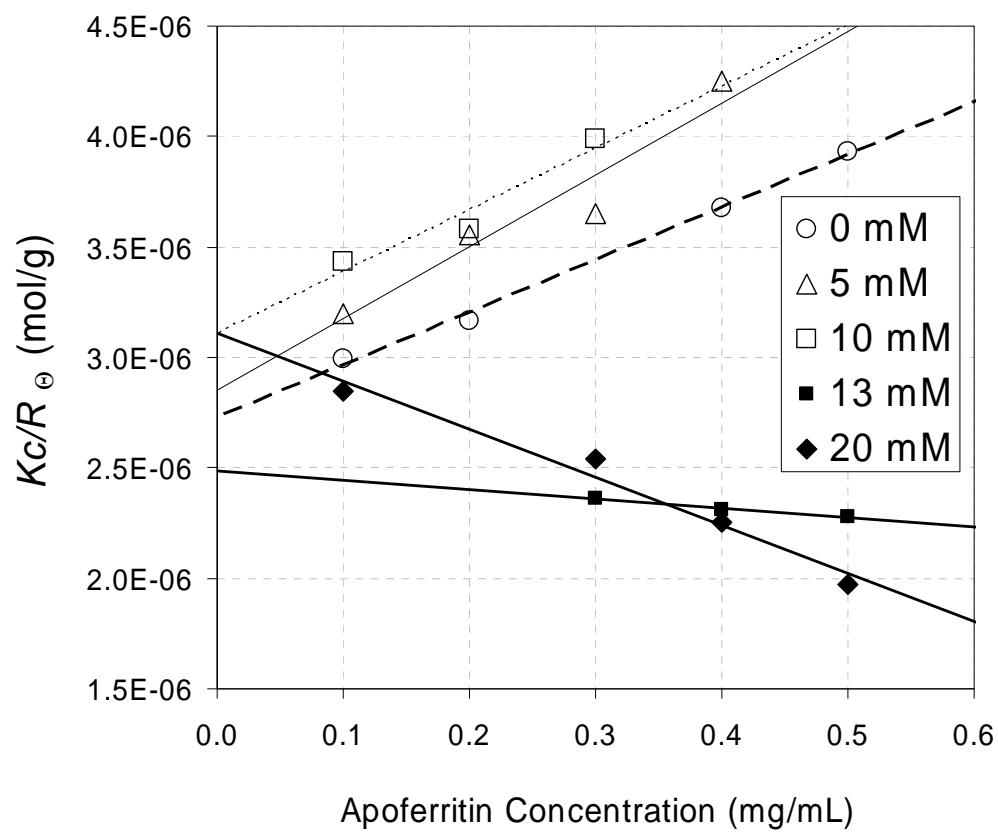
Figure 5-1: Results from simultaneous static and dynamic light scattering experiments. Values for Kc/R_θ obtained from light scattering (SLS) were plotted against apoferritin concentration. The molecular weight of apoferritin was obtained from the intercept.

At 0 mM, 5 mM and 10 mM $CdCl_2$, a positive second virial coefficient was obtained. A salting-in effect was observed as the solution with no added $CdCl_2$ had a smaller A than the solution with 5 mM $CdCl_2$. This salting-in effect was also reported by Bartling[10]. With 13 mM and 20 mM $CdCl_2$, negative A values were obtained. When parallel crystallization experiments were carried out under the same conditions, crystals were formed with 13 mM and 20 mM $CdCl_2$, whereas no crystals were detected in the other solutions (results not shown).
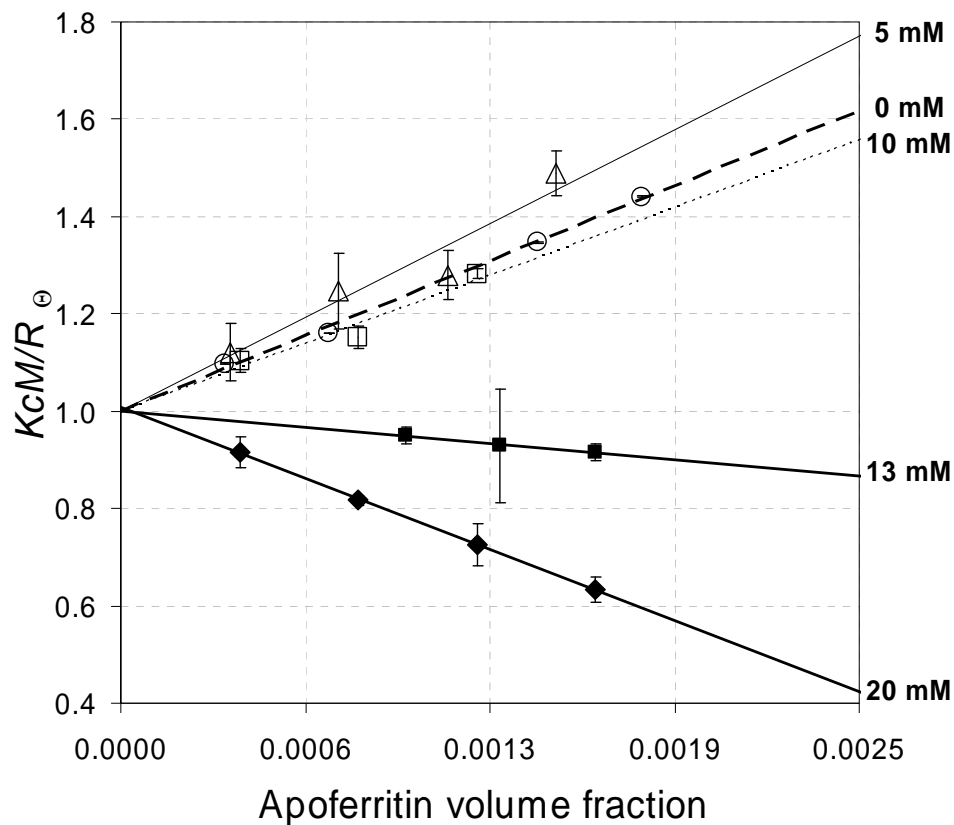
Figure 5-2: Results from simultaneous static and dynamic light scattering experiments. Static light scattering (SLS) used to measure the dimensionless second virial coefficient A from slope of plot of KcM/R_θ vs. φ. The error bars represent standard deviations with $n \geq 2$.

5.5.1.2 Dynamic Light Scattering

Dynamic light scattering carried out simultaneously with the static light scattering yielded the diffusivity slope k_D. The diffusivity values used to obtain k_D are shown in Table 5-2. As expected, k_D was positive for 0 mM, 5 mM and 10 mM $CdCl_2$, and negative for 13 mM and 20 mM $CdCl_2$. As Figure 5-3 shows, the salting-in effect was also observed with DLS, as the k_D of the 0 mM solution was smaller than that of the 5 mM solution. The hydrodynamic radius R_h was extrapolated to zero protein concentration to mimic infinite dilution at each $CdCl_2$ concentration. The results are shown in Figure 5-4 and summarized in Table 5-3. R_h increased from 6.33 nm at 0 mM $CdCl_2$ concentration to 27.80 nm at 20 mM $CdCl_2$, indicating that apoferritin monomers in solution were forming aggregates which increased in size as the $CdCl_2$ concentration increased.

DLS carried out alone begins measurement of R_h as soon as the experiment is started. With simultaneous SLS/DLS, however, background scattering is measured first. In addition, SLS/DLS takes 3 measurements and rejects measurements that deviate by 5% from the mean. In rapidly aggregating solutions, these delays may result in inaccurate values of B_{22} and R_h. This is reflected in Figure 5-4 which compares values of R_h obtained by DLS alone with those obtained by simultaneous SLS/DLS. The initial size of the aggregates in solution obtained by DLS alone is less than that measured by simultaneous SLS/DLS. This indicates that with DLS alone, measurements are taken early in the aggregation process. As the concentration of $CdCl_2$ increases, the gap increases between the R_h values measured by DLS and simultaneous SLS/DLS. Thus in

more supersaturated solutions, simultaneous SLS/DLS may measure skewed values of R_h and B_{22}.

Table 5-2: Diffusivity and normalized diffusivity (D/D_o) values obtained from the DLS portion of simultaneous SLS/DLS. These data are plotted in Figure 5-3.

$CdCl_2$ Concentration (mM)	Concentration (mg/mL)	D ($\mu m^2/s$)	D/D_o
	0.1	30.46	1.01
0	0.2	31.02	1.03
	0.3	31.36	1.04
	0.2	25.93	1.05
	0.3	28.57	1.16
5	0.4	27.70	1.13
	0.5	29.36	1.19
	0.2	26.38	1.03
	0.3	27.64	1.08
10	0.4	27.35	1.07
	0.5	28.26	1.11
	0.3	20.07	0.74
13	0.4	17.98	0.66
	0.5	15.45	0.57
	0.2	50.17	0.70
20	0.3	30.92	0.43
	0.4	26.45	0.37
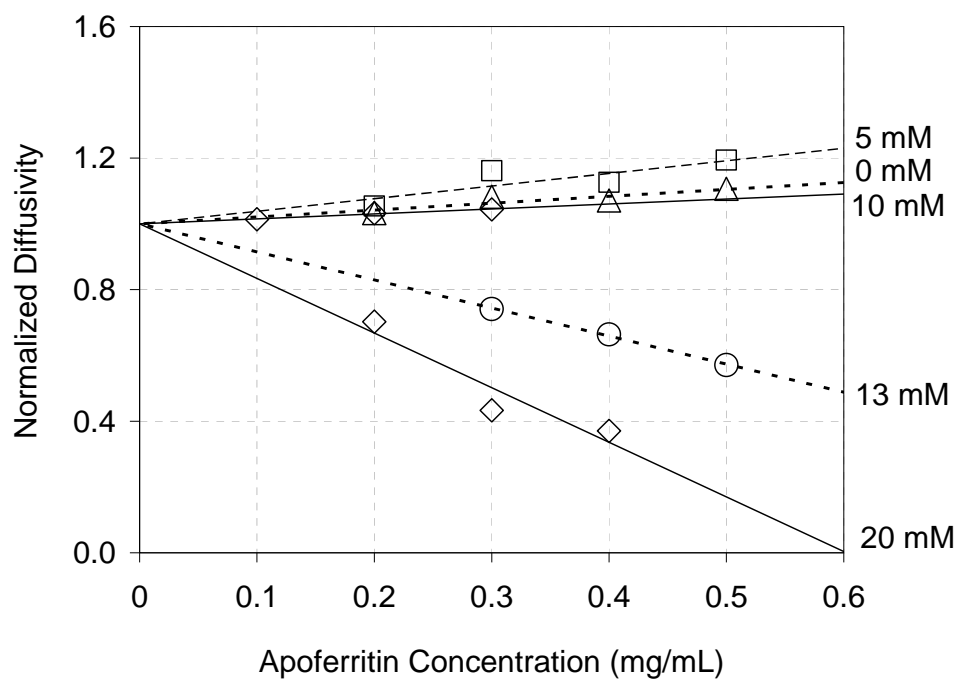
Figure 5-3: The diffusivity slope k_D was obtained as the slope of the plot of normalized diffusivity D/D_o vs. apoferritin concentration at different concentrations of $CdCl_2$.
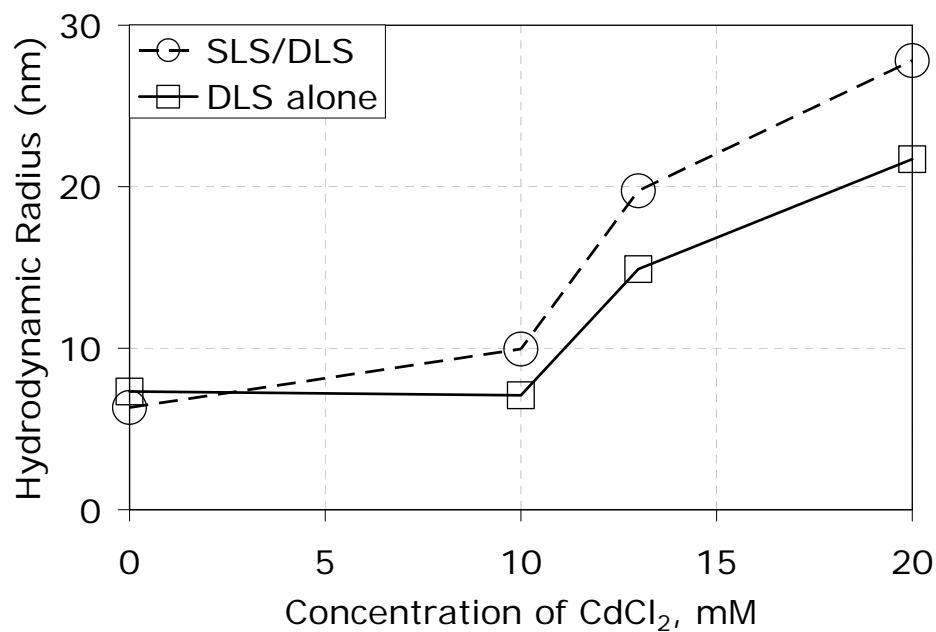
Figure 5-4: Hydrodynamic radii at various concentrations of $CdCl_2$ measured by simultaneous SLS/DLS and by DLS alone.

Table 5-3: Summary of terms obtained from the DLS portion of simultaneous SLS/DLS experiments. Simultaneous static and dynamic light scattering were carried out on apoferritin solutions at 5 different concentrations of CdCl$_2$. The diffusivity slope was obtained from diffusion coefficient data in Table 5-2. The hydrodynamic radius of apoferritin was also measured by dynamic light scattering at these conditions.

CdCl$_2$ concentration (mM)	Diffusivity slope, k_D (mL/mg)	Hydrodynamic radius, R_h (nm)
0	0.151	6.33
5	0.383	8.74
10	0.210	12.68
13	−0.853	19.75
20	−1.660	27.80

5.5.2 Dynamic Light Scattering Alone

In order to ascertain that scattering in the protein solutions was due to protein and not additives, dynamic light scattering (DLS) experiments were carried out on tris-HCl buffer with no additives, and tris-HCl buffer containing 10 mM CdCl$_2$, 10 mM CaCl$_2$ or 10 mM BaCl$_2$. None of the solutions contained any protein. Figure 5-5 shows a plot of R_h as a function of time for the solutions being tested. The size of R_h in these solutions averaged around 0 nm. DLS carried out on a solution of 0.2 mg/mL apoferritin yielded an average R_h of 7 nm, which is the size of an apoferritin monomer,[59] showing that the protein molecules were responsible for scattering observed in protein solutions.
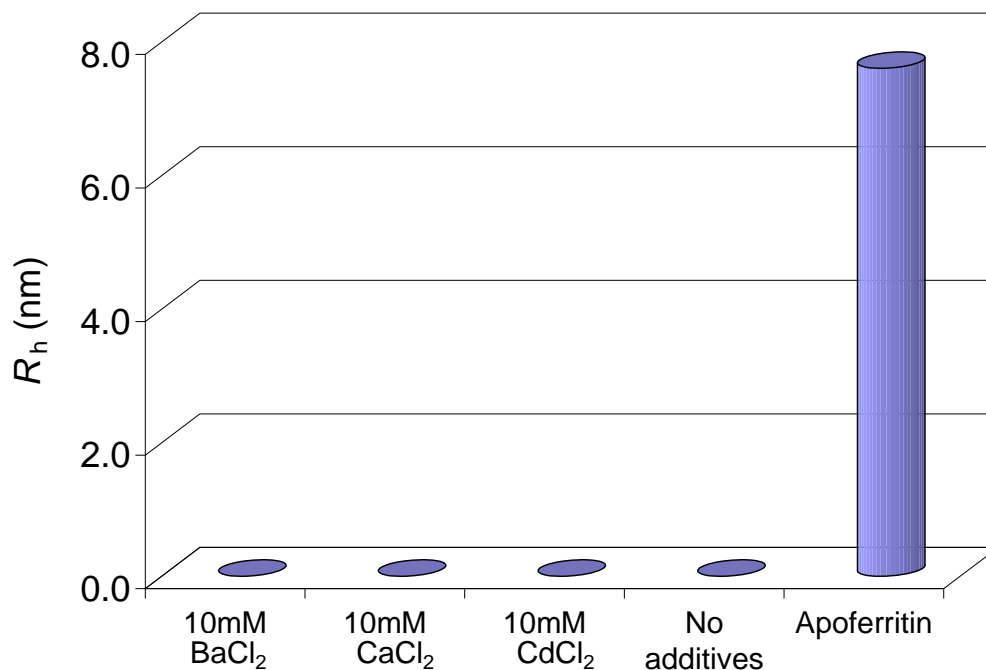
Figure 5-5: Dynamic light scattering of tris-HCl buffer containing various additives.
To determine whether the aggregates detected in protein solutions were due to protein or solvent, dynamic
light scattering (DLS) was carried out on solutions containing various additives but no protein and
compared with DLS results from 0.2 mg/mL of apoferritin. The hydrodynamic radii, shown here after 202
seconds, averaged around zero for the solutions with no protein, and around 7 nm for the apoferritin
solution, showing that particles detected in protein solutions were indeed proteins and not solvent particles.

Dynamic light scattering was carried out on 0.2 mg/mL apoferritin with 0 mM, 10
mM, 13 mM and 20 mM $CdCl_2$. Data obtained at 0 mM $CdCl_2$ was approximately the
same as data obtained at 10 mM $CdCl_2$. As such, results for 0 mM $CdCl_2$ have been
omitted from graphs to prevent cluttering. For these DLS measurements, the
autocorrelation function $G(t)$ and the hydrodynamic radius R_h were obtained as functions
of time. Values obtained for R_h are shown in Table 5-4.

The autocorrelation functions, $G(t)$, defined in Equation 5-1 are shown in Figure
5-6 for three $CdCl_2$ concentrations after 81 seconds. The autocorrelation function may be
used to determine relative aggregate sizes in the protein solutions. The autocorrelation

function decays more slowly when the size of the particles is bigger[103] indicating that the size of the apoferritin aggregates increases with increasing $CdCl_2$ concentration. It also indicates that the 20 mM $CdCl_2$ solution had the largest aggregates of all three solutions.
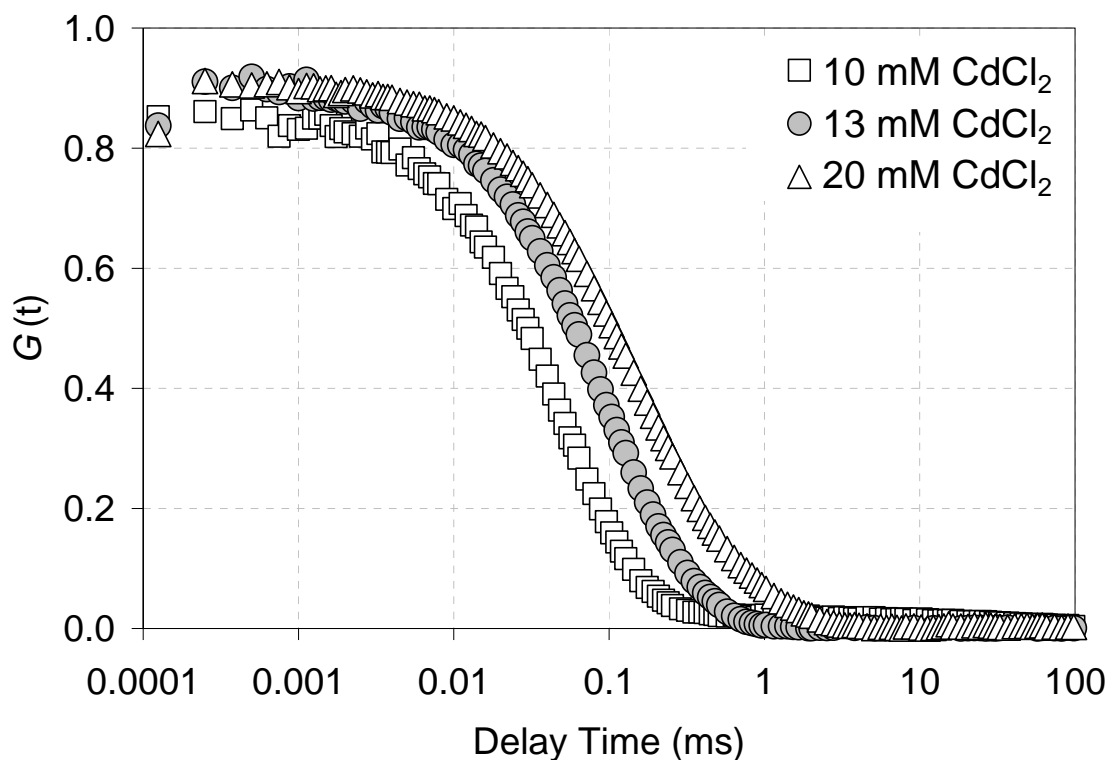
Figure 5-6: Autocorrelation functions obtained from dynamic light scattering (DLS) experiments after 81 seconds. The experiments were carried out on 0.2 mg/mL apoferritin at 10 mM, 13 mM and 20 mM $CdCl_2$.

The size of the hydrodynamic radius was tracked for approximately 11 hours. Figure 5-7 shows a plot of R_h against time for apoferritin in 10, 20 and 30 mM $CdCl_2$. It was shown at the beginning of this section that apoferritin monomers averaged around 7 nm. In the solution containing 10 mM $CdCl_2$, the apoferritin molecules had an average size of 8.05 nm, and therefore remained monomers.
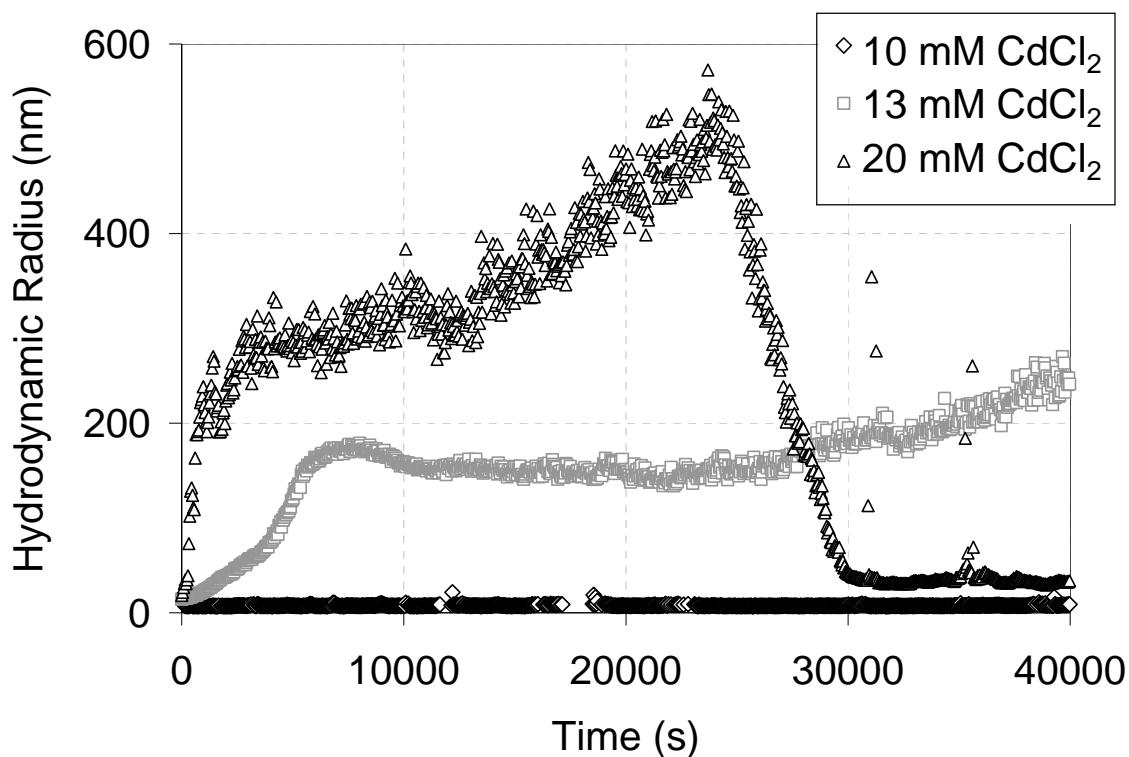
Figure 5-7: Time profile of the hydrodynamic radius of apoferritin aggregates tracked by DLS.

Table 5-4: Summary of data from DLS used to evaluate B_{22} and A.

CdCl$_2$ Concentration (mM)	R_h (nm)	D_o (µm^2/s)	D (µm^2/s)	k_D (mL/mg)	B_{22} (mol mL/g^2)	A
0	6.51	33.24	37.28	0.61	6.66 x 10^{-4}	107.20
10	7.55	28.83	32.17	0.58	6.35 x 10^{-4}	102.23
13	14.86	17.06	16.34	−0.21	−2.33 x 10^{-4}	−37.46
20	21.22	13.18	11.44	−0.66	−7.25 x 10^{-4}	−116.64
30	116.67	2.54	2.08	−0.90	−9.84 x 10^{-4}	−158.43

Aggregation began almost immediately in the 13 mM and 20 mM solutions but was faster in the 20 mM solution. This can be explained by the fact that the 20 mM

118

solution is more supersaturated and therefore nucleation is faster than in the 20 mM solution. Figure 5-7 also shows that after approximately 26000 seconds, the particle size in the 20 mM $CdCl_2$ solution dropped sharply. At the end of the experiment, a white crystalline deposit was observed at the bottom of the cuvette. Thus it is theorized that the drop in particle size was caused by the formed crystals falling to the bottom of the cuvette where they could no longer be detected by the laser.

The diffusivity slope k_D was calculated from the diffusion coefficient using Equation 5-6. The value of D_o was determined from the first R_h data point on each graph. Alternatively, a linear fit to the initial data points can be extrapolated to estimate the value of R_h at time zero. In the 13 mM $CdCl_2$ solution, the extrapolation method yielded an R_h value of 14.40 nm which is close to the initial data point value of 14.86 nm. Diffusion coefficient values calculated at each concentration of $CdCl_2$ using Equation 5-4 and R_h values from DLS are given in Table 5-4. As expected, k_D was positive for 10 mM $CdCl_2$ and negative for 13 mM and 20 mM $CdCl_2$. In the latter solutions, k_D decreased rapidly initially before leveling out. The dimensionless second virial coefficient A was calculated using Equations 5-7 and 5-25, and Figure 5-8 shows that it followed the same trend as k_D. The initial decrease explains why difficulties may arise when measuring the second virial coefficient of rapidly aggregating solutions by SLS. Muschol and Rosenberger[70] suggest that protein interaction rather than aggregation may explain difficulties encountered. However, since aggregation is caused by attractive protein interactions, the findings by Muschol and Rosenberger concur with the findings from the present study.
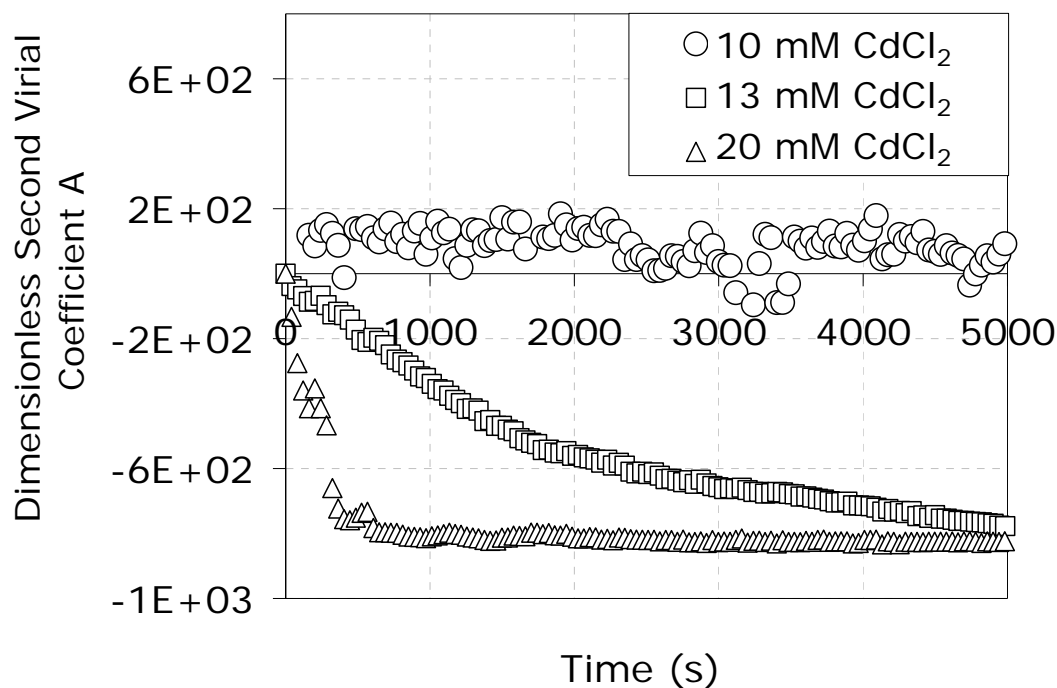
Figure 5-8: The dimensionless second virial coefficient *A* at 10 mM, 13 mM and 20 mM CdCl₂ determined over 5000 seconds.

The dimensional second virial coefficient B_{22} was evaluated for the first 20 seconds at each CdCl₂ concentration and converted to the dimensionless second virial coefficient *A* using Equation 5-25. Data obtained from DLS are summarized in Table 5-4 along with calculated values of B_{22} and *A*. The results were then compared with previously published studies.[10] Values of *A* are shown in Figure 5-9 and summarized in Table 5-5. It is clear that the dimensionless second virial coefficient calculated from k_D closely matched the values obtained by SLS both in the present study and the study by Bartling.[10]
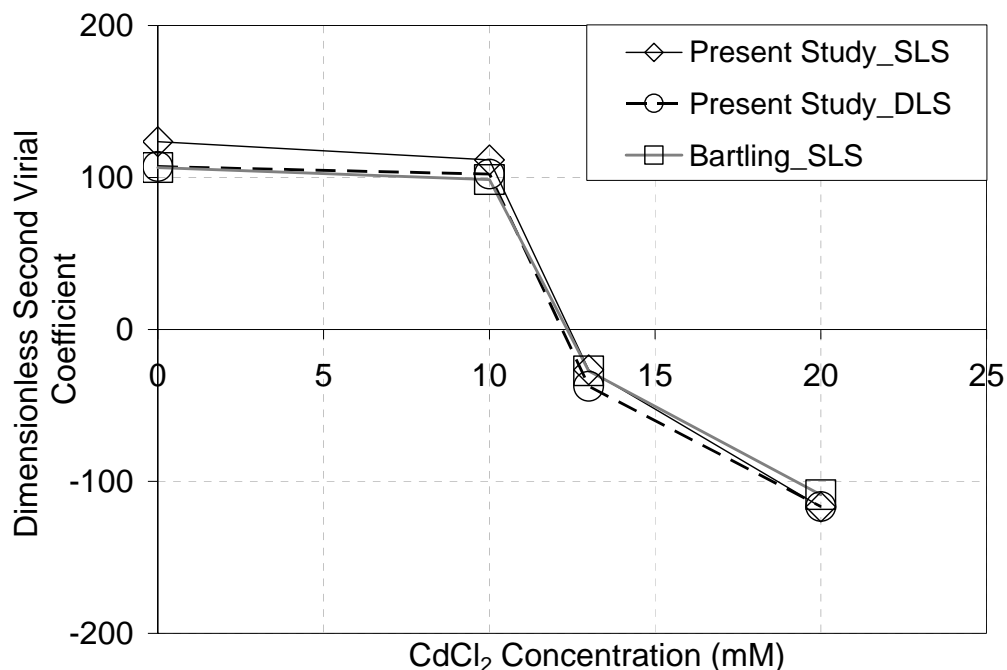
Figure 5-9: The values of the dimensionless second virial coefficient *A* obtained in the present study at 4 concentrations of $CdCl_2$ by SLS and by DLS were compared with each other and with SLS results previously obtained by Bartling.[10] There was an excellent match between the DLS- and SLS-obtained values showing that DLS is a useful alternative to SLS.

Table 5-5: Comparison of dimensionless second virial coefficient A obtained by static light scattering (SLS) and dynamic light scattering (DLS). The dimensionless second virial coefficient was obtained in the present study by static light scattering (SLS) and dynamic light scattering (DLS) and the results compared with previously published SLS results. The error reported for DLS is the deviation from the mean with n = 2. The error reported for SLS is the population standard deviation with n ≥ 2.

$CdCl_2$ concentration (mM)	SLS	DLS	Bartling[10] (SLS)
0	123.53 ± 3.12	107.20 ± 4.80	106.40 ± 9.60
10	111.51 ± 2.30	102.23 ± 7.77	98.55 ± 2.90
13	−26.59 ± 2.00	−37.46 ± 0.98	−27.33 ± 2.79
20	−116.78 ± 23.10	−116.64 ± 16.32	−108.84 ± 7.47

Both sign and magnitude of the second virial coefficient are important in predicting crystallization, and it should be noted that there is consistency in the sign of A at all concentrations of cadmium chloride. In all cases, there was a decrease in the absolute value of A from 0 mM to 13 mM and an increase from 13 mM to 20 mM. The crossover from a positive A to a negative A also occurred at the same cadmium chloride concentration of approximately 12.5 mM.

In order to determine the efficacy of the DLS method in rapidly aggregating systems, experiments were carried out with 30 mM $CdCl_2$. Aggregation proceeded so quickly that it was impossible to use SLS. However, as Figure 5-10 shows, DLS was effectively used to track aggregation and as a result, the second virial coefficient was successfully measured under these conditions. Figure 5-11 shows the dimensionless second virial coefficient A for the 30 mM $CdCl_2$ solution measured over time and compared with values of A for the solutions containing 10, 13 and 20 mM $CdCl_2$. As expected, A is more negative in the 30 mM $CdCl_2$ solution.
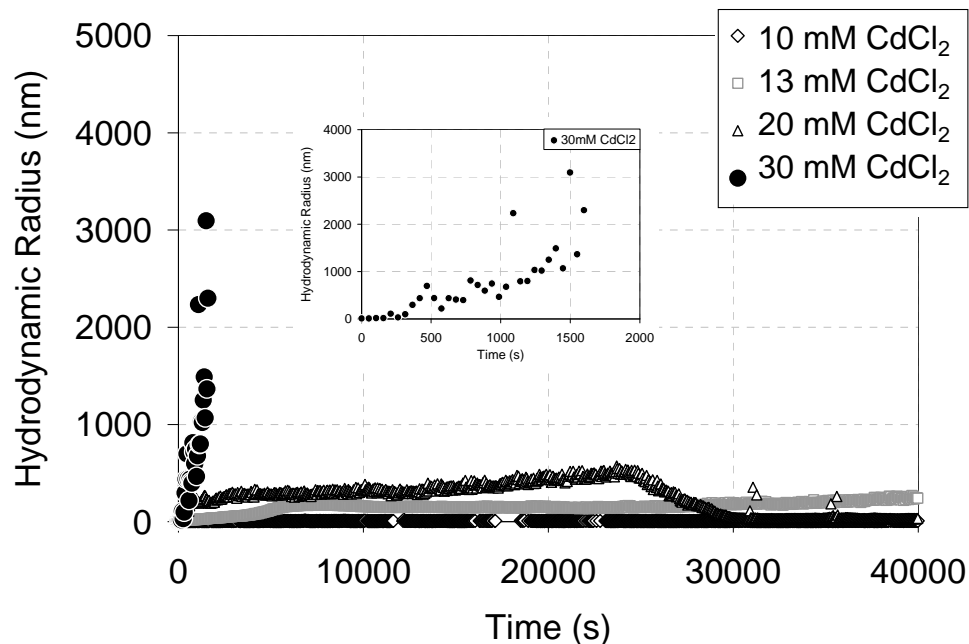
Figure 5-10: DLS was used to track aggregation in an apoferritin solution with 30 mM $CdCl_2$. This solution crystallized so rapidly that static light scattering could not be used to measure interactions. The rate of aggregation of the 30 mM $CdCl_2$ solution is shown relative to 10, 13, and 20 mM $CdCl_2$ solutions. Inset: the size of aggregates vs. time is shown for the 30 mM $CdCl_2$ solution by itself.
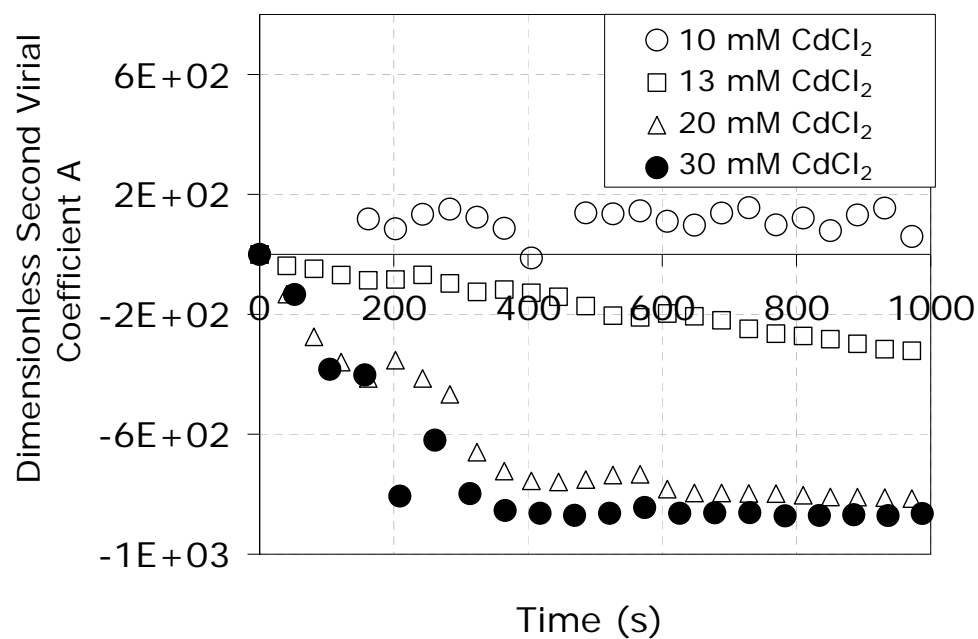
Figure 5-11: The dimensionless second virial coefficient A of the 30 mM $CdCl_2$ solution is shown as a function of time and relative to the other apoferritin-$CdCl_2$ solutions.

5.6 DISCUSSION AND CONCLUSIONS

The present study showed that, for apoferritin in solution with various $CdCl_2$ concentrations, the dimensionless second virial coefficient values obtained through dynamic light scattering (DLS) alone closely matched those obtained by static light scattering (SLS) in both this and previous studies. Additionally, the present study confirmed that the second virial coefficient reliably correlates with the protein crystallization outcome for apoferritin in $CdCl_2$ solutions. Thus, DLS constitutes a dependable method for measuring interactions between protein molecules in solution. As DLS is faster and requires less material than SLS, it is a sensible alternative to the latter even for cases where both methods produce accurate measurements. SLS requires 5 solutions of different protein concentration for each condition tested. In the present study, apoferritin concentrations used were 0.1, 0.2, 0.3, 0.4 and 0.5 mg/mL, whereas only one concentration was used for DLS, 0.2 mg/mL. The volume of each solution used for both SLS and DLS was 1 mL. Therefore, 1.5 mg of apoferritin were used for SLS for each condition whereas only 0.2 mg were used for DLS per condition tested. This represents an 87% reduction in the amount of material necessary for determination of B_{22}. This is significant especially for researchers working with limited amounts of protein, which is often the case.

If there is rapid protein aggregation at the start of an experiment, SLS may not accurately measure the interactions between the particles in solution, as it is not designed for dynamic systems. Furthermore, with biological fluids from experimental animals or human patients in which one wishes to assess the tendency of proteins to precipitate or

crystallize, the volume may be too small for SLS to be effectively applied. In such cases, DLS may be the only reliable alternative, as it is able to continuously capture the diffusivity in small sample volumes.

In summary, we have successfully derived a method by which the second virial coefficient may be accurately determined by dynamic light scattering alone. Furthermore, we confirmed that the second virial coefficient reliably correlates with the protein crystallization outcome in the apoferritin-$CdCl_2$ system.

CHAPTER 6: EFFECTS OF DIVALENT CATIONS ON NUCLEATION OF APOFERRITIN AND GAMMA D-CRYSTALLIN

6.1 ABSTRACT

Dynamic light scattering (DLS) was used to study the effect of divalent cations on aggregation and crystallization of two proteins found in the lens, gamma D-crystallin and apoferritin. In protein systems where crystallization was successfully induced, DLS was used to track aggregation and determine nucleation kinetics through estimation of key quantities such as the critical radius R_c, interfacial energy γ, and critical free energy ΔG. The fractal dimension, a measure of the compactness and regularity of aggregates formed during nucleation, was found to be approximately 1.5 for these systems indicating that aggregation occurred in the diffusion-limited cluster-cluster aggregation regime. This implies that aggregation that led to crystallization was limited only by diffusion, with particles sticking together irreversibly on contact. However, the presence of an energy barrier $> k_B T$ in the aggregating systems in the present study suggests that aggregation proceeded by reaction-limited cluster-cluster aggregation initially. Thus, initially, collisions between protein monomers or clusters did not always result in formation of aggregates. The second virial coefficient, B_{22}, was also determined for each system using

DLS and found to be negative under crystallizing conditions. Thus B_{22} was found to effectively predict crystallization for the conditions studied.

6.2 INTRODUCTION

Cataracts are the leading cause of blindness worldwide[104] and the only cure currently available is surgical removal of the lens and replacement with a plastic lens.[46; 48] This surgery is unaffordable for the majority of individuals suffering from cataract, making it vital that early, non-invasive diagnostics and alternative cures be developed.[48]

Many conditions are associated with the incidence of cataracts, including ageing and smoking.[3] These conditions are augmented by the lack of protein turnover in the lens.[32] The proteins in the center of the lens are approximately the same age as the individual.[15] As the lens proteins are continuously modified over a lifetime, they sustain substantial damage over time through modifications that result in their instability.[48; 105] Insolubilization of the lens proteins, i.e. crystallization, aggregation, or precipitation, may occur as a result, leading to cataract formation.[48; 105] The incidence of cataracts is also associated with an increase in the concentration of divalent cations in the lens.[3; 106]

Human gamma D-crystallin (HGD) is one of the two most abundant of the crystallin family and has a molecular weight of 20 kDa.[36] It has been linked to various congenital cataracts [87] and has also been implicated in the incidence of cold cataract where the lenses of animals grow cloudy at very low temperatures and clear up on warming.[107] Apoferritin, an iron-storage protein found throughout the body, including the lens, has a molecular weight of 456 kDa.[10] Mutations in the apoferritin gene have been

linked to Hereditary Hyperferritinemia Cataract Syndrome (HHCS)[41] which makes it of interest in the present study.

There are two quantities that have been related to the crystallization of proteins from solution: the osmotic second virial coefficient B_{22}, and an interaction parameter k_D, often referred to as the diffusivity slope.[70] The osmotic second virial coefficient B_{22} is a measure of the interaction of the protein molecules with the solvent compared with their interaction with each other.[5; 6; 44; 108] A negative B_{22} indicates overall attractive interactions between the protein molecules while a positive B_{22} indicates overall repulsive interactions.[68; 108] The diffusivity slope k_D is a measure of protein-protein interactions only.[70; 108] A negative k_D implies attractive interactions between protein molecules while a positive k_D implies repulsive interactions. Therefore both B_{22} and k_D are negative under crystallizing conditions. George and Wilson[5; 6] studied crystallization of a number of proteins including lysozyme, bovine serum albumin and ovalbumin, and found that there is a range of slightly negative values of B_{22} from -1×10^{-4} to -8×10^{-4} mol mL/g^2 within which protein crystallization is most likely to occur. They called this range of values the crystallization slot.[5] Subsequent studies with various proteins support the existence of a crystallization slot.[24; 109]

Calcium[48; 110] and barium[63] cations are found throughout the eye, including the lens, and elevated concentrations of both have been associated with cataracts, with concentrations of Ca^{2+} as high as 64 mM being found in cataractous lenses.[83; 110] In studies where frogs were injected with $BaCl_2$ and $CaCl_2$, cataracts formed in the lenses of the frogs.[57] Cataractous lenses extracted from human patients can contain up to 20 times as much Cd^{2+} as normal lenses.[3] In the present study, divalent cations were added to

solutions of HGD and of apoferritin to induce crystallization, and the size of protein aggregates in solution was tracked over time by dynamic light scattering.

Bartling.[10] observed that even at concentrations as high as 50 mM, Ca^{2+} and Ba^{2+} did not induce crystallization in apoferritin. Addition of Cd^{2+} to apoferritin has been shown to induce crystallization of this protein[44; 101] and therefore $CdCl_2$ was used in the present study to induce aggregation and crystallization of apoferritin. In the present study, addition of 10 mM $CdCl_2$ to HGD resulted in immediate precipitation. Since such a low concentration of $CdCl_2$ caused precipitation of HGD, it was deemed unsuitable for use in the present study. In the HGD systems investigated, $CaCl_2$ and $BaCl_2$ were used to induce crystallization since high concentrations of these cations have been linked to cataract disease.

In the present study, when crystallization occurred, DLS was used to evaluate interfacial energy, critical radius and critical free energy of nucleation. The second virial coefficient and the diffusivity slope were also determined for these systems and the results correlated with crystallization outcome showing that both quantities may be used to predict crystallization of HGD and apoferritin.

6.3 THEORY

6.3.1 Dynamic Light Scattering

Dynamic light scattering (DLS) was used to evaluate the diffusion coefficient D using an autocorrelation function $G(t)$ obtained directly from DLS measurements and defined by[69]

$$G(t) = A\exp\left(-2\frac{t}{\tau}\right) + B \qquad\qquad 6\text{-}1$$

where A is a system-specific constant, τ is delay time and B is the baseline. As explained in CHAPTER 5, the diffusion coefficient D can be obtained from $G(t)$. The hydrodynamic radius R_h of protein monomers and aggregates can be determined from D using the Stokes-Einstein equation:[70]

$$R_h = \frac{k_B T}{6\pi\eta_o D} \qquad\qquad 6\text{-}2$$

where k_B is the Boltzmann constant, T is absolute temperature and η_o is the solvent viscosity. The diffusion coefficient D is related to the diffusivity slope k_D as follows:

$$\frac{D(t)}{D_o} = 1 + k_D(t)c \qquad\qquad 6\text{-}3$$

where D_o is the diffusion coefficient at time zero, and c is the concentration. Once the diffusivity slope is determined at each time point, B_{22} may be determined using [69]

$$k_D = 2B_{22}M_w - k_s - v \qquad \qquad 6\text{-}4$$

where M_w is the molecular weight of the protein, k_s is a friction term, and v is the specific molar volume of the protein. The first term in the expression usually dominates in polymer solutions and is therefore used as an approximation in the present study.[69] The accuracy of this method was established in CHAPTER 5.

6.3.2 Energy and Nucleation Kinetics

The nucleation process is illustrated in Figure 6-1. Stochastic and reversible aggregation of protein monomers to form clusters of monomers or aggregates is thought to be the first step in the nucleation process according to the classical theory of nucleation.[17; 18] When the aggregates reach a critical size, they are called nuclei. Rearrangement of aggregates to a crystalline form occurs at the critical size and aggregation becomes irreversible, leading to growth of the crystal.[17] However, the exact nature of a nucleus and the process by which nuclei are formed are not known.[18] The changing size of aggregates in solution during aggregation can be tracked by dynamic light scattering. The free energy change ΔG for the formation of a spherical crystalline aggregate has two contributions: a volume term, which is the free energy released upon formation of a unit volume, and a surface term, which is the free energy difference between the surface of the aggregate and the

bulk of the aggregate. This may be illustrated as shown in Figure 6-2. The surface term is always positive while the volume term is always negative. The overall free energy change therefore goes through a maximum where the size of the aggregates is the critical size and ΔG_c is the critical free energy.
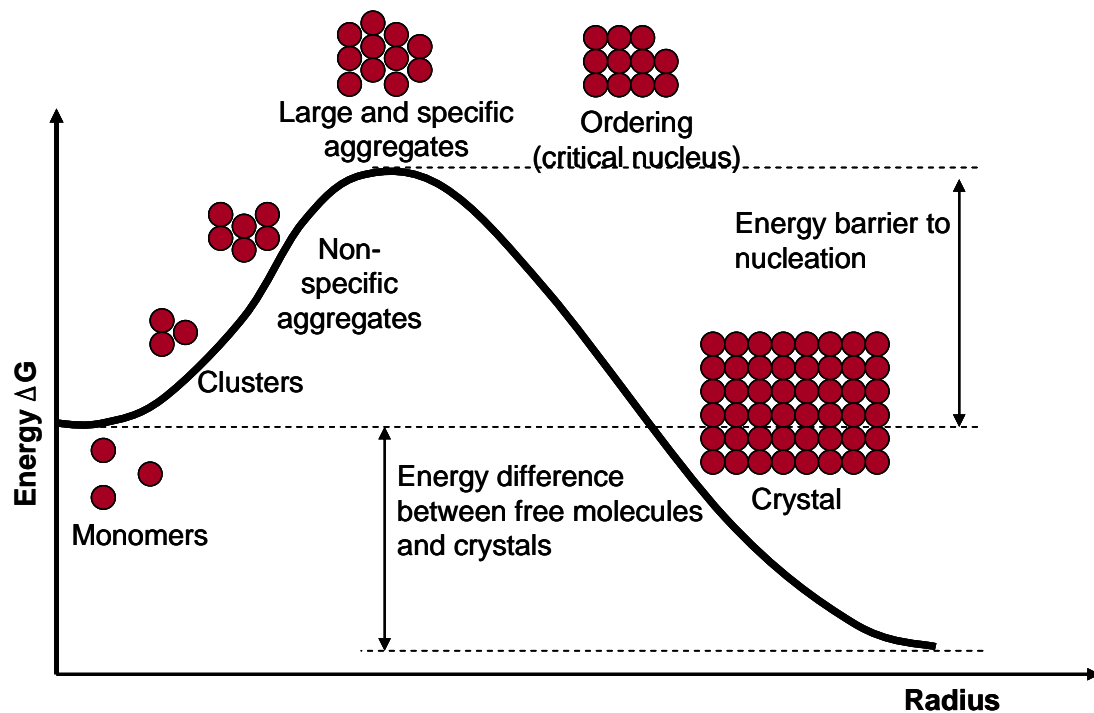
Figure 6-1: Free energy of nucleation as a function of radius illustrating the classical theory of nucleation. (Adapted from McPherson, 1998[17])
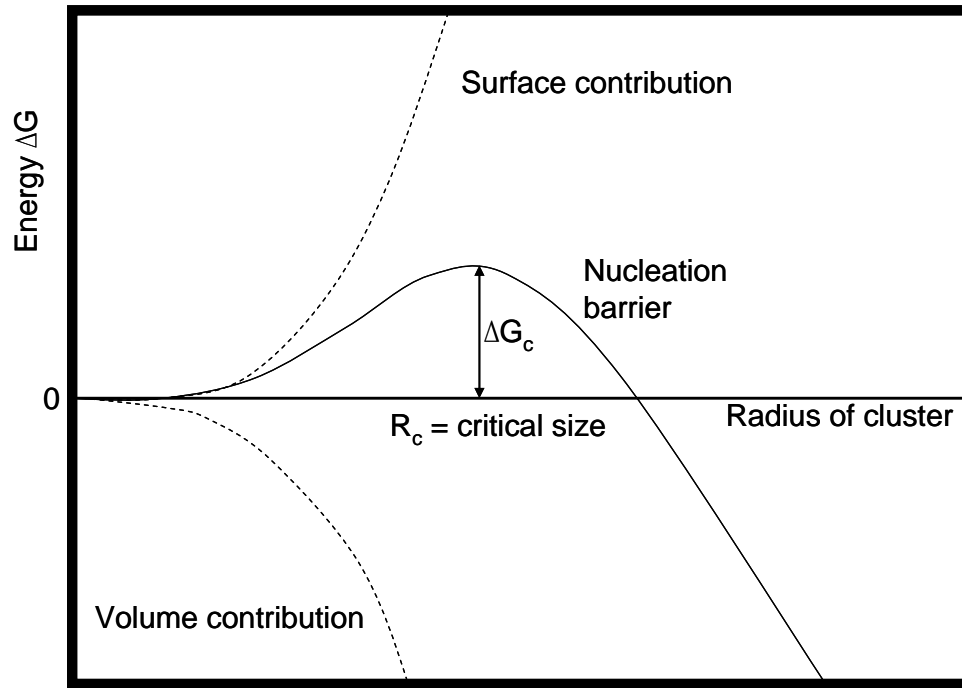
Figure 6-2: Free energy change of nucleation as a function of radius. The surface and volume energy contributions add up to the overall free energy. (Adapted from Mullin, 2001[18])

ΔG is calculated using [19]

$$\Delta G = \frac{-4\pi r^3 k_B T \sigma}{3\Omega} + 4\pi r^2 \gamma \qquad \text{6-5}$$

where r is the radius of the aggregate, k_B is Boltzmann's constant, T is the absolute temperature, σ is the supersaturation, Ω is the protein monomer volume in solution, and γ is the interfacial energy. Equation 6-5 may be used to obtain a plot of ΔG against r and the curve obtained would be similar to that shown in Figure 6-2. The interfacial energy γ

is the amount of energy necessary to create a unit of new surface area on the growing crystal face.[19] Many representations are available for supersaturation. In the present study, the solution supersaturation was determined from $\sigma = \ln(c/s)$ where c is the protein concentration and s is the solubility of the protein.[19] This representation is most often used when studying the energy changes associated with nucleation. As nucleation was investigated in the present study, this representation was appropriate.

The critical radius, R_c, is first determined and then the interfacial energy calculated using Equation 6-6 below. This equation is obtained by setting to zero the first derivative of ΔG with respect to the radius.

$$R_c = \frac{2\,\Omega\,\gamma}{k_B T \sigma} \qquad\qquad 6\text{-}6$$

Equation 6-6 is taken from an article by Malkin and McPherson.[19] However, the article contains a typographical error with a factor of 4 instead of a factor of 2. In the present work, Equation 6-6, which uses the correct factor of 2, is used to evaluate R_c. The critical radius is the size beyond which aggregation is no longer reversible. At this point, the aggregates have overcome the energy barrier and aggregation is irreversible resulting in growth. Below R_c the aggregates are unstable and stochastically grow and dissociate.

Upon determination of R_c and γ, the critical free energy, ΔG_c, may be calculated using Equation 6-7. This equation is obtained by combining Equations 6-5 and 6-6 and setting $\Delta G = \Delta G_c$. This gives

$$\Delta G_c = \frac{-4\pi(k_B T \sigma)}{3\Omega} \frac{8\Omega^3 \gamma^3}{(k_B T \sigma)^3} + 4\pi\gamma \frac{4\Omega^2 \gamma^2}{(k_B T \sigma)^2}$$

$$\Delta G_c = \frac{-32\pi}{3} \frac{\Omega^2 \gamma^3}{(k_B T \sigma)^2} + \frac{16\pi\gamma^3\Omega^2}{(k_B T \sigma)^2}$$

$$\Delta G_c = \frac{-\frac{32\pi}{3}\Omega^2\gamma^3 + 16\pi\gamma^3\Omega^2}{(k_B T \sigma)^2}$$

$$\Delta G_c = \frac{16.\pi.\Omega^2\gamma^3}{(k_B T \sigma)^2}\left(\frac{-2}{3} + 1\right)$$

$$\Delta G_c = \frac{16\pi.\Omega^2\gamma^3}{3(k_B T \sigma)^2} \tag{6-7}$$

The critical free energy is calculated using Equation 6-7. The lower the value of ΔG_c, the more likely it is that irreversible aggregation will occur and the faster the rate of aggregation. If ΔG_c is very low, strong attraction between protein molecules does not allow them adequate time to orient themselves as they come together. Thus, amorphous aggregates, i.e. precipitates, may form rather than crystals.[20]

According to classical nucleation theory, the nucleation rate J can be calculated using $J = A \exp[-\Delta G_c / (k_B T)]$ where A is a pre-exponential constant.[18] The main variables affecting J are interfacial energy, supersaturation, and temperature. The nucleation rate J decreases as the value of ΔG_c increases. Therefore, values of ΔG_c may

be used to gain insight into how the rate of nucleation is affected at different conditions even when A cannot be determined.

6.4 EXPERIMENTAL PROCEDURE

6.4.1 Materials

Horse spleen apoferritin was purchased from Sigma-Aldrich Co. (St. Louis, MO) and purified using size-exclusion chromatography as described in CHAPTER 5. Purified apoferritin was then concentrated via centrifugation with the Amicon centrifugal filter unit (Millipore Corporation, Billerica, MA) and stored in 50 mM Tris-HCl buffer (pH 7.4 with 150 mM NaCl and 10 mM NaN_3) at 4°C until use. HGD was prepared as described in CHAPTER 4. A single batch of HGD was used for the experiments in this chapter.

Protein concentration was determined by total protein assay using Bradford reagent (Pierce Biotechnology, Rockford, IL). Only one concentration of protein was used in every case, 0.2 mg/mL.

Stock solutions of $BaCl_2$ and $CaCl_2$ were prepared by dissolving the appropriate amount in tris-HCl buffer and a final concentration of 10 mM was used for each. Appropriate amounts of cadmium chloride (MP Biomedicals, Solon, OH) were dissolved in ultrapure HPLC-grade water (Alfa Aesar, Ward Hill, MA) to prepare stock solutions. The final concentrations of $CdCl_2$ used were 10, 13, 20 and 30 mM.

Protein solutions were prepared by first mixing tris-HCl buffer and stock protein solution and then adding the appropriate cation solution to obtain the final desired concentration of both protein and cation. Fresh solutions were prepared for each experiment and used within 1 hour for crystallization or 1 minute for dynamic light scattering.

6.4.2 Methods

6.4.2.1 Dynamic Light Scattering

Dynamic light scattering was carried out on a system that consisted of an ALV 5000/E/EPP instrument, an ALV/LSE-5004 digital correlator and ALV-60X0 4.0 software (ALV, Langen, Germany). A 22 mW laser (632.80 nm) served as the light source. Scattering intensity was measured at 90° for 30 seconds per run, 10 seconds between each run and a total of 1000 runs. The mixture was gently vortexed and transferred to 2.5 mL cylindrical glass cuvettes (ALV, Langen, Germany), capped and then placed inside the ALV 5000/E/EPP instrument (ALV, Langen, Germany). The samples were kept in the machine for the full duration of the experiment. The hydrodynamic radius of the particles in solution was obtained from the third cumulant of a computer-generated Cumulant analysis. All measurements were taken at 298 K.

6.4.2.2 Crystallization Experiments

Crystallization of apoferritin and HGD was carried out at 298 ± 0.43 K under the same solution conditions as the light scattering experiments using the multi-well microbatch crystallization set-up described by Bartling.[21]

6.4.2.3 Determination of phase diagrams

The microbatch multi-well system described by Bartling[21] was used to determine the phase diagrams for apoferritin and HGD. A crystallization grid was set up with protein concentration varied along the vertical axis and precipitant concentration varied along the horizontal axis. Each well had a unique concentration of protein and divalent cation i.e. each pair of concentrations was represented by one well. After approximately 4 weeks, crystals were obtained in some wells. Each of these points was noted on the graph and a plot was then obtained showing the solubility of the protein as a function of precipitant concentration. For the apoferritin experiments, the protein concentration was varied from 0 mg/mL to 0.3 mg/mL while Cd^{2+} concentration was varied from 0 mM to 30 mM. With HGD, protein concentration was varied from 0 mg/mL to 0.3 mg/mL and Ba^{2+} and Ca^{2+} concentrations were varied from 0 mM to 12 mM. Low protein concentrations were used to preserve material. All dynamic light scattering experiments used 0.2 mg/mL of HGD or apoferritin. The range of protein concentrations used in determining the phase diagrams straddled the concentrations used in DLS so that the results from both experiments could be correlated.

6.5 RESULTS AND DISCUSSION

6.5.1 Phase Diagrams

In a study by Bartling et al.,[10] it was observed that apoferritin could only be crystallized by addition of $CdCl_2$ and addition of up to 50 mM $BaCl_2$ and 50 mM $CaCl_2$ to apoferritin did not result in crystallization. In the present study, therefore, $CdCl_2$ was used to induce crystallization in apoferritin systems. The phase diagram for apoferritin in the presence of $CdCl_2$ was obtained from 2 experiments using the microbatch method at 298 K. Crystals were allowed to grow for 4 weeks. Table 6-1 shows a grid of apoferritin concentration versus $CdCl_2$ concentration. Apoferritin concentration was varied from 0.00 to 0.30 mg/mL along one axis while $CdCl_2$ concentration was varied from 0.0 to 30.0 mM along the second axis. Wells marked with an "X" indicate where crystals were observed while wells marked with an "O" indicate where no crystals were observed. These results were plotted on a graph of initial apoferritin concentration against $CdCl_2$ concentration as shown in Figure 6-3. The solid solubility line is obtained by joining the outer points of the region where crystals were obtained.

Table 6-1: Grid showing data obtained during microbatch experiments to determine the phase diagram of apoferritin in the presence of $CdCl_2$. Both apoferritin concentration and $CdCl_2$ concentration were varied. Each pair of concentrations was represented by a single well. Data shown were obtained with 2 different experiments. Wells where crystals were observed are marked with an "X" while wells where no crystals were observed are marked with an "O." The "X"es in red indicate the solubility line.

		$CdCl_2$ concentration, mM							
		0.0	**5.0**	**10.0**	**12.0**	**12.5**	**13.0**	**20.0**	**30.0**
	0.00	O	O	O	O	O	O	O	O
	0.01	O	O	O	O	X	X	X	X
Apoferritin concentration, mg/mL	**0.05**	O	O	O	O	O	O	X	X
	0.10	O	X	X	X	X	X	X	X
	0.15	O	X	X	X	X	X	X	X
	0.20	O	X	X	X	X	X	X	X
	0.30	X	X	X	X	X	X	X	X

The solubility of apoferritin was observed to decrease as $CdCl_2$ concentration increased, which indicates that higher concentrations of $CdCl_2$ favor crystallization of apoferritin. Cations are thought to induce crystallization of proteins by becoming hydrated in solution, binding to water molecules and thereby decreasing the concentration of protein in the "free" water.[82] The Hofmeister series ranks cations according to their degree of hydration in protein solutions, with divalent cations being more hydrated than monovalent cations due to their higher charge densities.[4] The decreased solubility of apoferritin at higher concentrations of $CdCl_2$ observed in the present study may be explained by the hydrating action of cations in protein solutions. At higher concentrations of Cd^{2+}, the effective concentration of apoferritin is decreased leading to decreased solubility of this protein.
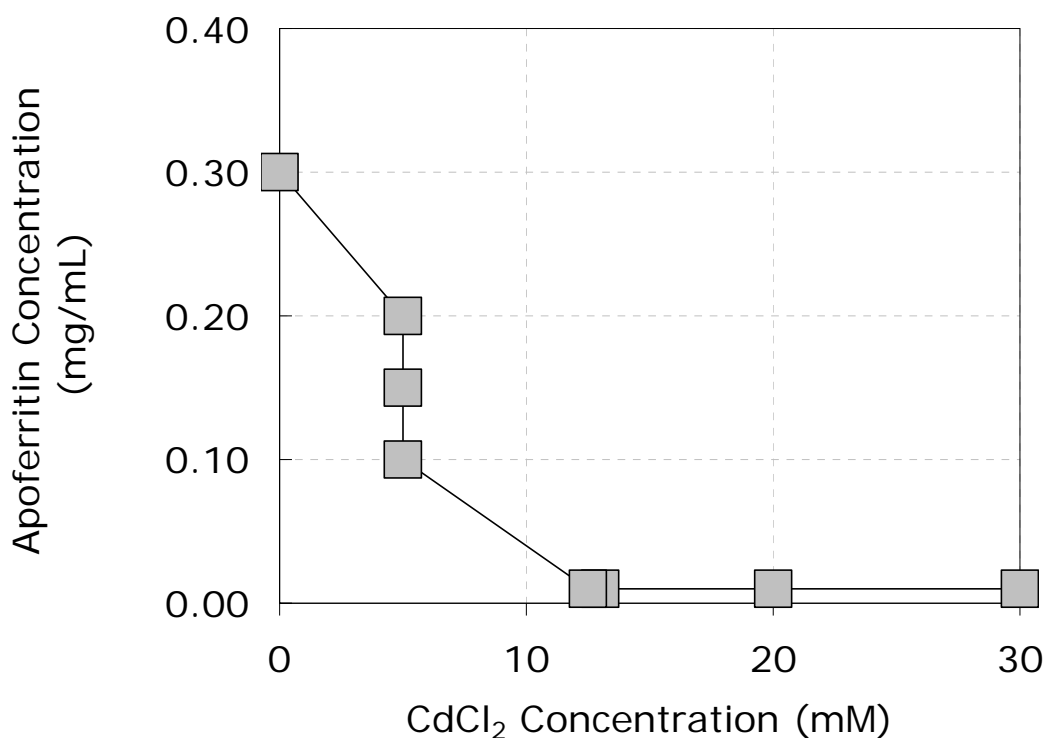
Figure 6-3: Plot showing apoferritin concentration as a function of $CdCl_2$ concentration. Apoferritin concentration was varied from 0.00 mg/mL to 0.30 mg/mL while $CdCl_2$ concentration was varied from 0.0 mM to 30.0 mM. The solid line is the solubility line and it is obtained by connecting the points at the edge of the region where crystals were observed.

In the apoferritin-$CdCl_2$ system, the size of the crystals obtained decreased as the concentration of $CdCl_2$ increased. Figure 6-4 shows photomicrographs of apoferritin crystals obtained with 0.2 mg/mL of apoferritin at 2 different concentrations of $CdCl_2$: 13 mM and 20 mM. The purpose of the photomicrographs was to compare average crystal size at each condition. A Meiji Techno (Santa Clara, CA) video-microscope was utilized for polarized light microscopy (PLM) and images of crystals were taken with a DKC-5000 digital camera (Sony Electronics, San Diego, CA). Average crystal size was determined by measuring crystal lengths using Image Pro Plus 4.0 (Media Cybernetics, Silver Spring, MD) which is an image analysis software. The crystals obtained in the 13

mM $CdCl_2$ solution averaged around 20 μm while in the 20 mM $CdCl_2$ solution, the crystals averaged around 10 μm. This is consistent with studies by Bartling *et al.*[44] where smaller crystals of apoferritin were obtained at higher $CdCl_2$ concentrations. Bartling *et al.*[44] found that csrystals grown in a solution containing 8 mg/mL of apoferritin and 15 mM $CdCl_2$ averaged around 80 μm, while crystals grown in a solution containing 8 mg/mL of apoferritin and 20 mM $CdCl_2$ averaged around 20 μm. The crystals in the present study were smaller because they were grown from a solution of 0.2 mg/mL compared with 8 mg/mL used in the study by Bartling *et al.*[44] In the present study, more crystals were observed in the 20 mM $CdCl_2$ solution implying that crystallization was occurring near the precipitation region of the phase diagram. Bartling *et al.*[44] reported a cubic octahedral shape for apoferritin crystallized in solutions of $CdCl_2$. In the present study, apoferritin crystals obtained exhibited the same cubic octahedral shape.
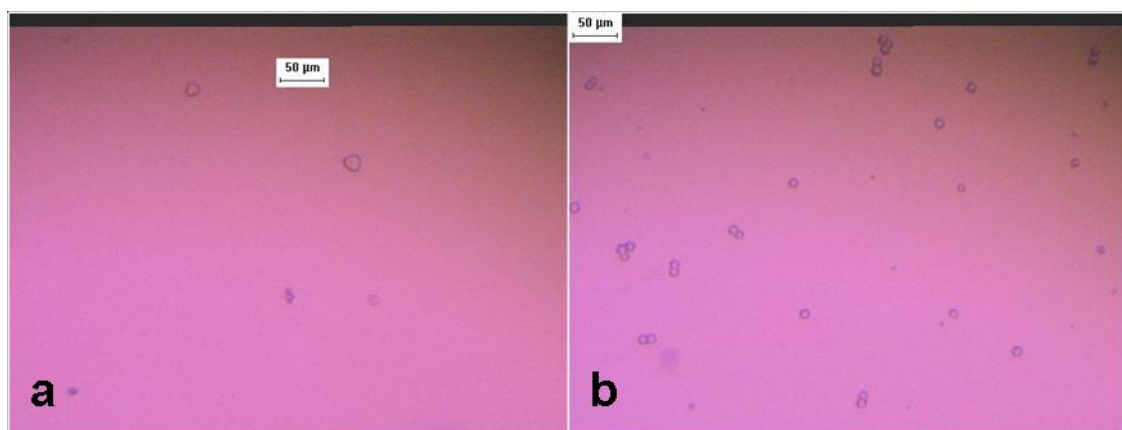
Figure 6-4: Photomicrographs of cubic apoferritin crystals obtained via PLM during determination of the phase diagram in the presence of $CdCl_2$. (a) 0.2 mg/mL apoferritin in solution containing 13 mM $CdCl_2$ (b) 0.2 mg/mL apoferritin in solution containing 20 mM $CdCl_2$

The microbatch method was used to determine precipitant phase diagrams for HGD-CaCl$_2$ and HGD-BaCl$_2$ at 298 K. The results are shown and discussed in CHAPTER 4.

6.5.2 Solubility and B_{22}

Using dynamic light scattering, the second virial coefficient B_{22} was evaluated for apoferritin at 0, 10, 13, 20 and 30 mM CdCl$_2$. Two experiments were performed for each concentration of CdCl$_2$. Values of B_{22} at each CdCl$_2$ concentration are reported in CHAPTER 5 in Table 5-4 along with values of D and R_h used to determine B_{22}. The phase diagram for apoferritin in the presence of CdCl$_2$ was compared with a plot of B_{22} as a function of CdCl$_2$ concentration. Figure 6-5 shows a plot of apoferritin concentration against CdCl$_2$ concentration (extracted from Figure 6-3), and a plot of the second virial coefficient B_{22} against CdCl$_2$ concentration. It was observed that both plots have a similar shape showing that B_{22} correlates well with solubility. Similar observations were made by George et al.[5] who observed that a plot of the solubility of lysozyme had the same shape as the plot of B_{22} against NaCl concentration. This serves to emphasize the role of B_{22} as a means for predicting crystallization. As the value of B_{22} is a measure of interactions between protein molecules, it is reasonable that as solution conditions change, B_{22} values also change. These changes in interaction between protein molecules are reflected in the changes in solubility as solution conditions change. Thus, both the plot of B_{22} against CdCl$_2$ concentration and the plot of apoferritin concentration against CdCl$_2$ concentration in Figure 6-5 follow the same trend. For each concentration of CdCl$_2$ used in the present

study for the B_{22} measurements, only one protein concentration, 0.2 mg/mL, was used. In contrast, a range of protein concentrations from 0.00 mg/mL to 0.30 mg/mL was used to determine the solubility curve. Thus establishing a B_{22} phase diagram using DLS requires less time for each pair of conditions i.e. protein concentration and $CdCl_2$ concentration than establishing a crystallization phase diagram using microbatch crystallization. In the absence of solubility data, B_{22} measurements may be used to establish how the solubility of a protein changes as solution conditions change.
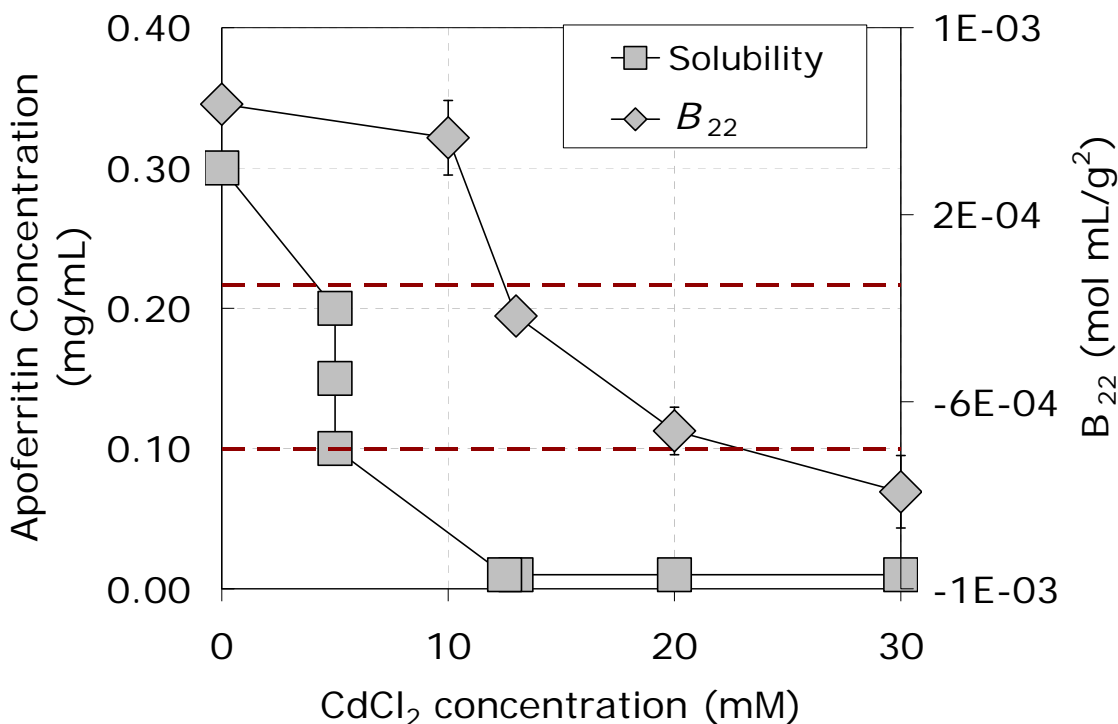
Figure 6-5: Solubility and B_{22} phase diagrams for apoferritin in solutions containing $CdCl_2$. The error bars for the B_{22} plot indicate two measurements at each point. The missing error bars are contained within the data points. The dotted lines indicate the limits of the crystallization slot.

6.5.3 Aggregation

It is theorized that stochastic aggregation of protein monomers is the first step in the nucleation process.[17; 18] When the aggregates reach a critical size, they are called nuclei, and further aggregation becomes irreversible, leading to crystal growth.[17] However, the exact nature of a nucleus and the process by which nuclei are formed are not known.[18] In the present work, crystallization of proteins was induced by addition of divalent cations. Dynamic light scattering (DLS) was used to track the size of the protein aggregates as a function of time. DLS could not distinguish between aggregates, nuclei and crystals, however, and only yielded the size of particles in solution regardless of their precise structure. DLS detected that upon addition of cations, the protein molecules in solution began to form aggregates. The DLS setup used in the present study can detect aggregates in solution ranging in radius from 1 nm to about 1000 nm. Outside of these limits, there can be little confidence in the R_h values measured.

Aggregation was induced in apoferritin by addition of $CdCl_2$ to final concentrations of 10, 13, 20 and 30 mM, and a final apoferritin concentration of 0.2 mg/mL in every case. Figure 6-6 shows a plot of R_h against time for apoferritin in the presence of the four different concentrations of $CdCl_2$; data for apoferritin by itself were omitted as they coincide with the data for the 10 mM $CdCl_2$ case. Aggregation was observed at all concentrations except in the 10 mM $CdCl_2$ case. In previous studies, the hydrodynamic radius of apoferritin monomers has been shown to average around 6.5 nm.[101] In the present study, the average hydrodynamic radius of apoferritin in a solution with no divalent cations was 7.3 nm showing that by itself, apoferritin did not exhibit any

aggregation. It can be seen in Figure 6-6 that after approximately 26,000 seconds, the size of the aggregates in the 20 mM solution dropped rapidly. It is theorized that sedimentation of particles occurred in the 20 mM solution resulting in the sudden drop in hydrodynamic radius.

Cations are thought to induce crystallization of proteins by becoming hydrated in solution, binding to water molecules and thereby decreasing the concentration of protein in the "free" water.[82] At higher concentrations of Cd^{2+}, the effective concentration of apoferritin is decreased leading to decreased solubility of this protein. Figure 6-6 shows that the initial rate of aggregation increased as the concentration of $CdCl_2$ added to apoferritin increased. This is possibly due to increased overall hydration of Cd^{2+} at higher concentrations of $CdCl_2$, leading to higher supersaturation of apoferritin hence faster nucleation. In addition, cadmium is a transition element and can form coordination bonds thus connecting molecules of apoferritin via specific "salt bridges."[59; 111] Higher concentrations of Cd^{2+} may result in formation of more salt bridges which may result in faster nucleation.
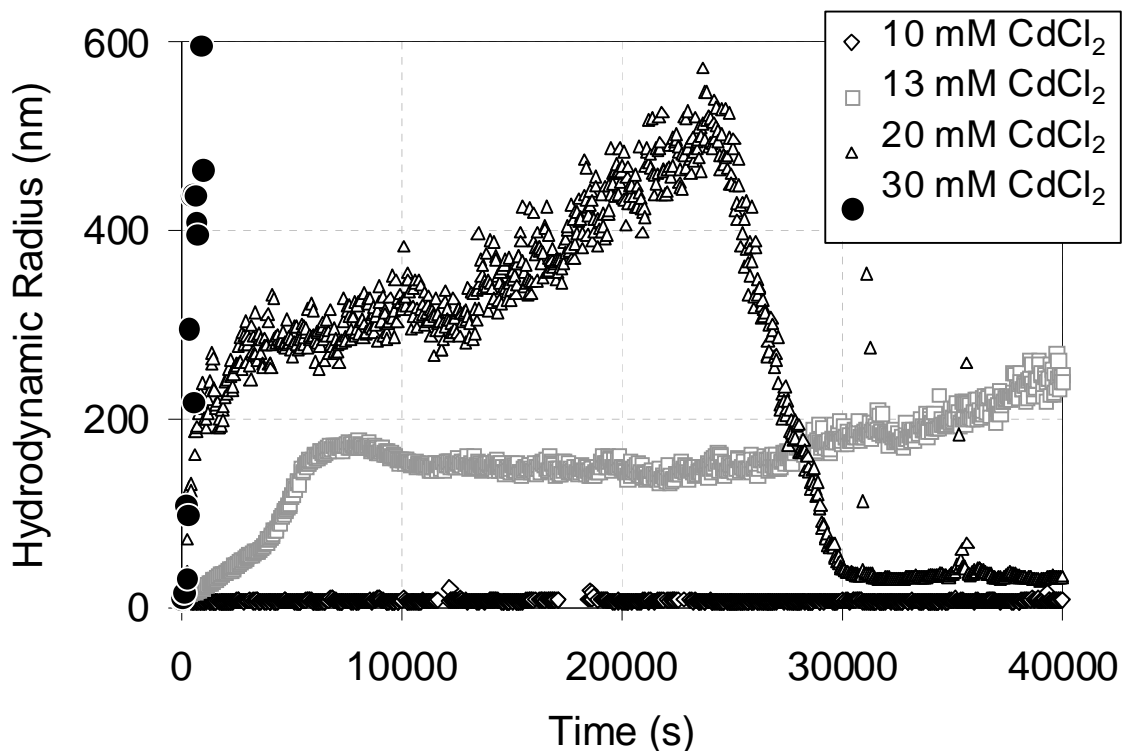
Figure 6-6: Time profile of the hydrodynamic radius of aggregates of apoferritin upon addition of various concentrations of $CdCl_2$. The drop in the size of R_h for the 20 mM solution is due to sedimentation that removed particles from the area of detection. The concentration of HGD used in every case was 0.2 mg/mL.

HGD is known to have attractive interactions between monomers so that stable baseline aggregates that do not yield crystals are normally present in HGD solutions.[13; 53] Monomers of HGD have an R_h of approximately 2.5 nm.[86; 87] In the present study, DLS measurements were carried out on a 0.2 mg/mL sample of HGD with no divalent cations added. These measurements showed that aggregates of HGD with $R_h = 18$ nm were present before the start of each experiment in the present study. HGD molecules tend to form aggregates via thiol-mediated aggregation. Typically, dithiothreitol (DTT) is used to reduce the aggregates to monomers. Pande *et al.*[13] used 20 mM DTT in their HGD

solutions and this was sufficient to prevent aggregation altogether. In the present study, 10 mM DTT was used in all HGD solutions. However, this concentration decreased aggregation but did not prevent it altogether which explains why 18 nm aggregates were present in the HGD solutions. Figure 6-7 shows a plot of hydrodynamic radius R_h of HGD aggregates as a function of time in a solution of HGD with no divalent cations, in a solution containing $BaCl_2$ and in a solution containing $CaCl_2$. The inset is the R_h-t plot of HGD in solution with no additives and it shows that the average size of the aggregates in that solution was 18 nm. Figure 6-7 shows that over a period of 14 hours, no further aggregation occurred in the solution of HGD by itself, showing that the aggregates already present in the solution were stable. Addition of $BaCl_2$ and $CaCl_2$ to HGD induced further aggregation which was tracked by DLS for approximately 11 hours. The figure also shows that the initial rate of aggregation was faster with $CaCl_2$ than with $BaCl_2$.

The autocorrelation function $G(t)$, which is defined in Equation 6-1, is derived by comparison of scattering intensities caused by movement of protein aggregates by Brownian motion.[103] At short time delays, where delay refers to the difference between the starting time and the present time, the value of $G(t)$ is high because molecules do not move to a great extent relative to their initial state. At longer delay times, movement of protein aggregates results in less correlation between the initial and final scattered intensity.[103] Thus $G(t)$ decays exponentially to zero at long delay times. The autocorrelation function for solutions with larger aggregates decays slower as the molecules move more slowly through the solution. Larger molecules move slower because diffusion is inversely proportional to size as shown in Equation 6-2. Figure 6-8 shows a partial logarithmic plot of autocorrelation function against delay time for the

HGD-BaCl$_2$ and HGD-CaCl$_2$ systems, and for HGD with no divalent cations added. The autocorrelation measurements shown were taken approximately 24,000 seconds after the start of the experiment. The autocorrelation function of HGD by itself decays first followed by that of HGD-BaCl$_2$, and then HGD-CaCl$_2$. This implies that the size of aggregates was largest in the HGD-CaCl$_2$ solution, showing that CaCl$_2$ induced more aggregation than BaCl$_2$.
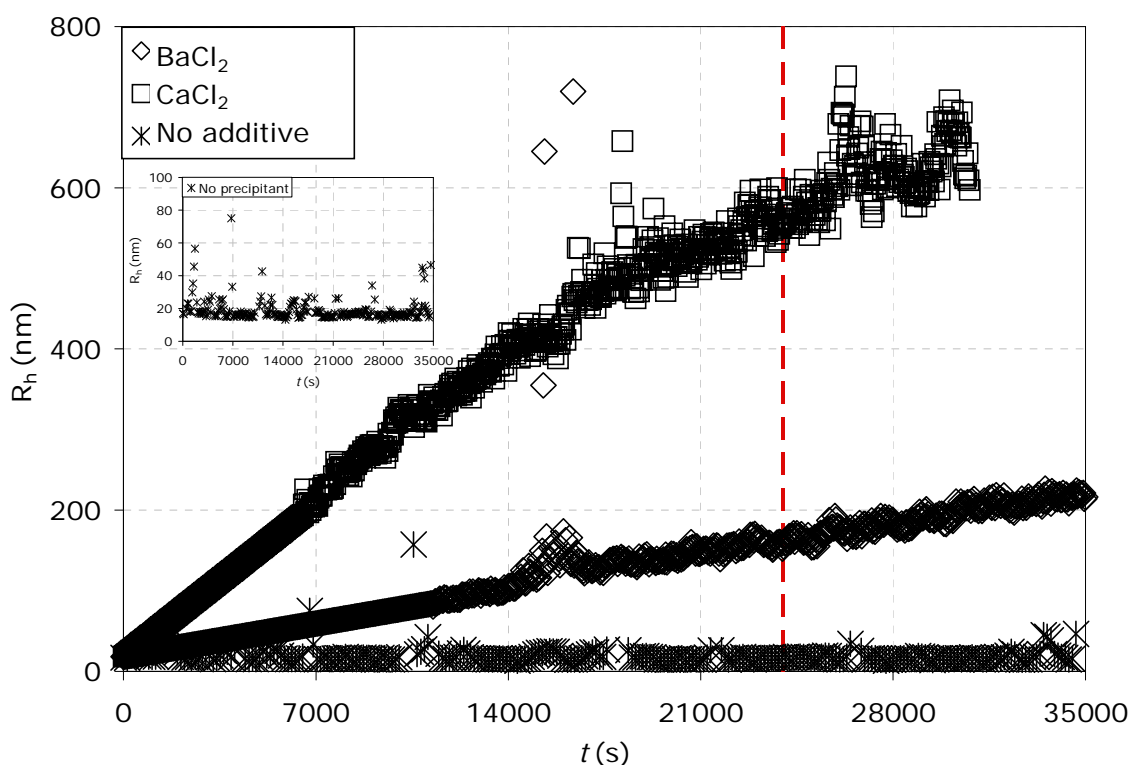
Figure 6-7: The time profile of the hydrodynamic radius of aggregates formed in HGD solutions upon addition of BaCl$_2$ and CaCl$_2$ to a final concentration of 10 mM each measured by DLS. HGD concentration was 0.2 mg/mL in all three systems. The dotted line is at 24,000 seconds. The autocorrelation functions shown in Figure 6-8 are taken from the data in the present figure at 24, 000 seconds. Inset: The R_h-t profile for HGD with no additives showing that the average R_h in this solution is 18 nm.
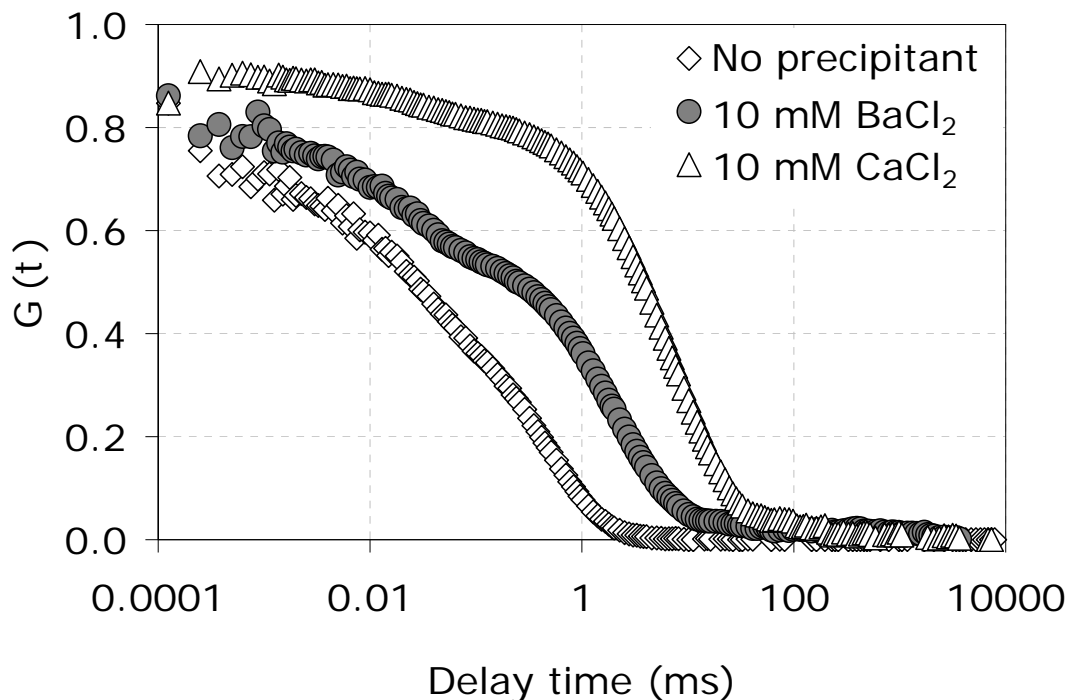
Figure 6-8: Autocorrelation functions for HGD with no precipitant, with $BaCl_2$, and with $CaCl_2$ added. Measurements were taken approximately 24,000 seconds after addition of divalent cations. In all three systems, HGD concentration was 0.2 mg/mL while the final concentration of the cations was 10 mM in each case.

There are 3 steps in the formation of an aggregate: diffusion of monomers, reaction or collision of the particles, and aggregation where the particles stick together. It is thought that there are 2 mechanisms by which aggregation occurs: diffusion-limited cluster-cluster aggregation (DLCA) where diffusion is the rate-limiting step, and reaction-limited cluster-cluster aggregation (RLCA) where reaction is the rate-limiting step.[112] In DLCA, almost every cluster-cluster collision leads to aggregation. With RLCA, an energy barrier to aggregation greater than k_BT is present and a large number of collisions must occur before aggregation occurs.[113; 114] Aggregation is also faster in the DLCA regime than in the RLCA regime.[112] The fractal dimension d_f is a measure of the compactness and regularity of the inner structure of an aggregate.[98; 115] Aggregates with

150

denser structures have higher values of d_f.[115] Faster aggregation results in aggregate structures that are less dense and therefore the value of d_f correlates to the rate of aggregation, with lower values of d_f corresponding to faster aggregation. The value of d_f may be used to determine the mechanism by which protein molecules aggregate: RLCA or DLCA. At long times, the dependence of R_h on d_f becomes a power law:[116]

$$R_h \sim t^{\frac{1}{d_f}}$$
6-8

A value of $d_f < 2$ implies aggregation proceeds by DLCA, while $d_f > 2$ implies aggregation proceeds by RLCA. Using Equation 6-8, d_f was determined for all protein systems exhibiting aggregation in the present study. Table 6-2 shows values of d_f determined for all aggregating solutions. The value of d_f was determined to be less than 2 for all aggregating systems, which implies that aggregation proceeded in DLCA regime. This implies that the aggregation rate was controlled by the diffusion rate of clusters between collisions. In the apoferritin-$CdCl_2$ system, the value of d_f decreased as the concentration of $CdCl_2$ increased, implying that aggregation proceeded faster at higher $CdCl_2$ concentrations. The increasing aggregation rates may be due to increasing hydration of Cd^{2+} at higher concentrations of $CdCl_2$, which in turn leads to decreased solubility of apoferritin.

In the HGD systems, $CaCl_2$ induced faster aggregation than $BaCl_2$. In an endeavor to explain this observation, the Hofmeister series was examined. The Hofmeister series is a scale that qualitatively compares the ability of different ions to precipitate or crystallize proteins from solution.[117] Cations are thought to induce crystallization by binding to

water, effectively increasing the concentration of the protein in the "free" water.[82] Ca^{2+} is slightly higher than Ba^{2+} in the Hofmeister series.[118] This implies that Ca^{2+} is more strongly hydrated than Ba^{2+}, and indeed effective salting-out agents are known to be strongly hydrated.[82] Ca^{2+} therefore increases the effective protein concentration more than Ba^{2+}, leading to faster aggregation. It is also hypothesized that binding of divalent cations to proteins may alter the solubility of the protein, although this mechanism is not well-understood.[118] Divalent cations are higher in the series than monovalent cations which may explain why monovalent cations are less effective than divalent cations at inducing aggregation.[4]

Table 6-2: Summary of nucleation factors in apoferritin and HGD solutions. The fractal dimension d_f was calculated using Equation 6-8 and R_h values obtained by DLS; the initial aggregation rate was determined from a linear fit to the initial data points on the R_h-t profile; R_c was determined from the R_h-log t profile; γ was evaluated using Equation 6-6; ΔG_c was evaluated using the R_c value previously determined and Equation 6-7.

	HGD		Apoferritin		
	10 mM BaCl$_2$	**10 mM CaCl$_2$**	**13 mM CdCl$_2$**	**20 mM CdCl$_2$**	**30 mM CdCl$_2$**
d_f , dimensionless	1.78	1.37	1.27	1.23	0.67
Initial aggregation rate (nm/s)	0.0059	0.0271	0.0124	0.1875	0.6943
R_c (nm)	30.63	27.56	65.10	39.10	31.70
γ (J/m^2)	2.58x 10^{-3}	2.32 x 10^{-3}	2.25 x 10^{-4}	1.35 x 10^{-4}	1.09 x 10^{-4}
ΔG_c (J/mol)	1.01 x 10^{-9}	7.39x 10^{-10}	9.10 x 10^{-9}	1.97 x 10^{-9}	1.05 x 10^{-9}
Exponential Nucleation factor $\Delta G_c/(k_B T)$, dimensionless	2400	1800	980	210	110

6.5.4 Second Virial Coefficient and Crystallization

As discussed in CHAPTER 5, the value of the osmotic second virial coefficient, B_{22}, may be used to predict crystallization in protein solutions.[6] George and Wilson[6] studied crystallization of a number of proteins including lysozyme, bovine serum albumin and ovalbumin, and induced crystallization by addition of precipitants such as NaCl and polyethylene glycol 8000. They found that values of B_{22} which correspond to crystallization lie within a narrow range of slightly negative values. They called this range of values from -1×10^{-4} to -8×10^{-4} mol mL g^{-2} the crystallization slot.[6] More negative values of B_{22} have been shown to correlate to precipitation while more positive values correlate to solutions where no crystallization occurs.[5; 6] Blouwolff and Fraden[119] found, however, that B_{22} of CLC-ecl, a membrane protein, in crystallizing solutions containing n-octyl-β-maltoside detergent and PEG400 were positive and hence did not fall within the crystallization slot. Hitscherich $et\ al.$[120] found that another membrane protein, OmpF porin, crystallized within a range of values of B_{22} from -0.5×10^{-4} to -2×10^{-4} mol mL g-^{2} which they suggested may be a crystallization slot for membrane proteins. Most proteins, other than membrane proteins, studied to date in crystallizing solutions have B_{22} values that fall within the crystallization slot.[29; 44] In general, for each protein, B_{22} measurements must be carried out to determine if they correlate to the occurrence of crystallization of that protein.

In the present study, the second virial coefficient B_{22} and the diffusivity slope k_D were determined for the HGD and apoferritin systems using results from dynamic light

scattering in Equations 6-3 and 6-4. The results for the HGD solutions are summarized in Table 6-3 while the results for apoferritin are summarized in CHAPTER 5 in Table 5-4 and plotted in Figure 6-5. In all HGD and apoferritin systems where crystallization occurred, the value of B_{22} fell within the crystallization slot except for the apoferritin-30 mM $CdCl_2$ system where it fell just outside the crystallization slot. No precipitate was observed in the apoferritin-30 mM $CdCl_2$ system which suggests that the crystallization slot is a rough guideline for crystallization and values outside the crystallization slot may also correlate to crystallization occurring. Addition of $BaCl_2$ and $CaCl_2$ to final concentrations of 10 mM each to HGD resulted in crystallization. While B_{22} for both HGD systems fell within the crystallization slot, it was more negative in the 10 mM $CaCl_2$ solution. Likewise, crystallization of apoferritin occurred upon addition of 13, 20 and 30 mM $CdCl_2$ with the value of B_{22} becoming more negative with increasing $CdCl_2$ concentration. Figure 6-5 shows that in the apoferritin systems where no crystallization occurred, i.e. in solutions containing 0 mM and 10 mM $CdCl_2$, B_{22} was positive. These results are consistent with the crystallization slot described by George et al.[5] They also show that the value of B_{22} can be used to predict crystallization of HGD and apoferritin under the conditions of the present study.

Table 6-3: Summary of B_{22} and k_D values for HGD solutions

Additives	R_h (nm)	D_o (μm^2/s)	D (μm^2/s)	k_D (mL/mg)	B_{22} (mol mL/g^2)
No additive	21.18	11.32	11.46	0.06	6.66×10^{-4}
10 mM $BaCl_2$	23.34	10.52	10.40	−0.05	-6.35×10^{-4}
10 mM $CaCl_2$	26.33	9.45	9.22	−0.11	-7.25×10^{-4}

6.5.5 Factors Influencing Nucleation Kinetics

The size of the critical nucleus and an approximation of the number of units comprising that nucleus can lead to an understanding and model of nucleation. An estimate of the size of the critical nucleus was obtained by examining the hydrodynamic radius R_h as a function of time. Figure 6-9 shows such a plot with a logarithmic timescale for apoferritin in solutions containing 13 mM, 20 mM and 30 mM $CdCl_2$. Using a logarithmic time-scale makes it easier to estimate the point where aggregation is no longer reversible as the point on the R_h -log t plot where the slope increases suddenly. In all three solutions, there is little increase in R_h until well into the runs: approximately 3648 seconds for the 13 mM solution, 283 seconds for the 20 mM solution, and 261 seconds for the 30 mM $CdCl_2$ solution. It is postulated that the rapid increase in R_h at these times correspond to embryos reaching the size of critical nuclei. Prior to these times, embryos grow and redissolve in the stochastic manner associated with classical nucleation theory.[18] After the critical nucleus has been achieved, dissolution no longer occurs and growth is rapid. After the rapid growth, the growth rate slows down for approximately 10,000 seconds and then increases again. It is postulated that the decreased growth rate corresponds to transitions on the ΔG–R_h curve, or rearrangement into a crystalline form, which suggests that rearrangement may not occur at the critical radius. It is also possible that the growth rate may slow down due to sedimentation of aggregates. Figure 6-10 shows a plot of R_h against log t for the apoferritin-13 mM $CdCl_2$ solution. An alternative method for determination of the critical radius involves using linear fits to the data below and above

the area where there is a sudden increase in the slope in the R_h-log t plot. The equations for both lines are set equal to each other and the solution gives the time when at which R_c occurs. Using this procedure and the linear fits in Figure 6-10, R_c was determined to be 67 nm in the apoferritin-13 mM $CdCl_2$ solution. This agreed closely with the value determined by visual inspection of the R_h-log t plot, which was 65 nm.

Figure 6-11 shows a plot of R_h against log t for HGD in 10 mM $BaCl_2$ and 10 mM $CaCl_2$ solutions. The value of R_c was greater in the $BaCl_2$ system than in the $CaCl_2$ system which is reasonable since supersaturation was higher in the $CaCl_2$ solution. The change in R_h with time was more gradual in the HGD solutions than in the apoferritin solutions. Therefore in the HGD systems, R_c was determined using linear fits to the data above and below the location of the sudden increase in R_h. Table 6-2 is a summary of nucleation factors, including R_c, evaluated for the protein solutions under study. Theory predicts that higher supersaturation leads to lower values for R_c.[18] As higher concentrations of $CdCl_2$ result in higher supersaturation in apoferritin, lower concentrations of $CdCl_2$ resulted in higher values of R_c. Greater hydration of Cd^{2+} at higher concentrations of $CdCl_2$ results in higher supersaturation and hence lower R_c.
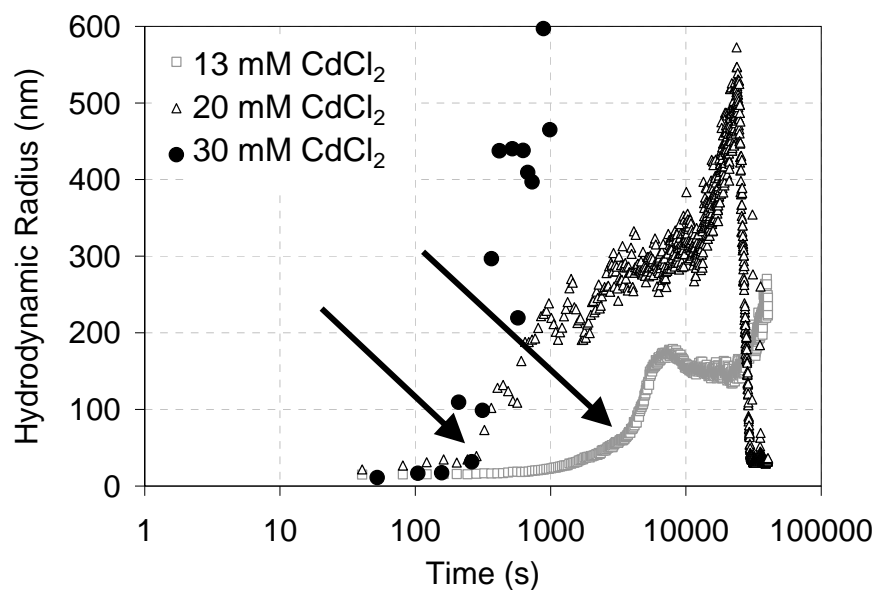
Figure 6-9: Semi logarithmic plot of hydrodynamic radius against time for 0.2 mg/mL apoferritin with three CdCl$_2$ solutions. The arrows indicate the approximate critical radius which is the point where the slope suddenly increases.
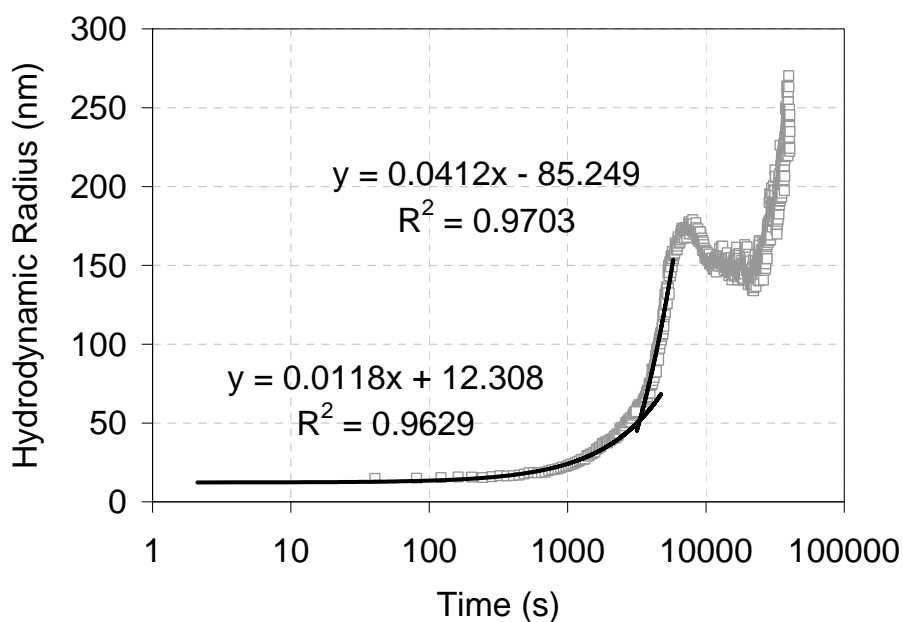
Figure 6-10: Semi logarithmic plot of hydrodynamic radius against time for 0.2 mg/mL apoferritin with 13 mM CdCl$_2$. The lines are linear fits to the data. The intersection of the lines represents the approximate value of the critical radius R_c.
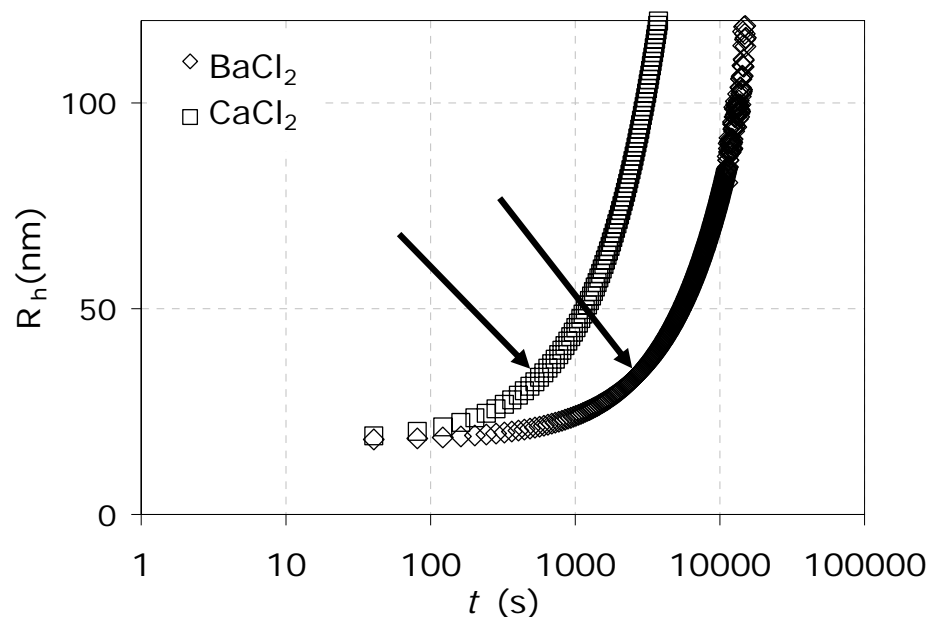
Figure 6-11: Semi logarithmic plot of hydrodynamic radius against time for 0.2 mg/mL HGD with 10 mM BaCl$_2$ and 10 mM CaCl$_2$ solutions. The arrows indicate the approximate critical radius which is the point where the slope suddenly increases.

Factors influencing nucleation were determined for the HGD-CaCl$_2$ and HGD-BaCl$_2$ systems. The energy barrier ΔG_c was evaluated from Equation 6-7 using the R_c value previously determined from the semi logarithmic R_h-t plot, and the interfacial energy γ evaluated using Equation 6-6. The value of ΔG_c was higher in the HGD-BaCl$_2$ system which is expected since Ba^{2+} is less hydrated and thus creates less supersaturation than Ca^{2+}. Figure 6-12 shows a plot of ΔG against R_h for apoferritin in solutions containing 13, 20 and 30 mM CdCl$_2$. The lines through the points are a third-order polynomial fit, which is the functional form associated with the free energy change according to the classical theory of nucleation, to guide the eye. The plot of ΔG against R_h for apoferritin with 30 mM CdCl$_2$ is shown in the inset in Figure 6-12 to show the complete curve below the x-axis. The maxima represent the critical energy barrier ΔG_c.

Values for ΔG_c are summarized in Table 6-2. Nicolis and Nicolis[121] report that the critical energy barrier to nucleation for proteins is of the order of 100 $k_B T$ which is of the order of 10^{-19} J, or 10^{-9} J/mol for apoferritin, at 298 K. The values obtained for ΔG_c in the present study are also of the order of 10^{-9} J/mol and are thus comparable with literature values. It was observed that increasing the concentration of $CdCl_2$ resulted in lower values of ΔG_c. This observation may be explained by the fact that there is a salting-out effect as the concentration of $CdCl_2$ increases. This implies there is a greater hydration of Cd^{2+} leading to a greater driving force to crystallization which lowers the energy barrier. This is reflected in the aggregation rates which also increase as the concentration of $CdCl_2$ increase. Table 6-2 shows that the surface energy γ decreased with increasing $CdCl_2$ concentration indicating that less work needed to be done to move particles to the growing surface. The critical energy barrier ΔG_c was greater than $k_B T$ which is unexpected since values for d_f indicate aggregation occurred in apoferritin solutions by DLCA. A possible explanation is that aggregation occurred by a combination of RLCA and DLCA, with initial aggregation occurring by RLCA and subsequent aggregation by DLCA. An examination of the R_h-log t plot in Figure 6-9 reveals that the R_h of the aggregates increases rapidly after a period where the aggregate size does not increase appreciably. This supports the theory that initial aggregation occurs by RLCA.
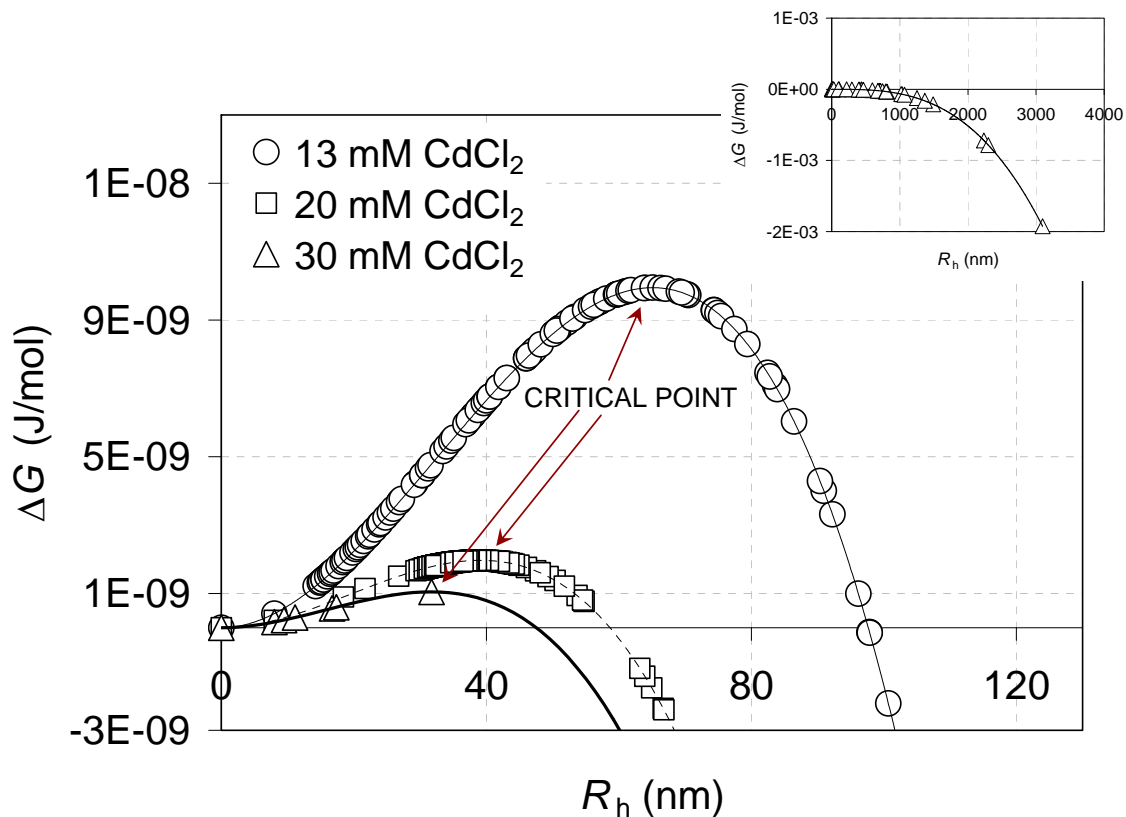
Figure 6-12: The overall free energy of apoferritin with CdCl$_2$ aggregating systems. The arrows point to the critical energy barriers to nucleation. The lines through the points are polynomial fits to guide the eye. The apoferritin concentration was 0.2 mg/mL in every case. The inset is the entire 30 mM CdCl$_2$ curve.

Theory predicts that the nucleation rate J should increase with increasing supersaturation.[18] In the present study, the exponential nucleation factor $\Delta G_c / (k_B T)$ was found to decrease with increasing CdCl$_2$ concentration implying that J increased with increasing CdCl$_2$ concentration as predicted by theory. In HGD solutions, addition of BaCl$_2$ resulted in a higher energy barrier, a higher surface energy, and a slower nucleation rate than CaCl$_2$. These values are summarized in Table 6-2.

In general, it was observed that HGD molecules had a greater tendency to aggregate than apoferritin molecules. Addition of 10 mM CdCl$_2$ to 0.2 mg/mL apoferritin

yielded no aggregation while precipitation occurred immediately upon addition of 10 mM CdCl$_2$ to 0.2 mg/mL HGD. Similarly, Figure 6-13 shows that the addition of 10 mM BaCl$_2$ did not cause aggregation of 0.2 mg/mL apoferritin, whereas it resulted in immediate aggregation in HGD. Bartling *et al.*[10] found that concentrations of BaCl$_2$ as high as 50 mM did not result in crystallization of apoferritin. It is possible that HGD is more sensitive to the divalent cations used in the present study. Also, apoferritin is a much larger molecule than HGD and higher concentrations of the divalent cations may be necessary to induce the same level of aggregation as in HGD. Therefore normalizing cation concentrations to protein moles rather than solution volumes may provide a better basis for comparison. Cadmium is a transition element and can form coordination bonds thus connecting molecules of apoferritin via specific "salt bridges."[59] In addition, apoferritin participates in iron storage in the body by binding iron to 24 nucleation sites in its inner cavity.[43] It is possible that the nucleation sites allow binding between apoferritin and Cd^{2+}.
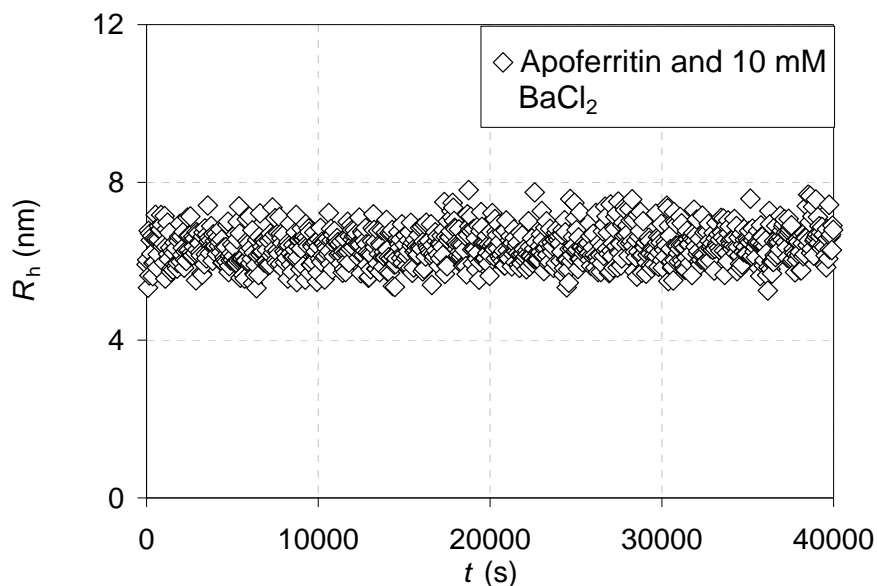
Figure 6-13: Time profile of hydrodynamic radius of 0.2 mg/mL apoferritin upon addition of 10 mM BaCl$_2$.

6.6 CONCLUSIONS

Phase diagrams were determined for HGD-BaCl$_2$, HGD-CaCl$_2$, and apoferritin-CdCl$_2$ systems using a microbatch method. Protein concentrations were varied from 0 to 0.3 mg/mL. Concentrations of CaCl$_2$ and BaCl$_2$ were varied from 0 to 12 mM while concentrations of CdCl$_2$ were varied from 0 to 30 mM. In the HGD systems, tetragonal crystals were obtained at all concentrations of BaCl$_2$ and CaCl$_2$. Crystals of apoferritin obtained under all conditions of the present study were cubic octahedral.

Dynamic light scattering (DLS) was applied to systems of human gamma D-crystallin (HGD) and apoferritin with and without selected divalent cations added. The diffusivity slope k_D and the second virial coefficient B_{22} were determined for all systems and both were negative in systems where crystallization occurred. This shows that values

162

for B_{22} and k_D can be used to predict the likelihood of a protein solution crystallizing. In HGD systems, addition of Ca^{2+} resulted in more negative values of B_{22} and k_D than upon addition of Ba^{2+}, implying that Ca^{2+} was more hydrated in HGD solutions than Ba^{2+}. In apoferritin-$CdCl_2$ systems, B_{22} and k_D decreased with increasing concentration of $CdCl_2$. The B_{22} vs. $CdCl_2$ concentration plot was found to have the same shape as the solubility plot for apoferritin-$CdCl_2$ system. Therefore in the absence of solubility data, B_{22} measurements, which require less material and time than solubility experiments, can be used to establish the solubility of apoferritin.

In systems of HGD and apoferritin where aggregation was successfully induced, the critical radius, the interfacial energy and the critical free energy were determined. As supersaturation increased, initial aggregation rates were found to increase while the critical radius decreased. The interfacial free energies obtained ranged from 0.11×10^{-3} to 3.06×10^{-3} J/m^2 while the range of energy barriers was from 1.05×10^{-9} to 9.10×10^{-9} J/mol.

Comparison of exponential nucleation factors in the apoferritin-$CdCl_2$ system at different concentrations of $CdCl_2$ showed that nucleation proceeded faster at higher concentrations of $CdCl_2$. Therefore, since nucleation is the rate limiting step for crystallization, faster crystallization can be induced in apoferritin systems by increasing the concentration of $CdCl_2$ added. These results provide evidence that DLS can be used to evaluate criteria such as critical energy and nucleation rates which allow characterization of aggregating systems. Knowledge of these criteria provides a means to manipulate crystallization processes to either induce or prevent crystallization.

In summary, phase diagrams were determined for HGD and apoferritin in the presence of selected divalent cations. DLS was used to measure the second virial coefficient and the values obtained confirm that the second virial coefficient can be used to predict the occurrence of crystallization. DLS measurements were used to evaluate nucleation factors leading to determination of the overall free energy of nucleation.

CHAPTER 7: EFFECT OF SOLUBILIZERS ON NUCLEATION AND CRYSTALLIZATION OF GAMMA D-CRYSTALLIN

7.1 ABSTRACT

Crystallization of proteins is thought to begin with stochastic aggregation of protein monomers. The effects of alpha A-crystallin on solutions of human gamma D-crystallin (HGD) where aggregation was induced were examined and compared with the effects of NDSB-201, a commercially available solubilizer. Aggregation and crystallization were induced in HGD by addition of $CaCl_2$ or $BaCl_2$ to solutions of the protein. Aggregation was tracked in HGD solutions by dynamic light scattering. While both alpha A-crystallin and NDSB-201 reduced the occurrence of crystallization, the solubilizing properties of alpha A-crystallin were far superior. Alpha A-crystallin decreased the size of the aggregates in solution and also prevented crystallization from occurring. NDSB-201 did not decrease the size of the aggregates but it decreased the size of crystals obtained and increased the energy barrier to nucleation compared to HGD-$CaCl_2$ solutions with no NDSB-201.

7.2 INTRODUCTION

The crystallins are structural water-soluble proteins that make up 90% of all the proteins found in the lens.[38] They are the major proteins that maintain lens transparency.[30] There are three classes of crystallins in the mammalian lens, namely alpha-, beta- and gamma-crystallins.

Gamma-crystallin has an average molecular weight of 20 kDa.[36] As Figure 7-1 illustrates, there are seven gamma-crystallin genes (gamma A, gamma B, gamma C, gamma D, gamma E, gamma F, gamma S), and the most abundantly expressed gamma-crystallin genes in the human lens are gamma C and gamma D.[15; 39; 40] Many genetic cataracts have been linked to point mutations in the gamma C and gamma D genes, which demonstrates the importance of these two proteins to lens transparency.[40] However, the genetic cataracts linked to gamma D-crystallin are more numerous.[87] Gamma D-crystallin has also been linked to cold cataract wherein the center of the lenses of young mammals becomes opaque when cooled but clear up rapidly upon warming.[14; 53] The 3-D structure of gamma D-crystallin is shown in Figure 7-2.

Alpha-crystallin is composed of heterogeneous complexes of alpha A-crystallin and alpha B-crystallin, as illustrated in the schematic in Figure 7-1, and makes up 40% of the soluble lens protein.[15] Alpha A-crystallin and alpha B-crystallin have molecular weights of 20-kDa each. Approximately 40 molecules of alpha A-crystallin and alpha B-crystallin in a ratio of approximately 3:2 make up the structure of alpha-crystallin. Expression of alpha A-crystallin is restricted to the lens cells. Alpha B-crystallin is

systemically expressed but is mainly found in the eye lens.[122] Alpha A-crystallin and alpha B-crystallin have not been crystallized successfully to date so the quaternary structure of alpha-crystallin remains unknown.[123] Alpha A-crystallin, alpha B-crystallin and alpha-crystallin inhibit insolubilization of the crystallin proteins, including themselves, due to conditions of stress[33] which may be generated by oxidation and chemical reduction, for example.[34] Studies carried out with a mutant form of gamma C-crystallin show that alpha-crystallin may prevent insolubilization of aggregating crystallins by forming complexes with them thus improving their solubility.[40] Results from a study with beta-crystallin and gamma-crystallin suggest that alpha-crystallin selectively binds to denatured proteins and inhibits pathways that lead to non-specific aggregation.[71; 124]
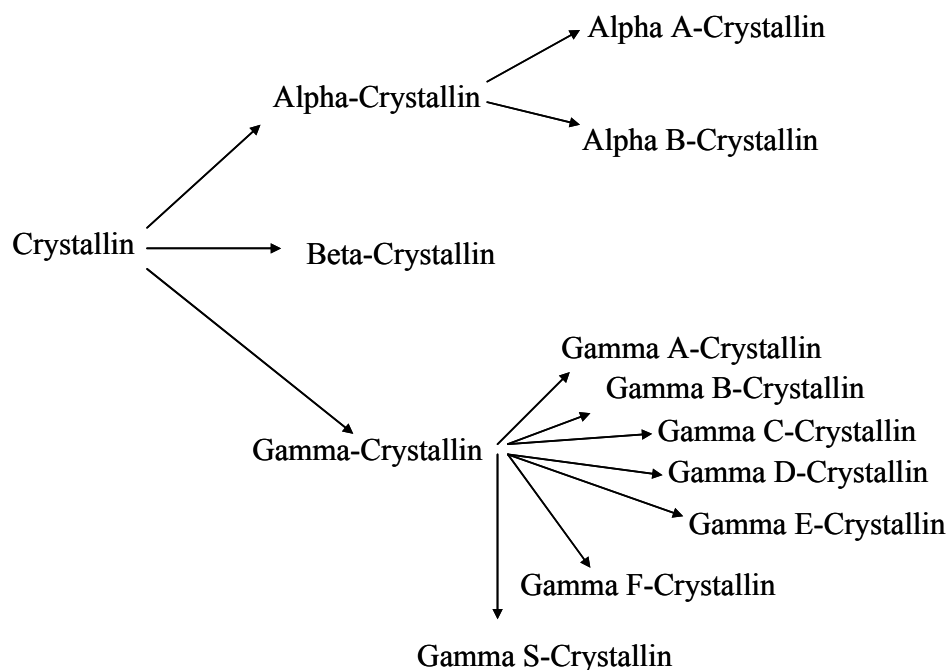
Figure 7-1: Schematic illustrating the relationship between the crystallins.

Cataracts, which are defined as opacity of the lens,[36] are the leading cause of blindness, affecting an estimated 16–20 million people worldwide. Currently, the only cure for cataracts is surgical removal of the lens and replacement with a plastic intraocular lens.[15] The crystallins have been implicated in cataract formation. The lack of protein turnover in the lens results in stress-induced damage to the crystallins accumulating over time.[15] This damage often leads to decreased solubility of the crystallins resulting in the formation of precipitates or crystals. Crystals or precipitates with molecular masses above 50 MDa diffract light and therefore interfere with vision[15; 51] leading to cataract formation.[15; 48; 49; 50] Cataracts have been associated with increased concentrations of divalent cations such as Ca^{2+}, Cd^{2+}, Pb^{2+} and Ba^{2+}.[3; 106]

The exact mechanism by which crystallization occurs is not known. According to the classical theory of nucleation,[95] stochastic aggregation of protein molecules is the first stage of protein crystallization. Aggregates that reach a critical size form a nucleus and rearrange to a crystalline form. More molecules are then added to the nucleus leading to growth of the crystal.

In the present study, Ca^{2+} and Ba^{2+} were added to solutions of HGD and aggregation leading to crystallization was tracked over time by dynamic light scattering. The chaperone activity of alpha A-crystallin was studied by addition of the protein to solutions of HGD where aggregation had been induced. The results were then compared with the solubilizing effects of 3-(1-Pyridino)-1-propane sulfonate (NDSB-201) whose structure is shown in Figure 7-3. NDSB-201 is a commercially available solubilizer

which is thought to prevent interaction between protein molecules, thus leading to increased solubility of the protein.[61]
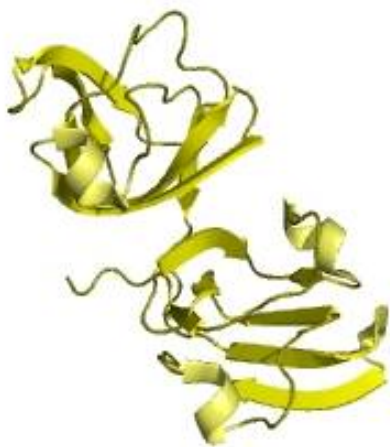
Figure 7-2: 3-D structure of human gamma D-crystallin.
(Source: http://www.ebi.ac.uk/pdbsum/1hk0)
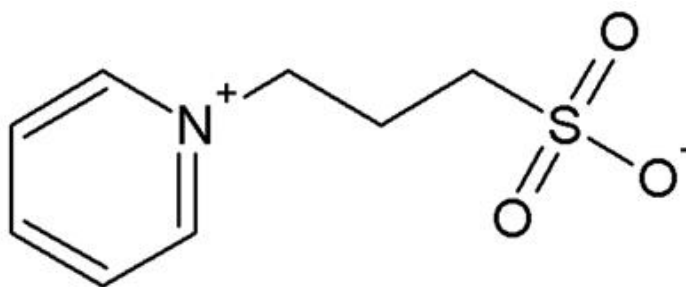
Figure 7-3: Structure of NDSB-201 showing oppositely charged ends of a carbon bridge
(Source: http://www.gbiosciences.com/NDSB_201-desc.aspx)

7.3 THEORY

7.3.1 Dynamic Light Scattering

Dynamic light scattering (DLS) makes use of fluctuations caused by Brownian motion to measure the diffusion coefficient of protein molecules in solution.[68] The hydrodynamic radius of the protein molecules or aggregates can be calculated from the diffusion coefficient using the Stokes-Einstein equation. The diffusion coefficient D_o is also used to calculate the diffusivity slope k_D and hence the second virial coefficient B_{22}. Details of the calculations involved are presented in CHAPTER 5.

7.3.2 Energy and Nucleation Kinetics

Figure 7-4 shows an illustration of a plot of the overall free energy of nucleation as a function of the radius of protein aggregates in solution. It is not known exactly how crystallization of proteins occurs. According to the classical theory of nucleation,[95] which is used in the present study, crystallization of proteins begins with aggregation of proteins. However, it is not known whether aggregation occurs by combination of protein monomers or oligomers, or by joining of clusters (small aggregates), or a combination of all three.[17] Aggregation of protein monomers is initially random, reversible and

stochastic, resulting in the formation of clusters which break apart to monomers. Aggregation is initially reversible due to the existence of an energy barrier ΔG_c. If the aggregates reach a critical size, they overcome the energy barrier and become critical nuclei. It remains unknown whether the critical nucleus is ordered at the start of aggregation or whether it undergoes reorganization at a later stage.[17] In the present study, it is assumed that reordering from random aggregates to crystals takes place after the energy barrier has been overcome. The crystals then grow bigger as more protein monomers or clusters are added.
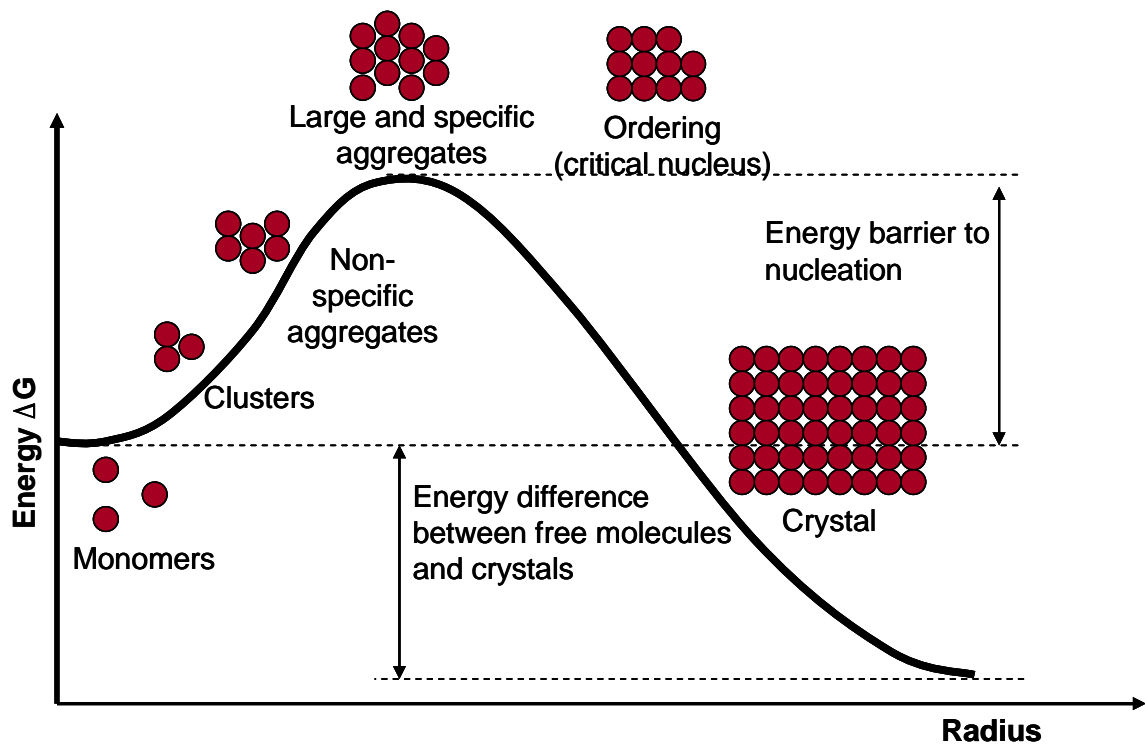
Figure 7-4: Free energy of nucleation as a function of radius. (Adapted from McPherson, 1998[17])

As described in SECTION 6.3.2, ΔG is calculated for a spherical radius by[19]

$$\Delta G = \frac{-4\pi r^3 k_B T \sigma}{3\Omega} + 4\pi r^2 \gamma \qquad 7\text{-}1$$

where r is the radius of the aggregate, k_B is Boltzmann's constant, T is the absolute temperature, σ is the supersaturation, Ω is the protein monomer volume in solution, and γ is the interfacial energy. The interfacial energy γ is the amount of energy necessary to create a unit of new surface area on the growing crystal face.[19]

The critical free energy ΔG_c is the energy barrier that must be overcome for stable nuclei to form. As described in SECTION 6.3.2, ΔG_c is calculated using[19]

$$\Delta G_c = \frac{16\pi \Omega^2 \gamma^3}{3(k_B T \sigma)^2} \qquad 7\text{-}2$$

Aggregates with an overall free energy less than ΔG_c dissociate while those with an overall free energy greater than ΔG_c continue to grow.[18]

Solubilizers like NDSB-201 work by increasing the solubility of proteins[17; 61] thus increasing the critical energy barrier ΔG_c which in turn may increase the interfacial energy γ. Alpha A-crystallin is thought to solubilize proteins by preventing aggregation of proteins,[33] which implies that ΔG_c is so great that it approaches infinity.

7.4 EXPERIMENTAL PROCEDURE

7.4.1 Materials

HGD was expressed using *E. coli* BL21-DE3 clones obtained from the Petrash Lab at Washington University in St. Louis, MO using the method described by Andley. [64] After purification, buffer exchange into 50 mM Tris-HCl buffer (pH 7.4 with 10 mM NaN$_3$) or the same buffer with 150 mM NaCl and 10 mM dithiothreitol (DTT) was accomplished by dialysis with 10 kDa molecular weight cutoff dialysis cassettes (Pierce Biotechnology, Rockford, IL). After dialysis, HGD was stored at 4°C until use. Human alpha A-crystallin was purchased from ProSpec (Rehovot, Israel) and used as received in 20 mM Tris-HCl buffer (pH 7.5).

Stock solutions of CaCl$_2$ or BaCl$_2$ (Sigma-Aldrich Co., St. Louis, MO) were prepared by dissolving the appropriate amounts of each in 50 mM tris-HCl buffer (pH 7.4 with 10 mM NaN$_3$). Appropriate amounts of NDSB-201 (EMD, Gibbstown, NJ) were dissolved in tris-HCl buffer (pH 7.4 with 10 mM NaN$_3$) to prepare stock solutions.

Protein solutions were prepared by first mixing buffer and stock protein solution and then adding $CaCl_2$ or $BaCl_2$ to obtain the final desired concentration of both the protein and the cation. Fresh solutions were prepared for each experiment and used immediately for crystallization or dynamic light scattering. Protein concentration was determined by total protein assay using Bradford reagent (Pierce Biotechnology, Rockford, IL). Only one concentration of HGD was used in every case, 0.2 mg/mL.

7.4.2 Methods

7.4.2.1 Dynamic Light Scattering

Dynamic light scattering measurements were carried out on a system which consisted of an ALV 5000/E/EPP instrument, an ALV/LSE-5004 digital correlator and ALV-60X0 4.0 software (ALV, Langen, Germany). A 22 mW laser (632.80 nm) served as the light source. More details are given in CHAPTER 6. All measurements were taken at 298 K.

7.4.2.2 Crystallization Experiments

Crystallization of apoferritin and HGD was carried out at 298 ± 0.43 K under the same solution conditions as the light scattering experiments using the multiwell microbatch crystallization set-up described by Bartling et al.[21]

7.5 RESULTS

7.5.1 Oxidized HGD vs. Non-oxidized HGD

HGD molecules have a tendency to form intermolecular disulfide bonds with other HGD molecules, resulting in aggregation of HGD. Dithiothreitol (DTT), which is a reducing agent, prevents aggregating of proteins by forming intermolecular disulfide bonds with them.[12] In the experiments in CHAPTER 4 and CHAPTER 6, 10 mM DTT was used in HGD solutions and the average R_h of HGD was 18 nm in these solutions. The HGD production and purification processes used in SECTION 7.5.2 were the same as for the HGD batch used in the experiments presented in CHAPTER 4 and CHAPTER 6, with the same migration of bands showing similar purity of HGD. However, in the experiments in SECTION 7.5.2, DTT was inadvertently left out of the HGD solution and this resulted in HGD solutions with an average R_h of 73 nm as determined by dynamic light scattering. In the present study, the HGD solution with an average R_h of 73 nm is referred to as oxidized HGD while the HGD solution with an average R_h of 18 nm is referred to as non-oxidized HGD. In the sections following, results are presented from experiments performed with both oxidized and non-oxidized HGD. Results from experiments with oxidized HGD are relevant because oxidation of lens proteins such as HGD has been implicated in cataract formation.[15]

7.5.2 Experiments With Oxidized HGD

Three different concentrations of $CaCl_2$ were added at 298 K to human gamma D-crystallin (HGD) to give a final HGD concentration of 0.2 mg/mL and final $CaCl_2$ concentrations of 20, 30 and 35 mM. Figure 7-5 shows a plot of R_h against time for HGD in solution with no $CaCl_2$ and in solution with 20, 30 and 35 mM $CaCl_2$ added. The plot shows that the 0.2 mg/mL sample of HGD with no $CaCl_2$ added had aggregates with an average R_h around 73 nm initially present in the solution. The aggregates did not increase in size and were therefore stable. As explained in SECTION 7.5.1, the aggregates were larger than the aggregates in the HGD sample used in CHAPTER 6 i.e. 18 nm. Thus, one could speculate that slight oxidation in the absence of DTT caused baseline aggregation.

Addition of all three concentrations of $CaCl_2$ resulted in aggregation of HGD. However, Figure 7-5 shows that it was difficult to distinguish significant differences between the dependence of size on time for the three concentrations of $CaCl_2$. Figure 7-6 shows an R_h-log t plot for the 30 mM $CaCl_2$ solution. An estimation of the critical radius was taken from the intersection of linear fits to the data above and below the point where the slope of the R_h-log t plot suddenly increases. The overall free energy of nucleation was compared for all three solutions. The critical free energy ΔG_c of all three solutions as well as the critical radius R_c and the interfacial energy γ are reported in Table 7-1 along with B_{22} values. The procedures for obtaining these quantities are given in CHAPTER 5 and CHAPTER 6. Figure 7-7 shows a plot of ΔG_c against radius for the 20, 30 and 35 mM $CaCl_2$ solutions. It can be seen that ΔG_c was lowest for the 20 mM $CaCl_2$ case, and highest for the 35 mM case. The higher the value of ΔG_c, the less likely it is that the

protein aggregates will overcome the energy barrier. Therefore, the protein solutions with high ΔG_c remain soluble. Conversely, protein solutions with low ΔG_c values are more likely to yield crystals. Applying this logic to Figure 7-7, it appears that since the value of ΔG_c increases as the concentration of $CaCl_2$ added to HGD increases from 20 to 35 mM, there is a salting-in effect i.e. an increase in the solubility of HGD. However, scatter in the data does not allow this conclusion to be drawn with certainty. This observation introduces another means by which salting-in and salting-out, or decreased solubility, may be observed in protein solutions. The B_{22} values calculated for each solution, and reported in Table 7-1, corroborate this conclusion as the 20 mM $CaCl_2$ solution had the highest B_{22} value and the 35 mM $CaCl_2$ solution had the lowest B_{22} value.
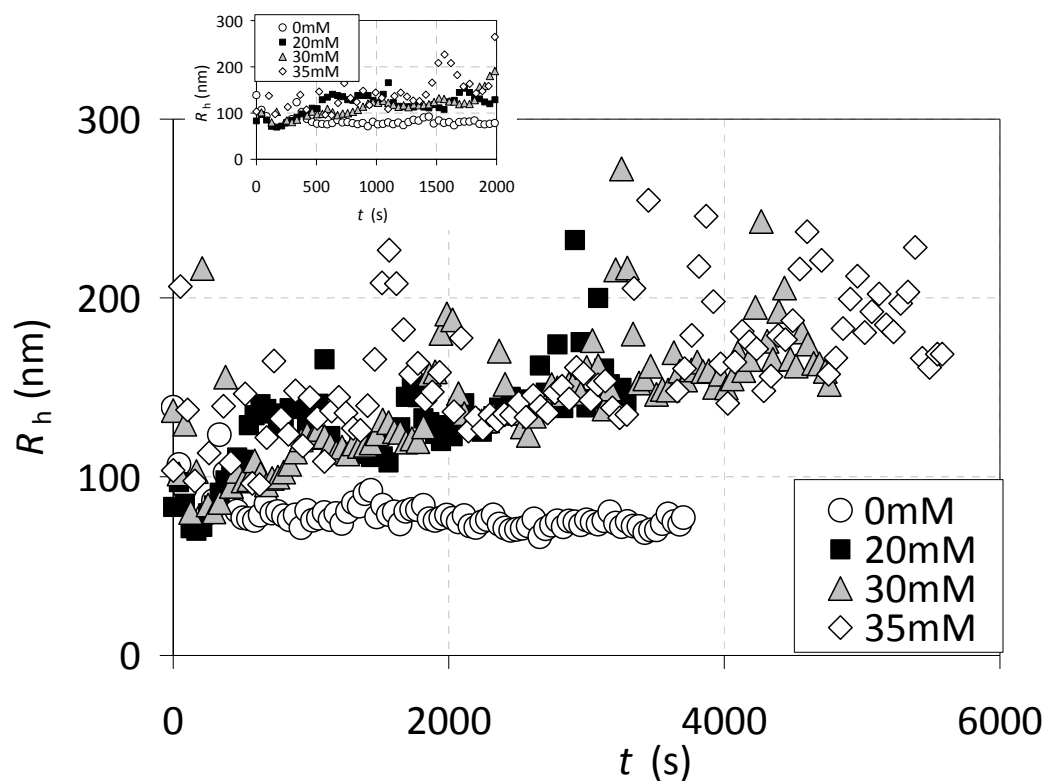
Figure 7-5: Time profile of hydrodynamic radii of HGD upon addition of 3 different concentrations of $CaCl_2$. It is impossible to determine from the plot which $CaCl_2$ concentration induced the greatest aggregation. Inset: The R_h-t plot for all three $CaCl_2$ concentrations over a shorter time scale.
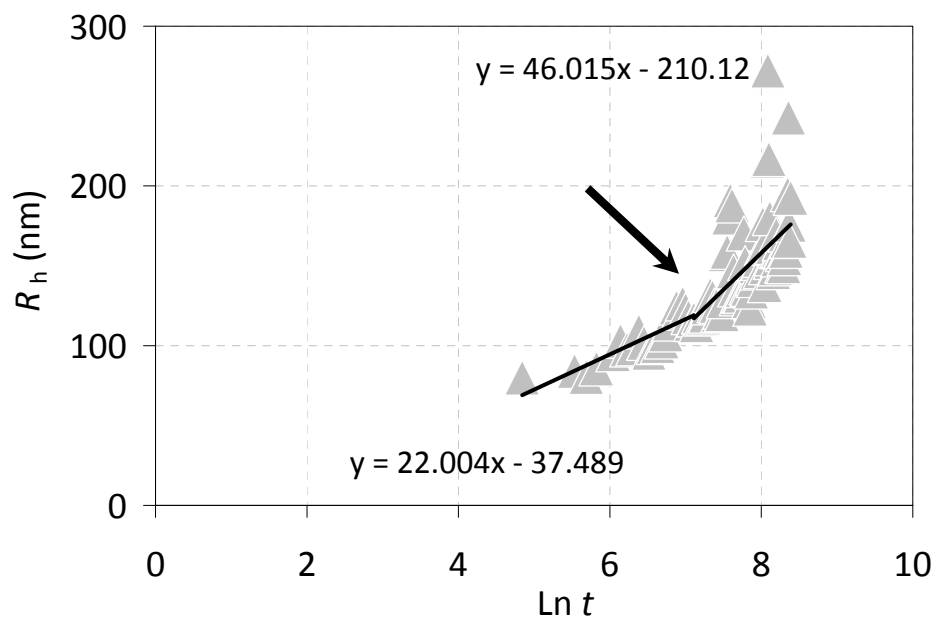
Figure 7-6: The R_h-log t profile of the 30 mM $CaCl_2$ solution with an arrow indicating the critical radius. The lines are linear fits to the data. The intersection of the lines represents the critical radius.

178

Table 7-1: Summary of factors affecting nucleation in oxidized HGD-CaCl$_2$ solutions

CaCl$_2$ Concentration (mM)	R_h (nm)	D_0 (μm^2/s)	D/D_o	k_D (mL/mg)	B_{22} (mol mL/g^2)	R_c (nm)	γ (J/m^2)	ΔG_c (J/mol)
20	92.33	3.48	0.76	−1.22	−7.63 x 10^{-4}	113.00	2.06 x 10^{-2}	1.10 x 10^{-7}
30	94.61	2.88	0.89	−0.55	−3.44 x 10^{-4}	120.71	2.20 x 10^{-2}	1.34 x 10^{-7}
35	103.52	2.54	0.92	−0.39	−2.41 x 10^{-4}	130.36	2.37 x 10^{-2}	1.69 x 10^{-7}
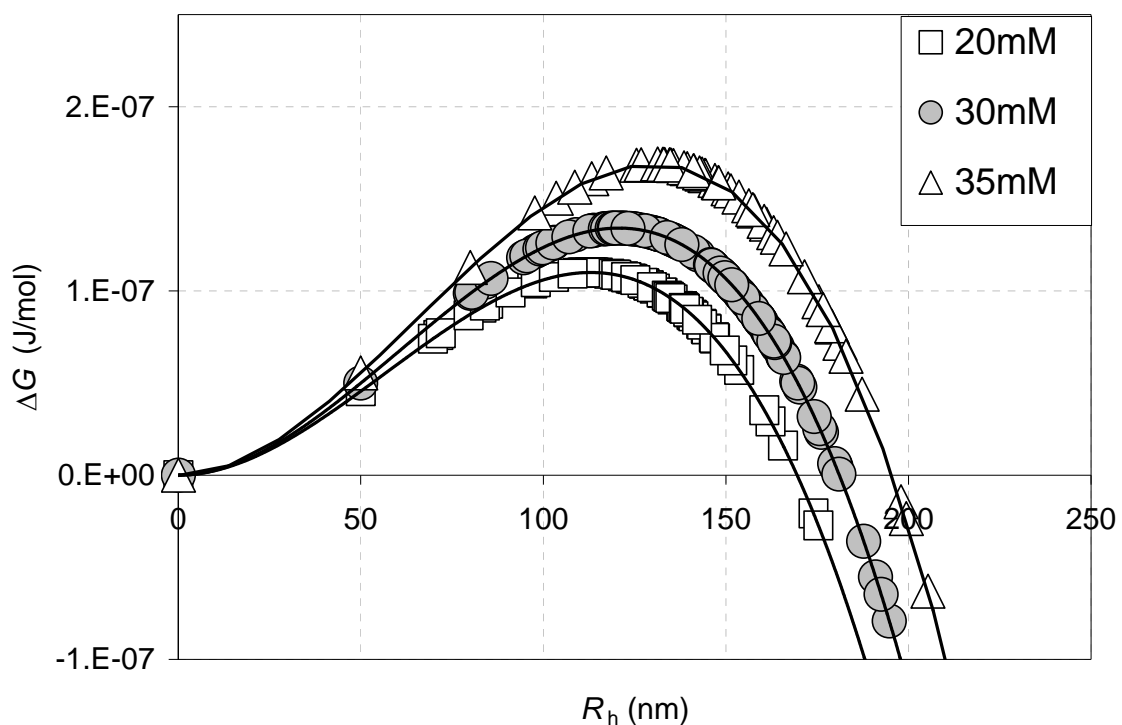
Figure 7-7: Nucleation energy profile for HGD on addition of 20, 30, and 35 mM CaCl$_2$. The energy barrier increases as the concentration of CaCl$_2$ added increases. The lines are polynomial fits of the data.

As suggested by its name, non-detergent sulfobetaine 201 (NDSB-201) is not a detergent. It solubilizes proteins without denaturing them, unlike detergents.[61] NDSB-201 has opposite charges at each end of a carbon bridge, which creates a dipole. Vuillard *et*

al.[61] suggested that the interaction of the dipole with the charges on the surface of the protein molecules may prevent interaction between protein molecules, leading to increased solubility of the protein.[61] The effect of NDSB-201 on an HGD-CaCl$_2$ solution was therefore examined.

Table 7-2 gives values of the second virial coefficient B_{22} for HGD obtained under different solution conditions. Values of R_h, D and k_D used to evaluate B_{22} are also given in Table 7-2. The first non-scattered point on the R_h-t curve was used to determine the second virial coefficient. Second virial coefficient values of HGD from Table 7-2 are plotted on the bar chart in Figure 7-8. It can be seen that the value of B_{22} did not change appreciably upon addition of NDSB-201 to the HGD-20mM CaCl$_2$ system. Previous studies with apoferritin in solutions containing 10 mM and 15 mM CdCl$_2$ showed that 1 M each of NDSB-195, NDSB-201 and NDSB-256 did not change the sign of the second virial coefficient, though they changed the magnitude of B_{22} slightly.[10] Figure 7-9 shows photomicrographs of HGD crystals obtained in the following solutions: 0.2 mg/mL HGD with 20 mM CaCl$_2$; 0.2 mg/mL HGD with 20 mM CaCl$_2$ and 100 mM NDSB-201; and 0.2 mg/mL HGD with 20 mM CaCl$_2$, and 0.1 mg/mL alpha a-crystallin. The results for the solution containing alpha A-crystallin will be discussed later in this section. The photomicrographs were obtained by examining approximately 20 μL from a 1 mL sample of each solution. The purpose of the examination was to compare the average size of crystals in each solution. Details of the apparatus used are described in CHAPTER 4. The crystals obtained in the solution containing NDSB-201 were approximately 5 μm while those in the solution with no NDSB-201 were approximately 20 μm. Therefore, even

though addition of NDSB-201 did not prevent crystallization, it may have resulted in smaller crystals being obtained.

Table 7-2: Second virial coefficient values for oxidized HGD in solution with various additives. The concentration of HGD used in all solutions 0.2 mg/mL HGD.

Additives	R_h (nm)	D_o (μm^2/s)	D/D_o	k_D (mL/mg)	B or B_{22} (mol mL/g^2)
No additives	73.26	3.08	1.08	0.38	2.40×10^{-4}
20 mM CaCl$_2$	92.33	3.48	0.76	-1.22	-7.63×10^{-4}
20 mM CaCl$_2$ with 100 mM NDSB	102.00	3.36	0.71	-1.46	-9.13×10^{-4}
20 mM CaCl$_2$ with 0.1 mg/mL alpha A-crystallin	70.90	2.96	1.16	0.78	4.86×10^{-4}

Values for R_c, γ and ΔG_c are reported in Table 7-3 for HGD solutions containing 20 mM CaCl$_2$, and HGD solutions containing both 20 mM CaCl$_2$ and 100 mM NDSB-201. Procedures for obtaining these data are explained in CHAPTER 6. Figure 7-10 shows a plot of overall free energy of nucleation as a function of aggregate size in the 0.2 mg/mL HGD with 20 mM CaCl$_2$ solution, and the 0.2 mg/mL HGD with 20 mM CaCl$_2$ and 100 mM NDSB-201 added. A similar plot was not made for the HGD solution containing 20 mM CaCl$_2$ and alpha A-crystallin because no aggregation occurred in that solution as can be seen from the R_h-t plot in Figure 7-11. It can be seen from Figure 7-10 that addition of NDSB-201 resulted in an increase in the free energy barrier. Thus NDSB-201 may have increased HGD solubility in this system by increasing the barrier to nucleation and thereby making it more difficult for crystals to form. The presence of large protein crystals in the lens results in diffraction of light and hence cataract. The use

of solubilizers such as NDSB-201, while not preventing crystallization, would at least

decrease the size of crystals obtained, thereby decreasing the amount of diffraction in the

lens and reducing the incidence of cataracts.
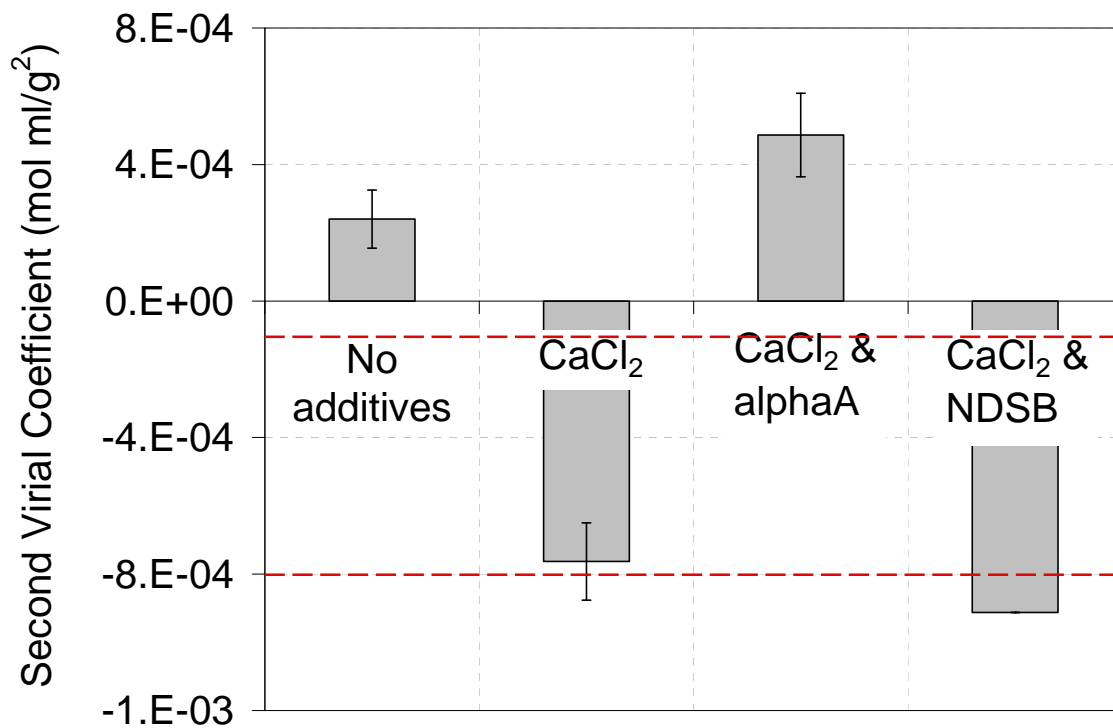
Figure 7-8: Second virial coefficient B_{22} values for HGD solutions with various additives. Two experiments were carried out at each condition except for the NDSB experiment where only one experiment was carried out. The error bars represent deviations from the mean. The HGD solution with no additives had a positive B_{22}. Addition of 20 mM $CaCl_2$ resulted in negative B_{22} which fell within the crystallization slot. Addition of a final concentration of 0.1 mg/mL alpha A-crystallin to a solution containing HGD and $CaCl_2$ increased B_{22} and actually resulted in a positive B_{22} higher than that of HGD with no additives. Addition of 100 mM NDSB-201 to a solution containing HGD and $CaCl_2$ did not affect B_{22}. The dotted lines represent the limits of the crystallization slot. The concentration of HGD used in every case was 0.2 mg/mL.
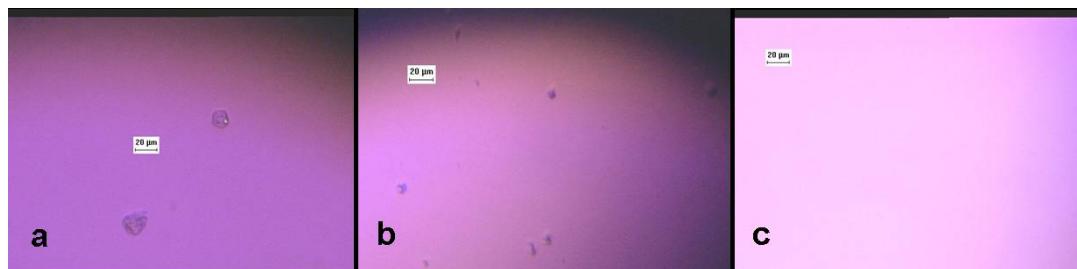
Figure 7-9: Photomicrographs of crystals of HGD obtained upon addition of the following solutions at 298 K (a) 20 mM $CaCl_2$ (b) 20 mM $CaCl_2$ and 100 mM NDSB-201 (c) 20 mM $CaCl_2$ and alpha A-crystallin. No crystals were obtained in the solution containing alpha A-crystallin.

Table 7-3: Summary of nucleation factors in oxidized HGD solutions

Additive	R_c (nm)	γ (J/m^2)	ΔG_c (J/mol)
20 mM $CaCl_2$	113.00	2.06 x 10^{-2}	1.10 x 10^{-7}
20mM $CaCl_2$ and 100mM NDSB-201	145.38	2.65 x 10^{-2}	2.34 x 10^{-7}
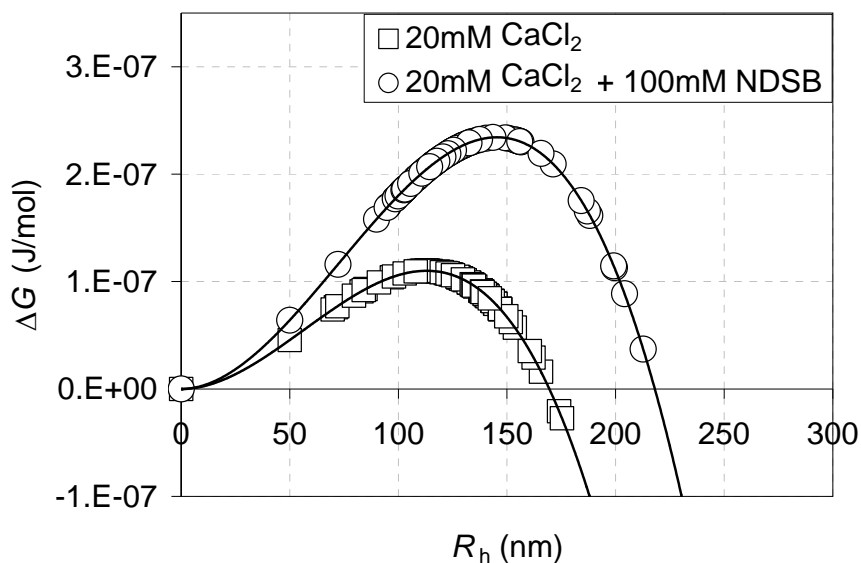
Figure 7-10: Overall nucleation energy profile of HGD upon addition of $CaCl_2$ by itself, and upon addition of $CaCl_2$ in the presence of NDSB-201. The lines through the points are polynomial fits to guide the eye.

Previous studies with alpha A-crystallin have shown that it acts as a molecular chaperone, i.e. it prevents aggregation of proteins in the lens and *in vitro*.[33; 64] Therefore, in the present study, an attempt was made to prevent aggregation of HGD by addition of alpha A-crystallin. Figure 7-12 shows a plot of R_h vs. t obtained by dynamic light scattering (DLS) for a sample of 0.1 mg/mL alpha A-crystallin in solution by itself. These data yielded an average R_h of 13.88 nm which is close to the R_h of 12.2 nm reported for monomers of alpha A-crystallin by Biswas *et al.*[125] The effect of 0.1 mg/mL alpha A-crystallin on the 0.2 mg/mL HGD with 20 mM $CaCl_2$ system was investigated. Figure 7-11 shows a plot of R_h against time for HGD in solution by itself, with 20 mM $CaCl_2$, and with 20 mM $CaCl_2$ and 0.1 mg/mL alpha A-crystallin. The solution of HGD by itself contained aggregates with an average size of 73 nm. As explained in SECTION 7.5.1, the 73 nm aggregates were caused by the absence of DTT in the HGD solution. Upon addition of $CaCl_2$ to HGD, aggregation of HGD occurred until approximately 800 seconds after the start of the experiment, at which point the size of the aggregates plateaued at approximately 140 nm. In the solution containing HGD, alpha A-crystallin and $CaCl_2$, stable aggregates of approximately 50 nm were formed. The ratio of alpha A-crystallin to HGD in the human lens is approximately 3.4:1.[126] In the present study, the ratio of alpha A-crystallin to HGD used was 0.5:1. This implies that much less alpha A-crystallin was used in the present study compared to actual lens conditions. In spite of this, alpha A-crystallin exhibited remarkable chaperoning properties, reducing the size of aggregates from 73 nm for pure HGD to 50 nm as shown in Figure 7-11. It is likely that the 50 nm aggregates are a complex of alpha A-crystallin and HGD since alpha A-crystallin has been reported to inhibit aggregation of proteins by forming complexes with

them.[33] The cross second virial coefficient B_{23}, which measures the effect of alpha A-crystallin on intermolecular interactions of HGD, was calculated using

$$B = y_2^2 B_{22} + 2B_{23}y_2y_3 + y_3^2 B_{33} \qquad\qquad 7\text{-}3$$

where B is the second virial coefficient of HGD and alpha A-crystallin in the 20 mM CaCl$_2$ solution; B_{22} is the second virial coefficient of HGD in a solution by itself with no CaCl$_2$ and no alpha A-crystallin; B_{33} is the second virial coefficient of alpha A-crystallin in a solution with no HGD and no CaCl$_2$; y_2 is the solvent-free mole fraction[20] of HGD; and y_3 is the solvent-free mole fraction of alpha A-crystallin. The mole fractions were CaCl$_2$-free because in solutions by itself, CaCl$_2$ did not scatter any light (data shown in CHAPTER 5). The values of B, B_{22} and B_{33} were determined by DLS and are given in Table 7-2 along with the corresponding R_h, D and k_D values. The value of the second virial coefficient for alpha A-crystallin with no additives (B_{33}) was determined to be 7.83 x 10^{-4} while that of HGD with no additives (B_{22}) was 2.40 x 10^{-4} mol mL/g^2. Upon addition of 20 mM CaCl$_2$, B_{22} of HGD decreased to -7.63 x 10^{-4} mol mL/g^2. Using Equation 7-3, and the measured B value of 4.86 x 10^{-4} mol mL/g^2, the cross second virial coefficient (B_{23}) value for HGD in the solution containing CaCl$_2$ and alpha A-crystallin was determined to be 6.58 x 10^{-4} mol mL/g^2, which was even higher than B_{22} of HGD with no CaCl$_2$ added. This shows that addition of alpha A-crystallin led to a more positive value of the second virial coefficient. The value of B_{23} is reported in Table 7-4 along with mole fraction values for HGD with CaCl$_2$ (y_2) and pure alpha A-crystallin (y_3).

The positive cross virial coefficient shows that alpha A-crystallin plays a solubilizing role in HGD solutions *in vitro*.

Table 7-4: Cross second virial coefficient (B_{23}) value for oxidized HGD with 20 mM $CaCl_2$ and 0.1 mg/mL alpha A-crystallin, and mole fraction values for pure oxidized HGD (y_2) and pure alpha A-crystallin (y_3)

B_{23}	6.58 x 10^{-4} mol mL g^{-2}
y_2	0.67
y_3	0.33

Figure 7-11 shows that alpha A-crystallin subdued aggregation of HGD in a solution containing 20 mM $CaCl_2$ at 298 K. However, oscillations were observed in the solution containing alpha A-crystallins. It is possible that the oscillations are due to clusters forming and dissipating as a result of not enough dissolved protein in the solution to take aggregates beyond the critical dimension. The photomicrographs in Figure 7-9 show a sample of the HGD-$CaCl_2$ with alpha A-crystallin solution. As Figure 7-9 shows, no crystals were obtained in this solution showing that alpha A-crystallin prevented crystallization of HGD. The reduced aggregation and absence of crystals confirm the solubilizing action of alpha A-crystallin under the conditions of the present study.
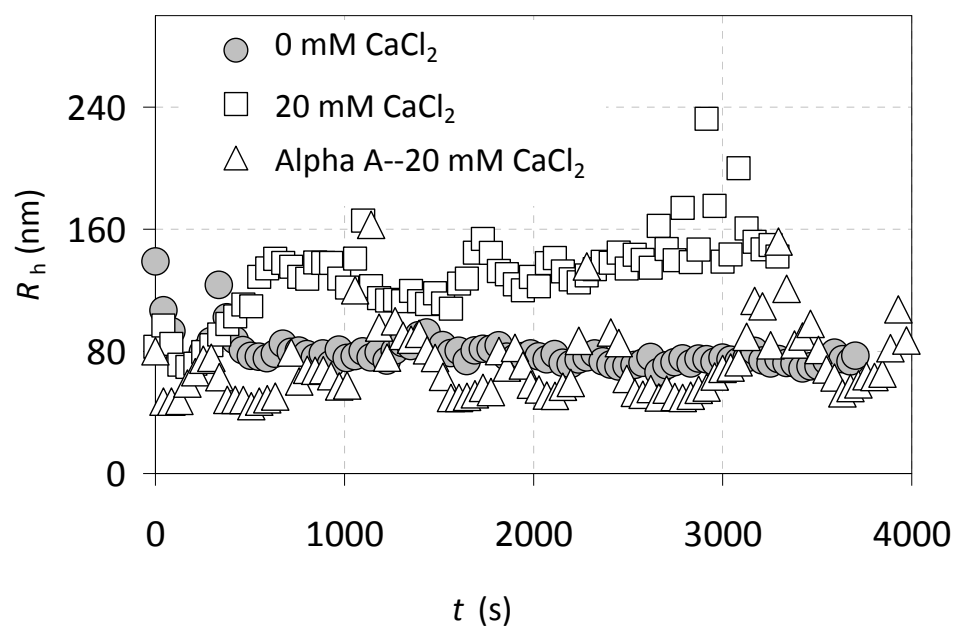
Figure 7-11: DLS results showing the hydrodynamic radius of HGD solutions as a function of time. Addition of CaCl$_2$ resulted in aggregation of HGD. Alpha A-crystallin prevented aggregation and reduced the size of aggregates of HGD below that of HGD with no additives.
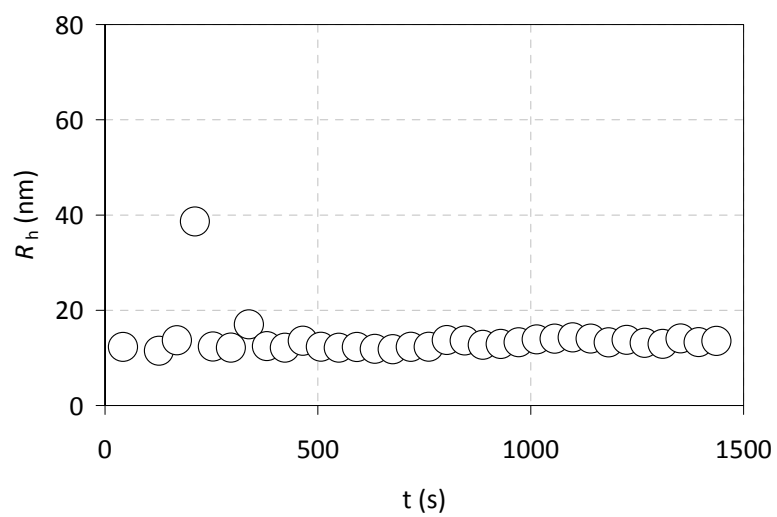
Figure 7-12: The R_h-t plot for alpha A-crystallin obtained from dynamic light scattering

7.5.3 Experiments With Non-oxidized HGD

In order to investigate the solubilizing action of alpha A-crystallin on non-oxidized HGD, experiments were carried out with non-oxidized HGD i.e. HGD containing 10 mM DTT. The purpose of DTT was to reduce thiol-mediated aggregation of HGD monomers. Figure 7-13 shows a plot of R_h against time for non-oxidized HGD with no additives, with 20 mM $CaCl_2$, in a solution containing 20 mM $CaCl_2$ and 0.1 mg/mL alpha A-crystallin, and in a solution containing 20 mM $CaCl_2$ and 100 mM NDSB-201. The same concentration of HGD, 0.2 mg/mL, was used for all three solutions. Figure 7-13 shows that the solution containing no additives had initial aggregates around 20 nm and exhibited no further aggregation over time whereas the solution containing 20 mM $CaCl_2$ exhibited aggregation. There was initial aggregation in the solution containing $CaCl_2$ and alpha A-crystallin, although alpha A-crystallin prevented further aggregation of HGD as can be seen in Figure 7-13, keeping the size of the aggregates constant at 56 nm. The R_h-t profile for the solution containing $CaCl_2$ and 100 mM NDSB-201 was similar to that of HGD with $CaCl_2$ and without NDSB-201, showing that NDSB-201 did not prevent aggregation of HGD.

Figure 7-14 shows a plot of R_h against time for non-oxidized HGD with no additives, with 20 mM $BaCl_2$, and in a solution containing 20 mM $BaCl_2$ and 0.1 mg/mL alpha A-crystallin. The results are similar to those from the $CaCl_2$ experiments although there was no initial aggregation upon addition of $BaCl_2$ as there was upon addition of $CaCl_2$. Alpha A-crystallin successfully suppressed aggregation induced by addition of $BaCl_2$.
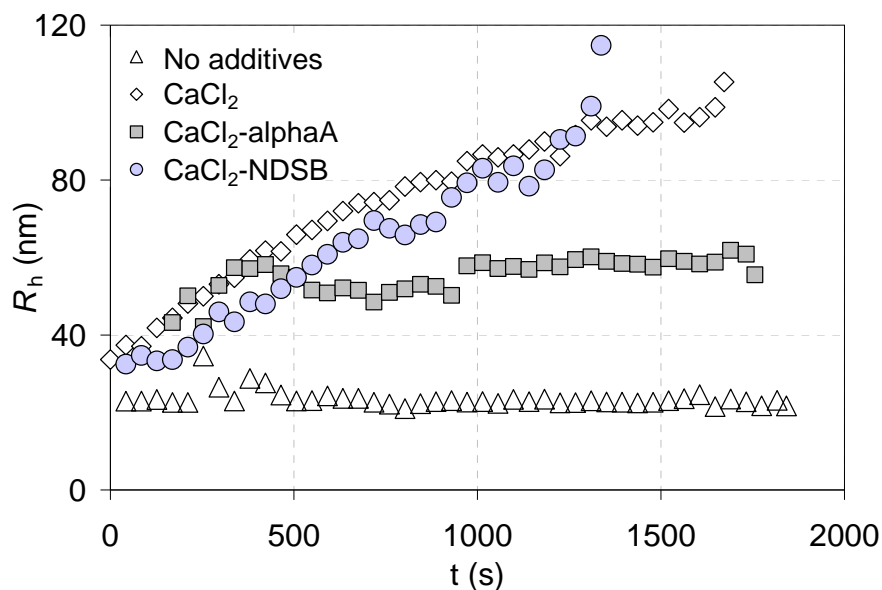
Figure 7-13: DLS results showing hydrodynamic radii of HGD solutions with DTT as a function of time. Addition of $CaCl_2$ to a final concentration of 20 mM resulted in aggregation of HGD. Although there was initial aggregation upon addition of $CaCl_2$, alpha A-crystallin prevented further aggregation and kept the size of aggregates of HGD below that of HGD with $CaCl_2$. NDSB-201 did not prevent aggregation.
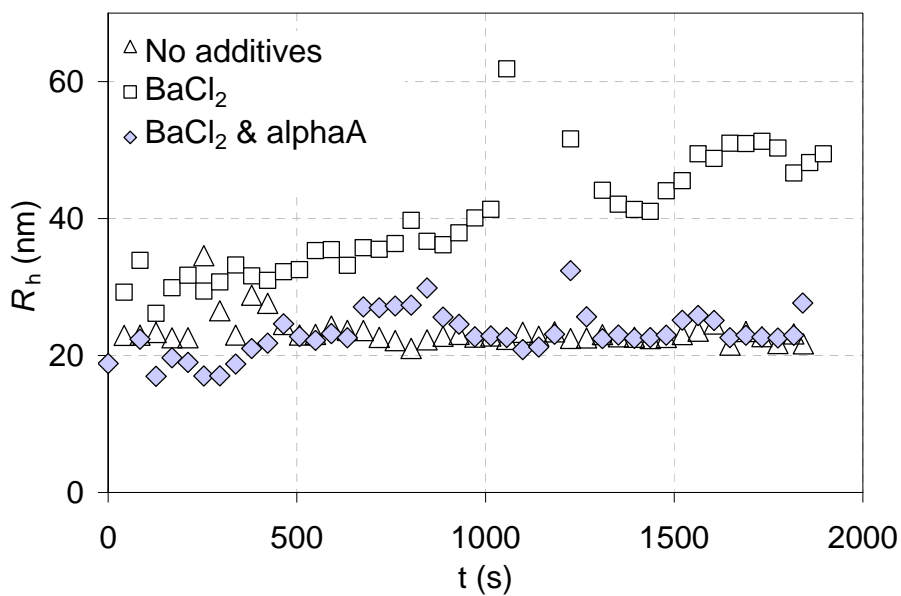
Figure 7-14: DLS results showing hydrodynamic radii of HGD solutions with DTT as a function of time. Addition of $BaCl_2$ to a final concentration of 20 mM resulted in aggregation of HGD. Alpha A-crystallin prevented aggregation and reduced the size of aggregates of HGD below that of HGD with $BaCl_2$.

The second virial coefficient values for all non-oxidized HGD solutions are reported in Table 7-5 along with the corresponding values of R_h, D and k_D. Figure 7-15 shows values of the second virial coefficient B_{22}, or B_{23} in the solution with alpha A-crystallin, for HGD obtained under the different solution conditions in the $CaCl_2$ experiments while Figure 7-16 shows second virial coefficient values for the $BaCl_2$ experiments. The cross second virial coefficient (B_{23}) values for the HGD solution containing $CaCl_2$ and alpha A-crystallin, and $BaCl_2$ and alpha A-crystallin, are reported in Table 7-6 along with mole fraction values for pure HGD (y_2) and pure alpha A-crystallin (y_3). The second virial coefficient was positive for HGD with no additives, negative with 20 mM $CaCl_2$ and 20 mM $BaCl_2$, and positive in the solution containing alpha A-crystallin and 20 mM $BaCl_2$, showing that for non-oxidized HGD, alpha A-crystallin was an effective solubilizer. However, the second virial coefficient was determined to be negative in the solution containing $CaCl_2$ and alpha A-crystallin. This negative second virial coefficient can be explained by the initial aggregation of HGD observed upon addition of $CaCl_2$ as shown in Figure 7-13. The fact that the value of the second virial coefficient did not change appreciably upon addition of alpha A-crystallin implies that higher concentrations of alpha A-crystallin are needed to prevent aggregation of HGD in the presence of 20 mM $CaCl_2$.

Table 7-5: Second virial coefficient values for non-oxidized HGD in solution with various additives. The concentration of HGD used in all solutions was 0.2 mg/mL. Procedures for obtaining these data are explained in CHAPTER 5.

Additives	R_h (nm)	D_o (μm^2/s)	D/D_o	k_D (mL/mg)	B or B_{22} (mol mL/g^2)
No additives	22.04	10.83	1.02	0.09	1.78×10^{-4}
20 mM CaCl$_2$	36.88	7.19	0.92	-0.42	-8.82×10^{-4}
20 mM CaCl$_2$ with 100 mM NDSB	35.52	7.47	0.92	-0.42	-8.83×10^{-4}
20 mM CaCl$_2$ with 0.1 mg/mL alpha A-crystallin	43.94	5.67	0.97	-0.13	-2.66×10^{-4}
20 mM BaCl$_2$	29.06	8.76	0.95	-0.23	-4.81×10^{-4}
20 mM BaCl$_2$ with 0.1 mg/mL alpha A-crystallin	22.99	9.78	1.08	0.40	8.29×10^{-4}

Table 7-6: Cross second virial coefficient (B_{23}) value for non-oxidized HGD with 20 mM CaCl$_2$ and 0.1 mg/mL alpha A-crystallin, and non-oxidized HGD with 20 mM BaCl$_2$ and 0.1 mg/mL alpha A-crystallin. Mole fraction values for pure non-oxidized HGD (y_2) and pure alpha A-crystallin (y_3) are given here and were the same in both solutions.

B_{23} (CaCl$_2$)	-9.10×10^{-4} mol mL g^{-2}
B_{23} (BaCl$_2$)	1.55×10^{-3} mol mL g^{-2}
y_2	0.67
y_3	0.33
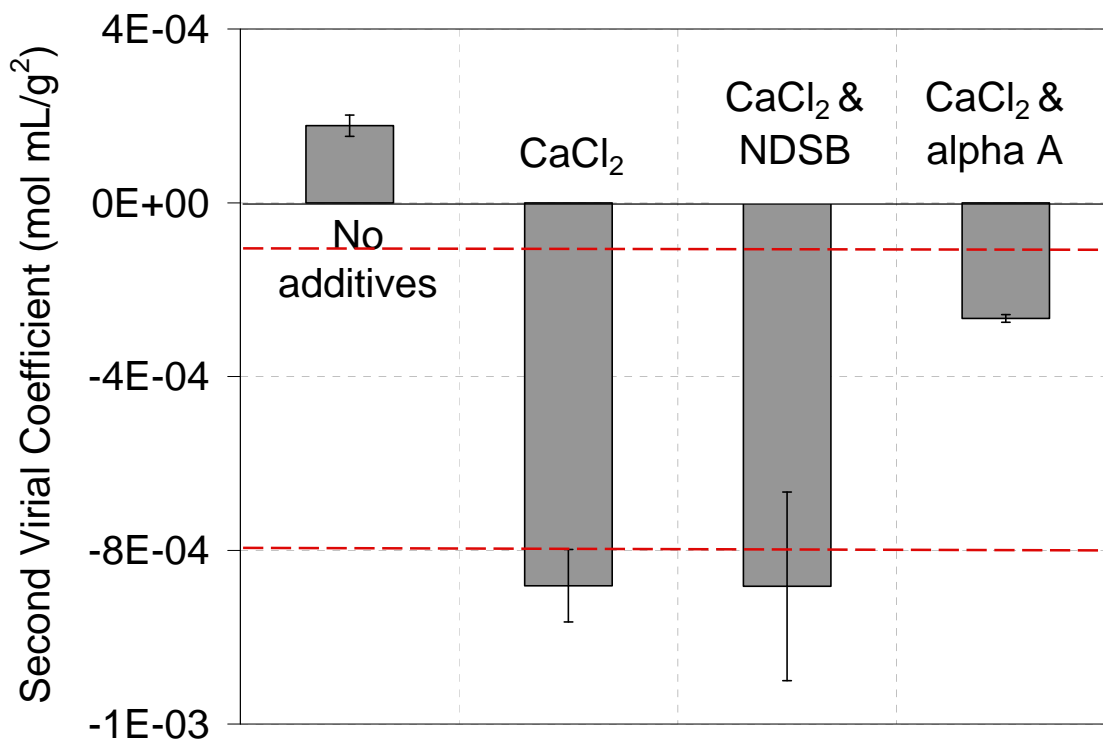
Figure 7-15: Second virial coefficient B_{22} (or B in solutions containing alpha A-crystallin) values for HGD solutions with various additives. Two experiments were carried out at each condition. The error bars represent deviations from the mean. The HGD solution with no additives had a positive second virial coefficient. Addition of 20 mM $CaCl_2$ resulted in negative B_{22} which fell within the crystallization slot. Addition of alpha A-crystallin to a solution containing HGD and $CaCl_2$ increased B_{22} although B_{22} remained negative. The dotted lines represent the limits of the crystallization slot. The concentration of HGD used in every case was 0.2 mg/mL.

Crystallization experiments were carried out for all the solutions studied. Photomicrographs obtained for the $CaCl_2$ experiments are shown in Figure 7-17 while those for the $BaCl_2$ experiments are shown in Figure 7-18. Crystals were obtained in HGD solution containing $CaCl_2$ and alpha A-crystallin, which correlates with the negative second virial coefficient calculated for HGD in this solution. The crystals obtained were less than 1 μm, and hence smaller than the average 12 μm of those obtained in the solution containing only $CaCl_2$. Therefore, even where alpha A-crystallin does not prevent crystallization, it may delay the onset of diseases by decreasing the size

of crystals obtained. Similarly, NDSB-201 also decreased the size of crystals obtained to

~ 5 μm.
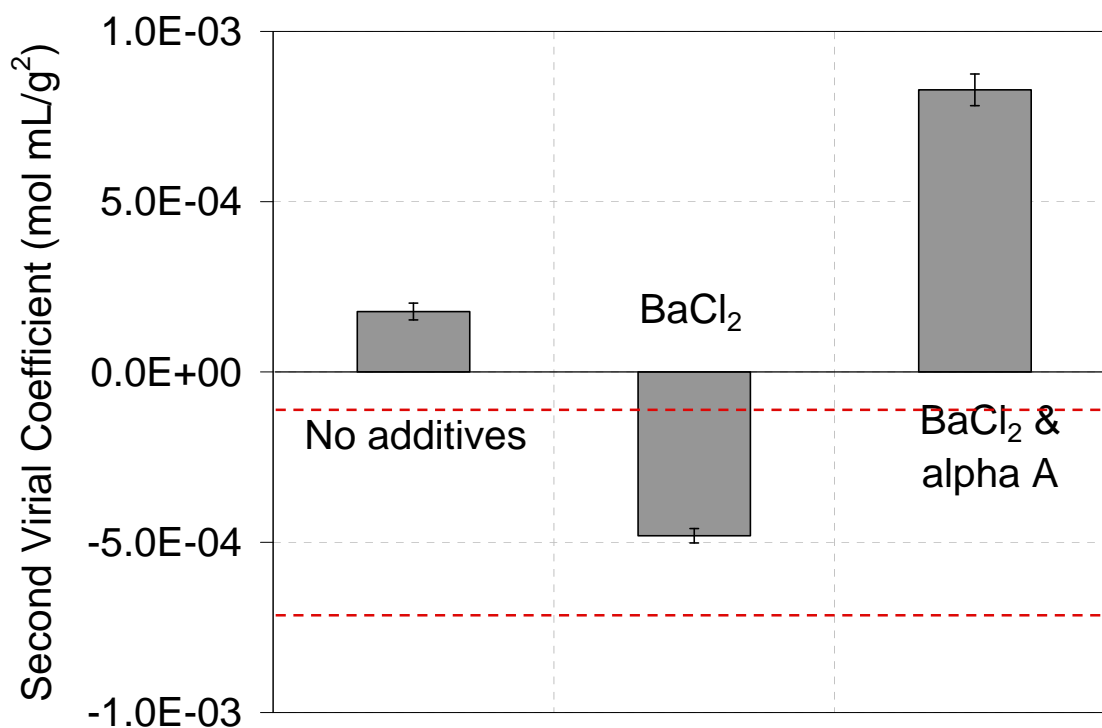
Figure 7-16: Second virial coefficient B_{22} values for HGD solutions with various additives. Two experiments were carried out at each condition. The error bars represent deviations from the mean. The HGD solution with no additives had a positive second virial coefficient. Addition of 20 mM $BaCl_2$ resulted in negative B_{22} which fell within the crystallization slot. Addition of alpha A-crystallin to a solution containing HGD and $BaCl_2$ increased B_{22} and actually resulted in a positive B_{22} higher than that of HGD with no additives. The dotted lines represent the limits of the crystallization slot. The concentration of HGD used in every case was 0.2 mg/mL.

Figure 7-17: Photomicrographs of crystals of non-oxidized HGD obtained upon addition of the following solutions at 298 K (a) 20 mM $CaCl_2$ (b) 20 mM $CaCl_2$ and 100 mM NDSB-201 (c) 20 mM $CaCl_2$ and alpha A-crystallin. Crystals were obtained in every solution.
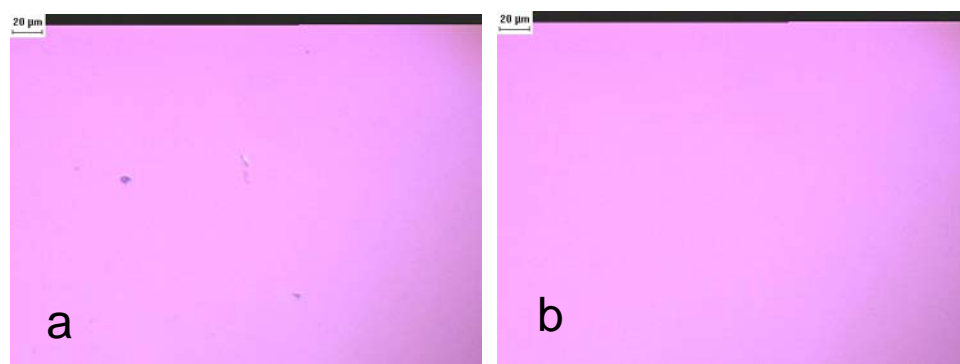
Figure 7-18: Photomicrographs of crystals of non-oxidized HGD obtained in the following solutions at 298 K (a) 20 mM $BaCl_2$ (b) 20 mM $BaCl_2$ and 0.1 mg/mL alpha A-crystallin. No crystals were obtained in the solution containing alpha A-crystallin.

7.6 DISCUSSION AND CONCLUSIONS

Various mechanisms have been suggested for the chaperone action of alpha A-crystallin, including incorporation of unfolded proteins into large complexes thus preventing their nonspecific aggregation[33] and selective binding to denatured proteins and inhibition of pathways that lead to non-specific aggregation.[71; 124; 127] In the present study, it is clear that alpha A-crystallin prevented aggregation of HGD although the exact mechanism is not known. Horwitz[127] discovered that thermally induced aggregation of gamma-

crystallin and a number of enzymes including alcohol dehydrogenase, enolase and aldolase was completely suppressed by alpha-crystallin under the conditions of his study. Horwitz induced aggregation in some solutions of gamma-crystallin with guanidine hydrochloride and precipitates formed within 20 minutes. After exhaustive dialysis of the denatured gamma-crystallin solution, addition of alpha-crystallin resulted in ~95% of the gamma-crystallin being solubilized and renatured.[127] This, coupled with the fact that aggregation was induced by addition of divalent cations in the present study, suggests that the alpha-crystallins can suppress aggregation irrespective of the method used to generate the aggregation. The results from Horwitz's study also demonstrate that alpha-crystallin can act as a chaperone for a wide range of proteins not just the crystallins. In the present study, aggregation was induced only by addition of $CaCl_2$ or $BaCl_2$ to HGD. It could be argued that alpha A-crystallin is a specific solubilizer for aggregation of HGD induced by $CaCl_2$ or $BaCl_2$. The studies carried out by Horwitz[127] suggest however that alpha A-crystallin acts as a solubilizer regardless of the driving force for aggregation and the results from the present study support this theory. The results from the present study are more physiologically relevant since Ba^{2+} and Ca^{2+} are found in the body whereas guanidine HCl, which was used by Horwitz, is not.

Alpha A-crystallin is a naturally occurring protein whose solubilizing properties are well demonstrated in the present study and in the literature. Therefore the use of alpha A-crystallin as a therapy for protein aggregation diseases should be considered. Examples of other commonly used solubilizers include urea, detergents and salts.[61] Urea is thought to solubilize proteins by disrupting the normal structure of water.[17] However, urea denatures proteins,[62; 128] which would negatively affect the body if urea was ingested or

injected as a therapy. Detergents attach their hydrophilic tails to the hydrophobic regions of the protein and thus allow the hydrophilic part of the protein to interact with water, increasing the solubility of the protein. However, detergents are known to denature proteins and are difficult to separate from proteins.[61] For these reasons, detergents are unsuitable for therapeutic use. Salts can increase the solubility of proteins but they can also decrease protein solubility at other concentrations. As elevated salt concentrations are associated with the occurrence of cataracts,[3] using salts as a therapy is not advisable. Sucrose has also been reported to maintain protein solubility under harsh conditions.[62] However, elevated concentrations of sucrose in the blood eventually lead to insulin resistance and hence diabetes.[129; 130] Chelating agents such as ethylenediaminetetraacetic acid (EDTA) form multiple bonds with metal ions thus inactivating them.[17] This prevents hydration of the metal ions and thus allows preferential hydration of the proteins in the solution. However, injection of chelating agents into dogs and rabbits resulted in retinal detachment and blindness.[63] This may be because divalent cations are essential for functioning of the body. As there is some danger associated with injecting chelating agents, more studies are required before they can be put to therapeutic use. Other delivery methods, such as transdermal or oral, may produce better results. Thus far, NDSBs have not been used *in vivo* so adverse effects of NDSBs are unknown. However, NDSBs do not denature proteins, do not significantly alter the pH of buffers, and are easily removed from protein solutions since they do not form micelles as do detergents.[61] These reasons make NDSBs a potential therapy for protein aggregation diseases such as cataracts.

Proteins in the body exhibit a natural solubility which may be compromised if the environment in the body changes e.g. due to pH changes or changes in the concentration

of cations. In the present study, it was observed that solubilization of oxidized HGD by alpha A-crystallin was more pronounced compared to solubilization of non-oxidized HGD. Based on these results, it could be speculated that alpha A-crystallin works best under conditions where the solubility of proteins is decreased. As it was not the purpose of the present study to compare the solubility of oxidized HGD to that of non-oxidized HGD, additional experiments need to be done to demonstrate reproducibility. However, these results do highlight the importance of alpha A-crystallin in solubilizing partially denatured proteins.

In conclusion, alpha A-crystallin was added to aggregating solutions of HGD in proportions that resulted in much less chaperone than is present in the lens. In spite of this, alpha A-crystallin exhibited extraordinary chaperoning ability, preventing or decreasing aggregation of HGD and even reducing the size of the aggregates of HGD in the case of the oxidized HGD solutions. Alpha A-crystallin also prevented crystallization of HGD altogether in the solution containing $BaCl_2$. In contrast, NDSB-201 did not prevent crystallization. It did, however, increase the energy barrier to nucleation and decrease the size of crystals obtained.

To the knowledge of the author, this is the first time the effects of alpha A-crystallin on solutions of HGD with $BaCl_2$ or $CaCl_2$ have been investigated. Since both Ba^{2+} and Ca^{2+} have been implicated in cataract formation, the results from the present study show that alpha A-crystallin may play a significant role in prevention of cataract disease. The results from the present study also suggest alpha A-crystallin and NDSB-201 may be potential therapies for cataract disease as well as other protein condensation diseases.

CHAPTER 8: CONCLUSIONS AND RECOMMENDATIONS

8.1 SUMMARY AND CONCLUSIONS

Crystallization of proteins plays a key role in the determination of protein structure and the separation and purification of therapeutic proteins such as insulin. Protein crystals have been linked to human diseases including Alzheimer's, cataracts and sickle cell anemia. In spite of the clear importance of crystallization of proteins, determination of conditions favorable for protein crystal growth remains empirical and involves extensive screening with no clear rationale for conditions tested. Protein crystallization is further complicated by the large number of variables and the fact that learnings from crystallization studies cannot be applied from one protein to another without further screening. The present study focused on relating protein solution conditions to thermodynamic properties of the solution as a means to predict the crystallization of clinically relevant proteins, specifically the lens protein, human gamma D-crystallin (HGD). However, protein crystallization is not always desired as in the case of the human diseases mentioned above. Therefore the possibility of subduing or preventing crystallization of proteins through the use of solubilizers was evaluated by examining the effects of natural and synthetic solubilizers on the nucleation and thermodynamic properties of human gamma D-crystallin (HGD) during crystallization.

Crystallization studies were carried out using HGD, a lens protein involved in cataract formation. The equilibrium phase diagram of HGD was determined

as a function of the concentrations of Ba^{2+} and Ca^{2+}. A salting-out effect was observed in both cases possibly because higher concentrations of the cations resulted in greater hydration of the cations and hence lower solubility of HGD. Addition of certain concentrations of Ca^{2+} to oxidized HGD appeared to result in a salting-in effect although scatter in the data does not allow this conclusion to be drawn with certainty. The equilibrium phase boundary for HGD was experimentally determined over a temperature range from 300 K to 305 K and the thermodynamics of crystallization were evaluated for HGD as a function of temperature. The dependence of solubility of HGD on temperature was found to be normal, i.e. higher solubility at higher temperatures which was consistent with previously published results from Pande *et al.*[13] However, the enthalpy determined in the present study did not match that from the study by Pande *et al.*[13] This discrepancy was attributed to the presence of aggregates in the HGD solution used in the present study which may have shifted the solubility curve.

The second virial coefficient, B_{22}, was identified in previous studies[5; 6] as having a correlation with the occurrence of crystallization of various proteins regardless of the driving force for crystallization. The driving force used in this part of the present study was the addition of divalent cations. While static light scattering (SLS) is most commonly used for measurement of B_{22}, this method was found unsuitable in the present study because the fast aggregation rates of HGD under the conditions studied resulted in inconsistent values of B_{22}. A new method was developed for measurement of B_{22} values through the use of dynamic light scattering (DLS). Whereas SLS averages out fluctuation intensities caused by Brownian motion of protein molecules, DLS makes use of the deviations from the average fluctuation to evaluate the diffusion coefficient and the

diffusivity slope k_D. DLS and SLS experiments conducted with apoferritin, another protein, in solutions containing $CdCl_2$ led to the development of a correlation between k_D and B_{22}. Therefore DLS provided an alternate method for measurement of B_{22}. The new method is more robust and efficient, requiring only a fraction of the time and material needed for SLS. This could be useful for assessment of the tendency of proteins in biological fluids taken from experimental animals or human patients to precipitate or crystallize. The volumes available in such cases may be too small for SLS to be effectively applied. DLS may be the only reliable alternative, as it is able to continuously capture the diffusivity in small sample volumes. DLS also worked well with the aggregating systems under study in the present work and yielded accurate and reliable values for B_{22}. As DLS measures aggregate size, it allowed tracking of the aggregation process and thus provided a means to determine kinetic nucleation and thermodynamic terms including the interfacial energy and the free energy barrier, leading to a better understanding of the nucleation process. Additionally, the present study confirmed that the second virial coefficient reliably correlates with protein crystallization outcome in the apoferritin-$CdCl_2$, HGD-$CaCl_2$, and HGD-$BaCl_2$ systems. The shapes of the apoferritin-$CdCl_2$ crystallization phase diagram and the B_{22} phase diagram under varying concentrations of $CdCl_2$ were similar; thus it can be concluded that simply measuring B_{22} provides an idea of how the solubility of apoferritin changes as the concentration of $CdCl_2$ changes. This could save time and material as it would greatly reduce the need for extensive screening for crystallization conditions.

The newly developed DLS method enabled determination of nucleation properties in the apoferritin-$CdCl_2$, HGD-$CaCl_2$, and HGD-$BaCl_2$ systems. Increasing the

concentration of $CdCl_2$ resulted in higher supersaturation in the apoferritin-$CdCl_2$ system. Higher supersaturation was induced by $CaCl_2$ than by $BaCl_2$ in the HGD systems, possibly because Ba^{2+} is less strongly hydrated than Ca^{2+}. Increasing the supersaturation resulted in higher critical radii, lower energy barriers and lower interfacial energies, which were all consistent with theory.

The solubilizing properties of alpha A-crystallin, a lens protein, in aggregating solutions of HGD-$CaCl_2$ were investigated and compared with the solubilizing effects of non-detergent sulfobetaine 201 (NDSB-201), a commercial solubilizer. Under the conditions of the present study, alpha A-crystallin decreased the size of HGD aggregates, prevented further aggregation of HGD and increased the second virial coefficient of the HGD molecules in solution. It ultimately prevented crystallization of HGD. It was observed that solubilization of oxidized HGD by alpha A-crystallin was more pronounced compared to solubilization of non-oxidized HGD which suggests that alpha A-crystallin works best under conditions where the solubility of proteins is decreased. The solubilizing properties of alpha A-crystallin were compared with those of NDSB-201. Upon addition of 100 mM NDSB to an HGD solution with 20 mM $CaCl_2$, aggregation was observed. However, smaller crystals were obtained compared with crystals obtained in HGD-$CaCl_2$ solutions containing no NDSB-201. The value of B_{22} did not change significantly but the free energy barrier to nucleation increased three-fold. This shows that NDSB-201 does solubilize HGD, increasing the energy barrier to nucleation and hence slowing down the crystal growth process. This observation shows potential for development of medications for protein aggregation and crystallization

diseases, based on the mechanisms of solubilizers, which could arrest or reverse protein aggregation.

The observations from the present study serve to increase understanding of protein interactions and the aggregation process especially in the presence of divalent cations. In addition, a new method was developed which makes it easier to quantify interactions between protein molecules. These results provide a stepping stone towards curing or preventing cataracts and other diseases associated with protein aggregation. These results could also ease the process of determining suitable conditions for crystal growth both for determination of crystal structure and in purification of therapeutic proteins. Measuring B_{22} could provide a quick and easy way to determine the type and strength of the intermolecular interactions in a protein solution, ultimately decreasing the number of crystallization trials necessary for determination of protein crystal growth conditions.

8.2 RECOMMENDATIONS FOR FUTURE WORK

1. The solubility plot determined in the present study used a partially oxidized form of HGD. The solubility plot should be determined for a solution of monomeric HGD.

2. The solubilizing properties of alpha A-crystallin on solutions of HGD should be further examined. Different ratios of alpha A to gamma D could be utilized to investigate whether there is an optimum ratio at which alpha A-crystallin exhibits

the most solubilization or at which the value of B_{22} is highest. A similar investigation could be carried out using different concentrations of NDSB-201. There is a possibility that the solubilizing action of alpha A-crystallin in HGD solutions is specific to Ca^{2+} and Ba^{2+}. As such, the solubilizing action of alpha A-crystallin on solutions of HGD containing other divalent cations should be studied.

3. Previous studies show that alpha A-crystallin is able to chaperone many different proteins both *in vivo* and *in vitro*.[40; 71; 127] At present, the exact mechanism employed by alpha A–crystallin is not known though studies suggest that the chaperone forms complexes with aggregating proteins and inhibits pathways that lead to non-specific aggregation.[40; 127] Studies should be set up to determine the mechanism(s) by which alpha A-crystallin is able to solubilize proteins. Evaluating the change in energy when alpha A-crystallin binds to aggregating proteins, for instance, could yield valuable information about the solubilizing mechanism.

4. Previous studies have shown that the only cation that can be used to crystallize apoferritin is cadmium cation[10; 44] although addition of polyethylene glycol created attractive interactions between apoferritin molecules ultimately resulting in crystallization.[59] Other divalent cations, including Ba^{2+} and Ca^{2+}, did not induce crystallization. Apoferritin possesses 24 nucleation sites to which iron can bind.[43] It is possibly the presence of the 24 nucleation sites that enables cadmium

to bind to apoferritin's crystal structure. In addition, cadmium is a transition element and can form coordination bonds thus connecting molecules of apoferritin via specific "salt bridges."[59] Further investigation could be carried out into the unique relationship between apoferritin and Cd^{2+}. Extensive studies could be carried out with other transition metals, such as chromium or nickel, to test if the ability of cadmium to form coordination bonds is a key factor. X-ray diffraction studies of crystals of apoferritin could be utilized to further examine the incorporation of Cd^{2+} into the crystal structure of apoferritin.

5. The new method developed for measurement of B_{22} could be further investigated to validate the assumptions made, especially the assumption that the friction term and the partial specific volume are negligible in the equation relating B_{22} and k_D. While this assumption holds for dilute solutions, it may be necessary to measure the friction term, which can be done by pulsed field gradient NMR. The investigation could also be extended to include other proteins to ensure that the method applies to other proteins.

6. It has been observed that the temperature in the eye decreases with age which most likely plays a part in cataractogenesis.[131] The effects of temperature on solubility of HGD in systems with divalent cations could be further investigated.

APPENDIX A: GAMMA D-CRYSTALLIN EXPRESSION

A.1 EXPRESSION OF GAMMA D-CRYSTALLIN

The procedure for expression and purification of HGD was obtained from Dr. Mark Petrash at Washington University in St. Louis. Dr. Petrash also provided the *E. coli* clones for HGD expression. An operations chart for the production and purification process is shown in Figure A-1.

Starter culture

↓

Culture

↓

Extraction

↓

Prepare for ion exchange

↓

IEX load and elute

↓

Screen purification fractions

↓

Pool and analyze γD-crystallin fractions
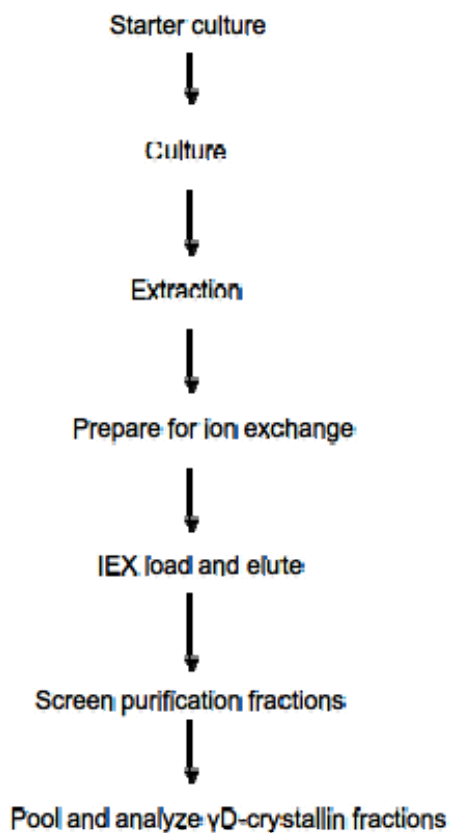
Figure A-1: Chart outlining the steps taken during expression and purification of HGD

A.1.1 Day 1 - Agar Culture

Materials

- YT medium

    o 10g Bactotryptone (N-Z-Amine-A)

    o 5 g Bacto yeast

    o 5 g NaCl

    o 1000 mL deionized water

    o 1 N NaOH for pH

    o 1 N HCl for pH

- For agar: 1.5g Bactoagar

- 100μL of 50mg/mL Antibiotic (Ampicillin)

- Bacteria

- 4 Tissue culture plates

Procedure

1. Prepare approx 2L of YT medium.

2. Start with 950 mL deionized water. Fill to 1000 mL after adjusting pH.

3. Pour into measuring cylinder then into flask.

4. Adjust pH to 7.4 with NaOH or HCl as necessary.

5. Mix all ingredients for YT-agar. Use 100 mL of YT for agar (in which case use 1.5g Bactoagar, etc.). Stir

6. Wait till solution is clear not cloudy

7. Autoclave media and agar mixture for 20 minutes on liquid cycle. Leave stir bar in agar mix.

8. Fill tray with water to minimize water loss. Also autoclave deionized water to replace lost water.

9. After cooling, add antibiotic (100μL of 50mg/mL) to agar mix.

10. Pour into tissue culture plates under hood (turn hood light on)

11. Pour about 10ml in each plate (about 4 plates). Pour slowly to prevent bubbles from forming.

12. Allow to cool. Keep covers cracked to allow cooling.

13. Streak different concentrations from 100 – 200 μL: e.g. bacteria only, half buffer, etc.

14. Sterilize spreader in ethanol and flame (allow to cool).

15. Add bacteria after mixing thoroughly with buffer

16. Pool buffer/bacteria in center of plate first

17. Once spreader is cool, spread buffer/bacteria on agar.

18. Dispose of leftover bacteria

19. Place plates in incubator at 37°C.

20. Flip plates after 10 minutes to prevent condensation.

21. Leave plates for approx 12 hours.

NOTE: Bactotryptone is the same as N-Z-Amine-A (Casein enzymatic hydrolysate) from bovine milk (Sigma-Aldrich Corporation, St. Louis, MO)

A.1.2 Day 2 - Starter Culture

Materials:

- Bunsen burner

- Agar bacterial culture

- Autoclaved YT Ampicillin Medium

- Sterilized volumetric flask

- Sterile pipette

Procedure

1. Flame flask

2. Pour ~50ml of YT medium into flask

3. Drag pipette across individual colony and dip into side of flask and medium.

4. Cover flask with foil. Label.

5. Place flask in shaker (~300rpm) at 37°C. Leave overnight or for approx 12 hours.

6. Cover agar jar with parafilm and store at 4°C for approx 1 week (just in case another starter culture is needed).

A.1.3 Day 3 – Cultures

<u>Materials</u>

- 3200µL Ampicillin (50mg/mL, autoclaved)

- 4 X 2L baffled flasks (autoclaved)

- 1600 mL YT medium (autoclaved)

- Sterile glycerol

- Bunsen burner

- Screw-top vial (autoclaved)

- Overnight starter culture

<u>Procedure</u> (*Multiply by 4 baffle flasks*)

1. Put 400mL of YT culture medium into each baffle flask

2. Add 800µL per 400mL of 50mg/mL ampicillin to flask

3. Flame the neck of the flask with the overnight culture

4. Add 8mL of overnight culture per 400ml of medium to flask. Swirl to mix. Label

5. Put baffle flasks in shaker at 37°C and ~100 rpm.

6. Leave until induction (OD_{600}~0.800), approx 2 hours. [Rule of thumb: cell concentration doubles every 45 minutes.]

7. (Meanwhile, add 800µL of remaining culture to 200µL of glycerol in sterile screw-top vial. Shake and store at -80°C.)

8. After 2 hours, measure turbidity using UV-Vis spec at $\lambda = 600nm$ (visible).

9. Use medium as blank

10. Flame medium flask before and after

11. After measuring, kill bacteria in cuvette with a drop of bleach and pour down the sink.

12. When $A_{600} \sim 0.800$, add 400μL of 1M IPTG to each 400mL culture

13. Leave for ~2.5 to 4 hours

14. Extract 1mL of culture from each flask.

15. Select even number of centrifuge bottles. Make sure they all fit into centrifuge snugly.

16. Pour equal amounts (or weights) of culture into centrifuge bottles. Balance weights with de-ionized water if necessary.

17. Make sure the bottles are not more than three quarters full or they will spill.

18. Centrifuge at 10,000 rpm for ~30 minutes.

19. Pour out supernatant into beaker. Add a few drops of bleach to kill the cells.

20. Label bottles. Freeze pellets overnight at -80°C overnight. Can keep frozen up to 1 week.

A.1.4 Day 4 - Extraction

The steps required for extraction and purification are outlined in Figure A-2.

Materials

- Lysozyme (20 mg X 4)

- N-Lysis buffer (40 mL X 4)

- Protease inhibitor (4 X 80 μL)

- Ice bath

- 10X Mg/Mn salt solution (16 mL)

- DNase (0.16 mg for 4 X 400 mL)

- Tissue homogenizer

- 2 boiled Dialysis tubes

- Short funnel

- 20 mM Tris-acetate buffer, pH = 6 (1600 mL), cold

- 3 X 2 L beakers = 4800 mL

- 1M DTT (0.8 mL)

- 500 mM EDTA (1.6 mL)

Procedure

1. Weigh out 80 mg lysozyme.

2. Add lysozyme to 160 mL of N-lysis buffer.

3. Add 320 μL of protease inhibitor to the N-Lysis buffer.

4. Put solution on ice until needed.

5.   Remove pellets from freezer. Warm pellets by putting centrifuge bottles under running tap.

6.   Remove all pellets and add to one centrifuge bottle.

7.   Place bottle in tap water bath at room temperature for approx 15 minutes to thaw. *Freeze-thaw helps break open cell walls.*

8.   Add 0.16 mg of DNase to 16 mL Mg/Mn salt solution.

9.   Put DNase + Mg/Mn salt solution mixture on ice until needed.

10.   Add lysozyme + N-lysis mixture to pellets. Mix with tissue homogenizer (*don't overdo it; heat is bad for the protein)*.

11.   Add Mg/Mn salt mixture to culture

12.   Leave on ice for ~2 hours.

Dialysis

13.   Wear gloves to protect dialysis tubing (12000-14000 kDa)

14.   Remove 2 already boiled dialysis tubes from ethanol (use 2 in case one ruptures)

15.   Wash thoroughly with de-ionized water, inside and out.

16.   Tie one end of each bag being careful to tug/tighten the end outside the knot (so as not to stretch membrane and increase pore size).

17.   Store in a beaker with de-ionized water until needed.

Pellets

18.   After 2 hours on ice, culture should be removed from ice and mixed with tissue homogenizer.

19.   Centrifuge solution for ~15 minutes at 10000rpm. (Don't forget to balance out the mass.)

20.   Use supe for dialysis

21.   (Pellets may be stored in case not all protein has been extracted.)

Dialysis: wear gloves

22.   Fill three 2L beakers each with cold 20mM Tris/Acetate buffer, pH = 6.0, 0.5mM DTT and 1.6ml of 500mM EDTA (*Total volume approx 1600ml = outside volume = ~ 20 times inside volume.)*

23.   Put stir bar in each beaker

24.   Fill each dialysis bag halfway with supernatant; use short funnel.

25.   Tie the top of each bag. Hold knot and tighten by pulling outside the knot.

26.   Make sure you leave some air in the bags to help them float.

27.   Fold dialysis bags in half and plop into beaker #1 in cold room

28.   Leave for ~3 hours. Move bags to beaker #2. Leave for 2 hours

29.   Throw away solution in beaker #1 to prevent confusion

30.   Move to beaker #3. Leave overnight

A.1.5 Day 5 - Cation Exchange Chromatography

1.   Prepare no-salt buffer: 20 mM Tris acetate, pH 6 + 0.5 mM DTT + 0.5 mM EDTA. Sterile filter.

2. Prepare salt buffer: 20 mM Tris acetate, pH 6 + 1 M Na acetate + 10 mM DTT + 0.5 mM EDTA. Sterile filter.

3. Prepare 6% v/v salt buffer i.e. 6% salt buffer + 94% no-salt buffer.

4. Measure whole cell lysate (WCL) concentration with Bradford reagent.

5. Mount column onto 5 mL syringe.

6. Wash column with 5 CV 100% salt buffer.

7. Equilibrate with 5 CV of no-salt buffer (4°C).

8. Load enough sample to put 44 mg protein on column (80% of max loading).

9. Re-equilibrate with 5 CV of no-salt buffer.

10. Run 6% salt over column to elute protein.

11. Check fraction with Bradford and save an aliquot to run a gel.

12. Wash with 5 CV of 100% salt.

13. Remove salt with 5 CV of no-salt buffer.

14. Collect samples for SDS-PAGE: crude lysate, flow-through, waste, 3% salt buffer (protein), and 100% salt buffer.

15. Repeat as necessary until all protein has been purified.

16. Wash column with 5 CV of 30% ethanol. Store in 30% ethanol in refrigerator.

A.1.6 Day 6 - SDS-PAGE

1. Run SDS-PAGE gels on samples.

2. Dialyze HGD (3% salt fraction) into storage buffer of your choice (100 mM phosphate buffer, pH 7.4, 10 mM DTT, 10 mM NaN_3; or 50 mM tris-HCl buffer, pH 7.4, 150 mM NaCl, 10 mM DTT, 10 mM NaN_3).

3. Freeze protein at $-80°C$.

```
                    Cell Pellet
                         |
                         |  N-Lysis, Lysozyme
                         |
                         |  Mg/Mn, DNase
                         |
                    Centrifuge
              _____|_____
             |                     |
          Pellet                 Supe
                                   |
                                   |
                                Dialysis
                                   |
                                   |  20mM Tris/Ace, 1mM DTT, 0.5mM EDTA
                                   |
                                Centrifuge
                           _____|_____
                          |                 |
                       Pellet              Supe
                                             |
                                             |
                                           Mac S
                                             |
                                             |  20mM Tris pH = 6, 1mM DTT, 0.5mM EDTA
                                             |
                                        0-0.5M Na Ace
```
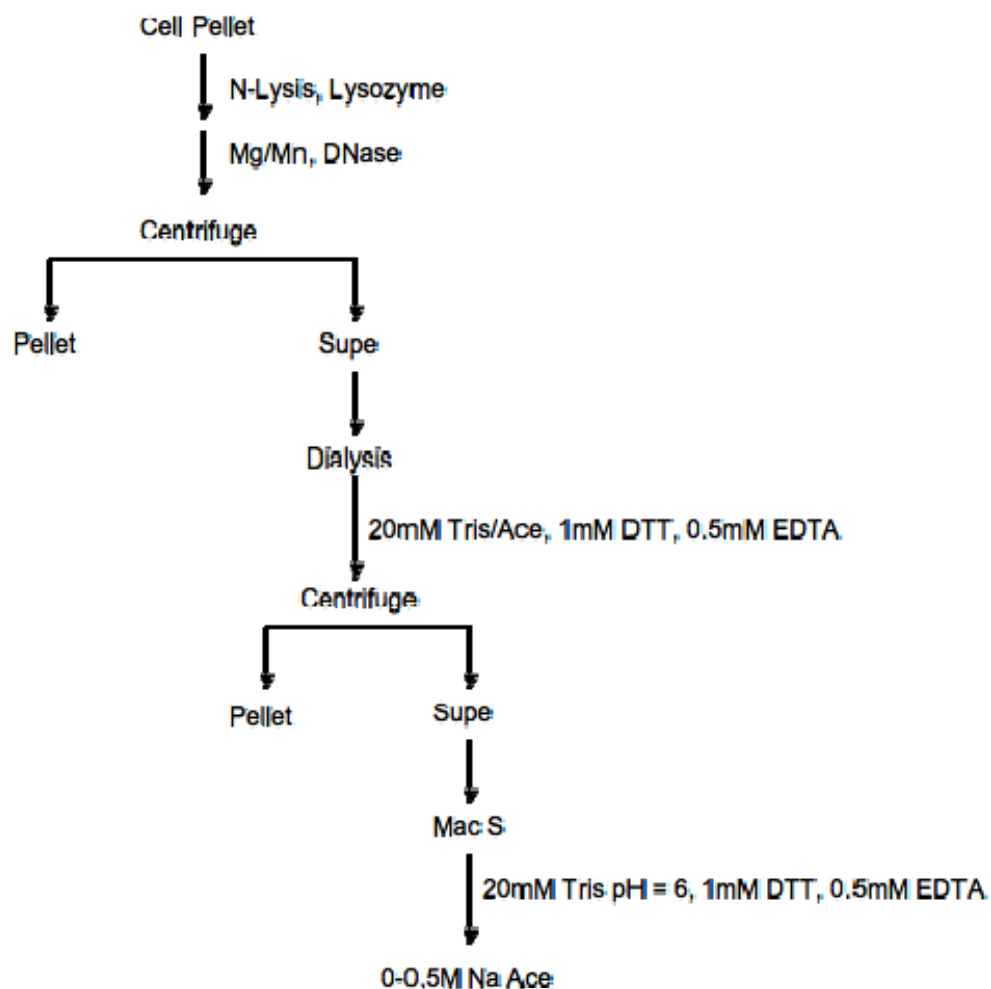
Figure A-2: Treatment of pellet after cell culture.

A.2 STOCK SOLUTIONS FOR EXPRESSION OF GAMMA D-CRYSTALLIN

(Adapted from documentation provided by Dr. Mark Petrash at Washington University in St. Louis)

ANTIBIOTIC (AMP)

AMP S/F store:-25°FR

0.5 g Antibiotic 10 mL diH_2O

Stir to dissolve, aliquot in 10 μL X 10 mL

1M DTT Dithiothreitol (Cleland reagent)

S/F   store: -25°FR thaw as needed

25   g $C_4H_{10}O_2S$

100   mL diH_2O

Stir to dissolve

Q.S. to 162 mL with diH_2O

Divide into 10-15ml aliquots

500 mM EDTA (ETHYLENEDIAMINETETRAACETIC ACID)

A/C stored: RTS

146.13 g $C_{10}H_{16}O_8N_2$ (186.13 g $C_{10}H_{14})_8$(Na·2H$_2$O)

900   mL diH_2O

20   g NaOH pellets(=~40pellets)

Stir to dissolve

PH TO 8.0 with 5 M NaOH

Q.S. to 1000 mL

Must be near pH = 6.0 to dissolve

1M TRIS/HCl pH=7.1

A/C store: RTS

121.14 g Tris [$NH_2C(CH_2OH)_3$]

900 mL diH2O stir until dissolved

pH to 7.4 with 12 N HCl

Q.S. to 1000 mL with diH$_2$O

PROTEASE INHIBITORS

NON-STERILE store: -25°FR

Using the weight designated on the manufacture's bottle

Add appropriate total volume of solvent

i.e.:

ANTIPAIN   resuspend to 1mg/mL diH$_2$O

BESTATIN   resuspend to 1mg/mL diH$_2$O

CHYMOSTATIN resuspend to 1mg/mL

      DMSO

LEUPEPTIN resuspend to1mg/mL diH$_2$O

PEPSTATIN resuspend to 1mg/mL

IPTG Isopropyl Thio-β-D-Galactoside (1M)

S/F store:-25°FR in 1-3ml aliquots

10 g IPTG

42 mL diH$_2$O

stir to dissolve, aliquot=1.0ml, freeze

YEAST TRYPTONE = YT=LB

A/C store: RTS in 100ml aliquots

10g Bacto-tryptone

5 g Bacto-Yeast extract

5 g NaCl

950 mL diH$_2$O

pH to 7.4 with NaOH

Q.S. to 1000ml with diH$_2$O

DESTAIN (40% Methanol/7.5% Acetic Acid)

NON STERILE stored: RTS

4200 mL diH$_2$O

3200 mL Methanol

 600 mL Glacial Acetic Acid*

YT AGAR

    A/C store: 4°CR

    10 g Bactotryptone

    5 g Bacto yeast

    5 g NaCl

    950 mL diH$_2$O

    pH to 7.4 with 1 M NaOH

    15 g Bactoagar

    Q.S. 1000 mL (**Remove stir bar)**

    Autoclave, cool to 50°C, add antibiotic(1/1000), pour into plates.

N-LYSIS BUFFER (50 mM Tris Cl pH = 7.5, 0.3M NaCl, 0.5 EDTA)

    NONSTERILE stored: 4°CB

    6.06g   Tris

    17.53g NaCl

    1.0 mL 0.5M EDTA

    pH$\rightarrow$ 7.5 with HCl

    Q.S. 1000ml

10X Mg/Mn SALTS (100mM MgCl$_2$, 10mM MnCl$_2$)

    NONSTERILE stored: 4°CB

    10.16g MgCl$_2$

0.99g   MnCl$_2$

Q.S. 500ml

DIALYSIS TUBING

NONSTERILE stored: 4°CB

Cut into 14-16" lengths

Boil for 10 minutes in large volume of :

2% Sodium Bicarb (60g/3000ml)

1mM EDTA pH=8.0(2ml/L 500mM)

Rinse thoroughly in diH$_2$O

Be sure to wash tubing inside with diH$_2$Oand out before using.

KEY

S/F = Sterile filter into previously autoclaved container

A/C = Autoclave for 30 minutes on liquid cycle with lid on but loose

4°CB = 4°C degrees cold box

4°CR = 4°C degrees cold room

RTS = Room Temperature Shelf

-25°FR = -25°C Freezer

Q.S. = Add deionized H$_2$O sufficient quantity to make...

*NOTE: When using concentrated acids it is advisable to add the acid to the water rather than the reverse. This prevents serious burns due to splattering or splashing as a result of heat generated.

APPENDIX B: HIGH PERFORMANCE LIQUID CHROMATOGRAPHY-SIZE EXCLUSION CHROMATOGRAPHY

B.1 OPERATION AND BUFFER RECIPES

Horse spleen apoferritin was purchased from Sigma-Aldrich Corporation (St. Louis, MO) and further purified to remove aggregates using high performance liquid chromatography – size exclusion chromatography (HPLC-SEC). A HiPrep 16/60 Sephacryl S-300 High Resolution column (GE Healthcare, Piscataway, NJ) was used. A flow-rate of 0.5 mL/min was used for running the protein sample and the running buffer over the column while the storage buffer and rinsing buffer were run at 0.3 mL/min. Three different buffers were utilized for this process: a storage buffer, a running buffer and a rinsing buffer. All buffers were prepared with ultrapure water (Alfa Aesar, Ward Hill, MA). The storage buffer was 20% v/v ethanol. The rinsing buffer comprised 0.6501 g of NaN_3 in 1000 mL of water.

The running buffer used was 50 mM Tris-HCl buffer, pH 7.4, with 150 mM NaCl and 10 mM NaN_3 added. The recipe for this buffer is below:

1000 mL of Solution A	1000 mL of Solution B
6.057 g Tris base	50 mL of 1 N HCl
8.766 g NaCl	8.766 g NaCl
0.6501 g NaN_3	0.6501 g NaN_3

The two solutions are then mixed until the right pH is reached.

All buffers were vacuum filtered prior to use. This removed particles from the solution to prevent clogging of the column and also degassed the solutions to ensure no air was passed over the column.

NOTE: Never let the column run dry.

B.2 PROCEDURE

The steps involved in this procedure are outlined below:

- The storage buffer is flushed out using 3-4 column volumes (CV) of rinsing buffer. One CV is 120 mL.

- The column is equilibrated with 3-4 CV of running buffer.

- The protein sample is injected into the column.

- After all the protein elutes, more protein can be loaded onto the column.

- Once all the protein is loaded and eluted, 3-4 CV of rinsing buffer is run over the column.

- Finally, the column is equilibrated with 3-4 CV of storage buffer and stored.

Step-by-step instructions for the operation of the HPLC process were first described by Bartling.[10] They are as follows:

- Turn on the LDC Analytical Pump (CM4000). Press "Lim" to set the pressure limits. The maximum pressure of the HiPrep 16/60 Sephacryl S-300 High Resolution column (Amersham Biosciences, Piscataway, NJ) is 21 psi. The minimum pressure is 0 psi. Confirm each entry by pressing "Ent."

Figure B-1: The LDC Analytical Pump (CM4000) showing the injection valve in the "inject" position.

- Close the spring-loaded valve of the transport syringe. Disconnect the syringe from the column and start the pump to purge the feed lines to the column. Connect the top of the column to the outlet of the injection valve. Connect the bottom of the column to the UV detector.

- If the column is not in use for 2 days or more, it is stored in 20% v/v ethanol. Start running the rinsing buffer over the column at 0.3 mL/min. Always begin at a low flow-rate, e.g. 0.1 mL/min, and gradually increase the flow-rate in steps of 0.1 mL/min.

- A maximum of 3 buffers can be connected to the column at the same time. Press "%" to check what line the buffer is being drawn from. To switch buffers, set the appropriate proportions of buffers and set the time delay to 0.1 min. The switch will be accompanied by a loud click after a few seconds. Stop the flow immediately and open the prime/purge valve. Draw approximately 10 mL of buffer from the prime/purge valve to remove any air trapped in the line. Close the valve and restart the flow.

- Equilibrate column with 3-4 CV of running buffer at 0.5 mL/min, then turn on UV lamp.

- Connect the outlet of the column to the inlet of the reference loop of the UV detector to purge the reference loop. Close the loop and set the detector to 280

nm.

- Switch the injection valve to the "Load" position (see Figure B-1). Use a blunt end needle to inject running buffer into the injection loop to rinse the loop. Remove the needle and switch the injection valve to the "inject" position.

- Switch the injection valve to the "Load" position. Use a blunt end needle to inject the protein sample into the injection loop to rinse the loop. Do not inject more than 2 mL of sample. Remove the needle and switch the injection valve to the "inject" position and start the timer.

- Turn on Shimadzu controller (Figure B-2), pump and UV detector. Turn on Shimadzu Class VP software (old HPLC). Instructions for operating the Shimadzu unit are below:

    1. Turn on the following IN ORDER:
        a. Controller
        b. Pump B
        c. Pump A
        d. Detector
    2. Turn on computer (log on)
    3. Open Class-VP 7.2.1 (by Shimadzu)

4. Fill vials with disposable pipette (minimum 0.5ml); number vials from zero (not one!).

5. Close vial. Shake.

6. Click on "Old HPLC;" listen for beep indicating connection has been made between computer and controller.

7. Click on LC setup icon

8. Open method:

   Desktop → HPLC users → kBartling → Method → Karsten 0.8ml-min…UV only

9. Click on pump in schematic

10. Start with flow-rate of 0.1ml/min. Increase flow gradually by 0.1ml/min. At each step, wait for pressure to equilibrate before increasing flow-rate further.

11. Increase flow-rate to 0.8 mL/min (or 1ml/min depending on method being used).

12. After reaching target flow-rate, wait about 15 minutes before loading sample.

13. Click "Sequence wizard" icon:

    Next → data path → HPLC users → name → data → ok

    Sample ID

    Data fill → Sample ID → Detection vial → number of unknowns in sequence

    Next → first vial → 0 →increment by 1

Autosampler injection volume → 0 µL → next → finish → next →

finish

14. Hit green arrow icon (Sequence run)

15. Name file in sequence. Save.

16. Make sure all buffers are connected.

17. Hit the "Start" button.

18. To turn off:

    a. Reduce flow-rate gradually to zero. Reduce by 0.1ml/min each

        time, waiting for pressure to equilibrate before further

        reducing.

    b. Close window. Wait for beep (controller and computer

        disconnecting).

    c. Turn off detector, *then* pumps A and B, *then* controller last.

    d. Close final window. Log off.

Figure B-2: Shimadzu system used for UV detection. The controller is on the left, and pumps A and B and the UV detector are on the right.

- Apoferritin oligomers elute first followed by monomers, followed by subunits. At a flow-rate of 0.5 mL/min, the oligomers elute after approximately 1 hour, the monomers after approximately 1 hour and 27 minutes, and the subunits after approximately 3 hours. These times are approximate so monitor the UV readings carefully.

- Collect the monomers by placing a 50 mL centrifuge tube at the exit of the UV detector.

- Continue running the running buffer until the UV reading returns to zero.

- Switch to rinsing buffer and equilibrate with 3-4 CV. Never allow the column to sit in running buffer for more than 2 days. The salts in the buffer may crystallize, compromising the ability of the column to separate proteins effectively.

- Decrease the flow-rate to 0.3 mL/min and equilibrate the column with 3-4 CV of storage buffer.

- Attach the spring-loaded transport syringe to the bottom of the column while the buffer is still running. Open the valve and let the syringe fill up to the 26 mL mark. Filling it more may result in very high back pressure. Leave the valve open.

- Stop flow and turn off the pump and UV detector. Unscrew the inlet tube at the top of the column. Close the top of the column with a blind connector.

Occasionally, an SCL Communications error is encountered when dealing with the Shimadzu UV detector. This arises because the Shimadzu pump is not being used. To erase errors, carry out the steps outlined below before turning on the software.

- On the Shimadzu Controller, press the F3 and Power buttons together until the Run and Act lights blink
- Press F2 and wait until controller says Pass
- Turn off power

- Turn on

- Press F5 (for menu)

- Press 4 (system)

- Press F3; make the following changes

  - CLASS-VP = 5.X

  - Interface = RS-232C

  - Baud rate = 19200

  - Level = enhanced

- Turn off and restart system.

- Wait about 3 minutes then turn on software.

APPENDIX C: DYNAMIC LIGHT SCATTERING

PROCEDURE

1. Prepare protein solution minus the additive (NDSB, Cd^{2+}, etc), i.e. just protein solution and buffer in the required amounts in (micro) centrifuge tube. (If carrying out experiment with protein alone, add buffer right before taking measurements (step 7).

2. Turn on correlator and leave on for at least one minute (instrument: ALV/LSE-5004 light scattering electronics and multiple tau digital correlator).

3. Open ALV software (ALV 5000/E/EPP).

4. Go to "Set up" → "option setup" → "ALV/LSE-5004" (last option). Select "COM 3." Click "OK."

5. Clean cuvette(s) as follows: scrub with soapy water and soft scrubber inside and out. Rinse thoroughly several times with deionized water. Rinse thoroughly several times with acetone inside and out. Dry outside of cuvette wit lens paper. Hold cuvette by top end until the inside is completely dry.
   Note: never touch the lower end of the cuvette. If this is necessary, use lens paper.

6. Lay cuvette on lens paper. Add required amount of additive to centrifuge tube and mix thoroughly with vortexer.

7. Transfer mixture to cuvette using syringe (no needle or cuvette may be scratched).

8. Cap cuvette and place in holder in machine. Adjust opening if necessary. Cover holder with lid. Open laser shutter.

9. Hit play to get an idea of the signal strength. If count rate is 10 or less, duration should be set to 2 minutes rather than 30 seconds (step 10).

10. For a quick run to determine R_h, do the following: Go to "Set up" → "ALV correlator set up" → "Manual run" → "Duration" → 30 s (or up to 2 minutes if signal strength is 10 or less).

11. For a long run over time, do the following: Go to "Set up" → "ALV correlator set up" → "Manual run" → "Create experiment schedule via script" → "Edit script." Change duration to 2 minutes if count rate was less than 10. Adjust number of runs as necessary. Click "Compile and run." Click "Yes" to save. After saving, software shows how long entire experiment will take including rest time (10 seconds) between each run. If too short or too long, change number of runs and click on compile and run again. After saving, click "Ok" to exit.

12. Go to "File" → "Auto save" → "data" → "name-folder." Enter name of experiment. If name-folder has not been created yet, go to "start" → "my computer" → "programs and files" → "ALV_V3.0" → "data." Create own folder in data folder. Return to ALV program and set up auto save.

13. Hit play button.

14. After experiment is over, open name-folder. Data summary is stored in DYNADYST file. Open this file, select all, copy and paste into excel. Save and email to self. Each run has its own individual file. Right-click one of them and open with notepad. Select all, copy and paste into excel, and save. Write down date and conditions. Email to self.

15. Close laser shutter.

16. To exit ALV program, go to "file" and select "exit." Click "ok." *(DO NOT exit program without going through file → exit. Failure to exit properly could result in errors next time the program is opened.)*

17. Turn off autocorrelator.

18. Remove cuvette and pour solution back into centrifuge tube. Wash cuvette as described above.

19. Close cuvette holder.

APPENDIX D: STATIC LIGHT SCATTERING DATA

OBTAINED FOR APOFERRITIN IN CdCl$_2$ SOLUTIONS

0 mM CdCl$_2$

Apoferritin Conc (mg/mL)	Kc/R (mol/g)	Kc/R (mol/g)	Kc/R (mol/g)	Average
0.1	2.90E-06	3.00E-06	3.09E-06	3.00E-06
0.2	3.29E-06	3.05E-06	3.17E-06	3.17E-06
0.4	3.72E-06	3.60E-06	3.71E-06	3.68E-06
0.5	3.89E-06	3.92E-06	3.99E-06	3.93E-06

Apoferritin Conc (mg/mL)	KcM/R	KcM/R	KcM/R	Average	Standard deviation	phi
0.1	1.06	1.10	1.13	1.10	0.028	0.00035
0.2	1.21	1.12	1.16	1.16	0.036	0.00071
0.4	1.36	1.32	1.36	1.35	0.021	0.00141
0.5	1.43	1.43	1.46	1.44	0.015	0.00176

5 mM CdCl$_2$

Apoferritin Conc (mg/mL)	Kc/R (mol/g)	Kc/R (mol/g)	Kc/R (mol/g)	Average
0.1	3.17E-06	3.01E-06	3.42E-06	3.20E-06
0.2	3.46E-06	3.35E-06	3.86E-06	3.56E-06
0.3	3.66E-06	3.82E-06	3.47E-06	3.65E-06
0.4	4.18E-06	4.13E-06	4.44E-06	4.25E-06

Apoferritin Conc (mg/mL)	KcM/R	KcM/R	KcM/R	Average	Standard deviation	phi
0.1	1.11	1.05	1.20	1.12	0.059	0.00037
0.2	1.21	1.17	1.35	1.25	0.077	0.00074
0.3	1.28	1.34	1.22	1.28	0.050	0.00111
0.4	1.46	1.45	1.56	1.49	0.047	0.00147

10 mM CdCl$_2$

Apoferritin Conc (mg/mL)	Kc/R (mol/g)	Kc/R (mol/g)	Kc/R (mol/g)	Average
0.1	3.40E-06	3.36E-06	3.54E-06	3.43E-06
0.2	3.54E-06	3.52E-06	3.68E-06	3.58E-06
0.3	3.96E-06	4.02E-06		3.99E-06

Apoferritin Conc (mg/mL)	KcM/R	KcM/R	KcM/R	Average	Standard deviation	phi
0.1	1.09	1.08	1.14	1.10	0.025	0.00040
0.2	1.14	1.13	1.18	1.15	0.022	0.00080
0.3	1.27	1.29		1.28	0.010	0.00121

13 mM CdCl$_2$

Apoferritin Conc (mg/mL)	Kc/R (mol/g)	Kc/R (mol/g)	Kc/R (mol/g)	Average
0.3	2.34E-06	2.33E-06	2.42E-06	2.36E-06
0.4	2.29E-06	1.97E-06	2.68E-06	2.31E-06
0.5	2.31E-06	2.22E-06	2.30E-06	2.28E-06

Apoferritin Conc (mg/mL)	KcM/R	KcM/R	KcM/R	Average	Standard deviation	phi
0.3	0.94	0.94	0.97	0.95	0.016	0.00096
0.4	0.92	0.79	1.08	0.93	0.116	0.00129
0.5	0.93	0.89	0.93	0.92	0.017	0.00161

20 mM CdCl$_2$

Apoferritin Conc (mg/mL)	Kc/R (mol/g)	Kc/R (mol/g)	Kc/R (mol/g)	Average
0.1	2.89E-06	2.71E-06	2.94E-06	2.85E-06
0.3	2.51E-06	2.57E-06		2.54E-06
0.4	2.17E-06	2.15E-06	2.44E-06	2.25E-06
0.5	1.90E-06	2.08E-06	1.93E-06	1.97E-06

Apoferritin Conc (mg/mL)	KcM/R	KcM/R	KcM/R	Average	Standard deviation	phi
0.1	0.93	0.87	0.95	0.92	0.032	0.00040
0.2	0.81	0.83		0.82	0.001	0.00080
0.3	0.70	0.69	0.79	0.73	0.042	0.00120
0.4	0.61	0.67	0.62	0.63	0.025	0.00161

REFERENCES

1.   Lewis, C. S. (1952). The Humanitarian Theory of Punishment. *20th Century: An Australian Quarterly Review* **3**, 5-12.

2.   Schmidt, S., Havekost, D., Kaiser, K., Kauling, J. & Henzler, H. K. (2005). Crystallization for the downstream processing of proteins. *Engineering in Life Sciences* **5**, 273-276.

3.   Cekic, O. (1998). Effect of cigarette smoking on copper, lead, and cadmium accumulation in human lens. *British Journal of Ophthalmology* **82**, 186-188.

4.   Benas, P., Legrand, L. & Ries-Kautt, M. (2002). Strong and specific effects of cations on lysozyme chloride solubility. *Acta Crystallographica Section D-Biological Crystallography* **58**, 1582-1587.

5.   George, A., Chiang, Y., Guo, B., Arabshahi, A., Cai, Z. & Wilson, W. W. (1997). Second virial coefficient as predictor in protein crystal growth. *Macromolecular Crystallography, Pt A* **276**, 100-110.

6.   George, A. & Wilson, W. W. (1994). Predicting Protein Crystallization from a Dilute-Solution Property. *Acta Crystallographica Section D-Biological Crystallography* **50**, 361-365.

7.   Tessier, P. M., Sandler, S. I. & Lenhoff, A. M. (2004). Direct measurement of protein osmotic second virial cross coefficients by cross-interaction chromatography. *Protein Science* **13**, 1379-1390.

8.   Ansari, R. R. (2004). Ocular static and dynamic light scattering: a noninvasive diagnostic tool for eye research and clinical practice. *Journal of Biomedical Optics* **9**, 22-37.

9.   Simpanya, M. F., Ansari, R. R., Suh, K. I., Leverenz, V. R. & Giblin, F. J. (2005). Aggregation of lens crystallins in an in vivo hyperbaric oxygen guinea pig model of nuclear cataract: Dynamic light-scattering and HPLC analysis. *Investigative Ophthalmology & Visual Science* **46**, 4641-4651.

10.   Bartling, K. (2006). Apoferritin Crystallization in Relation to Eye Cataract. PhD Thesis, Georgia Institute of Technology.

11.   Belter, P. A., Cussler, E. L. & Hu, W.-S. (1988). *Bioseparations: Downstream Processing for Biotechnology*, John Wiley & Sons.

12.   Scopes, R. K. (1988). *Protein Purification: Principles and Practice*. 2 edit. Springer Advanced Texts in Chemistry (Cantor, C. R., Ed.), Springer-Verlag.

13.   Pande, A., Pande, J., Asherie, N., Lomakin, A., Ogun, O., King, J. & Benedek, G. B. (2001). Crystal cataracts: Human genetic cataract caused by protein crystallization. *Proceedings of the National Academy of Sciences of the United States of America* **98**, 6116-6120.

14.   Benedek, G. B. (1997). Cataract as a protein condensation disease - The Proctor Lecture. *Investigative Ophthalmology & Visual Science* **38**, 1911-1921.

15.   Bloemendal, H., de Jong, W., Jaenicke, R., Lubsen, N. H., Slingsby, C. & Tardieu, A. (2004). Ageing and vision: structure, stability and function of lens crystallins. *Progress in Biophysics & Molecular Biology* **86**, 407-485.

16.   Neal, B. L., Asthagiri, D., Velev, O. D., Lenhoff, A. M. & Kaler, E. W. (1999). Why is the osmotic second virial coefficient related to protein crystallization? *Journal of Crystal Growth* **196**, 377-387.

17.   McPherson, A. (1998). *Crystallization of Biological Macromolecules*, Cold Spring Harbor Laboratory Press.

18.   Mullin, J. W. (2004). *Crystallization*. Fourth Edition edit, Elsevier Butterworth-Heinemann, Oxford.

19.   Malkin, A. & Mcpherson, A. (1994). Light-Scattering Investigations of Nucleation Processes and Kinetics of Crystallization in Macromolecular Systems. *Acta Crystallographica Section D-Biological Crystallography* **50**, 385-395.

20.   Moon, Y. U., Curtis, R. A., Anderson, C. O., Blanch, H. W. & Prausnitz, J. M. (2000). Protein-protein interactions in aqueous ammonium sulfate solutions. Lysozyme and bovine serum albumin (BSA). *Journal of Solution Chemistry* **29**, 699-717.

21.   Bartling, K., Sambanis, A. & Rousseau, R. W. (2005). Multiwell microbatch crystallization on a thermal gradient. *Crystal Growth & Design* **5**, 1559-1564.

22.   Cantor, C. R. & Schimmel, P. R. (1980). *The Behavior of Biological Macromolecules*. Biophysical Chemistry, MacMillan.

23.   Valente, J. J., Payne, R. W., Manning, M. C., Wilson, W. W. & Henry, C. S. (2005). Colloidal behavior of proteins: Effects of the second virial coefficient on solubility, crystallization and aggregation of proteins in aqueous solution. *Current Pharmaceutical Biotechnology* **6**, 427-436.

24. Tessier, P. M., Vandrey, S. D., Berger, B. W., Pazhianur, R., Sandler, S. I. & Lenhoff, A. M. (2002). Self-interaction chromatography: a novel screening method for rational protein crystallization. *Acta Crystallographica Section D-Biological Crystallography* **58**, 1531-1535.

25. Valente, J. J., Verma, K. S., Manning, M. C., Wilson, W. W. & Henry, C. S. (2005). Second virial coeffcient studies of cosolvent-induced protein self-interaction. *Biophysical Journal* **89**, 4211-4218.

26. Bloustine, J., Berejnov, V. & Fraden, S. (2003). Measurements of protein-protein interactions by size exclusion chromatography. *Biophysical Journal* **85**, 2619-2623.

27. Mccarty, B. W. & Adams, E. T. (1987). Osmotic-Pressure Measurements of Ovalbumin and Lysozyme Mixtures. *Biophysical Chemistry* **28**, 149-159.

28. Smith, J. M., Ness, H. C. V. & Abbott, M. M. (1996). *Introduction to Chemical Engineering Thermodynamics*. Fifth edit. Chemical Engineering Series, McGraw-Hill.

29. Wilson, W. W. (2003). Light scattering as a diagnostic for protein crystal growth - A practical approach. *Journal of Structural Biology* **142**, 56-65.

30. Neal, R., Aykin-Burns, N., Ercal, N. & Zigler, J. S. (2005). Pb2+ exposure alters the lens alpha A-crystallin protein profile in vivo and induces cataract formation in lens organ culture. *Toxicology* **212**, 1-9.

31. Delaye, M. & Tardieu, A. (1983). Short-Range Order of Crystallin Proteins Accounts for Eye Lens Transparency. *Nature* **302**, 415-417.

32. Biswas, S., Harris, F., Dennison, S., Singh, J. P. & Phoenix, D. (2005). Calpains: enzymes of vision? *Medical Science Monitor* **11**, Ra301-Ra310.

33. Aquilina, J. A., Benesch, J. L. P., Ding, L. L., Yaron, O., Horwitz, J. & Robinson, C. V. (2004). Phosphorylation of alpha B-crystallin alters chaperone function through loss of dimeric substructure. *Journal of Biological Chemistry* **279**, 28675-28680.

34. Kumar, M. S., Reddy, R. Y., Sreedhar, B. & Reddy, G. B. (2005). alpha B-crystallin-assisted reactivation of glucose-6-phosphate dehydrogenase upon refolding. *Biochemical Journal* **391**, 335-341.

35. Slingsby, C., Norledge, B., Simpson, A., Bateman, O. A., Wright, G., Driessen, H. P. C., Lindley, P. F., Moss, D. S. & Bax, B. (1997). X-ray diffraction and structure of crystallins. *Progress in Retinal and Eye Research* **16**, 3-29.

36.   Meehan, S., Berry, Y., Luisi, B., Dobson, C. M., Carver, J. A. & MacPhee, C. E. (2004). Amyloid fibril formation by lens crystallin proteins and its implications for cataract formation. *Journal of Biological Chemistry* **279**, 3413-3419.

37.   Sergeev, Y. V., Hejtmancik, J. F. & Wingfield, P. T. (2004). Energetics of domain-domain interactions and entropy driven association of beta-crystallins. *Biochemistry* **43**, 415-424.

38.   Andley, U. P. (2007). Crystallins in the eye: Function and pathology. *Progress in Retinal and Eye Research* **26**, 78-98.

39.   Pande, A., Pande, J., Asherie, N., Lomakin, A., Ogun, O., King, J. A., Lubsen, N. H., Walton, D. & Benedek, G. B. (2000). Molecular basis of a progressive juvenile-onset hereditary cataract. *Proceedings of the National Academy of Sciences of the United States of America* **97**, 1993-1998.

40.   Pigaga, V. & Quinlan, R. A. (2006). Lenticular chaperones suppress the aggregation of the cataract-causing mutant T5P gamma C-crystallin. *Experimental Cell Research* **312**, 51-62.

41.   Levi, S., Girelli, D., Perrone, F., Pasti, M., Beaumont, C., Corrocher, R., Albertini, A. & Arosio, P. (1998). Analysis of ferritins in lymphoblastoid cell lines and in the lens of subjects with hereditary hyperferritinemia-cataract syndrome. *Blood* **91**, 4180-4187.

42.   Harrison, P. M. & Arosio, P. (1996). Ferritins: Molecular properties, iron storage function and cellular regulation. *Biochimica Et Biophysica Acta-Bioenergetics* **1275**, 161-203.

43.   Granier, T., Comberton, G., Gallois, B., d'Estaintot, B. L., Dautant, A., Crichton, R. R. & Precigoux, G. (1998). Evidence of new cadmium binding sites in recombinant horse L-chain ferritin by anomalous Fourier difference map calculation. *Proteins-Structure Function and Bioinformatics* **31**, 477-485.

44.   Bartling, K., Sambanis, A. & Rousseau, R. W. (2007). Dependence of apoferritin crystal growth on temperature and cadmium concentration. *Crystal Growth & Design* **7**, 569-575.

45.   Yau, S. T., Petsev, D. N., Thomas, B. R. & Vekilov, P. G. (2000). Molecular-level thermodynamic and kinetic parameters for the self-assembly of apoferritin molecules into crystals. *Journal of Molecular Biology* **303**, 667-678.

46.   Balasubramanian, D. (2005). Photodynamics of cataract: An update on endogenous chromophores and antioxidants. *Photochemistry and Photobiology* **81**, 498-501.

47.   Truscott, R. J. W. (2005). Age-related nuclear cataract - oxidation is the key. *Experimental Eye Research* **80**, 709-725.

48.   Biswas, S., Harris, F., Dennison, S., Singh, J. & Phoenix, D. A. (2004). Calpains: targets of cataract prevention? *Trends in Molecular Medicine* **10**, 78-84.

49.   Basak, A., Bateman, O., Slingsby, C., Pande, A., Asherie, N., Ogun, O., Benedek, G. B. & Pande, J. (2003). High-resolution X-ray crystal structures of human gamma D crystallin (1.25 angstrom) and the R58H mutant (1.15 angstrom) associated with aculeiform cataract. *Journal of Molecular Biology* **328**, 1137-1147.

50.   Sun, Y. & MacRae, T. H. (2005). The small heat shock proteins and their role in human disease. *Febs Journal* **272**, 2613-2627.

51.   Brooks, D. G., Manova-Todorova, K., Farmer, J., Lobmayr, L., Wilson, R. B., Eagle, R. C., St Pierre, T. G. & Stambolian, D. (2002). Ferritin crystal cataracts in hereditary hyperferritinemia cataract syndrome. *Investigative Ophthalmology & Visual Science* **43**, 1121-1126.

52.   Xu, W. Z., Zheng, S., Xu, S. J., Huang, W., Yao, K. & Zhang, S. Z. (2004). Autosomal dominant coralliform cataract related to a missense mutation of the gamma D-crystallin gene. *Chinese Medical Journal* **117**, 727-732.

53.   Tardieu, A., Veretout, F., Krop, B. & Slingsby, C. (1992). Protein Interactions in the Calf Eye Lens - Interactions between Beta-Crystallins Are Repulsive Whereas in Gamma-Crystallins They Are Attractive. *European Biophysics Journal with Biophysics Letters* **21**, 1-12.

54.   Korlimbinis, A., Hains, P. G., Truscott, R. J. W. & Aquilina, J. A. (2006). 3-Hydroxykynurenine oxidizes alpha-crystallin: Potential role in cataractogenesis. *Biochemistry* **45**, 1852-1860.

55.   Korlimbinis, A. & Truscott, R. J. W. (2006). Identification of 3-hydroxykynurenine bound to proteins in the human lens. A possible role in age-related nuclear cataract. *Biochemistry* **45**, 1950-1960.

56.   Christiansen, G. & Mohney, B. G. (2007). Hereditary hyperferritinemia-cataract syndrome. *Journal of Aapos* **11**, 294-296.

57.   Burnett, J. C. (1889). *Cataract: Its Nature, Causes, Prevention, and Cure*, The Homeopathic Publishing Company, London.

58.   Wu, J. Z., Bratko, D. & Prausnitz, J. M. (1998). Interaction between like-charged colloidal spheres in electrolyte solutions. *Proceedings of the National Academy of Sciences of the United States of America* **95**, 15169-15172.

59. Tanaka, S. & Ataka, M. (2002). Protein crystallization induced by polyethylene glycol: A model study using apoferritin. *Journal of Chemical Physics* **117**, 3504-3510.

60. Cekic, O. (1998). Copper, lead, cadmium and calcium in cataractous lenses. *Ophthalmic Research* **30**, 49-53.

61. Vuillard, L., Braunbreton, C. & Rabilloud, T. (1995). Non-Detergent Sulfobetaines - a New Class of Mild Solubilization Agents for Protein-Purification. *Biochemical Journal* **305**, 337-343.

62. Conti, M., Galassi, M., Bossi, A. & Righetti, P. G. (1997). Capillary isoelectric focusing: The problem of protein solubility. *Journal of Chromatography A* **757**, 237-245.

63. Sowden, E. & Pirie, A. (1958). Barium and Strontium Concentrations in Eye Tissue. *Biochemical Journal* **70**, 716-717.

64. Andley, U. P., Mathur, S., Griest, T. A. & Petrash, J. M. (1996). Cloning expression, and chaperone-like activity of human alpha A-crystallin. *Journal of Biological Chemistry* **271**, 31973-31980.

65. Hay, R. E., Andley, U. P. & Petrash, J. M. (1994). Expression of Recombinant Bovine Gamma-B-Crystallin, Gamma-C-Crystallin and Gamma-D-Crystallin and Correlation with Native Proteins. *Experimental Eye Research* **58**, 573-584.

66. Petrash, J. M., Harter, T. M., Devine, C. S., Olins, P. O., Bhatnagar, A., Liu, S. Q. & Srivastava, S. K. (1992). Involvement of Cysteine Residues in Catalysis and Inhibition of Human Aldose Reductase - Site-Directed Mutagenesis of Cys-80, Cys-298, and Cys-303. *Journal of Biological Chemistry* **267**, 24833-24840.

67. Prescott, L. M., Harley, J. P. & Klein, D. A. (2002). *Microbiology*. Fifth edit, McGraw-Hill.

68. Bonnete, F., Malfois, M., Finet, S., Tardieu, A., Lafont, S. & Veesler, S. (1997). Different tools to study interaction potentials in gamma-crystallin solutions: Relevance to crystal growth. *Acta Crystallographica Section D-Biological Crystallography* **53**, 438-447.

69. Adel, A., Nadia, M., Mohamed, O. & Abdelhafidh, G. (2008). Study of thermally and chemically unfolded conformations of bovine serum albumin by means of dynamic light scattering. *Materials Science & Engineering C-Biomimetic and Supramolecular Systems* **28**, 594-600.

70.   Muschol, M. & Rosenberger, F. (1995). Interactions in undersaturated and supersaturated lysozyme solutions: Static and dynamic light scattering results. *Journal of Chemical Physics* **103**, 10424-10432.

71.   Horwitz, J., Bova, M. P., Ding, L. L., Haley, D. A. & Stewart, P. L. (1999). Lens alpha-crystallin: function and structure. *Eye* **13**, 403-408.

72.   Purkiss, A. G., Bateman, O. A., Goodfellow, J. M., Lubsen, N. H. & Slingsby, C. (2002). The x-ray crystal structure of human gamma S-crystallin C-terminal domain. *Journal of Biological Chemistry* **277**, 4199-4205.

73.   Fu, L. & Liang, J. J. N. (2002). Conformational change and destabilization of cataract gamma C-crystallin T5P mutant. *Febs Letters* **513**, 213-216.

74.   Hegde, K. R. & Varma, S. D. (2005). Prevention of cataract by pyruvate in experimentally diabetic mice. *Molecular and Cellular Biochemistry* **269**, 115-120.

75.   Racz, P. & Erdohelyi, A. (1988). Cadmium, Lead and Copper Concentrations in Normal and Senile Cataractous Human Lenses. *Ophthalmic Research* **20**, 10-13.

76.   Shi, H. L., Zhang, R. L., Chandrasekher, G. & Ma, Y. F. (1994). Simultaneous Detection and Quantitation of Sodium, Potassium, Calcium and Magnesium in Ocular Lenses by High-Performance Capillary Electrophoresis with Indirect Photometric Detection. *Journal of Chromatography A* **680**, 653-658.

77.   Chirgadze, Y. N., Nikonov, S. V., Garber, M. B. & Reshetnikova, L. S. (1977). Crystallographic Study of Gamma-Crystallins from Calf Lens. *Journal of Molecular Biology* **110**, 619-624.

78.   Asherie, N. (2004). Protein crystallization and phase diagrams. *Methods* **34**, 266-272.

79.   Broide, M. L., Berland, C. R., Pande, J., Ogun, O. O. & Benedek, G. B. (1991). Binary-Liquid Phase-Separation of Lens Protein Solutions. *Proceedings of the National Academy of Sciences of the United States of America* **88**, 5660-5664.

80.   Boggon, T. J. & Shapiro, L. (2000). Screening for phasing atoms in protein crystallography. *Structure with Folding & Design* **8**, R143-R149.

81.   Carlisle, C. H., Lindley, P. F., Moss, D. S. & Slingsby, C. (1977). Preliminary X-Ray Crystallographic Study of Bovine Lens Protein, Nu-Crystallin Fraction-2. *Journal of Molecular Biology* **110**, 417-419.

82.   Dumetz, A. C., Snellinger-O'Brien, A. M., Kaler, E. W. & Lenhoff, A. M. (2007). Patterns of protein - protein interactions in salt solutions and implications for protein crystallization. *Protein Science* **16**, 1867-1877.

83. del Valle, L. J., Escribano, C., Perez, J. J. & Garriga, P. (2002). Calcium-induced decrease of the thermal stability and chaperone activity of alpha-crystallin. *Biochimica Et Biophysica Acta-Proteins and Proteomics* **1601**, 100-109.

84. Bergeron, L., Filobelo, L. F., Galkin, O. & Vekilov, P. G. (2003). Thermodynamics of the hydrophobicity in crystallization of insulin. *Biophysical Journal* **85**, 3935-3942.

85. Vekilov, P. G., Feeling-Taylor, A. R., Yau, S. T. & Petsev, D. (2002). Solvent entropy contribution to the free energy of protein crystallization. *Acta Crystallographica Section D-Biological Crystallography* **58**, 1611-1616.

86. Annunziata, O., Ogun, O. & Benedek, G. B. (2003). Observation of liquid-liquid phase separation for eye lens gamma S-crystallin. *Proceedings of the National Academy of Sciences of the United States of America* **100**, 970-974.

87. Pande, A., Annunziata, O., Asherie, N., Ogun, O., Benedek, G. B. & Pande, J. (2005). Decrease in protein solubility and cataract formation caused by the Pro23 to Thr mutation in human gamma D-crystallin. *Biochemistry* **44**, 2491-2500.

88. Vekilov, P. G., Feeling-Taylor, A. R., Petsev, D. N., Galkin, O., Nagel, R. L. & Hirsch, R. E. (2002). Intermolecular interactions, nucleation, and thermodynamics of crystallization of hemoglobin C. *Biophysical Journal* **83**, 1147-1156.

89. Gunton, J. D., Shiryayev, A. & Pagan, D. L. (2007). *Protein Condensation: Kinetic Pathways to Crystallization and Disease*, Cambridge University Press.

90. Tanford, C. (1980). *The Hydrophobic Effect: Formation of Micelles and Biological Membranes*, John Wiley, New York.

91. Thurston, G. M. (2006). Liquid-liquid phase separation and static light scattering of concentrated ternary mixtures of bovine alpha and gamma B crystallins. *Journal of Chemical Physics* **124**, -.

92. Pellicane, G., Costa, D. & Caccamo, C. (2004). Microscopic determination of the phase diagrams of lysozyme and gamma-crystallin solutions. *Journal of Physical Chemistry B* **108**, 7538-7541.

93. McManus, J. J., Lomakin, A., Ogun, O., Pande, A., Basan, M., Pande, J. & Benedek, G. B. (2007). Altered phase diagram due to a single point mutation in human gamma D-crystallin. *Proceedings of the National Academy of Sciences of the United States of America* **104**, 16856-16861.

94. Bhamidi, V., Varanasi, S. & Schall, C. A. (2002). Measurement and modeling of protein crystal nucleation kinetics. *Crystal Growth & Design* **2**, 395-400.

95.   Gibbs, J. W. (1948). *The Collected Works of J. Willard Gibbs*, 1. 2 vols, Yale University Press, New Haven, CT.

96.   Tsekova, D., Popova, S. & Nanev, C. (2002). Nucleation rate determination by a concentration pulse technique: application on ferritin crystals to show the effect of surface treatment of a substrate. *Acta Crystallographica Section D-Biological Crystallography* **58**, 1588-1592.

97.   Rosenbaum, D., Zamora, P. C. & Zukoski, C. F. (1996). Phase behavior of small attractive colloidal particles. *Physical Review Letters* **76**, 150-153.

98.   Onuma, K. & Kanzaki, N. (2007). Multi-angle static and dynamic light scattering investigation of lysozyme association: From crystallization to liquid-liquid phase separation. *Journal of Crystal Growth* **304**, 452-459.

99.   Brown, W. & Zhou, P. (1991). Solution Properties of Polyisobutylene Investigated by Using Dynamic and Static Light-Scattering and Pulsed Field Gradient Nmr. *Macromolecules* **24**, 5151-5157.

100.   Yamakawa, H. (1971). *Modern Theory of Polymer Solutions*, Harper and Row, New York.

101.   Petsev, D. N., Thomas, B. R., Yau, S. T. & Vekilov, P. G. (2000). Interactions and aggregation of apoferritin molecules in solution: Effects of added electrolytes. *Biophysical Journal* **78**, 2060-2069.

102.   Bjork, I. (1973). Association-Dissociation Behavior and Hydrodynamic Properties of Apoferritin Monomer and Dimer. *European Journal of Biochemistry* **36**, 178-184.

103.   Brown, W. & Mortensen, K. (2000). *Scattering in Polymeric and Colloidal Systems*, CRC Press.

104.   Taylor, A. & Hobbs, M. (2001). 2001 assessment of nutritional influences on risk for cataract. *Nutrition* **17**, 845-857.

105.   Yan, H., Willis, A. C. & Harding, J. J. (2003). gamma III-crystallin is the primary target of glycation in the bovine lens incubated under physiological conditions. *Biochemical Journal* **374**, 677-685.

106.   Shukla, N., Moitra, J. K. & Trivedi, R. C. (1996). Determination of lead, zinc, potassium, calcium, copper and sodium in human cataract lenses. *Science of the Total Environment* **181**, 161-165.

107.   Finet, S., Skouri-Panet, F., Casselyn, M., Bonnete, F. & Tardieu, A. (2004). The Hofmeister effect as seen by SAXS in protein solutions. *Current Opinion in Colloid & Interface Science* **9**, 112-116.

108.   Giannopoulou, A., Aletras, A. J., Pharmakakis, N., Papatheodorou, G. N. & Yannopoulos, S. N. (2007). Dynamics of proteins: Light scattering study of dilute and dense colloidal suspensions of eye lens homogenates. *Journal of Chemical Physics* **127**, -.

109.   Bonnete, F. & Vivares, D. (2002). Interest of the normalized second virial coefficient and interaction potentials for crystallizing large macromolecules. *Acta Crystallographica Section D-Biological Crystallography* **58**, 1571-1575.

110.   Churchill, G. C. & Louis, C. F. (2002). Ca2+ regulation in differentiating lens cells in culture. *Experimental Eye Research* **75**, 77-85.

111.   Granier, T., Gallois, B., Dautant, A., DEstaintot, B. L. & Precigoux, G. (1997). Comparison of the structures of the cubic and tetragonal forms of horse-spleen apoferritin. *Acta Crystallographica Section D-Biological Crystallography* **53**, 580-587.

112.   Lin, M. Y., Lindsay, H. M., Weitz, D. A., Ball, R. C., Klein, R. & Meakin, P. (1990). Universal Reaction-Limited Colloid Aggregation. *Physical Review A* **41**, 2005-2020.

113.   Brantley, S., Kubicki, J. & White, A. (2007). *Kinetics of Water-Rock Interaction*, Springer.

114.   Matijevic, E. & Borkovec, M. (2004). *Surface and Colloid Science*, 17, Springer.

115.   Koutsoukos, P. G. (2001). *Trends in Colloid and Interfce Science XV*. European Colloid and Interface Society Conference, Springer.

116.   Panyukov, Y., Yudin, I., Drachev, V., Dobrov, E. & Kurganov, B. (2007). The study of amorphous aggregation of tobacco mosaic virus coat protein by dynamic light scattering. *Biophysical Chemistry* **127**, 9-18.

117.   Piazza, R. & Pierno, M. (2000). Protein interactions near crystallization: a microscopic approach to the Hofmeister series. *Journal of Physics-Condensed Matter* **12**, A443-A449.

118.   Arakawa, T. & Timasheff, S. N. (1984). Mechanism of Protein Salting in and Salting out by Divalent-Cation Salts - Balance between Hydration and Salt Binding. *Biochemistry* **23**, 5912-5923.

119. Blouwolff, J. & Fraden, S. (2007). Crystallization conditions of membrane protein CLC-ec1: An example outside the crystallization slot. *Journal of Crystal Growth* **303**, 546-553.

120. Hitscherich, C., Kaplan, J., Allaman, M., Wiencek, J. & Loll, P. J. (2000). Static light scattering studies of OmpF porin: Implications for integral membrane protein crystallization. *Protein Science* **9**, 1559-1566.

121. Nicolis, G. & Nicolis, C. (2003). Enhancement of the nucleation of protein crystals by the presence of an intermediate phase: a kinetic model. *Physica a-Statistical Mechanics and Its Applications* **323**, 139-154.

122. Reddy, G. B., Das, K. P., Petrash, J. M. & Surewicz, W. K. (2000). Temperature-dependent chaperone activity and structural properties of human alpha A- and alpha B-crystallins. *Journal of Biological Chemistry* **275**, 4565-4570.

123. Horwitz, J. (2009). Alpha Crystallin: The Quest for a Homogeneous Quaternary Structure. *Experimental Eye Research* **88**, 190-194.

124. Tanksale, A., Ghatge, M. & Deshpande, V. (2002). alpha-crystallin binds to the aggregation-prone molten-globule state of alkaline protease: Implications for preventing irreversible thermal denaturation. *Protein Science* **11**, 1720-1728.

125. Biswas, A., Miller, A., Oya-Ito, T., Santhoshkumar, P., Bhat, M. & Nagaraj, R. H. (2006). Effect of site-directed mutagenesis of methylglyoxal-modifiable arginine residues on the structure and chaperone function of human alpha A-crystallin. *Biochemistry* **45**, 4569-4577.

126. Siezen, R. J., Fisch, M. R., Slingsby, C. & Benedek, G. B. (1985). Opacification of Gamma-Crystallin Solutions from Calf Lens in Relation to Cold Cataract Formation. *Proceedings of the National Academy of Sciences of the United States of America* **82**, 1701-1705.

127. Horwitz, J. (1992). Alpha-Crystallin Can Function as a Molecular Chaperone. *Proceedings of the National Academy of Sciences of the United States of America* **89**, 10449-10453.

128. Bennion, B. J. & Daggett, V. (2003). The molecular basis for the chemical denaturation of proteins by urea. *Proceedings of the National Academy of Sciences of the United States of America* **100**, 5142-5147.

129. Fukuchi, S., Hamaguchi, K., Seike, M., Himeno, K., Sakata, T. & Yoshimatsu, H. (2004). Role of fatty acid composition in the development of metabolic disorders in sucrose-induced obese rats. *Experimental Biology and Medicine* **229**, 486-493.

130. Ten, S. & Maclaren, N. (2004). Insulin resistance syndrome in children. *Journal of Clinical Endocrinology and Metabolism* **89**, 2526-2539.

131. Alio, J. & Padron, M. (1982). Influence of Age on the Temperature of the Anterior Segment of the Eye - Measurements by Infrared Thermometry. *Ophthalmic Research* **14**, 153-159.